Novel layered silicates HUSs: potential application for functionalized material

(新規層状ケイ酸塩 HUSs:機能材料としての応用展望)

Nao Tsunoji

Submitted to Hiroshima University

In partial fulfillment of the requirements for the degree of Philosophy of Doctor

Supervisor: Professor Dr. Tsuneji Sano

Department of Applied Chemistry,
Graduate School of Engineering,
Hiroshima University

March 2015

Referee in Chief: Professor Tsuneji Sano

Referees: Professor Takeshi Shiono

Professor Kei Inumaru

Professor Shinjiro Hayakawa

Associate Professor Masahiro Sadakane

Department of Applied Chemistry,
Graduate School of Engineering,
Hiroshima University

Contents

Chapter 1

Introduction

1.1 General introduction

Silica based materials are promising due to the abundance of this natural resource, relatively high resistance to heat and chemicals, and the potential of wide variety of possible structures and functionalities. They are composed of combination of SiO_4 tetrahedron, which has the possibility for bonding various elements (Al, Zn, P, Ti, B etc.) with relative free bond length and angle. Therefore, silica based materials having numerous characteristics based on own specific structural features are available (Fig. 1-1). They are very important in both the chemical industrial field and the research for new applications.

Zeolites are one of the most important crystalline silicates material having microporous (2.0 nm $\geq$ d_P) in industry.[1,2] Because of their attractive properties (adsorption, catalytic and ion exchange) attributed to their crystalline defined, rigid and stable framework structure, they are utilized for the environmentally friendly and economically benefit application such as petrochemical industries, oil refineries and fine chemicals industries.[3-6] To date, new type of zeolites with various framework structures, morphologies and compositions can be hydrothermally prepared by changing a large number of variable synthesis methods such as utilization of complex organic structure directing agent (OSDA), ionic liquid, and unique hydrothermal synthesis process.[8-11] In

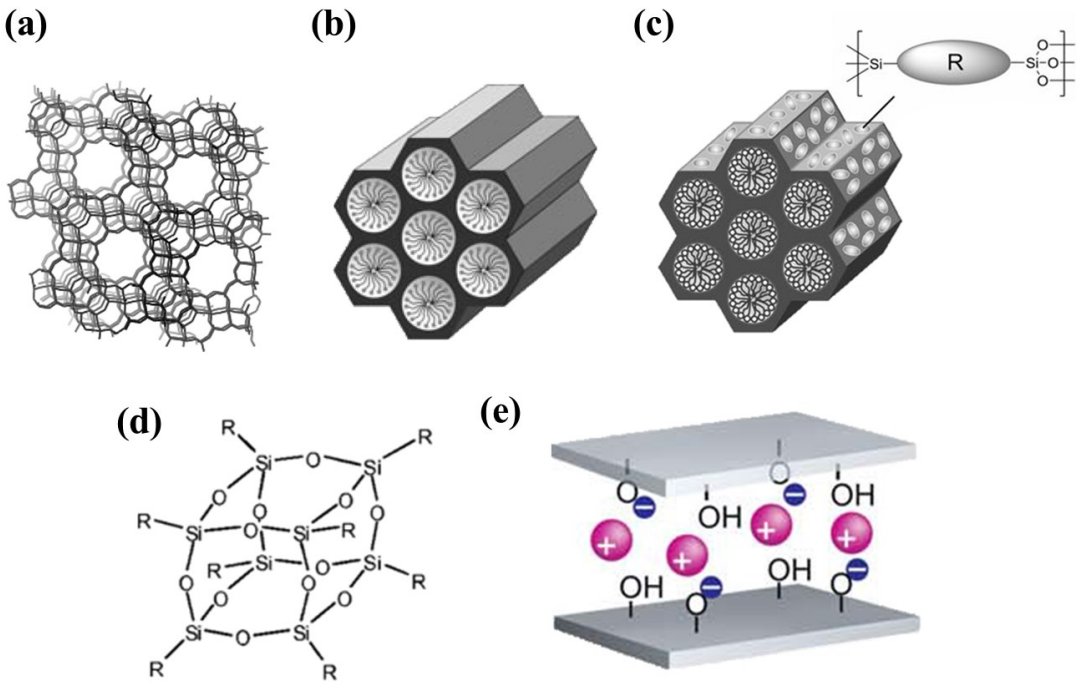

Fig. 1 Illustrations of representive silica based materials with various structural features: (a) zeolite, (b) mesoporous silica,[21] (c) periodic mesoporous organosilica,[23] (d) silisesuquioxane,[25] and (e) crystalline layered silicate.[34]

spite of such many efforts, even today, the design of zeolite synthesis with desirable structure and composition is very difficult. In other words, these results indicate that their structural features, including the metastable nature of zeolites, the complex crystallization mechanism and the limit of method for functionalization due to the stable crystalline structure, inhibit the potential for more free and precise design of their own features.

On the other hand, from the view point of silica based materials for more flexible structural design, ordered mesoporous silicas, have been considerable attracted. Mesoporous silicas, FSM-16[12,13] and MCM-41[14,15], a new class of ordered porous material with “meso” pore having diameter larger than 2 nm, were successfully synthesized by Kuroda group and a research group in Mobil Corp, respectively.

Although zeolites have excellent catalytic properties by virtue of their crystalline framework network, their applications are limited by the relatively small pore opening. Therefore, mesoprous silicas opened novel application area of porous materials with different directionality of zeolite, including drug delivery, photochemical, and other catalysts for reaction of more bulky molecules, because huge matter such as complex organic molecules, metal oxide, and biomolecules were enabled to access into the internal large meso space.[16,17] In addition, as the flexible synthesis strategy of mesoporous silica, that self-assembly between ionic or nonionic surfactants (such as long-chain alkyltrimethylammonium) and building unit of their mesoporous frameworks (silica or other element),[14,15,18] periodic mesoporous organo silica can be synthesized using organic-hybrid alkoxysilane precursors as a functional building unit instead of simple silica monomer.[19-22] These novel organic-inorganic hybrid mesoporous materials have numerous potential for application as fluorescent sensor, charge-transporting material and new type of solid state catalyst.[23] However, almost of these material have amorphous pore wall, which could limit their potential utility for industrial catalyst and more accurate surface design.

In addition, molecular and polymeric organic-inorganic hybrid materials, silicone polymer and silsesquioxane, which are composed of polymeric structures based on R_2SiO and $RSiO_{3/2}$, respectively, are prepared using organosilane.[24-26] These compounds have a formula unit between the inorganic materials and the more organic materials and have often been described as having “hybrid” properties, which are the chemically inert and thermally stable inorganic Si-O-Si fragment and the potentially reactive and readily modified R-Si fragment. Especially, a wide variety of polymeric structures based on $RSiO_{3/2}$ are known, such as random polymers through ladder polymers to more highly

ordered discrete molecular species such as POSS and double-decker. Therefore, silsesquioxane polymers are utilized for material chemistry fields based on organic and polymer science as photoresist coatings for electronics and optical devices,[27] protective coating films for semiconductor devices,[28] liquid crystal display elements,[29] and gas separation membranes.[30] It is well known that the synthesis of these polymer are performed by hydrolysis and subsequent condensation reaction of organosilane monomer in the presence of acid or alkali mediums with very high reaction rate. Typically, as it is difficult to completely control this polymerization process, it mainly gives disordered 3-dimensional network, which lead to decrease of their utility depending on insolubility to solution.

Thus, these wide varieties of silica based materials have different structural features, flexibility for materials design and regularity or stability, which can be regard as both of merits and demerits. Because these all factors are important for materials design, the other class of silica based material having both of high flexibility for material design and structural regularity will be a key to more desirable material synthesis. From such a view point, in this thesis, the detail and background of crystalline layered silicate are described separately in the following section.

1.2 Introduction to layered silicate

Crystalline layered silicates[31,32] composed of 2-dimentional silicate sheets with nanometer thickness having the silicate framework composed SiO_4 tetrahedron possess interlayer exchangeable cations and large interlayer space. By using reactive silanol

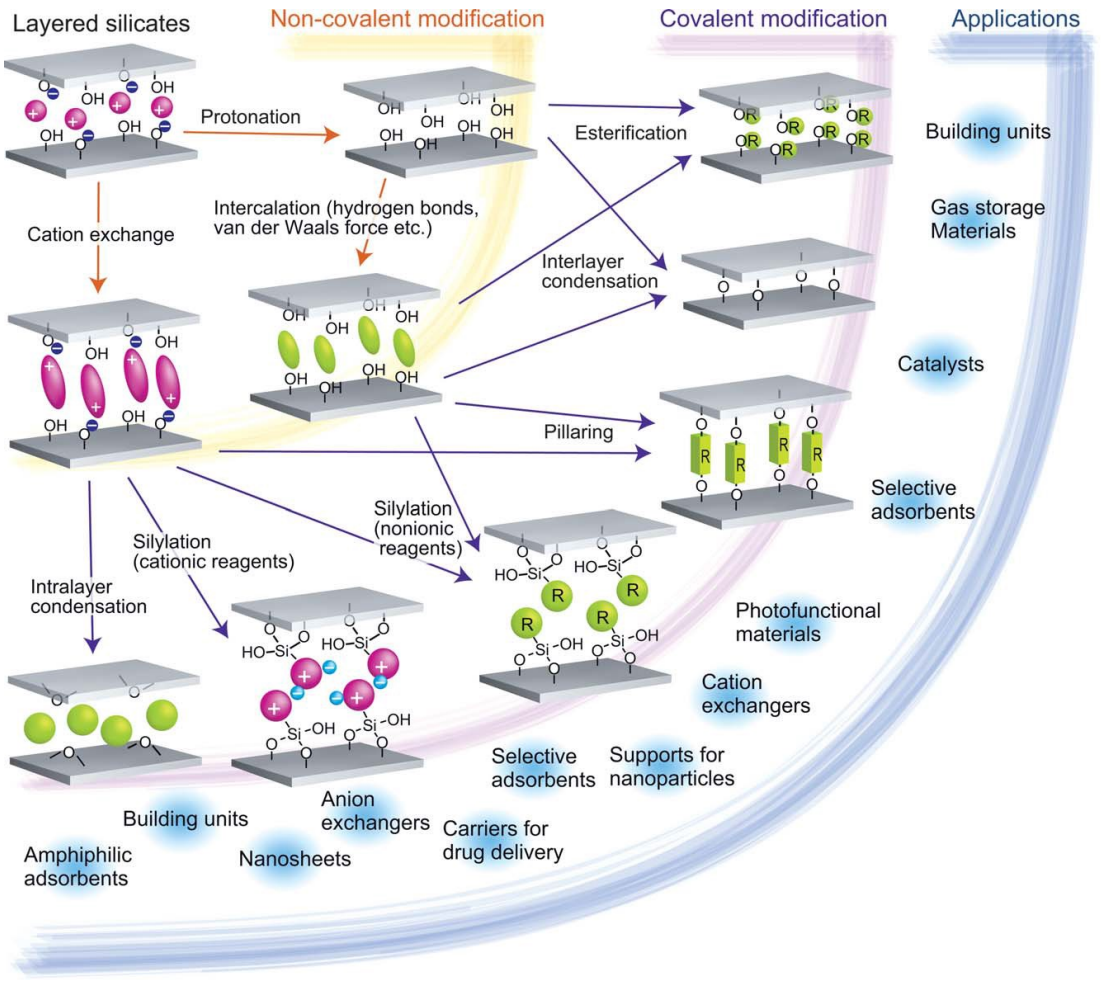

Fig. 1-2 Materials design of layered silicates with non-covalent and covalent modifications.[34]

(SiOH) and silanolate (SiO^-) groups, neighboring silanol (SiOH/SiO^-) groups, in the interlayer, various post treatment including ion-exchange, silylation and pillaring are available[33-37] (Fig. 1-2). Although the macroscopic structures of other silica based materials such as zeolite and mesoporous silica are hardly changed during the post treatment due to hardness of their frameworks, the interlayer of layered silicate space can be flexibly swelled depending on the size of incorporated guest compounds into the interlayer. In addition, accurate arrangement of SiOH/SiO^- groups located in the

crystallographically defined position that reflects their original silicate framework structure enable control of the surface structural features at an angstrom level. These structural features of layered silicate facilitate more free design of advanced and innovative inorganic materials with desired property optimized in accordance with the purpose by combination with the various compound introduced and accurate design of interlayer structure.

1.2.1 Layered alkali silicate

Magadiite ($Na_2Si_4O_{10}\cdot 5H_2O$),[38-40] kenyaite,[38,41] makatite,[42–44] and kanemite ($NaHSi_2O_5\cdot 3H_2O$),[45–49], are widely known as natural layered silicates which composed single silicate sheets and hydrated Na^+ cation in the interlayer. Kanemite and makatite have similar silicate framework topology. The silicate frameworks are constructed from

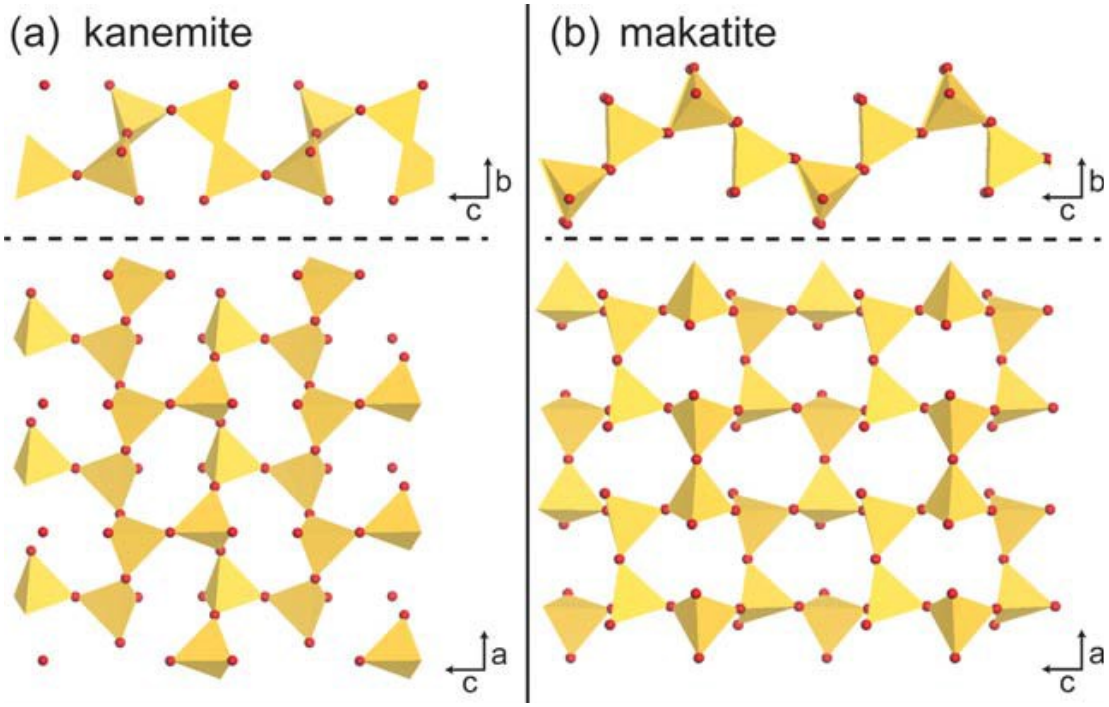

Fig. 1-3 Silicate frameworks of (a) kanemite and (b) makatite.[34]

only six-membered (Si-O-Si) rings with Q^3 ($(HO)Si(OSi)_3$ or $(O^-)Si(OSi)_3$) and Q^4 ($Si(OSi)_4$) structure (Fig. 1-3). In the framework of kanemite, the SiO_4 tetrahedra are ordered with crank-like along *c* axis (Fig. 1-3a). The silicate layer of makatite show zigzag ordering along c axis (Fig. 1-3b). In contrast, crystal structures of magadiite and kenyaite have not been well defined. Other sodium layered silicates, for example, layered octosilicate ($Na_8[Si_{32}O_{64}(OH)_8]\cdot 32H_2O$ also known as ilerite or RUB-18),[50–57] α-$Na_2Si_2O_5$,[58] β-$Na_2Si_2O_5$,[59] ε-$Na_2Si_2O_5$,[60] and δ-$Na_2Si_2O_5$,[61] which is a precursor of kanemite, are also synthesized. In addition, layered silicates having other alkali cations than Na^+ in the interlayer are also known, such as apophyllite,[62] $KHSi_2O_5$,[63] $LiNaSi_2O_5\cdot 2H_2O$ (Silinaite),[64] $Li_2Si_2O_5$, $K_2Si_2O_5$,[65] $Na_{1.55}K_{0.45}Si_2O_5$,[66] $NaKSi_2O_5$, $Na_{0.67}K_{1.33}Si_2O_5$,[67,68] $Cs[Si_3O_6(OH)]$, $Rb[Si_3O_6(OH)]$,[69] $CsHSi_3O_7$,[70] and $K_4[H_4Si_8O_{20}H_4]$ (named as K-LDS).[71,72] Although, the frameworks of layered silicates are usually composed of Q^3 and/or Q^4 units. Arroyabe et al. reported unusual single-layer silicate ($K_2Ca_4Si_8O_{21}$) containing Q^2 ($(O^-/HO)_2Si(OSi)_2$) and Q^3 units.[73]

1.2.2 Layered zeolite precursor

Although most of zeolites contain 3-D connecting framework structures, some zeolites are obtained from 2 dimensional layered silicate precursors. This layered zeolite precursor can be categorized as layered silicates because of their structure composed of the silicate framework with SiO_4 tetrahedral units and $SiOH/SiO^-$ groups with $SiOH^{\cdots -}OSi$ hydrogen bridge. To date, layered zeolite precursors and layered silicates with various framework structures were hydrothermally synthesized using various organics such as quaternary ammonium and amines as structure directing agents (SDA). The details are described in the following section (Section 1.3.3).

Layered silicate has several specific structural features, (1) internal large surface area, (2) ordered interlayer space crystallographically defined, and (3) silicate framework topology. In following section, their application and functionalization are summarized by showing the several characters of layered silicate based on these structural features.

1.3 Application and functionalization of layered silicate

1.3.1 Interlayer large surface area

As crystalline inorganic nanosheets, such as clay and LDH, are applicable for polymer/nanosheets composites,[74] active and long-lived catalysts,[75,76] catalyst supports[77] and various hybrid materials including Langmuir-Blodgett films,[78,79] layer-by-layer films,[80,81] hydrogels,[82] and self-standing films,[83] effective utilization of the surface of silicate layer as nanosheets has received considerable attention as a method for significant expansion in applications.

As their specific features of layered silicate, exfoliation of silicate layers also leads to the formation of high surface and modifiable materials. Novel catalysts consisting of exfoliated zeolite 2D-precursors provides the wide range of reactions.[84-88] ITQ-2 was firstly reported by Corma et al. as exfoliated catalysts with alumino silicate layers, which were prepared by the delamination of the zeolite layered precursor material MCM-22(P) (Fig. 1-4).[84] Each individual MWW-type layer, has a thickness of 2.5 nm and contains a 10 member-ring (MR) sinusoidal channel, expanded the range of application that zeolites catalyze by providing access for larger reactant molecules as

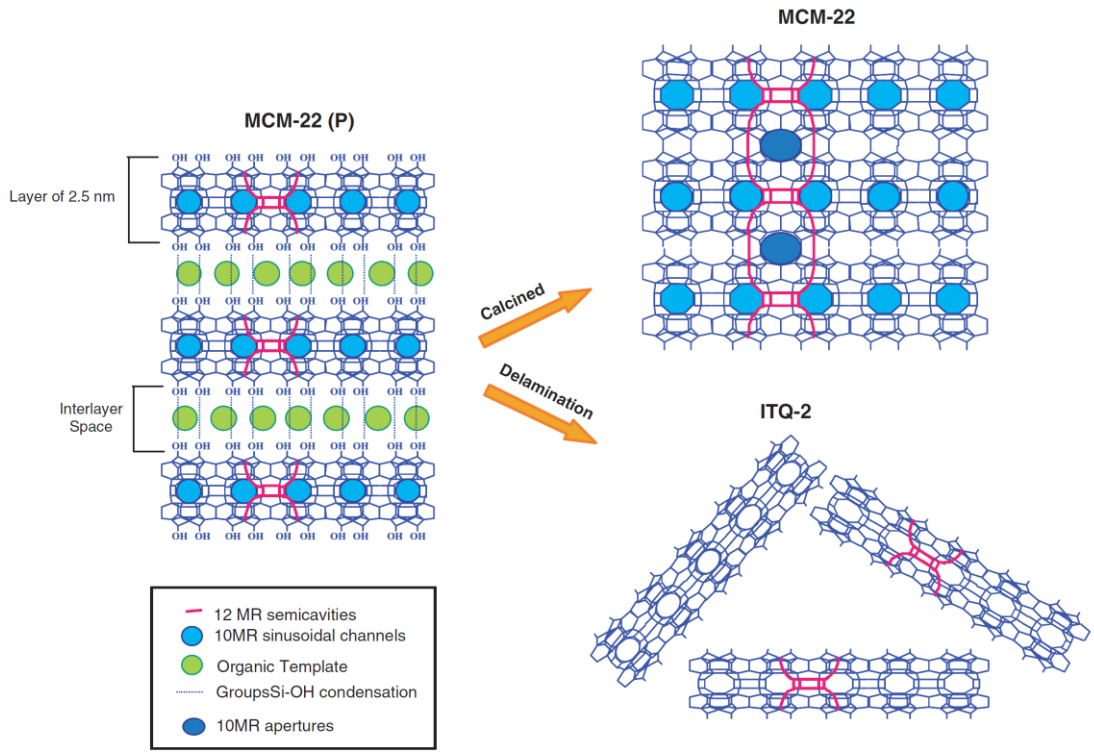

Fig. 1-4 Structural schematic representation of MWW-type zeolites and ITQ-2 delaminated zeolite.[93]

accessible sheets with shape-selective catalytic ability.[89-96] On the basis of this prospective, delamination or exfoliation of various layered zeolite precursor and layered silicate has been investigated. Delaminated zeolites have been prepared from the delamination of lamellar precursors such as AMH-3,[97] PREFER[85] and Nu-6(1).[86,87] The relevant parameters for delamination (exfoliation) of cetyltrimethylammonium bromide exchanged layered silicate magadiite were reported by Bi et al.[98] The framework element of exfoliated silicate sheet is not limited to aluminium, a new porous material, UZAR-S1 and UZAR-S2 has been obtained by exfoliation of the layered titanosilicate precursors JDF-L1 and AM-4, respectively.[99,100] Also, [V,Al]-Nu-6(1), containing vanadium and aluminium in the silicate layers, was delaminated in basic medium and treated with acid as well affording [V,Al]-ITQ-18. It is well known that the synthesis of

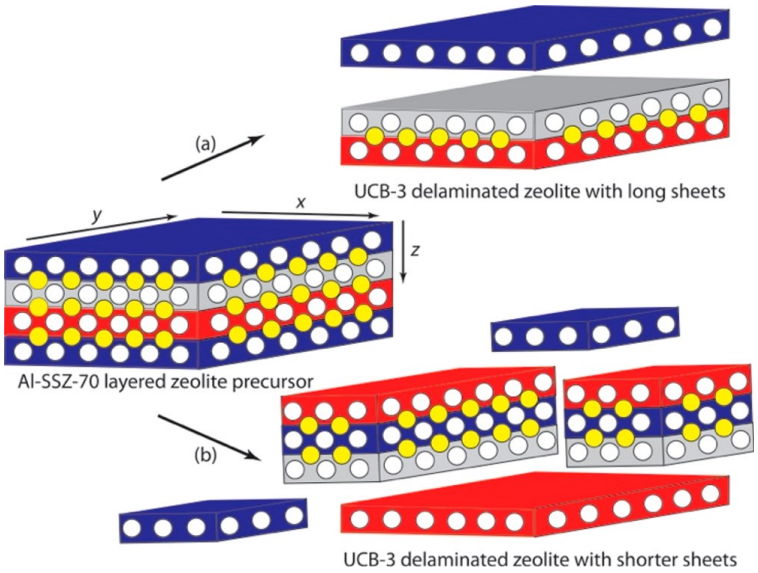

Fig. 1-5 Schematic representation of two possible benefits of Al-SSZ-70 delamination: (a) conventional benefit consisting of separated long sheets and (b) proposed new benefit of delamination, in which UCB-3 delaminated zeolite consists of shorter sheets formed by the breakage of layers during delamination.[108]

exfoliated layered silicate materials has required a high-pH medium during precursor material swelling, typically in the pH range of 13.5−13.8.[102-104] Because of the high solubility of silica in such a basic aqueous solution, hypotheses of partial amorphization of the zeolite layers during delamination have been invoked. Therefore, to prevent unexpected collapse of silicate layer, the search for milder conditions for delamination was carried out. Ogino et al. reported the synthesis of UCB-1, which results from MCM-22 (P) exfoliation using a combination of tetrabutylammonium fluoride and chloride surfactants in aqueous solution.[105] It was concluded that this fluoride/chloride exfoliation method presented delaminates layered zeolite precursors at a pH of 9 in aqueous solution. In this mild condition, the delamination of borosilicate layered zeolite precursors SSZ-70 was also achieved without leaching boron.[106] Boron (B) atoms often are post-synthetically exchangeable with other metal atoms, such as aluminum (Al) and

titanium (Ti), to synthesize active catalysts.[107] Therefore, this results may be enable the synthesis of a wide variety of catalysts consisting of heteroatoms on external surfaces within well-defined coordination environments. The catalytic activities of delaminated zeolite UCB-3 was particularly investigated by the same group.[108] Delaminated zeolite UCB-3 exhibited considerable higher catalytic activity comparison to its three-dimensional (3D) zeolite counterpart, Al-SSZ-70. In contrast, when the internal active sites was formed as a result of sheet breakage during delamination, catalytic

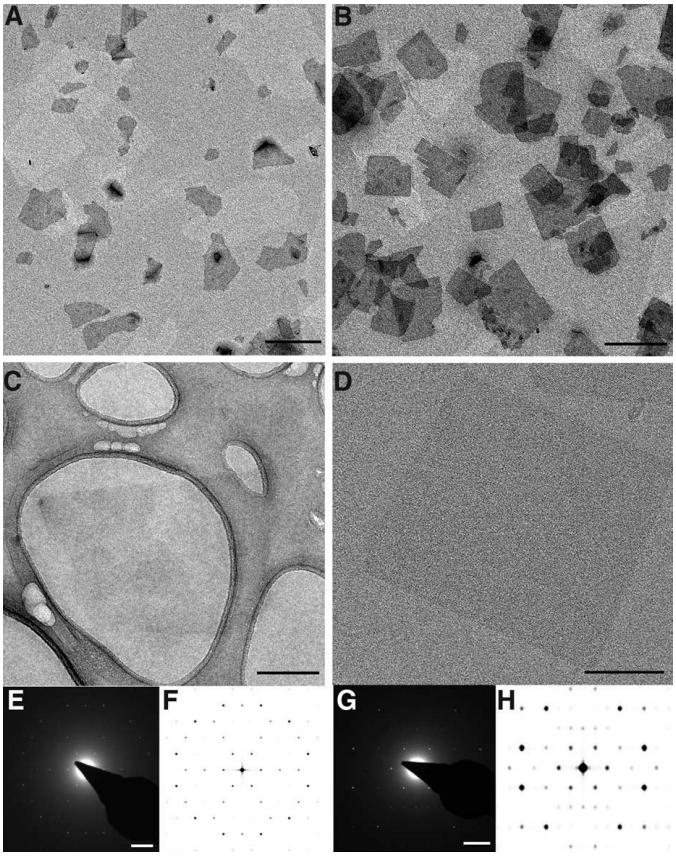

Fig. 1-6 Low-magnification TEM images of c-oriented MWW (A) and b-oriented MFI nanosheets (B). TEM images of single MWW and MFI nanosheets are shown in (C) and (D), respectively. (E) and (G) are the corresponding ED patterns of the same particles shown in (C) and (D), respectively. Simulations of the ED patterns of proposed structures of nanosheets down the c axis (MWW) and b axis (MFI) are shown in (F) and (H), respectively. Scale bars in (A) to (C), 200 nm; in (D), 50 nm; in (E) and (G), 1 nm. [108]

performance increased (Fig. 1-5).

Furthermore, these exfoliated lamellar zeolite particles also have potential in a number of applications without catalytic use, for example such as enhancing the permselectivity of polymer–zeolite nanocomposite membranes,[109] the immobilization of enzymes,[110] and producing polymer-layered silicate nanocomposites with improved tensile properties.[111]

As stated above, exfoliated silicate sheets are useful for functionalized materials with high surface area. In contrast, suspensions of exfoliated silicate nanosheets are also important. Tsapatsis groups reported the synthesis of thin membrane constructed from zeolite nanosheet films using the dispersed suspension of MFI and MWW type zeolite nanosheets via exfoliation in the polystyrene and toluene and subsequent stacking of each silicate layers (Fig. 1-6).[112] Fig. 1-6 shows the TEM images of dispersed MFI and MWW zeolite nanosheets. As shown in the Fig. 1-6A, high-aspect-ratio MWW and MFI zeolite nanosheets with flakelike morphologies were observed. Electron diffraction (ED) from single MWW and MFI nanosheets (Fig. 1-6 bottom) confirmed that the nanosheets are highly crystalline materials of the MWW and MFI type, respectively. In addition, thin film membranes, prepared by filtration and subsequent hydrothermal treatment of MFI type zeolite nanosheets, separated xylene isomers (p-xylene from o-xylene) with a p-xylene/o-xylene separation factor of 40 to 70, whereas and p-xylene permeance of 3×10^{-7} mol $m^{-2}s^{-1}$ Pa^{-1} at 150 °C. In addition, MWW membranes exhibited molecular sieving properties with ideal selectivies for He/H_2 and He/N_2 up to 3 and 17, respectively, derived from the small transport-limited aperture of MWW along the direction of layer stacking. The high layer charge density than that of layered clay minerals and strong hydrogen bonds between hydrated cations and silanol groups

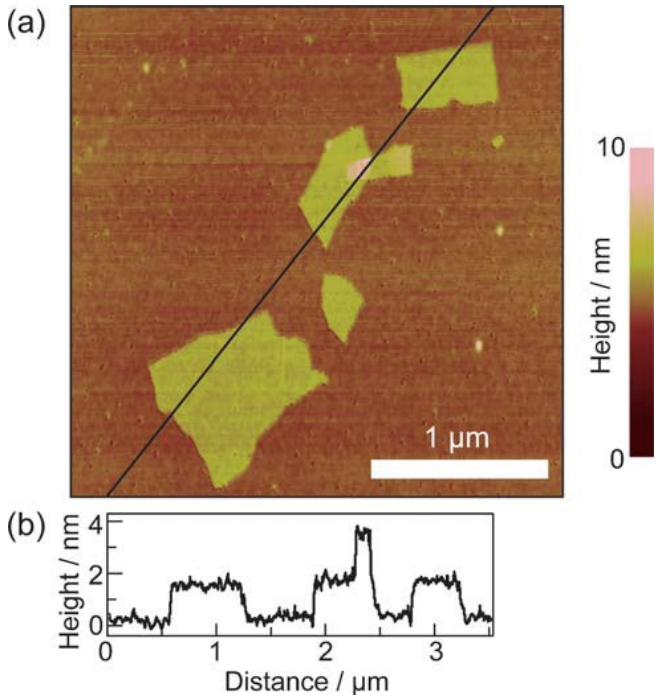

Fig. 1-7 (a) AFM image of exfoliated Bim-Oct cast on a silicon wafer and (b) height profile on the black line of the AFM image. [108]

normally prevents exfoliation. To overcome such limitation, surface modification are often performed. Kuroda group reported that exfoliation of layered sodium octosilicate in water can be achieved by silylation with 1-butyl-3-(3-triethoxysilylpropyl)-4,5-dihydroimidazolium (Bim-Oct).[77] AFM images of the nanosheets of layered silicate silylated derivative obtained from the colloidal solution show the formation of thin nanosheets with thickness of 1.9 nm (Fig. 1-7). Furthermore, didecyldimethylammonium ion-exchanged octosilicate was exfoliated by stirring in pentane with ultrasonication.[113]

To obtain exfoliated silicate nanosheets, several post-treatment including interlayer expansion, acid or alkali treatment, composition with the polymer and ultrasonication are performed. However several groups achieved direct synthesis of 2-dimensional

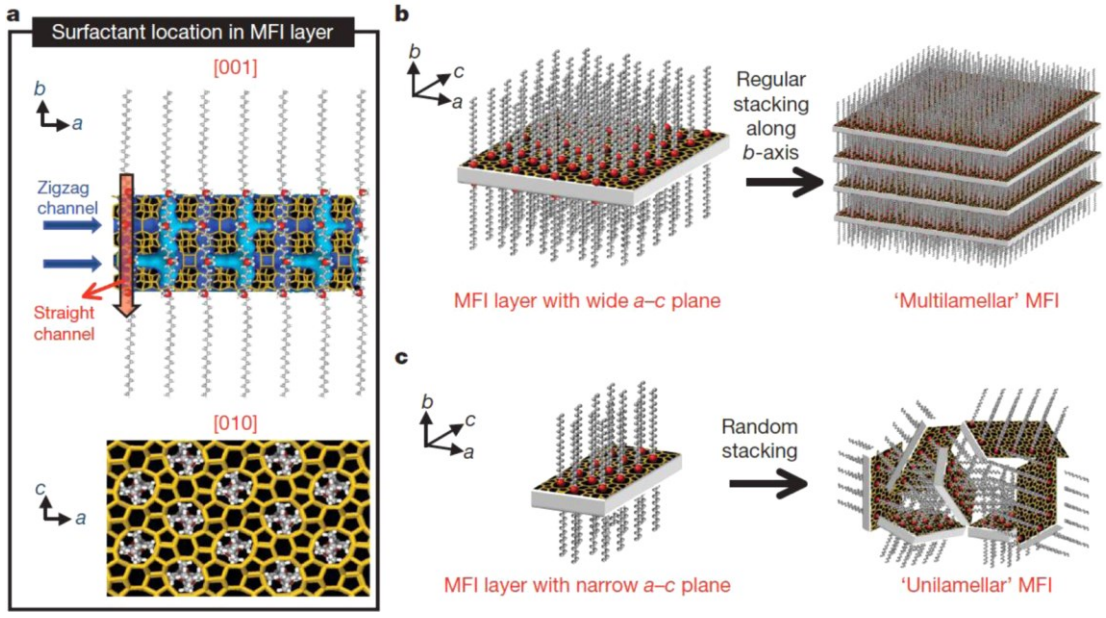

Fig. 1-8 Use of a surfactant with a cationic headgroup that can direct the MFI structure to nanosheets with approximately 1 and 0.5 unit cell thickness. These nanosheets can either stack in an ordered fashion or be randomly stacked to form different types of material. Reprinted with permission from ref 114. Copyright 2009 Nature Publishing Group.

zeolite nanosheet without post-treatment. Ryoo's work has been spectacularly successful and has resulted in several families of new zeolites constructing from MFI type zeolite nanosheets.[114] In that work, bifunctional surfactant, $C_{22}H_{45}$-$N^+(CH_3)_2$-C_6H_{12}-$N^+(CH_3)_2$-C_6H_{13} with a long and short alkyl chain, was designed so that the dicationic headgroup would be a suitable structure-directing agent for the synthesis of a zeolite with the MFI structure (Fig. 1-8). Recently, using different strategy, zeolite nanosheets with the silicate framework crossed each other containing micro- and mesoporosity were reported by using tetrabutylphosphonium cations as an OSDA.[115] Okubo groups also reported formation of hierarchically organized zeolite nanosheet by sequential intergrowth (Fig. 1-9).[116] These two reports about the zeolite nanosheet crossed each other selected an appropriate OSDA that can form plate-like

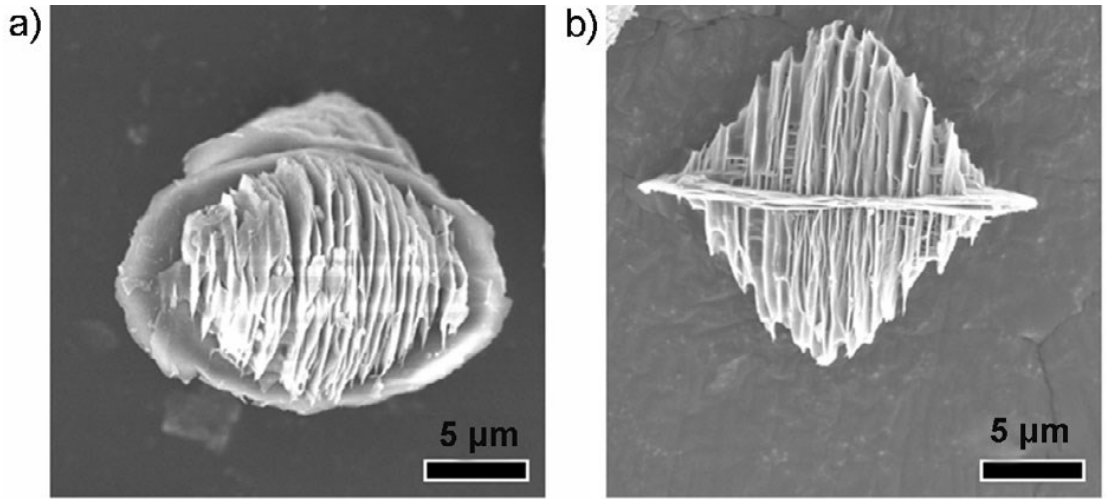

Fig. 1-9 FE-SEM images of formation of hierarchically organized MFI type zeolites nanosheet by sequential intergrowth.[116]

zeolites with enhanced 90° rotational intergrowths. These researches are much valuable because both of the bifunctional surfactant and intergrowths concepts would be applicable to other zeolite frameworks and related porous crystalline materials that can form such unique structure. For example, titanosilciate[117] and stannosilicate[118] zeolite nanosheets, which showed notable catalytic activities for bulky molecular selective oxidation reactions such as epoxidation of alkene and Baeyer−Villiger oxidation of cyclic ketones using H_2O_2 as oxidant, were hydrothermally synthesized by using a dual porogenic surfactant with formula $C_{16}H_{33}–N^+(CH_3)_2–C_6H_{12}–N^+(CH_3)_2–C_6H_{13}$ as the SDA.

The interlayer space of layered materials is easily expanded by incorporation of various matters into the interlayer. Pillaring of layered precursors is a general and older concept to obtain porous material with high surface areas. Pillaring of layered precursors is based on the idea that transformation of layered material into high-surface-area molecular sieves with larger interlayer space. The “pillars” are

typically amorphous and not orderly arranged in interlayer space. As the crystalline silicate layers play the important role as building block in pillared marterial, more various material design are available. The first example of pillared layered zeolite is that, Kresge et al. reported the MCM-36 pillared zeolite which is formed by MWW-type inorganic layers and insertion of silica pillars in to the interlyaer, leading to outstanding catalytic performance.[94-96] In the work, pillaring is accomplished by absorption of pillar precursor such as tetraethylorthosilicate (TEOS) into the organophilic interlayer space of exfoliated layered precursors, where it is converted to a metal oxide pillar. To remove the interlayer molecules such as water, preswollen ammonium ions and organic byproducts, the final silica-pillared product is produced by calcination. After the treatment of TEOS pillaring, pillared material (MCM-36) showed high BET surface area of 711 m^2g^{-1} compared with original MCM-22 (432 m^2g^{-1}). From characterization of this material, they concluded that MCM-36 was comprised of MWW layers, ca. 2.5 nm thick, separated by 2−2.5 nm interlayer space filled partially with silica pillars with the structure exhibiting mesopores and the large amount of strong Brønsted acid sites was located in this original zeolite layer. Therefore, this material also exhibited excellent catalytic activity and adsorption property for bulky molecule. Derivatives of pillared zeolites with various silicate frameworks, including MWW (MCM-36),[95] FER (ITQ-36),[86] NSI [MCM-39(Si)],[119] MFI,[76] ilerite,[120] kanemite,[121] and PCR[122], were successfully synthesized. Pillaring of layered zeolite precursors has been exclusively carried out by using TEOS, having a suitable rate of hydrolysis. Of course, alternative oxides are available as pillaring units. By the several group of reports, introduction of other metal oxide copomosites pillars including aluminium, magunesium and barium, were tried, and pillared materials exhibiting similar porosities like one in which silica

was as pillars were obtained.[123-125] These materials also showed additional Brønsted acid sites of higher strength than those in the zeolitic sheets generated by pillaring with (mixed) aluminum oxides. The presence of Mg and Ba also generated basic sites. In addition, an organic type of pillaring units, arylsilsesquioxane[126] or 1,4-bis(triethoxysilyl)benzene (BTEB),[127] were reported. By several treatments including swelling with organic reactants, porous material with high BET surface area (500-650 m^2g^{-1}) and large mesopore volume 0.2 mlg^{-1} were obtained. The pillars

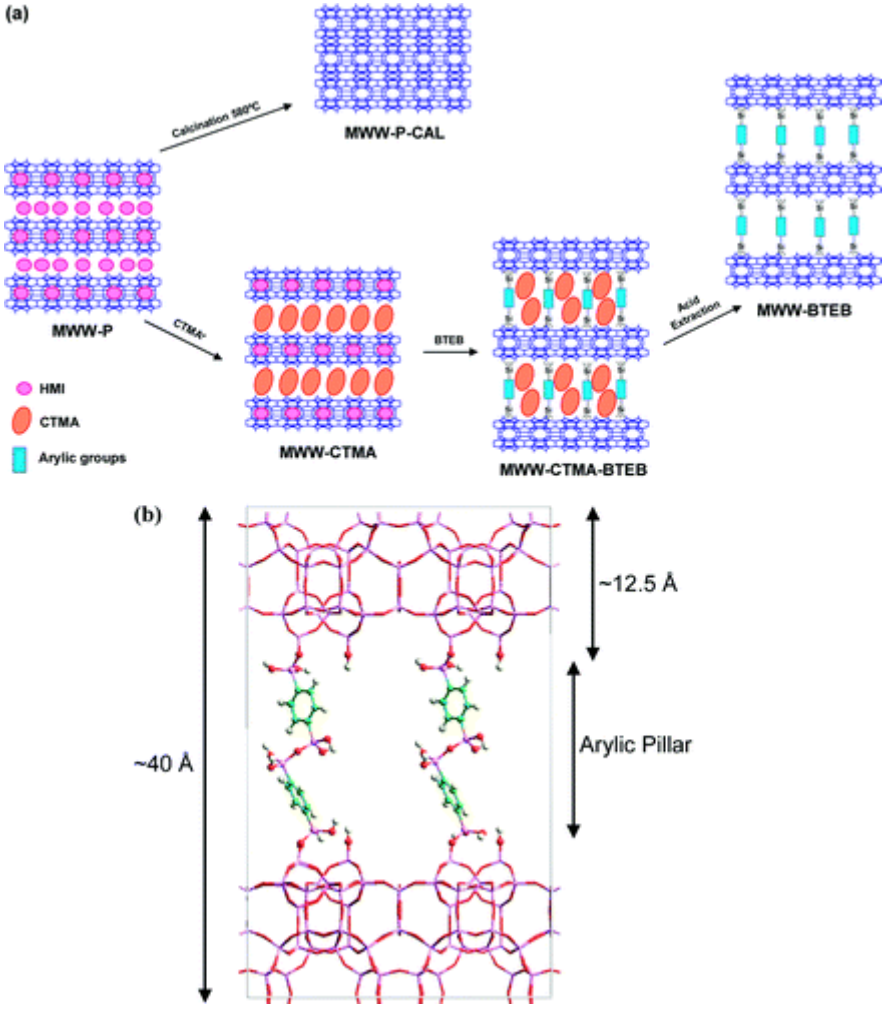

Fig. 1-10 Artistic Representation of (a) Methodology Employed to Obtain Pillared Hybrid Zeolitic Materials from MWW Precursors and (b) Layered Hybrid Material Obtained by Pillaring with BTEB Silsesquioxane Molecules (MWW-BTEB).[127]

comprised BTEB molecules have two connection parts of (aryl)-Si-O-Si-(aryl) bridge and an aryl-Si-O-MWW bord (Fig. 1-10). Through amination post-treatment of BTEB molecules, it has been possible to prepare bifunctional acid-base catalysts where the acid sites are of the zeolitic part located in the inorganic building blocks and the basic sites are a part of the organic structure. This catalyst can act as bifunctional catalysts for performing a two-step cascade reaction that involves the catalytic conversion of benzaldehyde dimethylacetal into benzylidene malononitrile. Other layered zeolitic organic−inorganic materials have been synthesized using a two-dimensional zeolite precursor IPC-1P and siloxane with biphenyl, phenylene, and ethanediyl groups.[128]

Formation of ordered mesoporous silica, with high internal surface area and mesopore having narrow pore diameter, derived from layered silicates, especially kanemite, was extensively investigated by the Kuroda group.[129] The formation mechanisms of mesophase silicates derived from layered silicates are summarized in Fig. 1-11. The two-dimensional (2D) hexagonal symmetry of one-dimensional (1D) mesopores can be obtained by alkali treatment using layered intermediates composed of fragmented silicate sheets and C_nTMA cations (Fig. 1-11 bottum). The materials were called FSM-16 (Folded Sheets Mesoporous Materials) in 1994.[130,131] On other hand, the mesoporous material with different pore structure, named KSW-1 (mesoporous silica derived from Kanemite Sheets performed at Waseda University), were also reported.[132] This material was obtained by following two step procedure; a layered $C_{16}TMA$–kanemite complex were prepared, and then this layered complex was treated under mild acidic conditions and calcined. The synthetic strategy of KSW-2 prepared from a layered silicate is the bending of individual silicate sheets and condensation of surface silanol. The bending was induced by the partial elution of $C_{16}TMA$ ions from

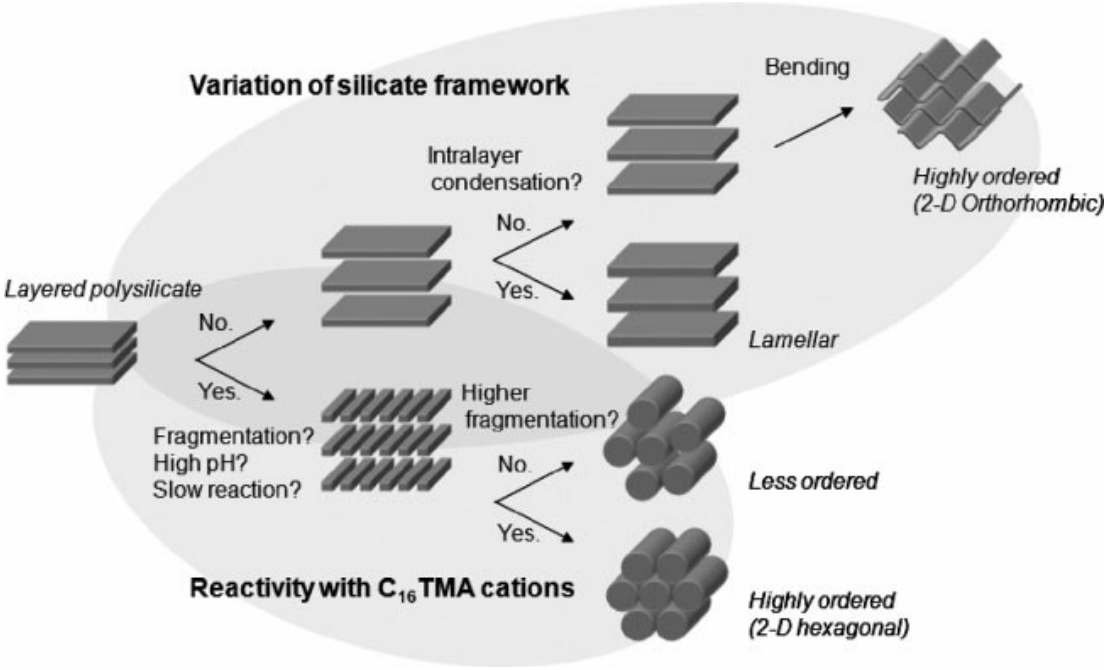

Fig. 1-11 Schematic formation routes of mesostructured C16TMA–silicates derived from layered -silicates.[129]

the interlayer spaces, and C_{16}TMA assemblies in the interlayer region were structurally changed during the acid treatment of the layered compounds with intralayer condensation by lowering pH values down to 6–4. As the result, the formation unique squared mesopores were performed. There have been reports on the incorporation of metal species into the silicate frameworks of KSW-2.[133,134] When Al-KSW-2 was prepared by using Al incorporated layered crystalline silicate, incorporated Al atoms are kept as AlO_4 units in all the preparation stages of kanemite, as-synthesized KSW-2, and calcined KSW-2. Temperature-programmed desorption measurements of ammonia (NH_3-TPD) of Al-KSW-2 showed a broad pattern with two peaks at around 250 and 400 °C, suggesting a wide distribution of acid strength. In addition, silylation of KSW-2 was also reported by the authors.[135,136] Formation of more ordered mesostructure of KSW-2 was achieved by silylation with $C_8H_{17}OSiCl_3$ and hydrolyzed. From XRD, the

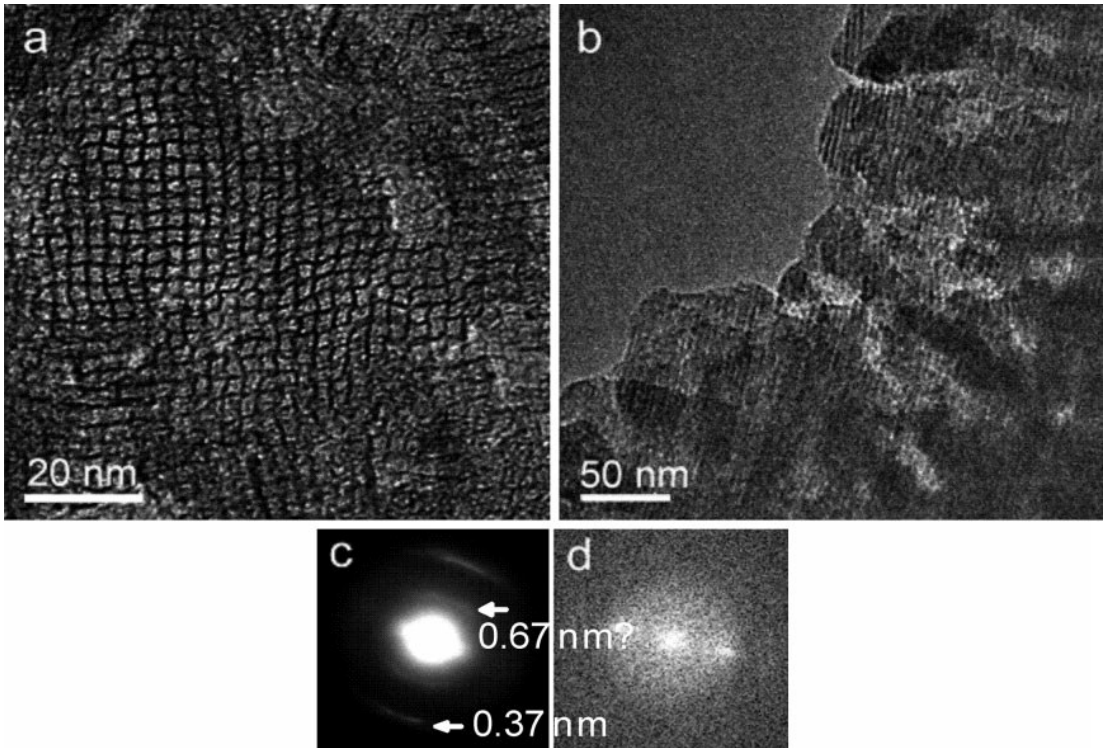

Fig. 1-12 TEM images along the a) [100] and b) [110] directions of KSW-2 silylated directly with $C_8H_{17}OSiCl_3$ and hydrolyzed. c) The corresponding SAED image and d) the Fourier transform image of (b).[135]

peaks due to the kanemite-based periodic structure were observed at high diffraction angles. Also, TEM observation directly shows the presence of the periodic structure in the silicate framework with the mesostructural ordering (Fig. 1-12). Other groups also reported the formation of mesoporous silica using layered silicate as a silica source. Ion-exchanged layered silicates, RUB-18[137,138] and helix layered silicate (HLS),[139] were transformed into meso structure by hydrothermal treatment. In these reports, the morphology of original layered silicate, i.e., plate-like particles, was unchanged during the transformation to mesostructured materials.

1.3.2 Ordered interlayer space or surface crystallographically defined

Layered silicates are consists of anionic silicate layers, with cation-exchangable

ability, and interlayer cations. Furthermore, layered silicates have silanol (SiOH) and silanolate (SiO^-) groups regularly located at crystallographically defined positions in the interelayer. This surface silanol (SiOH) and silanolate grousps can be modified covalently (covalent modification) such as condensation, silylation and esterification. As the spatially limited two dimensional space of layered material gives the specific interaction between the gest species into the interlayer and the host inorganic layers, interlayer space of layered materials can be utilized as the specific space that exhibits molecular recognitive ability. Namely, by using modification ability and spatial limitation of layered silicates, materials design on the interlayer surface becomes possible. In this section, the synthesis of layered silicate material are summarized and discussed focused on ordered interlayer space or surface.

In the case of layered silicate, conventional intercalation reactions coming from hydrogen bonding, cation exchange, dipole–dipole interaction, van der Waals force, and acid–base reaction, are widely investigated as well as other layered material.[140] In clay minerals, the determination of exact position of reactive sites is very difficult, whereas the ordering of SiOH/SiO^- groups, namely interlaction point, of layered silicates can be defined specifically on the basis of their crystal structures.

Iler[141] reported the cation exchange reaction of layered silicate with metal cations (Li^+, Na^+, Mg^{2+}, Ni^{2+}, and Cu^{2+}) and hexadecyltrimethylammonium cation. Also, layered silicates are used for softener of water by using the cation exchange property for divalent cations in water.[142,143] Intercalation of organic cations, alkylammoniums and alkylamines, were firstly studied by Lagaly et al. They reported that the possibility of the intercalation of alkylamine, quaternary alkylammonium, and alkylpyridinium cations into magadiite.[144] It has been also reported that interlayer of several layered

silicates gave selective adsorption spaces. For example, it has been reported that magadiite exhibits selective adsorption of Zn^{2+} from seawater.[145] Ogawa et al. reported the photoluminescence of Eu^{3+} intercalated into various layered silicates (kanemite, octosilicate, magadiite, and kenyaite).[146] Exchange reaction of interlayer cations with proton is often performed for the accomplishment other intercalation reactions because alkali metal cations prevents other intercalation reactions due to the strong interactions between the cations and anionic silicate layer. Protonated layered silicates can act host materials for alkylamines which are intercalated by acid–base reactions between SiOH and RNH_2.[147,148] Other polar organic molecules, such as formamide and dimethylsulfoxide, can also be intercalated into protonated layered silicates.[148,149] In addition, the highly selective adsorption of phenol from water containing benzene on protonated magadiite during photocatalytic oxidation were reported by Ide et al.[150] They reported that phenol could be recovered with unprecedentedly high efficiency and selectivity (purity) when the photocatalytic oxidation of benzene in water over TiO_2 under simulated solar light was conducted in the presence of a layered silicic acid (protonated magadiite).

Interlayer covalent modification including silylation, and esterification of $SiOH/SiO^-$ groups are also expected to exhibit more interesting interlayer spaces due to the possibility of controlled spatial distribution of specific functional groups in the interlayer. The silylation reaction onto layered silicates was firstly reported by Ruiz-Hitzky and Rojo in 1980.[151] They used protonated layered silicates (e.g. magadiite) and treated it with polar organic solvents, such as dimethylsulfoxide (DMSO), for the expansion of the interlayer spaces and then trimethylchlorosilane and hexamethyldisilazane were reacted with surface silanol groups for 24-48 hours at reflex.

The silylated layered silicates can be regarded as a new family of macromolecular organosilicon compounds and named as *planar silicone*. This discovery indicated that interlayer silanol groups of layered silicates can be regarded as reactive sites for various kinds of reactants providing covalent bond. By Ruiz-Hitzky, Rojo, and Lagaly, the mechanism of silylation reactions by using various organosilanes was extensively investigated. They used various organo silanes such as (chloromethyl)dimethylchlorosilane, dimethylphenylchlorosilane, triphenylchlorosilane, and hexaethyldisilazane.[152] According to their paper, it was concluded that (i) it is necessary for silylation that hydrogen bonds between interlayer surfaces are attenuated by intercalation of polar organic solvents, and (ii) diffusion of silylation reagents occurs simultaneously with desorption of the polar organic guest molecules. In contrast, by Kato and Kuroda groups, silylation of dodecyltrimethylammonium (C_{12}TMA) ion-exchanged layered silicates, such as magadiite, kenyaite, and layered octosilicate, was investigated by using several silylation reactants including trimethylchlorosilane, diphenylmethylchlorosilane, triethylchlorosilane, triisopropylchlorosilane, butyldimethylchlorosilane, octyldimethylchlorosilane, and octadecyldimethylchlorosilane.[152–156] By Park et al., octyltriethoxysilane was also used for silylation.[157] Kuroda et. al claimed that reaction intermediates intercalated with polar organic solvents have some disadvantages of (i) relatively low stability of the solvents in air and (ii) small basal spacings, which prevents the modification of bulkier silylating reagents. In contrast, they also showed that the alkyltrimethylammonium ion-exchanged layered silicates were stable and the guest molecules could not be eliminated by washing with acetone. As the basal spacings of intercalated compounds were larger than 2 nm and adjustable by choosing the length of alkyl chain, bulky silylation reagents,

such as octadecyldimethylchlorosilane, could be immobilized into interlayers.[119]

As explained above, in the silyation reaction of layered silicates, various reactants (silane coupling agents) with different structure are available. Furthermore, as the degree of silylation on the interlayer surface directly affect to special distribution of reactants immobilized onto the surface, silyation reaction can be utilized for the design of surface properties of layered silicates. Ogawa et al. reported that the distance between adjacent organic functional groups can be controlled to make nanospace accessible for guest species (Fig. 1-13). They prepared the silylated layered silicate derivatives by silylation of magadiite with octyltrichlorosilane and octyldimethylchlorosilane. Then, the distance of functional groups has been controlled (0.52–0.66 nm; 0.28–0.44 nm^2 per group) by changing the amount of covalent attachment of octylsilyl groups (Fig. 14).[158–160] Alkyl alcohols were adsorbed into the magadiites modified with controlled amounts of octylsilyl groups (0.44 nm^2 per group), while alkanes were not. From these results, they concluded that this surface property was comming from the cooperative effect of the geometry and the chemical nature of the surface covered the octyl groups and silanol groups. Furthermore, the adsorption capacity of alcohols was affected by the surface cover ratio (the distance between the adjacent functional groups). This concept was developed using more complex silylation system. It has been reported that trimethylsilylated- kanemite adsorbed benzene rather than water because of hydrophobic interlayer region by Toriya et al.[161] Also, magadiite immobilized with [2-(perfluorohexyl)-ethyl]dimethylchlorosilane is advantageous for preparation of the films and showed high thermal stability.[162] Ide et al. reported the silylation of layered silicate octosilicate with two types of reactants with octadecyl and phenyl groups to control the spatial distribution and the silylated derivatives achieved the effective and

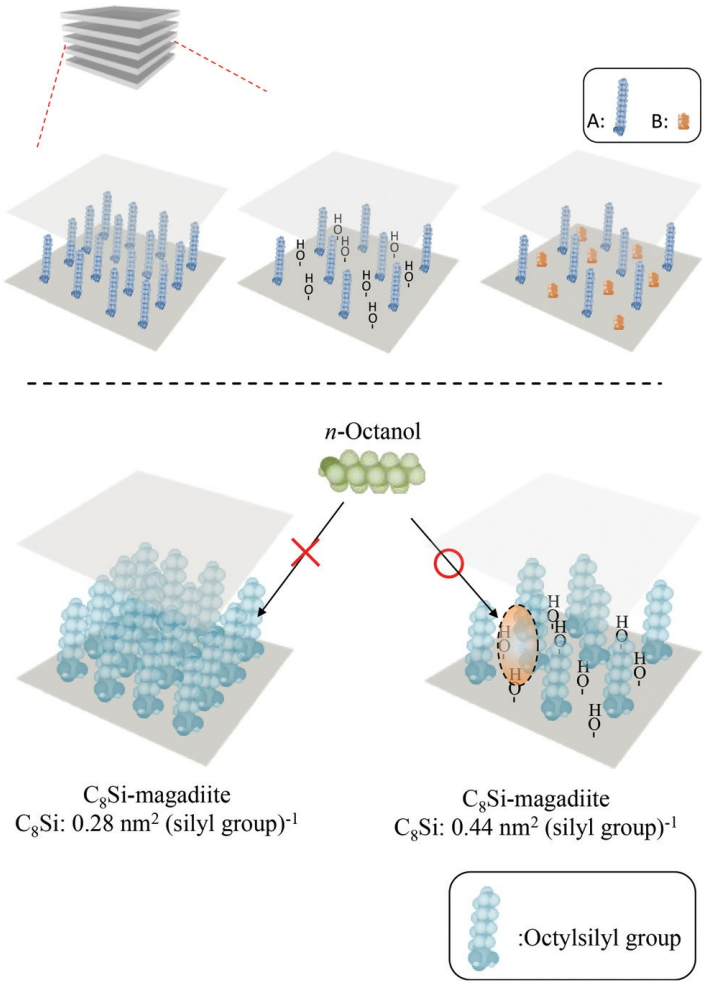

Fig. 1-13 Schematic drawings of possible variation of the spatial distribution of functional units

selective adsorption of 4-nonylphenol from aqueous solution.[163]

The immobilization of functional groups except a simple hydrocarbon on the layered silicates was also reported to exhibit different surface property. Immobilization of aminopropyltriethoxysilane (APTES), which exhibits base catalytic and cationic properties, onto the interlayer surfaces of magadiite and kenyaite was reported.[164,165] Leu et al. synthesized APTES immobilized kenyaite.[166] They utilized the derivative as an intermediate for layered silicate/polyimide nanocomposites. The nanocomposites exhibited a maximum degradation temperature of 36 °C and a maximum moisture

absorption reduction of 54%. Selective adsorption of metal cations by using amino-functionalized magadiite was studied by Zhang et al.[167] They used (3-(2-aminoethylamino) propyltrimethoxysilane with two amino groups, denoted as AAPTMS) and immobilized its onto magadiite. The layered hybrid selectively adsorbed Cu^{2+} from diluted aqueous solutions. Adsorption property of silylated derivatives by using silylation reagents with one (APTES), two (AAPTMS), and three (N-3-trimethoxysilylpropyldiethylenetriamine) amino group(s) were extensively studied by Airoldi group.[168–172] Ishii et al. reported the silylation of octosilicate with p-aminophenyltrimethoxysilane (APhTES) using pre-intercalated n-hexylamine.[140] Takahashi et al. reported the synthesis of novel anion exchangeable layered materials by immobilization of imidazolium chloride salts onto octosilicate (Fig. 1-14).[174] They utilized 1-butyl- (or 1-octyl-) 3-(3-triethoxysilylpropyl)-4,5-dihydroimidazolium chloride, which are applicable for ‘‘designer solvents’’ as ionic liquid and conductor, for immobilization into octosilicate, and the products were named Bim-Oct and Oim-Oct. By the immobilization process, the $SiOH/SiO^-$ groups on octosilicate are converted to one anion exchangeable sites of imidazolium groups. In general layered double hydroxides (LDH), representative anionic exchangeable inorganic layered material, anion exchange at relative lower pH value is hardly occurred due to the its lower acid resistance, whereas the Bim-Oct is stable at pH 1.0, and can adsorbed several anions such as Cl^-, Br^-, I^-, and NO_3^-.

Also, silylation using various silylation reagents with sulfide, thiol and cyano groups has been performed. Bis[3-(triethoxysilyl)propyl]tetrasulfide and 3-cyanopropyltriclorosilane were used for silylation.[175,176] These siylated derivatives have an ability to remove divalent cations, such as Co^{2+}, Ni^{2+}, Cu^{2+}, Zn^{2+}, Cd^{2+}, and

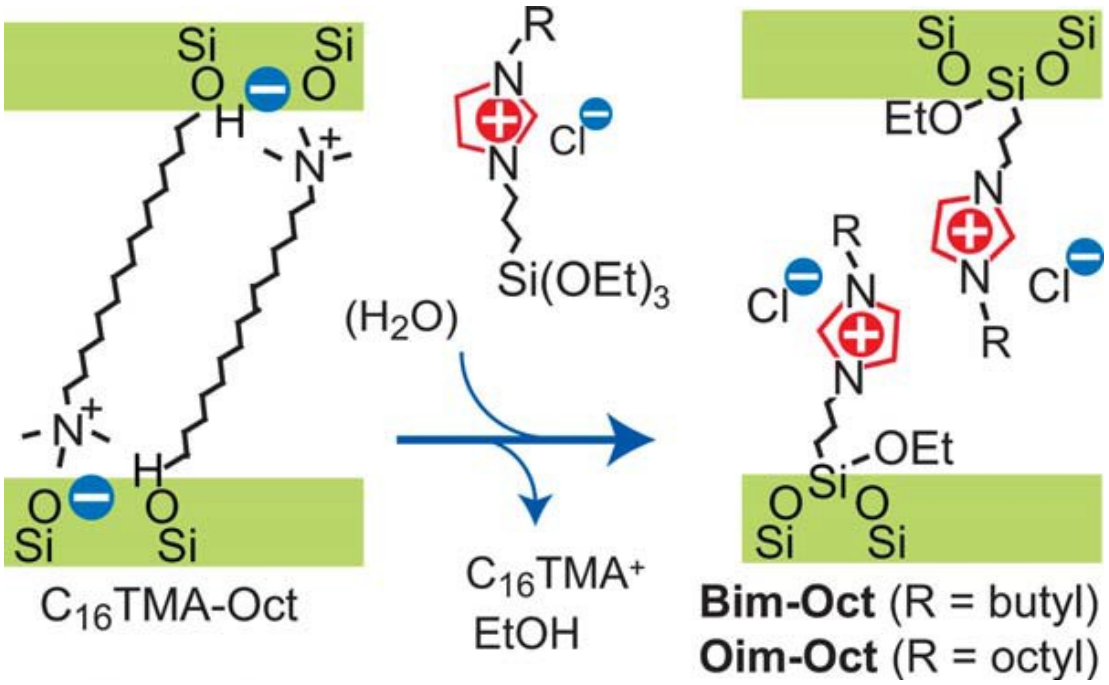

Fig. 1-14 Synthetic pathway of anion exchangeable layered silicates.[174]

Hg^{2+} from aqueous solutions. Ogawa, Ide, and co-workers have studied the immobilization of thiol group onto layered silicates.[177,178] They utilized the layered octosilicate hybrid (MPS-Oct) silylated with 3-mercaptopropyltrimethoxysilane (MPTMS) for preparation of Au nanoparticles in the interlayer space.[177] They though that the Au nanoparticles was disc-like or polygonal plate-like because of the confinement in the interlayer space. Thiol groups immobilized on layered octosilicate can be converted to sulfonic acid groups by oxidation with nitric acid.[178] The sulfonated octosilicates are well dispersed and swollen in water, which is applicable for transparent colloidal suspensions. In addition, Ide et al. reported several co-modification processes for preparation of gas adsorbents and acid catalysts.[179,180] They synthesized the silylated derivatives of a layered alkali silicate, magadiite, modified with propylsulfonic or arylsulfonic acid, and used as catalysts for an acid catalyzed condensation of phenol

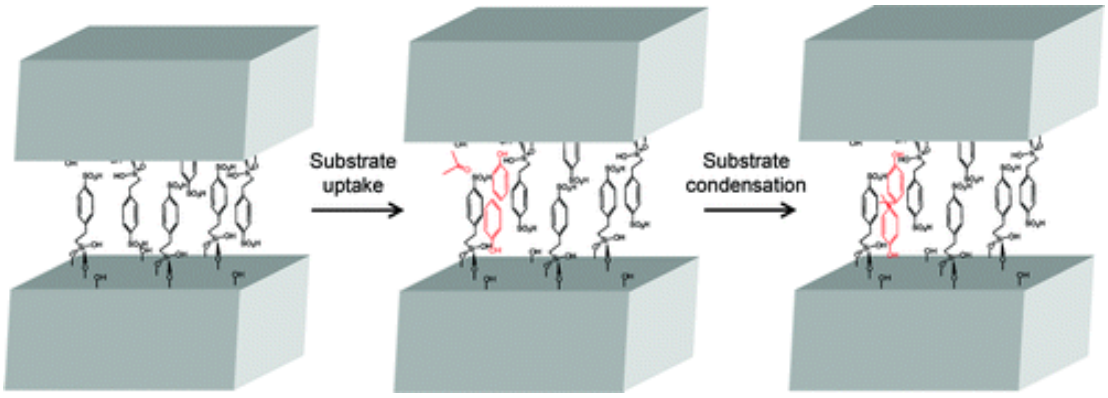

Fig. 1-15 Schematic drawing of p,p' bisphenol A formation in the interlayer space of silyalted layered silicate catalyst.[179]

with acetone (Fig. 1-15). The yield and selectivity of p,p' bisphenol A, desired product, were successfully obtained by controlling the amount of the attached propylsulfonic or arylsulfonic acid.[179] They also exhibited that organic derivative of a layered silicate co-modified with amino and octadecyl groups adsorbed CO_2 effectively and very selectively from the gaseous mixture with N_2 and H_2O.[180] Recently, octosilicate was successfully modified with the controlled amount of phenethyl group and the immobilized phenethyl group was subsequently sulfonated by the reaction with chlorosulfonic acid. In this report, a systematic expansion of the interlayer space was observed by the ion exchange with alkyltrimethylammonium ions to show the variation of the layer charge density.[181]

Silylation of layered silicates is also applicable for the preparation strategy of new crystalline layered silicates because functional groups can be regurely immobilized in an ordered manner on the surfaces.[182] These silylated 2D silicate derivatives can be regarded as building units for formation of novel high-ordered structure. Alkoxysilylation of layered silicates can expand the possibility of design of the crystal

structure at the atomic level. The ordered silylation of layered silicate using various alkoxychlorosilanes ($(RO)_nSiCl_{4-n}$, R = alkyl, n = 1, 2) have been studied by Kuroda groups. They have paid attention to layered octosilicate (also known as RUB-18 or ilerite) as one of the most suitable layered silicates for silylation. In their research, siylation of alkyltrimethylammonium-exchanged octosilicate with dialkoxydichlorosilanes was mainly performed, then one silylating agent reacted with the two confronting $SiOH/SiO^-$ groups, they it called "dipodal silylation".[183,184] As the silyl groups could be immobilized on the surfaces of layered silicate, reflecting the crystallinity of the original layers, construction of several ordered 2D and 3D silicate structures were achieved by alkoxysilylation of layered octosilicate (Fig. 1-16). When the silylation of octosilicate with monoalkoxytrichlorosilanes was performed, alkoxy(chloro)silyl groups were immobilized on the surfaces by dipodal silylation. Furthermore, alkoxy groups could be hydrolyzed by post-treatment with a mixture of water and polar organic solvent. The obtained structure was varied according to the kind of the organic solvents (dimethylsulfoxide (DMSO) or acetone). The H_2O/DMSO treatment of the silylated product gave hydrolysis of alkoxy groups and intercalation of DMSO into the interlayer spaces to form a novel 2D silicate structure. In contrast, when the H_2O/acetone treatment was carried out, interlayer condensation between the neighboring layers and formation of a novel 3D silicate structure were observed (Fig. 1-16). They explained that such a difference was caused by the difference in the amount of the solvent molecules present in the interlayer spaces by hydrogen-bonding with SiOH groups. Although the 3D structure has no micropores because the acetone molecules are stuffed into the pores, formation of micropores has been successful when the similar procedure was applied to a layered silicate magadiite.[185] However, the

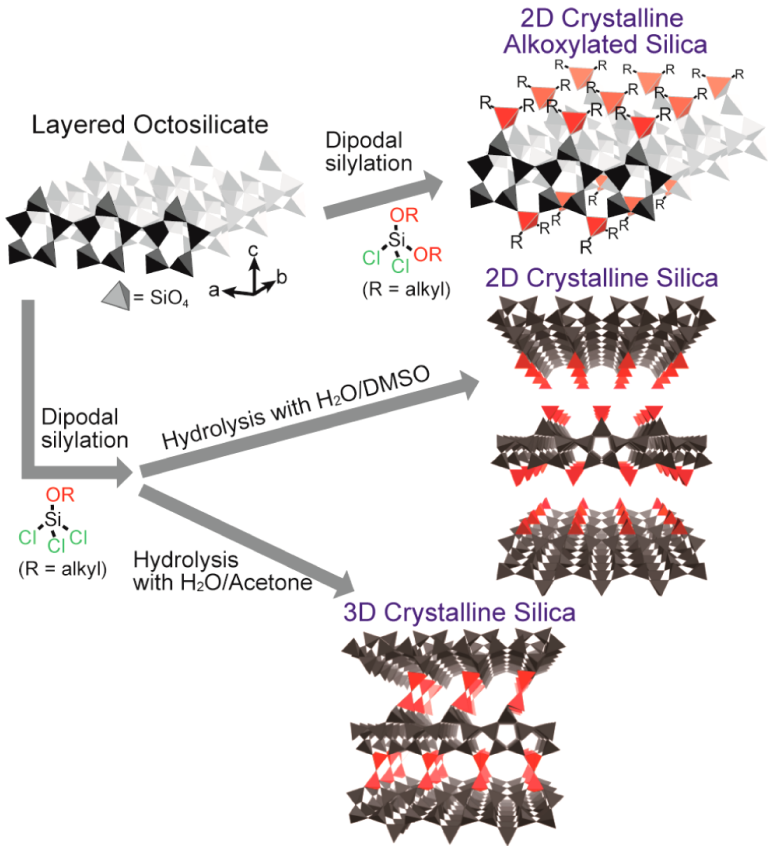

Fig. 1-16 Construction of 2D and 3D silicate structures by alkoxysilylation of layered octosilicate followed by hydrolysis of alkoxy groups. Reprinted with permission from ref 183. Copyright 2002 American Chemical Society.

detailed structure was unclear because the crystal structure of magadiite has not been determined yet. In the above systems, each pillar between the layers consists of silicon. On the other hand, pillaring of layered silicates with organically bridged silanes (Si−R−Si; R = phenylene or biphenylene) was also performed to give inorganic−organic hybrid materials.[186,187] Mochizuki et al. used 1,4-bis(trichlorosilyl)benzene or 1,4-bis(dichloromethylsilyl)benzene as of pillaring unit of octosilicate.[187] The silylation degrees were high, which was from 83% to 88%, calculated from the Q^3/Q^4 ratios of the products, indicating high ordered silylation of octpsilicate. Also, the pore size distribution was narrow, suggesting the formation of uniform pores due to well-ordered

immobilization of silylation reagents. The obtained micropores derived from 1,4-bis-(trichlorosilyl)benzene exhibited a hydrophilic nature due to formed Si–OH groups by hydrolysis of chlorosilyl groups. In contrast, those derived from 1,4-bis(dichloromethylsilyl)benzene exhibited a hydrophobic nature. The adsorption behavior of phenol and water onto these microprous materials is due to the difference in the hydrophilicity/hydrophobicity of pores.

Recently, silylation of other type of layered silicate, RUB-51, was also performed by Asakura et al. Silylattion of RUB-15 with half-sodalite cages with dichlorodimethylsilane and trichloromethylsilane was perfomed.[188,189] Silylation of RUB-51 gave the bidentate silylation, in which one silylating agent reacted with the two conforming SiOH/SiO^- groups. RUB-51 silylated with dichlorodimethylsilane could be delaminated and flocculated through ultrasonication in cyclohexane.[188] Furthermore,

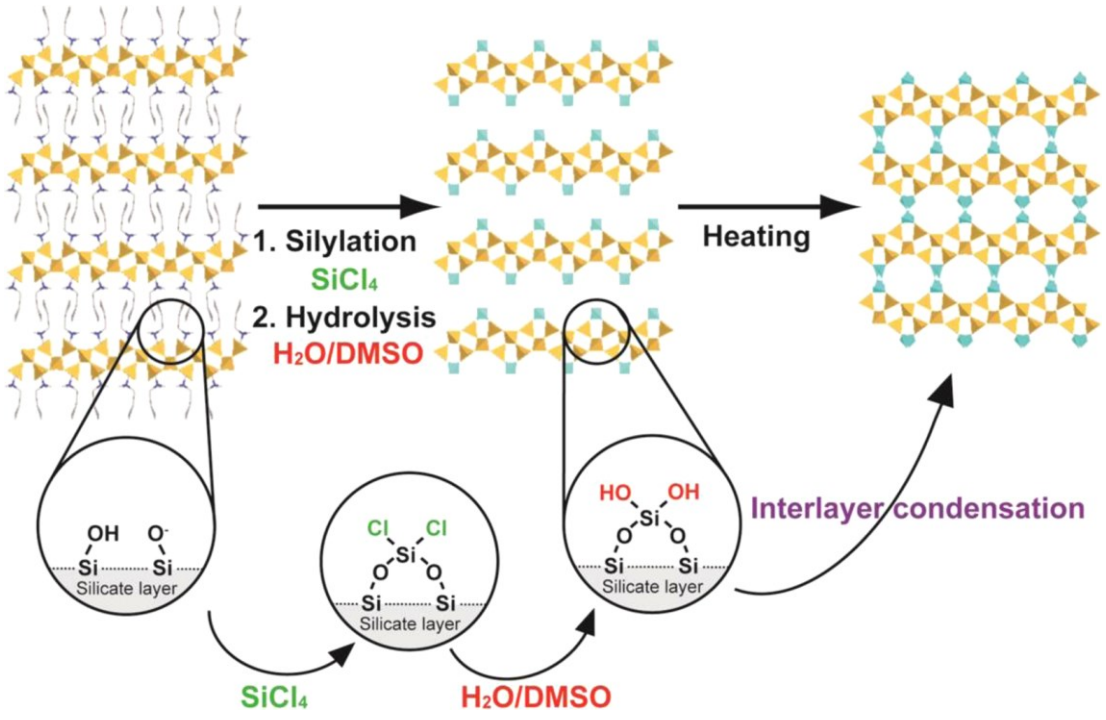

Fig. 1-17 Formation of a Microporous Material from RUB-51.[189]

Asakura et al. studied that synthesis of a novel crystalline microporous material derived from silylation of layered silicate RUB-51 with tetrachlorosilane ($SiCl_4$) (Fig. 1-17).[189] In the formation process of this material, to form interlayer micropore, three step treatment including silylation, hydrolysis, and heat treatment were performed. First, one $SiCl_4$ molecule reacted with two confronting groups, SiO^- and Si−OH, on the interlayer surfaces of RUB-51 and then hydrolysis reaction of the unreacted SiCl groups of immobilized silyl groups were performed by the treatment of H_2O/DMSO solution. Subsequent heat treatment gave the condensation reaction between neighboring remaining silanol groups, and the condensed material composed of layers of RUB-51 was obtained. Although RUB-51 before treatment hardly adsorbed CO_2, the large amount of adsorbed CO_2 on the obtained material was observed. In addition, the amount of adsorbed CO_2 on the microporous material is larger than that of CH_4. They suggest that this result processes the potential of this material as a separation medium between CO_2 and CH_4.

1.3.3 Silicate framework topology

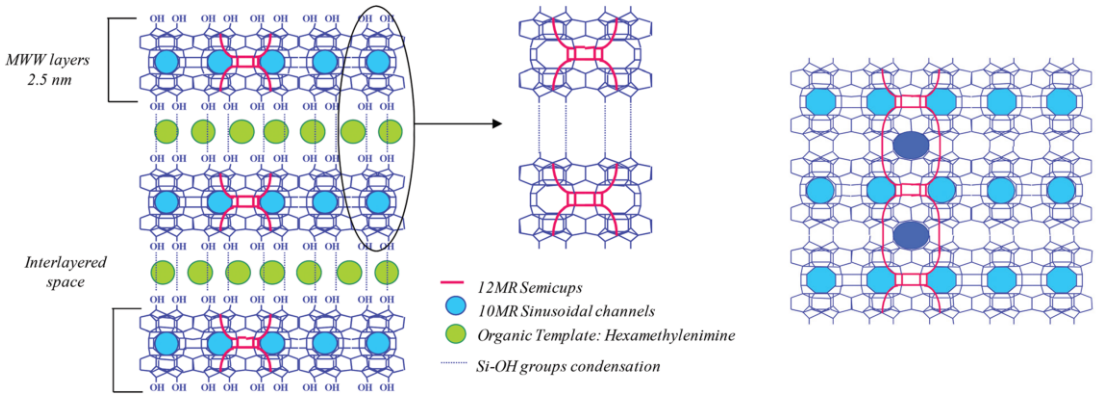

Fig. 1-18 (left) Artistic representation of MWW(P) layered zeolitic precursor and (right) zolite MCM-22.[193]

Layered silicates, whose frameworks are composed of only SiO_4 tetrahedra are also well-known as precursor of zeolite.[190-194] In this transformation process, silanol groups on the interlayer surface of layered silicates are condensed between layers, and the 2D layered structures are transformed to 3-D structures retaining the crystallinity of the original layers. This transformation process of a layered silicate into zeolite is called topotactic conversion. The topotactic conversion via interlayer condensation has received keen interests from the viewpoint of the synthesis of zeolites from layered silicates (layered zeolitic materials). In conventional zeolite synthesis, hydrothermal

Table 1-1 Zeolite synthesis by topotactic concersion of layered silicates.[191,200,204,206]

Lyaered silicate	Zeolite	Zeolite framework type	Reference
β-HLS	Cal-DPA-HLS	AST	200
EU-19	EU-19	CAS	201
MCM-65(as made)	MCM-65(calcined)	CDO	218
PLS-1	CDS-1	CDO	202
UZM-13, UZM-17, UZM-19	UZM-25	CDO	219
RUB-36, RUB-38, RUB-48	RUB-37	CDO	215, 216
PLS-4	unnamed	CDO	214
ERS-12(as made)	ERS-12(calcined)	Incomplete condensation	225
MCM-47(as made)	MCM-47(calcined)	Highly disprdered	226
PREFER	Ferrierite	FER	203
PLS-3	CDS-3	FER	214
HPM-2	unnamed	MTW	204
MCM-22(P)	MCM-22	MWW	195
ERB-1	ERB-1(calcined)	MWW	198
ITQ-1(as made)	ITQ-1(calcined)	MWW	199
Nu-6	Nu-6(2)	NSI	205
IPC-1P	IPC-4	IPC	206
RUB-39	RUB-41	RRO	220
R-RUB-18	RUB-24	RWR	221
AA-RUB-18	Zeolite RWR	RWR	222
HAcRUB-15	Silica-Sodalite	SOD	224
HOAc-RUB-15	RUB-15-SOD	SOD	223

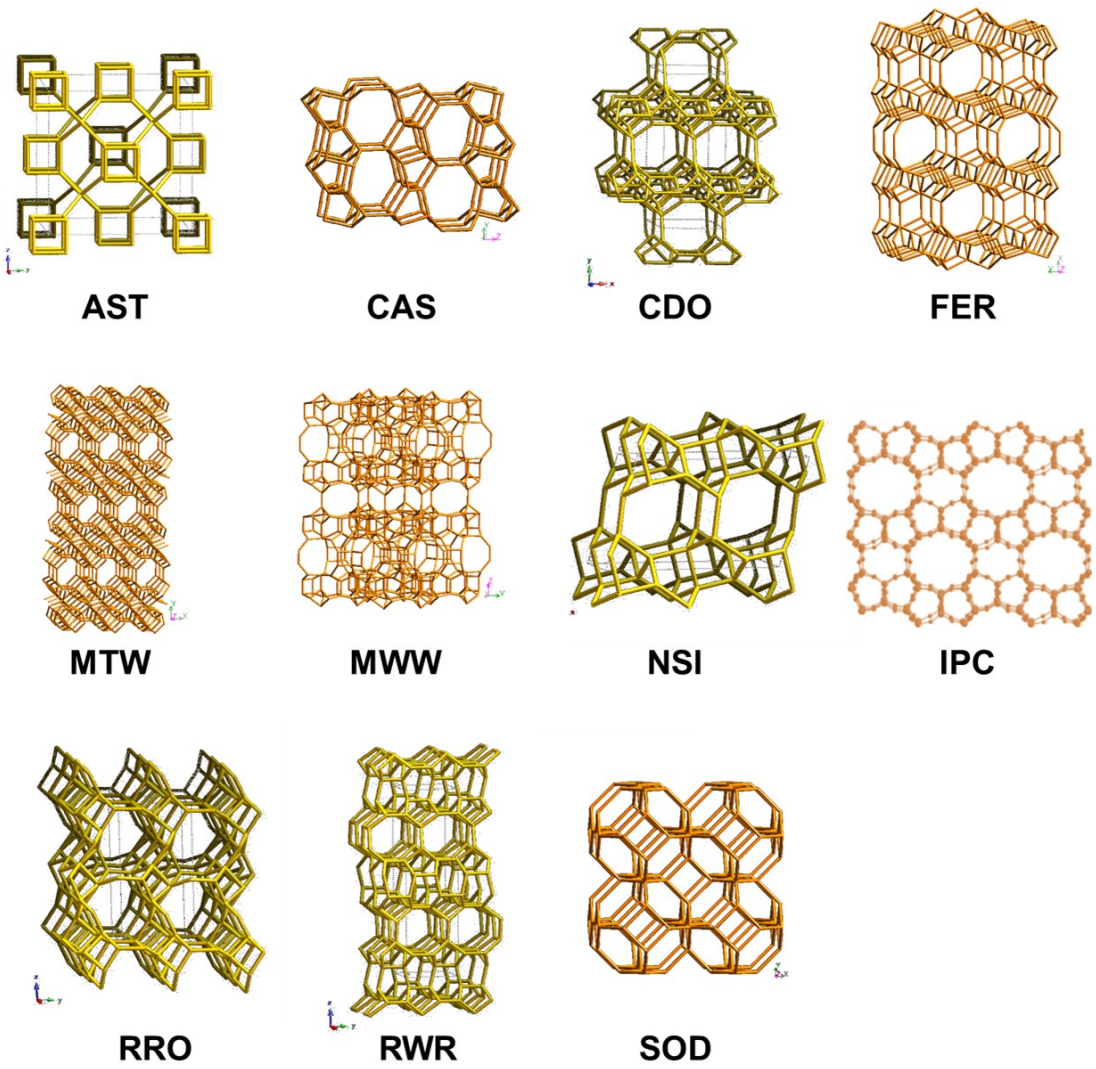

Fig. 1-19 Zerolites framework topologies obtained by topotactic conversion of layered silciates.

synthesis has been very successful and has produced various framework types of zeolites. However, as the synthesis of zeolites with desirable structure and composition is very difficult, there is a continuous search for alternative synthesis route. Topotactic conversion of layered silicate has been attracted as a very promising method to obtain new zeolite materials. Because, if the crystal structures of the layered silicate nanosheets are determined, we can easily determine the framework structures of zeolites obtained by topotactic conversion using the interlayer dehydration–condensation process. The

Table 1-2 Structural parameters and synthesis condition of layered silicates.[191]

Lyaered silicate	Lyaer type	Synthesis condition		Reference
		Interlayer cation or molecule	H_2O/SiO_2 ratio	
β-HLS	ast	Tetramethylammonium + Na^+	15.9	213
EU-19	cas	Piperazinium	40	201
NU-6(1)	cas	4,4'-bipyridine or 4,4'-bipyridinium	11.1	205
ERS-12(as made)	fer	Tetramethylammonium	40	225
PLS-1	fer	Tetramethylammonium + K^+	5.0	202
RUB-20	fer	Tetramethylammonium	-	234
RUB-40	fer	Tetramethylphosphonium	-	234
MCM-47(as made)	fer	Tetramethylene-bis(N-Methyl-pyrrolidinium)	40	217
MCM-65(as made)	fer	Quinclidinium	30	218
RUB-38	fer	Methyltriethylammonium	-	234
UZM-13	fer	Diethyldimethylammnium	-	219
RUB-36	fer	Diethyldimethylammnium	-	234
RUB-48	fer	Trimethylisopropylammonium	-	234
PLS-4	fer	Diethyldimethylammnium	5.3-15.9	214
PREFER	fer	Amino-tetramethyl-piperidinium	10-30	203
PLS-3	fer	Tetraethylammonium	2.3-11.4	214
RUB-39	heu	Dimethyldipropylammonium	8-12	220
Kanemite	kan	$[Na(H_2O)_6]^+$	-	48
H-LDS	kan	H^+	-	235
ERB-1	mww	Piperidinium + Na^+	10-15	198
RUB-18	rwr	$[Na(H_2O)_6]^+$	-	222
DLM-2	sod	Tetramethylammonium	5.5	236
RUB-15	sod	Tetramethylammonium	55.52	223
RUB-51	sod	Benzyltrimethylammonium	3-4	237
RUB-52	r52	Diethyldimethylammonium	-	228
RUB-53	r52	Choline	-	228

first successful example of synthesis of zeolite from layered silicate precursor was given by MWW framework type. These materials were described by several researchers.[195-199] Silicate layer of MWW-type has a thickness of 2.5 nm and contains a 10 member-ring (MR) sinusoidal channel present along the in-plane direction (Fig. 1-18). In the surface of each silicate sheet, a large amount of terminal silanol groups (Si–OH) are presented.

Table 1-3 Structural parameters various silicate layers.[191]

Lyaer type	Composition of per 2D unit cell	Q^3:Q^4	Distance of (OH…OH) [Å]	Max. layer charge [z/Å^2]	Thickness of layer [Å]
kan	Si8O20	1:0	Ca. 2.5	0.056	4.4
ast	Si20O48	1:0.25	Ca. 2.6	0.051	7.2
sod	Si12O28	1:0.5	Ca. 2.5	0.041	6.3
rwr	Si8O18	1:1	Ca. 2.3	0.037	7.1
r52	Si10O22	1:1.5	Ca. 2.5	0.032	7.7
cas	Si24O52	1:2	Ca. 6.0	0.029	8.3
fer	Si18O38	1:3.5	Ca. 5.7	0.019	9.5
heu	Si18O38	1:3.5	Ca. 7.0	0.017	7.8
mww	Si72O146	1:15	Ca. 8.2	0.011	24.9

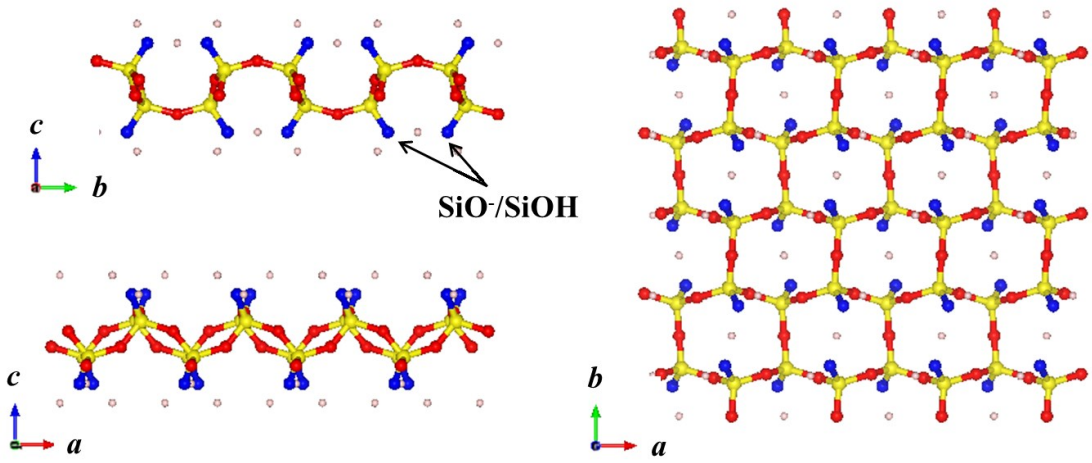

Fig. 1-20 Framework topology of kan silicate layer.

This interlayer silanol is condensed after the calcination process, generating the 3D zeolitic structure MCM-22. After the formation of zeolitic 3D structure, an additional second pore system delimited by 12 MR located on the surface of each MWW layer is formed. Several studies have been conducted on the synthesis of zeolites from layered silicates or alumino silicate. Layered silicates which have successfully been converted in to zeolite are summerized in Table 1-1. Via topotactic conversion of layered silicate with different framework topology, AST,[200] CAS,[201] CDO,[202] FER,[203] MTF,[204] MWW,[195]

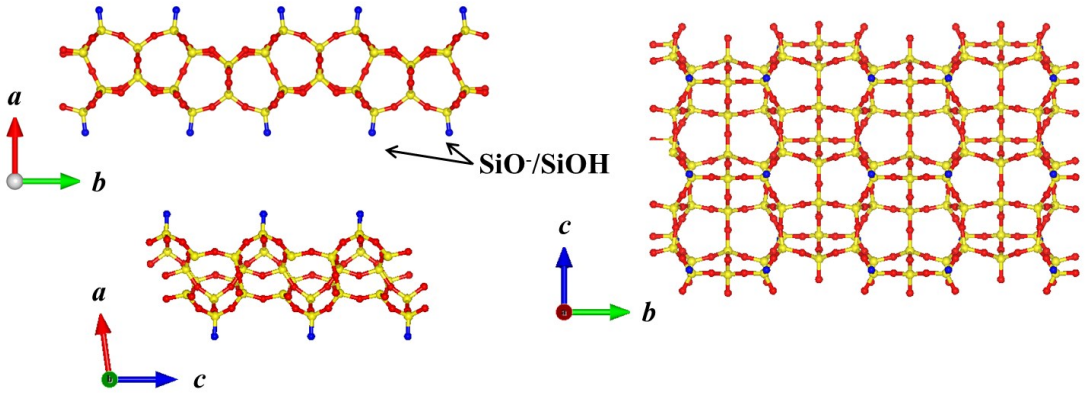

Fig. 1-21 Framework topology of fer silicate layer.

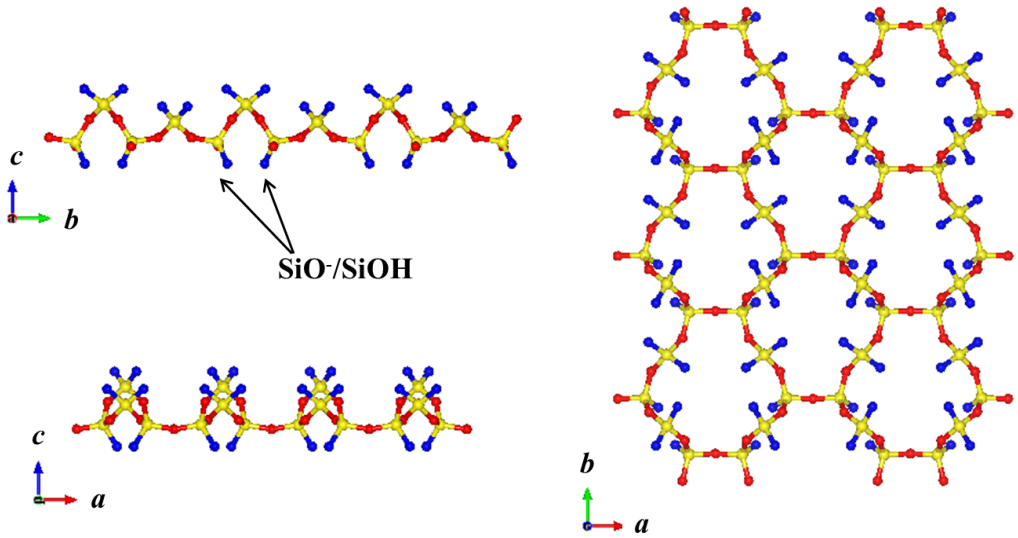

Fig. 1-22 Framework topology of sod silicate layer.

NSI,[205] PCI,[206] RRO,[207] RWR,[208–210] and SOD,[211] -type zeolites were prepared using layered silicates β-HLS,[200,212,213] EU-19,[201] PLS-1,[202] (isomorphic materials: PLS-4,[214] RUB-36,[215,216] MCM-47,[217] MCM-65,[218] UZM-13, UZM-17, and UZM-19[219]), PREFER (PLS-3[214]), HPM-2,[204] MCM-22(P)[197] (ERB-1,[198] ITQ-1(as-mage)[199]), Nu-6(1),[205] IPC-1P,[206] RUB-39,[220] RUB-18,[221,222] and RUB-15,[223,224] respectively. The framework topology of several zeolite can be obtained by topotactic conversion of layered silicate are shown in Fig. 1-19. In addition, further layered silicate have not

been transformed into zeolite, for example ERS-12,[225] MCM-47,[226] MCM-69(p),[227] RUB-52 and RUB-53[228] with known crystal structure and several materials with unknown structure such as EU-22,[229] MCM-20,[230] MCM-56[231] and KLS1[232,233] (similar to β-HLS), are available. The names (lab codes) of layered silciates with similar structure are listed as follows: RUB-36 ≈ PLS-4 ≈ UZM-13, ERS-12 ≈ PLS-1 ≈ RUB-20 ≈ FLS1, EU-19 ≈ MCM-69(p), RUB-18 ≈ Na-RUB-18 ≈ Octosilicate ≈ Ilerite and precursors of ERB-1 ≈ ITQ-1 ≈ MCM-22 ≈ PSH-1 ≈ SSZ-25.

As described above, various layered silicates with different silicate frameworks are available. Marler and Gies proposed that the corresponding 3-letter code of the zeolite

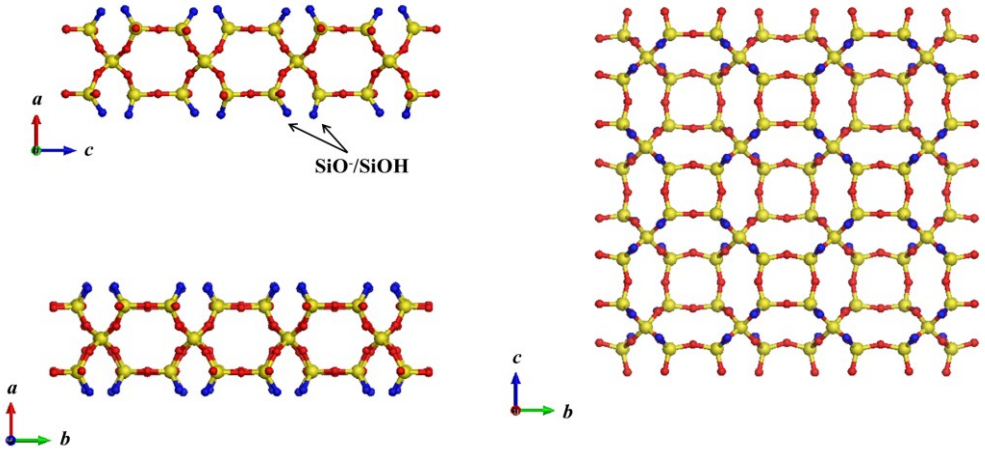

Fig. 1-23 Framework topology of ast silicate layer.

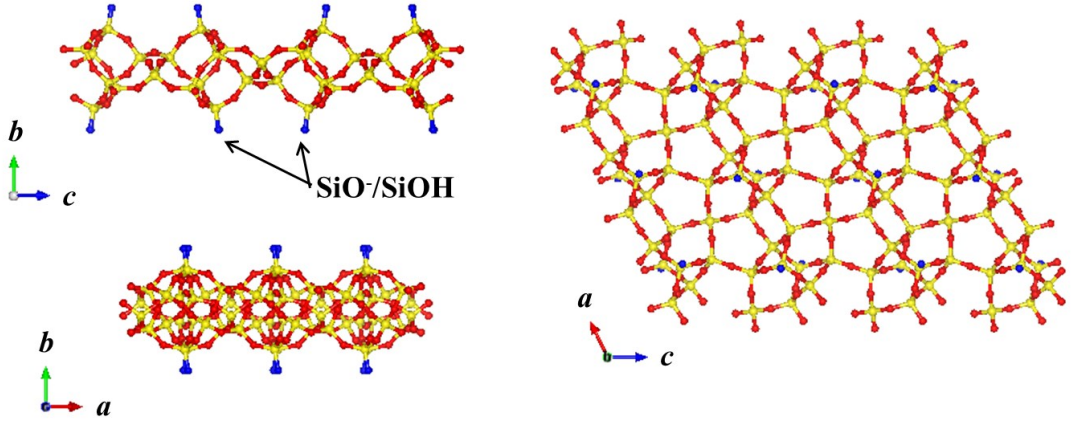

Fig. 1-24 Framework topology of heu silicate layer.

framework is used as acronym for categorization of silicate framework topology of layered silicates.[191] For example, the layer-like building units of the zeolite framework type of FER are named fer. In the case of layered silicate which has not been transformed into zeolite, identical codes are named: the silicate layer of RUB-52 and RUB-53 is designated r52 (RUB-52) and also that of kanemite is named kan. Table 1-2 lists the structural parameter and synthesis condition of layered silicate.

These silicate layers have different structural parameters including Q^3: Q^4 ratio, thickness of layer, and the distance of surface silanol/siloxy groups. These parameters are summarized in Table 1-3. The thicknesses of silicate layers are considerably

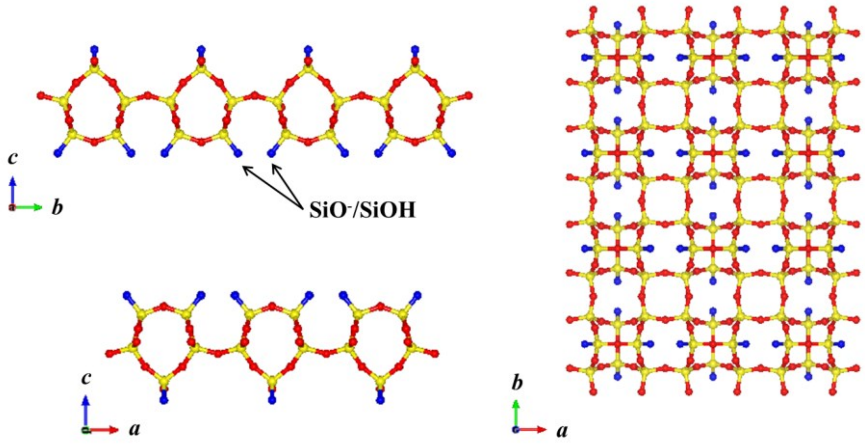

Fig. 1-25 Framework topology of rwr silicate layer.

different among layered silicates. The kan layer in framework of kanemite exhibits thickness of 4.4 Å (Fig. 1-20), whereas thick layer like the mww layer with thickness of 24.9 Å is available. General structure of the silicate layers can be described as rugged sheet with SiOH/SiO^- groups onto the interlayer surface. PREFER are constructed from fer silicate layer with 5 Si-O-Si ring (Fig. 1-21). The silicate layer of RUB-15 and RUB-51 (sod) are composed of truncated octahedral that are cut halves sodalite-cages (Fig. 1-22). If the layer condensed each other, sodalite structure is formed. In the case of

β-HLS, the silicate framework with ast (Fig. 1-23) consists of interconnected truned octahedra cut into halves. However, the condensation of each layers give a framework larger [$4^6 6^{12}$]-cages and additional double four rings which is AST type zeolite framework. Distance between neighbouring SiOH/SiO^- groups of each silicate layers are important for consideration of their structural feature as a precursor of porous materials. The silicate layer of fer exhibits large intra-layer distance of SiOH/SiO^-, which is 5.7 Å, preventing condensation of these groups. If we attempt these groups to be condensed by calcination, only inter-layer condensation of interlayer silanol groups occurs due to the large distance of neighbouring SiOH/SiO^- groups. Therefore, as the several researchers reported, layered silicate with fer, heu and cas silicate layer easily converted to 3-dimensional structure (FER, CDO and NSI type zeolite, respectively) by simple calcination. Novel layered silicate named as PLS-1 (Pentagonal-cylinder Layered Silicate) with fer layer was synthesized by Ikeda et al.[202] The PLS-1 was converted into a novel zeolite with COD type framework topology (CDS-1). They showed the crystal structures of both PLS-1 and CDS-1, and the topotactic conversion of PLS-1 to CDS-1 via interlayer condensation of silanol groups, indicating the topotactic conversion is applicable for design of new type of zeolite structure. The crystal structure of layered silicate Nu-6(1) which can be converted to zeolite (Nu-6(2)) by topotactic conversion was reported by Zanardi et al.[205] In addition, layered silicate RUB-39 with heu layer (Fig. 1-24) can be transformed into zeolite with RRO type framework.[220]

In contrast, rwr, ast and sod silicate layers have shorter distance between silanol groups (2.3, 2.6 and 2.5 Å, respectively), which lead to intra-layer condensation and decrease of structural order of condensed product. To form interlayer micropore via

topotactic conversion, several literatures utilized organics-post-intercalated layered silicate.[203] Marler et al. reported that alkylammonium-intercalated octosilicate was transformed into RUB-24 zeolite with rwr layer (Fig. 1-25) by topotacitic conversion.[208] Also, Oumi et al. reported the topotactic conversion of acetic-acid-intercalated octosilicate (Ac-Oct) into RWR-type zeolite.[209] Afterwards, the effect of the layer stacking sequence for the topotactic conversion to RWR-zeolite was investigated by using structural analysis of before and after calcination (Fig. 1-26).[210] As the inappropriate layer stacking sequence, original Na-type layered octosilicate, H-octosilicate, and tetramethylammonium-intercalated octosilicate (TMA-Oct) become amorphous by calcination. However, acid-treated TMA-Oct can be converted to a RWR-type zeolite. According to their literatures, the important factors for topotactic conversion to 3-D zeolite structures are (1) closer contacts between silanol groups and (2) control of stacking layers having silanol groups which should face each other appropriately. They reported a similar phenomenon by using magadiite.[238]

Also, sod silicate layer has the possibility for the formation of zeolite structure by the similar strategy. Moteki and Okubo et al. reported that acetic acid intercalated RUB-15 can be transformed into the silica sodalite zeolite, which exhibited adsorption ability of H_2.[211] They also studied the variable effects of carboxylic acids on the formation of pure silica sodalite and concluded that propionic acid treatment suitable for obtaining high ordered silica sodalite.[239] Two key factors: (i) proton exchange of interlayer TMA^+ cations to shorten the interlayer distance and to form Si-OH groups and (ii) intercalation of carboxylic acid molecules between the layers to maintain the well-ordered layered structure prior to calcination were also shown in the literature. Recently, Asakura and Kuroda et al. proposed topotactic conversion via polar organic molecule intercalated

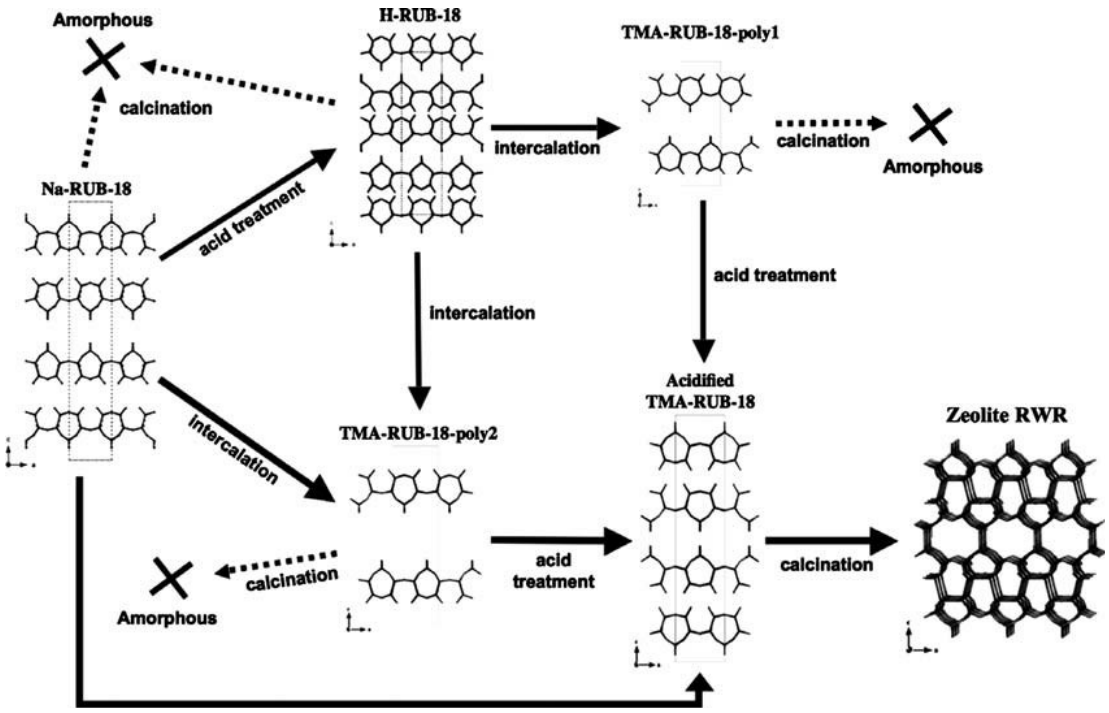

Fig. 1-26 Schematic diagram of the topotactic conversion route from Na-RUB-18 (layered octosilicate) to zeolite RWR. (Reprinted from ref. 210 with permission; copyright 2008 Elsevier Inc.)[34]

intermediate. They reported the synthesis of AST-type zeolite by topotactic conversion of a layered silicate β-HLS, N,N-dimethylpropionamide (DPA) was used to control the layer stacking of silicate layers and the subsequent interlayer condensation.[200] In this literature, they judiciously selected amide molecule for control of the stacking sequence of silicate layers and the interlayer condensation occurred by calcination at 800 °C for 3h.

As stated above, topotactic conversion process is transformation of 2D layered structure into 3D porous structure via interlayer dehydration reaction. It is easily considered that the pore size of product, obtained by topotactic conversion depend on the original crystal structure of silicate layer. In contrast, layered silicate can be converted into another crystalline microporous material by ordered interlayer

modification process using covalent modification. As the layered precursor retains these regularity and modified pillar position between the layer through modification process, novel microporous material, having both of ordered silicate layer and pillared unit position, can be formed. The products are called interlayer expanded zeolites (IEZ), having enlarged pore openings between the layers.

First IEZ like material was reported by Fan and Tatsumi et al. They synthesized Interlayer-Expanded Zeolite (IEZ) which was pillared with monomeric pillaring reagents.[240] When the acid post-treatment processes were carried out on Ti-MWW precursors to effectively remove the extra-framework octahedral Ti species, interlayer modification with titanium species was observed, resulting in obtaining a novel 3D titanosilicate denoted Ti-YNU-1. This zeolitic material exhibited a more expanded pore window between the crystalline MWW sheets, due to the immobilization of additional pillar units in the interlayer space, obtaining a interlayer expansion by the formation of further interlayered 12 MR channels.[241] They concluded that as Ti centers could occupy the pillar sites, having a higher accessibility compared to the case that they were in network positions in conventional 3D MWW, their sites act effective active centers for olefins' epoxidations. Tatsumi and Wu et al. applied this method to preparation of IEZ materials by using silylation reagents.[242,243] They initially demonstrated preparation of IEZ materials with MWW, CDO, and FER framework structures (Fig. 1-27). To date, layered silicates and layered zeolitic materials including PLS-1,[242-244] PLS-3,[245] PLS-4,[245] RUB-36,[246-250] RUB-39,[246,251,252] RUB-51,[189] Nu-6(1),[253] MWW(P),[243,244,254] MCM-47,[254] IPC-1P[206] and PREFER,[243,255,245] have been silylated with chlorosilane or alkoxysilane. Silylattion of layered silicate PLS-1 with dichlorodimethylsilane and then calcination were performed.[242] In this case, the silylation reagent with two reactive

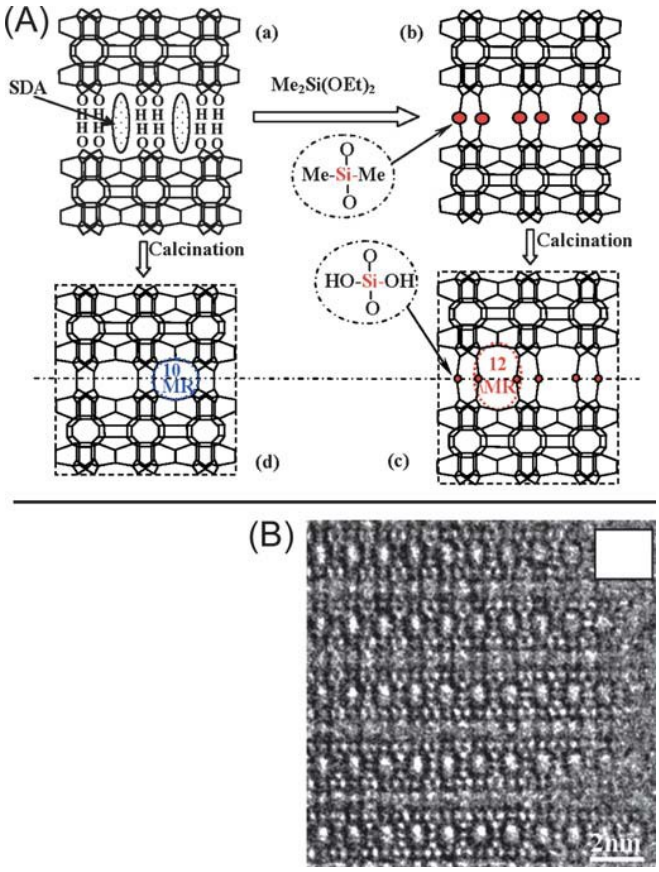

Fig. 1-27 (A): Sequence of synthesis of IEZs. (a) MWW lamellar precursor, (b) the interlayer structure expanded by silylation, (c) 3-D structure with enlarged pore window, and (d) common 3-D MWW structure obtained by a direct interlayer condensation. (B): Corresponding HRTEM image of calcined IEZ-MWW. (Reproduced from ref. 243 with permission; copyright 2008, American Chemical Society.)

groups (Si–Cl) acts as a single molecular pillaring agent. The direct topotactic conversion of layered silicate PLS-1 leads to the formation of CDS-1 with 8MRs, whereas the pillared product possesses 10MRs because of two additional pillaring molecular reagents. Ikeda et al. reported that thermal acid treatment of layered silicates using alkoxysilane (PLS-1, PLS-3, PLS-4, and PREFER) leads to the formation of a monomeric Si pillared structure.[245] Terasaki and co-workers determined the crystal structure of these IEZs by electron microscopic investigations (Fig. 1-27B).[243] Although

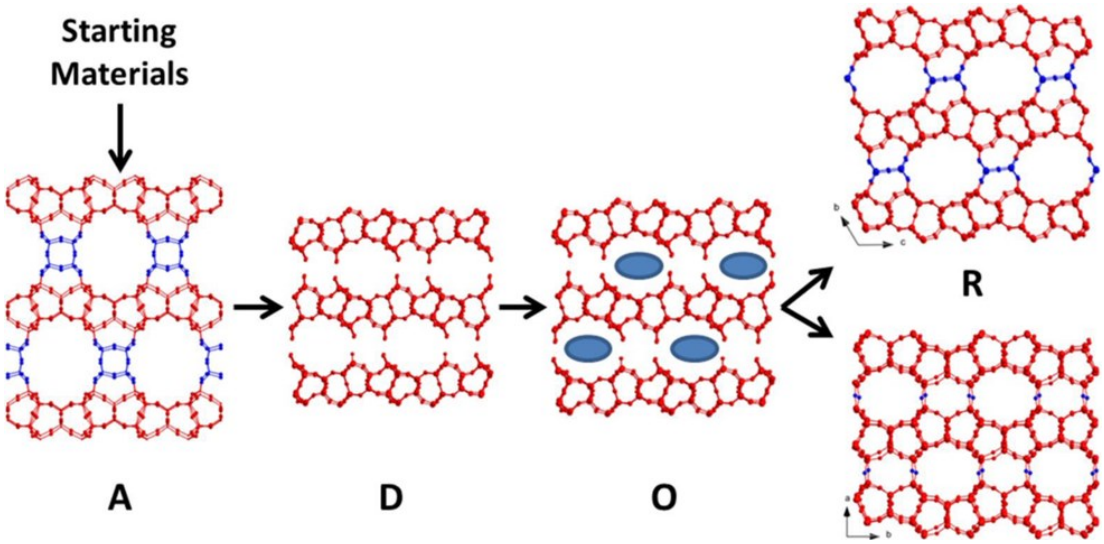

Fig. 1-28 ADOR strategy for the preparation of zeolites. Stage A is the assembly of a zeolite from the starting materials; D is the controlled disassembly of the zeolite; O is an organization step whereby a new linking unit or a structure-directing agent (blue oval) is incorporated; and R is the final reassembly step. In the case of zeolites IPC-2 (OKO) and IPC-4 (PCR), there is no direct synthesis route yet available. (Reproduced from ref. 192 with permission; copyright 2014, American Chemical Society.)

MWW type zeolite obtained by direct topotactic conversion leads to the creation of pores with 10MRs, the pillared IEZ has pores with 12MRs. The crystal structure determination of IEZ like materials using XRD was also performed by Ikeda et al.[245] and Gies et al.[247,251] Vapor-phase silylation procedure was proposed by Inagaki et al. for more effective interlayer silylation.[256] Because the conventional liquid-phase silylation is performed in a strongly acidic condition, the number of acid sites in the framework considerably decreases due to leaching of a part of framework Al. However, when the vapor-phase silylation was carried out, the dealumination from in the framework was hardly observed and the product obtained by vapor-phase silylation exhibited higher catalytic activity than that by the liquid phase.

As stated above, the synthesis of 2D layered precursors represents the bottom-up

preparation, usually by hydrothermal synthetic methodology. Čejika and co-workers proposed an alternative top-down approach, where a 3D framework is selectively disassembled into a 2D layered material. There are several reports about the synthesis of new type of zeolite containing germanium in double four (D4R) and double three (D3R) rings as secondary building units.[257-259] However, despite the great interest in their topologies, there are few reports about the applications of Ge zeolites. This is due to the rather low hydrothermal stability of the materials. In contrast, several groups focused on the facts that Ge is significantly more reactive than other framework atoms in many ways; it is especially sensitive toward hydrolysis.[260,261] If there is enough Ge in the material, removing completely the germanium units is available. This method was so-called (assembly−disassembly−organization−reassembly) strategy.[206,262] Fig. 1-28 shows the ADOR strategy via chemical removal of Ge from the UTL structure. As a result, the lamellar zeolite precursor IPC-1P obtained through this original 3D to 2D zeolite conversion was suitable for the formation of fully connected zeolite topologies. Two different ways to produce a family of zeolite structures with PCR and OKO topologies were performed.[206,262] After the calcination process, the layered zeolite with regular stacking of ferrierite-like layers with octylamine can be transformed into 3D zeolite like porous structure (IPC-4).[206] IEZ like material (IPC-2) was prepared by adding a S4R unit to replace the D4R unit. The ethoxy groups in the silylated material are available to condense with the silanols of the layers by calcination at high temperature and the Si–O–Si linkages of the S4R unit formed.[206] In addition, theoretical studies that inverse sigma transformation of a zeolite framework to generate new open structures by sheets' removal of intra-framework atoms could be extrapolated to other 3D zeolites have also shown.[262] They mentioned the attractive feature of the ADOR

process that while Ge is selectively incorporated between the layers of the starting UTL structure, other elements are not incorporated in the same way.[263,264] Therefore, aluminum still presented in the layered framework through the whole process. As a result, the catalytic sites in UTL are available in the PCR material. Also, isomorphous substitution of B, Al, Fe, and Ga into the UTL framework has been achieved, suggesting the catalytic potential of this new family of zeolites and zeolite-related materials.[265-267] The critical issue in this 3D to 2D transformation, as well as in the subsequent condensation, is proof of preservation of the structural integrity of UTL layers. These results indicate that the ADOR mechanism can operate also for other germanosilicates having D4R or D3R rings connecting zeolitic layers.

The crystal structure of obtained these materials reflects the structure of those building units, namely silicate layer. This is quite different from conventional hydrothermal zeolite synthesis. Therefore, synthesis of zeolite from layered silicate can avoid the ‘‘black box’’ routes and open the door to designed chemical conversion by using silicate layer as “desired building units”.

1.4 Objective of the thesis

As described the previous sections, layered silicate are attractive due to unique structural features and they have been already utilized in various research areas. This success of layered silicate is derived from development of myriad treatment methods by effective utilizing their structural features including (1) interlayer large surface area, (2) ordered interlayer space, and (3) unique silicate framework. Also, as these essential

features are directly affected from the original crystal structure of layered silicates, synthesis and application of novel layered silicate with new crystal structure and framework topology are quite attractive as a formation of desirable precursor for novel class of material synthesis. Of course, diversity of various modification processes on layered silicate as the primary functionalization tool as well as diversity of novel layered silicate often must be very encouraging the potential for more numerous applications. If their advantage is shown through the synthesis, structural grasp and functionalization in one path, the novel route of material design may become open. Therefore, in this thesis, to expand the applications of the layered silicate based functionalized materials, I focused on following six research areas on the synthesis and application of novel layered silicate Hiroshima University Silicates (HUSs).

In chapter 2, first, synthesis and structural analysis of novel layered silicate HUS-2 and HUS-3 are described. Three kinds of layered silicates, HUS-2, HUS-3, and HUS-4, were synthesized using choline hydroxide as an organic template, structure-directing agent (SDA). Structural analyses revealed that HUS-2 had novel layered structure. I also demonstrated that the layered silicates HUS-2 and HUS-3 exhibited high catalytic activities as base catalysts in a Knoevenagel condensation reaction.

Chapter 3 also described synthesis and structural analysis of novel layered silicate HUS-7 synthesized using benzyltrimethylammonium hydroxide as a structure-directing agent (SDA). HUS-7 gave the unique interlayer space and adsorption behavior. HUS-7 selectively and effectively adsorbed phenol from acetonitrile solution containing benzene and phenol. The adsorption of phenol occurred through the exchange of water molecules in the interlayers with phenol.

Chapter 4 described selective adsorption of propionic acid on HUS-2 inspired from

the relationship interlayer structure and adsorbed state of propionic acid. This chapter focused on the utilization of the framework topology of HUS-2.

In chapter 5, the potential of layered silicate HUS-5 for the precursor of porous materials was investigated by focusing the interlayer large surface area of layered silicate.

In chapters 6 and 7, design of ordered interlayer space of HUSs for catalysts and adsorbent are shown. Chapter 6 showed the preparation of effective titanosilicate photo catalyst by the immobilization of titanium acetylacetonate in the ordered interlayer space of HUS-2 and also investigated the photocatalytic acitivity of Ti-incorporated HUS-2 toward the partial oxidation of cyclohexane to cyclohexanol and cyclohexanone under solar light irradiation.

In chapter 7, I also focused on the framework topology of HUS-2. The HUS-2 was successfully converted to crystalline microporous material HUS-10 with molecular sieve ability and the high potential for CO_2 adsorptive separation.

In Chapter 8, conclusions of this thesis and future perspectives were descrived.

Through my study, it was clarified that the novel layered silicates HUSs have the high potential for designable innovative materials.

References

1 D. W. Breck, Zeolite Molecular Sieves: Structure, Chemistry, and Use, Wiley-Interscence publication, New York, 1974.

2 Handbook of Zeolite Science and Tech nology, ed by S. M. Auerbach, K. A. Carrodo, P. K. Dutta, Marcel Dekker, New York, 2003.

3 Corma, A. *Chem. Rev*., 1995, **95**, 559

4 Davis, M. E. *Nature*, 2002, **417**, 813−821.

5 M. E. Davis, *Chem. Mater*., 2014, **26**, 239

6 M. Moliner, C. Martínez and A. Corma *Chem. Mater*., 2014, **26**, 246

7 S. I. Zones, *Microporous Mesoporous Mater*., 2011, **144**, 1.

8 R. M. Barrer, Zeolites and their synthesis. *Zeolites*, 1981, **1**, 130.

9 M. E. Davis and R. F, Lobo, *Chem. Mater*., 1992, **4**, 756.

10 C. S. Cundy, P. A. Cox, *Chem. Rev*., 2003, **103**, 663.

11 J. X. Jiang, J. H. Yu and A. Corma, *Angew. Chem., Int. Ed*., 2010, **49**, 3120.

12 T. Yanagisawa, T. Shimizu, K. Kuroda and C. Kato, *Bull. Chem. Soc. Jpn*., 1990, **63**, 988.

13 S. Inagaki, Y.Fukushima and K. Kuroda, C. *J. Chem. Soc., Chem. Commun*., 1993, 680.

14 C.T. Kresge, M.E. Leonowicz, W.J. Roth, J.C. Vartuli and J.S. Beck, *Nature*, 1992, **359**, 710.

15 J.S. Beck, J.C. Vartuli, W.J. Roth, M.E. Leonowicz, C.T. Kresge, K.D. Schmitt, C. T-W. Chu, D.H. Olson, E.W. Sheppard, S.B. McCullen, J.B. Higgins and J.L. Schlenker, *J. Am. Chem. Soc*., 1992, **114**, 10834.

16 Y. Wan and D. Zhao, *Chem. Rev*., 2008, **107**, 2821.

17 K. Ariga, A. Vinu, Y. Yamauchi, Q. Ji, and J. P. Hill, *Bull. Chem. Soc. Jp*n., 2012, **85**, 1.

18 C.Y. Chen, S.Q. Xiao and M.E. Davis, *Microporous. Mater*., 1995, **4**, 1.

19 T. Asefa, M. J. MacLachlan, N. Coombs and G. A. Ozin, *Nature,* 1999, **402**, 867.

20 S. Inagaki, S. Guan, T. Ohsuna and O. Terasaki, *Nature,* 2002, **416**, 304.

21 F. Hoffmann, M. Cornelius, J. Morell and M. Fröba, *Angew. Chem., Int. Ed*., 2006, **45**, 3216.

22 S. Fujita and S. Inagaki, *Chem. mater.,* 2008, **20**, 891.

23 N. Mizoshita, T. Tani and S. Inagaki, *Chem. Soc. Rev*., 2011, **40**, 789.

24 P. D. Lickiss and F. Rataboul, *In Advances in Organometallic Chemistry*; Hill, A. F., Fink, M. J., Eds.; Academic Press: Oxford, U.K., 2008; Vol. 57, pp 1-116.

25 G. Li, L. Wang, H. Ni, and C. U. Pittman, *J. Inorg. Organomet. Polym.*, 2001, **11**, 123.
26 D. B. Cordes, P. D. Lickiss, and F. Rataboul, *Chem. Rev.*, 2010, **110**, 2081.
27 H. Lin, S. Wu, P. Huang, C. Huang, S. Kuo and F. Chang, *Macromol. Rapid Commun*., 2006, **27**, 1550.
28 Y. Li, S. Mannen, J. Schulz and J. Grunlan *J. Mater. Chem*., 2011, **21**, 3060.
29 R. Elsäßer, G. Mehl, J. Goodby and D. Photinos, *Chem. Commun*., 2000, 851.
30 K. Madhavan and B.S.R. Reddy, *J. Membr. Sci*,. 2009, **342**, 291.
31 W. Schwieger and G. Lagaly, *Alkali Silicates and Crystaline Silicic Acids in Handbook of Layered Materials*, Marcel Dekker, Inc., New York, 2004, pp. 541–629.
32 E. Burzo, *Phyllosilicates in Magnetic Properties of Non-Metallic Inorganic Compounds Based on Transition Elements*, Springer-Verlag, Berlin Heidelberg, 2009.
33 M. Ogawa and K. Kuroda, *Bull. Chem. Soc. Jpn*., 1997, **70**, 2593
34 N. Takahashi and K. Kuroda, *J. Mater. Chem*., 2011, **21**, 14336.
35 T. Okada, Y. Ide and M. Ogawa, *Chem.–Asian J*., 2012, **7**, 1980.
36 M. Ogawa, K. Saito and M. sohmiya, *Dalton Trans*., 2014, **43**, 10340.
37 T. Selvam, A. Inayat and W. Schwieger, *Dalton Trans*., 2014, **43**, 10365.
38 H. P. Eugster, *Science*, 1967, **157**, 1177.
39 G. W. Brindley, *Am. Mineral*., 1969, **54**, 1583.
40 J. M. Rojo, E. Ruiz-Hitzky and J. Sanz, *Inorg. Chem*., 1988, **27**, 2785.
41 K. Beneke and G. Lagaly, *Am. Mineral*., 1983, **68**, 818.
42 R. L. Hay, Contrib. *Mineral. Petrol*., 1968, **17**, 255.
43 R. A. Sheppard, A. J. Gude and R. L. Hay, *Am. Mineral*., 1970, **55**, 358.
44 H. Annehed, L. Falth and F. J. Lincoln, Z. *Kristallogr*., 1982, **159**, 203.
45 Z. Johan and G. F. Maglione, Bull. Soc. Fr. *Mineral. Cristallogr*., 1972, **95**, 371.
46 K. Beneke and G. Lagaly, *Am. Mineral*., 1977, **62**, 763.
47 H. Gies, B. Marler, S. Vortmann, U. Oberhagemann, P. Bayat, K. Krink, J. Rius, I. Wolf and C. Fyfe, *Microporous Mesoporous Mater*., 1998, **21**, 183.
48 L. A. J. Garvie, B. Devouard, T. L. Groy, F. C.□amara and P. R. Buseck, *Am. Mineral*., 1999, **84**, 1170.
49 S. Vortmann, J. Rius, B. Marler and H. Gies, *Eur. J. Mineral*., 1999, **11**, 125.
50 R. K. Iler, *J. Colloid Sci*., 1964, **19**, 648.
51 W. Schwieger, D. Heidemann and K.-H. Bergk, Rev. *Chim. Miner*., 1985, **22**, 639.
52 G. Borbely, H. K. Beyer, H. G. Karge, W. Schwieger, A. Brandt and K.-H. Bergk, *Clays Clay Miner*., 1991, **39**, 490.

53 S. Vortmann, J. Rius, S. Siegmann and H. Gies, *J. Phys. Chem. B*, 1997, **101**, 1292.
54 I. Wolf, H. Gies and C. A. Fyfe, *J. Phys. Chem. B*, 1999, **103**, 5933.
55 U. Brenn, H. Ernst, D. Freude, R. Herrmann, R. J€ahnig, H. G. Karge, J. Köarger, T. K€onig, B. M€adler, U. T. Pingel, D. Prochnow and W. Schwieger, *Microporous Mesoporous Mater*., 2000, **40**, 43.
56 M. Borowski, I. Wolf and H. Gies, *Chem. Mater*., 2002, **14**, 38.
57 M. Borowski, O. Kovalev and H. Gies, *Microporous Mesoporous Mater*., 2008, **107**, 71.
58 A. K. Pant and D. W. J. Cruickshank, *Acta Crystallogr., Sect. B: Struct. Crystallogr. Cryst. Chem*., 1968, **24**, 13.
59 A. K. Pant, Acta Crystallogr., Sect. B: Struct. *Crystallogr. Cryst. Chem*., 1968, **24**, 1077.
60 M. E. Fleet and G. S. Henderson, *J. Solid State Chem*., 1995, **119**, 400.
61 V. Kahlenberg, G. Döorsam, M. Wendschuh-Josties and R. X. Fischer, *J. Solid State Chem*., 1999, **146**, 380.
62 W. H. Taylor and S. Naray-Szabo, Z. Kristallogr., 1931, **77**, 146–158.
63 D. Benbertal and A. Mosset, *J. Solid State Chem*., 1994, **108**, 340.
64 K. Beneke, P. Thiesen and G. Lagaly, *Inorg. Chem*., 1995, **34**, 900.
65 B. H. W. S. de Jong, H. T. J. Super, A. L. Spek, N. Veldman,G. Nachtegaal and J. C. Fischer, *Acta Crystallogr., Sect. B: Struct.Sci*., 1998, **54**, 568.
66 S. Rakic and V. Kahlenberg, *Eur. J. Mineral*., 2001, **13**, 1215.
67 S. Rakic, V. Kahlenberg and B. C. Schmidt, Z. *Kristallogr*., 2003, **218**, 413.
68 A. L. Spek and B. H. W. S. d. Jong, *Acta Crystallogr., Sect. E: Struct. Rep. Online*, 2005, **61**, 188.
69 I. Bull and J. B. Parise, *Acta Crystallogr., Sect. C: Cryst. Struct. Commun*., 2003, **59**, 100.
70 X. Wang, L. Liu, J. Huang and A. J. Jacobson, *J. Solid State Chem*., 2004, **177**, 2499.
71 K. Komura, T. Ikeda, A. Kawai, F. Mizukami and Y. Sugi, *Chem. Lett*., 2007, **36**, 1248.
72 T. Ikeda, M. Uenaka, K. Komura and Y. Sugi, *Chem. Lett*., 2010, **39**, 747.
73 E. Arroyabe, R. Kaindl, D. M. Töobbens and V. Kahlenberg, *Inorg. Chem*., 2009, **48**, 11929.
74 P. Podsiadlo, A. K. Kaushik, E. M. Arruda, A. M. Waas, B. S. Shim, J. Xu,H. Nandivada, B. G. Pumplin, J. Lahann, A. Ramamoorthy and N. A. Kotov, *Science*, 2007, **318**, 80.

75 M. Choi, K. Na, J. Kim, Y. Sakamoto, O. Terasaki and R. Ryoo, *Nature*, 2009, **461**, 246.

76 K. Na, M. Choi, W. Park, Y. Sakamoto, O. Terasaki and R. Ryoo, *J. Am. Chem. Soc*., 2010, **132**, 4169.

77 N. Takahashi, H. Hata and K. Kuroda, *Chem. Mater*., 2011, **23**, 266.

78 B. Brahimi, P. Labbe and G. Reverdy, *Langmuir*, 1992, **8**, 1908.

79 Y. Umemura, A. Yamagishi, R. Schoonheydt, A. Persoons and F. De Schryver, *J. Am. Chem. Soc*. 2002, **124**, 992.

80 Z. Tang, N. A. Kotov, S. Magonov and B. Ozturk, *Nat. Mater*., 2003, **2**, 413.

81 G. Decher, J. Maclennan, U. Sohling and J. Reibel, *Thin Solid Films* 1992, **210-211**, 504–507.

82 K. Haraguchi and T. Takehisa, *Adv. Mater*., 2002, **14**, 1120.

83 Y. Suzuki, R. Matsunaga, H. Sato, T. Kogure, A. Yamagishi and J. Kawamata, *Chem. Commun*., 2009, 6964.

84 A. Corma, V. Fornes, S. B. Pergher, T. L. M. Maesen and J. B. Buglass, *Nature*, 1998, **396**, 353.

85 A. Corma, U. Díaz, M. E. Domíne and V. Fornes, *J. Am. Chem. Soc*., 2000, **122**, 2804.

86 A. Corma, U. Díaz, M. E. Domíne and V. Fornes, *Angew. Chem., Int. Ed*., 2000, **39**, 1499.

87 A. Corma, V. Fornes and U. Díaz, *Chem. Commun*., 2001, 2642.

88 U. Diaz, V. Fornés and A. Corma, *Micropor. Mesopor. Mater*. 2006, **90**, 73.

89 J. Aguilar, S. B. C. Pergher, C. Detoni, A. Corma, F. V. Melo and E. Sastre, *Catal. Today*, 2008, **133**, 667.

90 A. Corma, V. Fornes, J. Martínez-Triguero and S. Pergher, *J. Catal*., 1999, **186**, 57.

91 I. Rodríguez, M. J. Climent, S. Iborra, V. Fornes and A. Corma, *J. Catal*., 2000, **192**, 441.

92 P. Botella, A. Corma, S. Iborra, R. Monton, I. Rodríguez and V. Costa, *J. Catal*., 2007, **250**, 161.

93 A. Corma, H. García and J. Miralles, *Microporous Mesoporous Mater*. 2001, **43**, 161.

94 C. T. Kresge, W. J. Roth, K. G. Simmons and J. C. Vartuli, WO Patent, 9211934, 1992.

95 W. J. Roth, C. T. Kresge, J. C. Vartuli, M. E. Leonowicz, A. S. Fung and S. B. McCullen, *Stud. Surf. Sci. Catal*., 1995, **94**, 301.

96 F. Eder, Y. He, G. Nivarthy and J. A. Lercher, *Recl. Trav. Chim. Pays-Bas*, 1996, **115**, 531.

97 S. Choi, J. Coronas, E. Jordan, W. Oh, S. Nair, F. Okamoto, D. F. Shantz and M. Tsapatsis, *Angew. Chem. Int. Ed*. 2008, **47**, 552.

98 Y. Bi, J.-F. Lambert, Y. Millot, S. Casale, J. Blanchard, S. Zeng, H. Nie and D. Li, *J. Mater. Chem*., 2011, **21**, 18403.

99 C. Rubio, C. Casado, P. Gorgojo, F. Etayo, S. Uriel, C Téllez and J.Coronas, *Eur. J. Inorg. Chem*., 2010, 159.

100 C. Casado, D. Ambroj, Á. Mayoral, E. Vispe, C. Téllez1 and J. Coronas, *Eur. J. Inorg. Chem*., 2011, 2247.

101 M. K. Pietrea, F. A. Bonka, C. Rettorib, F. A. Garciab and H. O. Pastore, *Microporous Mesoporous Mater*., 2012, **156**, 244.

102 R. Schenkel, J. O. Barth, J. Kornatowski and J. Lercher, *Stud. Surf. Sci. Catal*. 2002, **142A**, 69.

103 S. Maheshwari, E. Jordan, S. Kumar, F. S. Bates, R. L. Penn, D. F. Shantz and M. Tsapatsis, *J. Am. Chem. Soc*., 2008, **130**, 1507.

104 W. J. Roth and J. C. Vartuli, *Stud. Surf. Sci. Catal*., 2002, **141**, 273.

105 I. Ogino, M. M. Nigra, S.-J. Hwang, J.-M. Ha T. Rea, S. I. Zones and A. Katz, *J. Am. Chem. Soc*., 2011, **133** 3288.

106 I. Ogino, E. A. Eilertsen, S.-J. Hwang, T. Rea, D. Xie, X. Ouyang, S. I. Zones and A. Katz, *Chem. Mater*. 2013, **25**, 1502.

107 C. Y. Chen and S. I. Zones, *Stud. Surf. Sci. Catal*., 2001, **135**, 1710.

108 R. C. Runnebaum, X. Ouyang, J. A. Edsinga, T. Rea, I. Arslan, S.-J. Hwang, S. I. Zones and A. Katz, *ACS Catal*., 2014, **4**, 2364.

109 S. Choi, J. Coronas, J. A. Sheffel, E. Jordan, W. Oh, S. Nair, D. F. Shantz and M. Tsapatsis, *Microporous Mesoporous Mater*., 2008, **115**, 75.

110 A. Corma, F. Vornés, J. L. Jordá, F. Rey, R. Fernandez-Lafuente adn J. M. Guisan, B. Mateo, *Chem. Commun*., 2001, 419.

111 Z. Wang and T. J. Pinnavaia, *Chem. Mater*., 1998, **10**, 1820.

112 K. Varoon, X. Zhang, B. Elyassi, D. D. Brewer, M. Gettel, S. Kumar, J. A. Lee, S. Maheshwari, A. Mittal, C.-Y. Sung, M. Cococcioni, L. F. Francis, A.n V. McCormick, K. A. Mkhoyan and M. Tsapatsis, *Science*, 2011, **334**, 6052.

113 S. Osada, A. Iribe and K. Kuroda, *Chem. Lett*. 2013, **42**, 80.

114 M. Choi1, K. Na, J. Kim, Y. Sakamoto, O. Terasaki and R. Ryoo, *Nature*, 2009, **461**, 246.

115 X. Zhang, D. Liu, D. Xu, S. Asahina, K. A. Cychosz, K. V. Agrawal, Y. A.Wahedi, A. Bhan, S. A. Hashimi, O. Terasaki, M. Thommes and M. Tsapatsis, *Science*, 2012, **336**, 1684.

116 W. Chaikittisilp, Y. Suzuki, R. R. Mukti, T. Suzuki, K. Sugita, K. Itabashi, A. Shimojima and T. Okubo, *Angew. Chem. Int. Ed*., 2013, **52**, 3355.

117 K. Na, C. Jo, J. Kim, W. Ahn and R. Ryoo, *ACS catal*., 2011, **1**, 901.

118 H. Y. Luo, L. Bui, W. R. Gunther , E. Min and Y. R. Leshkov, *ACS catal*., 2012, **2**, 2695.

119 W. J. Roth and C. T. Kresge, *Microporous Mesoporous Mater*. 2011, **144**, 158.

120 K. Kosuge and A. Tsunashima, *J. Chem. Soc., Chem. Commum*., 1995, 2427.

121 S. Toriya, Y. Tamura, T. Takei, M. Fuji, T. Watanabe and M. Chikazawa, *J. Colloid Interface Sci*., 2002, **255**, 171.

122 P. Chlubna, W. J. Roth, H. F. Greer, W. Z. Zhou, O. Shvets, A. Zukal, J. Čejka and R. E. Morris, *Chem. Mater*., 2013, **25**, 542.

123 J. O. Barth, J. Kornatowski and J. A. Lercher, *J. Mater. Chem*., 2002, **12**, 369.

124 J. O. Barth, A. Jentys, J. Kornatowski and J. A. Lercher, *Chem. Mater*., 2004, **16**, 724.

125 J. Kornatowski, J. O. Barth, K. Erdmann and M. Rozwadowski, *Microporous Mesoporous Mater*., 2006, **90**, 251.

126 U. Díaz, Á. Cantín and A. Corma, *Chem. Mater*., 2007, **19**, 3686.

127 A. Corma, U. Diaz, T. Garcia, G. Sastre, A. Velty, *J. Am. Chem. Soc*., 2010, **132**, 15011.

128 M. Opanasenko, W. O'N. Parker, M. Shamzhy, E. Montanari, M. Bellettato, M. Mazur, R. Millini and J. Čejka, *J. Am. Chem. Soc*. 2014, **136**, 2511.

129 T. Kimura and K. Kuroda, *Adv. Funct. Mater*. 2009, **19**, 511.

130 S. Inagaki, A. Koiwai, N. Suzuki, Y. Fukushima and K. Kuroda, *Bull. Chem. Soc. Jpn.*, 1996, **69**, 1449.

131 S. Inagaki, Y. Fukushima and K. Kuroda, *Stud. Surf. Sci. Catal*. 1994, **84**, 125.

132 T. Kimura, T. Kamata, M. Fuziwara, Y. Takano, M. Kaneda, Y. Sakamoto, O. Terasaki, Y. Sugahara, K. Kuroda, *Angew. Chem. Int. Ed*., 2000, **39**, 3855.

133 Q. Kan, V. Fornés, F. Rey ans A. Corma, *J. Mater. Chem*. 2000, **10**, 993.

134 T. Shigeno, K. Inoue, T. Kimura, N. Katada, M. Niwa and K. Kuroda, *J. Mater. Chem*. 2003, **13**, 883.

135 T. Kimura, H. Tamura, M. Tezuka, D. Mochizuki, T. Shigeno, T. Ohsuna and K. Kuroda, *J. Am. Chem. Soc*., 2008, **130**, 201.

136 T. Kimura, H. Tamura, M. Tezuka, D. Mochizuki, T. Shigeno and K. Kuroda, *Stud. Surf. Sci. Catal*., 2007, **170**, 1740.
137 R. García, I. Díaz, C. M. Álvarez and J. P. Pariente, *Chem. Mater*., 2006, **18**, 2283.
138 N. Alama and R. Mokaya, *J. Mater. Chem*., 2008, **18**, 1383.
139 M. Songa, Y. Kiyozumib and J. Kima, *Colloids Surf. A*, 2014, **443**, 1.
140 W. Schwieger, G. Lagaly, *Alkali Silicates and Crystaline Silicic Acids in Handbook of Layered Materials*, Marcel Dekker, Inc., New York, 2004, pp. 541–629.
141 R. K. Iler, *J. Colloid Sci*., 1964, **19**, 648.
142 E. N. Coker and L. V. C. Rees, *J. Mater. Chem*., 1993, **3**, 523.
143 A. de Lucas, L. Rodriguez, J. Lobato and P. Sanchez, *Chem. Eng. Sci*., 2002, **57**, 479.
144 G. Lagaly, K. Beneke and A. Weiss, *Am. Mineral*., 1975, **60**, 642.
145 Y. Ide, N. Ochi and M. Ogawa, *Angew. Chem., Int. Ed*., 2011, **50**, 654.
146 M. Ogawa, Y. Ide and M. Mizushima, *Chem. Commun*., 2010, **46**, 2241.
147 G. Lagaly, K. Beneke, P. Dietz and A. Weiss, *Angew. Chem., Int. Ed. Engl*., 1974, **13**, 819–821.
148 K. Beneke and G. Lagaly, *Am. Mineral*., 1989, **74**, 224.
149 G. Lagaly, K. Beneke and A. Weiss, *Am. Mineral*., 1975, **60**, 650.
150 Y. Ide, M. Torii and T. Sano, *J. Am. Chem. Soc.*, 2013, **135**, 11784.
151 E. Ruiz-Hitzky and J. M. Rojo, *Nature*, 1980, **287**, 28.
152 E. Ruiz-Hitzky, J. M. Rojo and G. Lagaly, *Colloid Polym. Sci*., 1985, **263**, 1025.
153 T. Yanagisawa, K. Kuroda and C. Kato, *React. Solids*, 1988, **5**, 167.
154 T. Yanagisawa, K. Kuroda and C. Kato, *Bull. Chem. Soc. Jpn*., 1988, **61**, 3743–3745.
155 K. Endo, Y. Sugahara and K. Kuroda, *Bull. Chem. Soc. Jpn*., 1994, **67**, 3352.
156 S. Okutomo, K. Kuroda and M. Ogawa, *Appl. Clay Sci*., 1999, **15**, 253.
157 K.-W. Park, J. H. Jung, S.-K. Kim and O.-Y. Kwon, *Appl. Clay Sci*., 2009, **46**, 251–254.
158 M. Ogawa, S. Okutomo and K. Kuroda, *J. Am. Chem. Soc*., 1998, **120**, 7361.
159 I. Fujita, K. Kuroda and M. Ogawa, *Chem. Mater*., 2003, **15**, 3134.
160 I. Fujita, K. Kuroda and M. Ogawa, *Chem. Mater*., 2005, **17**, 3717–3722.
161 S. Toriya, S. Kobayashi, T. Takei, M. Fuji, T. Watanabe and M. Chikazawa, *Colloid Polym. Sci*., 2003, **281**, 1121.
162 M. Ogawa, M. Miyoshi and K. Kuroda, *Chem. Mater*., 1998, **10**, 3787.
163 Yusuke Ide, Shota Iwasaki and Makoto Ogawa, *Langmuir*, 2011, **27**, 2522.
164 K.-W. Park, S.-Y. Jeong and O.-Y. Kwon, *Appl. Clay Sci*., 2004, **27**, 21.

165 S.-F. Wang, M.-L. Lin, Y.-N. Shieh, Y.-R. Wang and S.-J. Wang, *Ceram. Int*., 2007, **33**, 681.
166 C.-M. Leu, Z.-W. Wu and K.-H. Wei, *Chem. Mater*., 2002, **14**, 3016.
167 Z. Zhang, S. Saengkerdsub and S. Dai, *Chem. Mater.*, 2003, **15**, 2921.
168 V. S. O. Ruiz, G. C. Petrucelli and C. Airoldi, *J. Mater. Chem*., 2006, **16**, 2338.
169 T. R. Macedo and C. Airoldi, *Dalton Trans*., 2009, 7402.
170 T. R. Macedo and C. Airoldi, *New J. Chem*., 2009, **33**, 2081.
171 T. R. Macedo and C. Airoldi, *Microporous Mesoporous Mater*., 2010, **128**, 158.
172 T. R. Macedo, G. C. Petrucelli and C. Airoldi, *Thermochim. Acta*, 2010, **502**, 30.
173 R. Ishii, T. Ikeda and F. Mizukami, *J. Colloid Interface Sci*., 2009, **331**, 417.
174 N. Takahashi, H. Hata and K. Kuroda, *Chem. Mater*., 2010, **22**, 3340.
175 V. S. O. Ruiz, G. C. Petrucelli and C. Airoldi, *J. Mater. Chem*., 2006, **16**, 2338.
176 T. R. Macedo and C. Airoldi, *Dalton Trans*., 2009, 7402.
177 Y. Ide, A. Fukuoka and M. Ogawa, *Chem. Mater*., 2007, **19**, 964.
178 Y. Ide, G. Ozaki and M. Ogawa, *Langmuir*, 2009, **25**, 5276.
179 Y. Ide, N. Kagawa, M. Itakura, I. Imae, M. Sadakane and T. Sano, *ACS Appl. Mater. Interfaces*, 2012, **4**, 2186.
180 Y. Ide, N. Kagawa, M. Sadakane and T. Sano, *Chem. Commun*., 2013, **49**, 9027-9029.
181 T. Nakamura and M. Ogawa, *Langmuir*, 2012, **28**, 7505.
182 K. Kuroda, A. Shimojima, K. Kawahara, R. Wakabayashi, Y. Tamura, Y. Asakura, and M. Kitahara, *Chem. Mater*. 2014, 26, 211.
183 D. Mochizuki, A. Shimojima, K. Kuroda, *J. Am. Chem. Soc*., 2002, **124**, 12082.
184 D. Mochizuki, A. Shimojima, T. Imagawa, K. Kuroda, *J. Am. Chem. Soc*., 2005, **127**, 7183.
185 D. Mochizuki and K. Kuroda, *New J. Chem*., 2006, **30**, 277.
186 R. Ishii and Y. Shinohara, *J. Mater. Chem*. 2005, **15**, 551.
187 D. Mochizuki, S. Kowata and K. Kuroda, *Chem. Mater*., 2006, **18**, 5223.
188 Y. Asakura, Y. Matsuo, N. Takahashi and K. Kuroda, *Bull. Chem. Soc. Jpn*. 2009, **84**, 968.
189 Yusuke Asakura, Yasuhiro Sakamoto and Kazuyuki Kuroda, *Chem. Mater.* 2014, **26**, 3796.
190 W. J. Roth and J. Čejka, *Catal. Sci. Technol*., 2011, **1**, 43.
191 B. Marler and H. Gies, *Eur. J. Mineral*., 2012, **24**, 405.
192 W. J. Roth, P. Nachtigall, Russell E. Morris, and J. Čejka, *Chem. Rev*., 2014, **114**, 4807.

193 U. Díaz and A. Corma, *Dalton Trans*., 2014, **43**, 10292.
194 W. J. Roth, B. Gil and B. Marszalek, *Catalysis Today* 2014, **224**, 9.
195 Puppe, L. and Weisser, J. U.S. Patent 4,439,409, 1984.
196 S. I. Zones, Patent 231,860, 1987.
197 M. E. Leonowicz, J. A. Lawton, S. L. Lawton and M. K. Rubin, *Science*, 1994, **264**, 1910.
198 R. Millini, G. Perego, W.O. Parker, Jr., G. Bellussi and L. Carluccio, *Microporous Materials* 1995, **4**, 221.
199 M. Camblor, C. Corell, A. Corma, M. Díaz-Cabańas, S. Nicolopoulos, J. González-Calbet, and M. Vallet-Regí, *Chem. Mater*., 1996, **8**, 2415.
200 Y. Asakura, R. Takayama, T. Shibue and K. Kuroda, *Chem. Eur. J.*, 2014, **20**, 1893.
201 B. Marler, M. A. Camblor and H. Gies, *Microporous Mesoporous Mater*., 2006, **90**, 87.
202 T. Ikeda, Y. Akiyama, Y. Oumi, A. Kawai and F. Mizukami, *Angew. Chem., Int. Ed*., 2004, **43**, 4892.
203 L. Schreyeck, P. Caullet, J. C. Mougenel, J. L. Guth and B. Marler, *Microporous Mater*., 1996, **6**, 259.
204 A. Rojas and M. A. Camblor, *Chem. Mater*., 2014, **26**, 1161.
205 S. Zanardi, A. Alberti, G. Cruciani, A. Corma, V. Fornes and M. Brunelli, *Angew. Chem., Int. Ed*., 2004, **43**, 4933.
206 W. J. Roth, P. Nachtigall, R. E. Morris, P. S. Wheatley, V. R. Seymour, S. E. Ashbrook, P. Chlubná, L. Grajciar, M. Položij, A. Zukal, O. Shvets, J. Čejka, *Nat. Chem*., 2013, **5**, 628.
207 Y. Wang, B. Marler, H. Gies and U. Muller, *Chem. Mater*., 2005, **17**, 43.
208 B. Marler, N. Stroter and H. Gies, *Microporous Mesoporous Mater*., 2005, **83**, 201.
209 Y. Oumi, T. Takeoka, T. Ikeda, T. Yokoyama and T. Sano, *New J. Chem*., 2007, **31**, 593.
210 T. Ikeda, Y. Oumi, T. Takeoka, T. Yokoyama, T. Sano and T. Hanaoka, *Microporous Mesoporous Mater*., 2008, **110**, 488.
211 T. Moteki, W. Chaikiiisilp, A. Shimojima and T. Okubo, *J. Am. Chem. Soc*., 2008, **130**, 15780.
212 Y. Akiyama, F. Mizukami, Y. Kiyozumi, K. Maeda, H. Izutsu and K. Sakaguchi, *Angew. Chem*., 1999, **111**, 1510; *Angew. Chem*. Int. Ed. 1999, **38**, 1420.
213 T. Ikeda, Y. Akiyama, F. Izumi, Y. Kiyozumi, F. Mizukami and T. Kodaira, *Chem. Mater*., 2001, **13**, 1286.

214 T. Ikeda, S. Kayamori and F. Mizukami, *J. Mater. Chem*., 2009, **19**, 5518.
215 J. Song and H. Gies, *Stud. Surf. Sci. Catal*., 2004, **154A**, 295.
216 B. Marler, Y. Wang, H. Song and H. Gies, *Abstracts of Papers, 15th International Zeolite Conference*, 2007, Beijing, China, August 12–17, 2007, p. 599.
217 A. Burton, R. J. Accardi, R. F. Lobo, M. Falcioni and M. W. Deem, *Chem. Mater*., 2000, **12**, 2936.
218 D. L. Dorset and G. J. Kennedy, *J. Phys. Chem. B*, 2004, **108**, 15216.
219 L. M. Knight, M. A. Miller, S. C. Koster, M. G. Gatter, A. I. Benin, R. R. Willis, G. J. Lewis and R. W. Broach, *Stud. Surf. Sci. Catal*., 2007, **170A**, 338.
220 Y. X. Wang, H. Gies and J. H. Lin, *Chem. Mater*., 2007, **19**, 4181.
221 A. J. Blake, K. R. Franklin and B. M. Lowe, *J. Chem. Soc*., *Dalton Trans*., 1988, 2513.
222 S. Vortmann, J. Rius, S. Siegmann and H. Gies, *J. Phys. Chem. B*, 1997, **101**, 1292.
223 U. Oberhagemann, P. Bayat, B. Marler, H. Gies and J. Rius, *Angew. Chem., Int. Ed*., 1996, **35**, 2869.
224 H. Voss, J. Therre, H. Gies and B. Marler, WO Patent, WO/2010/037690 A1, 2010.
225 R. Millini, L. C. Carluccio, A. Carati a, G. Bellussi, C. Perego, G. Cruciani and S. Zanardi, *Microporous and Mesoporous Mater*. 2004, **74**, 59.
226 A. Burton, R. J. Accardi and R. F. Lobo, *Chem. Mater*., 2000, **12**, 2936.
227 L. D. Rollmann, J. L. Schlenker, S. L. Lawton, C. L. Kennedy, G. J. Kennedy, *Microporous and Mesoporous Mater*, 2002, **53**, 179.
228 B. Marler, Z. Li, G. Wang and H. Gies, *Acta Cryst*., 2011, **A67**, 650..
229 *Stdies in Surface Science and Catalysis*, K. R. Franklin and B. M. Lowe, ed by P. A. Jacobs and R. A. Santen, 48, Elsevier, Amsterdum, 1989, 179-188.
230 G. H. Kuehl and M. E. Landis, US Patent, 4,861,570, 1989.
231 A. S. Fung, S. L. Lawton and W. J. Roth, US Patent, 5,362,697, 1994.
232 F. Kooli, *J. Mater. Chem*., 2002, **12**, 1374.
233 F. Kooli, Y. Kiyozumi and F. Mizukami, *New J. Chem*., 2001, **25**, 1613.
234 B. Marler, Y. Wang, J. Song, H. Goes, Book of Abstruct " I*II International Workshop on Lyaered Materials*", 2010, 67.
235 T. Ikeda, M. Uenaka, K. Komura and Y. Sugi, Chem Lett., 2010, **39**, 747.
236 L. Massüger, C. Baerlocher, L. B. McCusker and M. A. Zwijnenburg, *Microporous Mesoporous Mater*. 2007, **105**, 75.
237 Z. Li, B. Marler and H. Gies, *Chem. Mater*., 2008, **20**, 1896.
238 Y. Oumi, K. Takagi, T. Ikeda, H. Sasaki, T. Yokoyama and T. Sano, *J. Porous Mater*., 2008, **16**, 641.

239 T. Moteki, W. Chaikiiisilp, Y. Sakamoto, A. Shimojima and T. Okubo, *J. Am. Chem. Soc*., 2008, **130**, 15780.
240 W. Fan, P. Wu, S. Namba and T. Tatsumi, *Angew. Chem., Int. Ed*., 2004, **43**, 236.
241 J. Ruan, P. Wu, B. Slater and O. Terasaki, *Angew. Chem., Int. Ed*., 2005, **44**, 6719.
242 S. Inagaki, T. Yokoi, Y. Kubota and T. Tatsumi, *Chem. Commun*., 2007, 5188.
243 P. Wu, J. Ruan, L. Wang, L. Wu, Y. Wang, Y. Liu, W. Fan, M. He, O. Terasaki and T. Tatsumi, *J. Am. Chem. Soc*., 2008, **130**, 8178.
244 S. Inagaki, H. Imai, S. Tsujiuchi, H. Yakushiji, T. Yokoi and T. Tatsumi, *Microporous Mesoporous Mater*., 2011, **142**, 354.
245 T. Ikeda, S. Kayamori, Y. Oumi and F. Mizukami, *J. Phys. Chem. C*, 2010, **114**, 3466.
246 F.-S. Xiao, B. Xie, H. Zhang, L. Wang, X. Meng, W. Zhang, X. Bao, B. Yilmaz, U. Müller, H. Gies, H. Imai, T. Tatsumi and D. De Vos, *ChemCatChem*, 2011, **3**, 1442.
247 H. Gies, U. Muller, B. Yilmaz, M. Feyen, T. Tatsumi, H. Imai, H. Y. Zhang, B. Xie, F. S. Xiao, X. H. Bao, W. P. Zhang, T. De Baerdemaeker and D. De Vos, *Chem. Mater*., 2012, **24**, 1536.
248 B. Yilmaz, U. Muller, M. Feyen, H. Zhang, F.-S. Xiao, T. De Baerdemaeker, B. Tijsebaert, P. Jacobs, D. De Vos, W. Zhang, X. Bao, H. Imai, T. Tatsumi and H. Gies, *Chem. Commun*., 2012, **48**, 11549.
249 H. Li, D. Zhou, D. Tian, C. Shi, U. Müller, M. Feyen, B. Yilmaz, H. Gies, F.-S. Xiao, D. De Vos, T. Yokoi, T. Tatsumi, X. Bao and W. Zhang, *ChemPhysChem,* 2014, **15**, 1700.
250 T. De Baerdemaeker, W. Vandebroeck, H. Gies, B. Yilmaz, U. Müller, M. Feyen and D. De Vos, *Catalysis Today*, 2014, **235**, 169.
251 H. Gies, U. Muller, B. Yilmaz, T. Tatsumi, B. Xie, F. S. Xiao, X. H. Bao, W. P. Zhanga and D. De Vos, *Chem. Mater*., 2011, **23**, 2545.
252 B. Tijsebaert, M. Henry, H. Gies, F.-S. Xiao, W. Zhang, X. Bao, H. Imai, T. Tatsumi, U. Müller, B. Yilmaz, P. Jacobs and D. Vos, D. *J. Catal*., 2011, **282**, 47.
253 J. G. Jiang, J. L. Jia, B. T. Yang, H. Xu and P. Wu, *Chem. Mater*., 2013, **25**, 4710.
254 H. Xu, B. Yang, J.-G. Jiang, L. Jia, M. He and P. Wu, *Microporous Mesoporous Mater*., 2013, **169**, 88.
255 J. F. Ruan, P. Wu, B. Slater, Z. L. Zhao, L. L. Wu and O. Terasaki, *Chem. Mater*., 2009, **21**, 2904.
256 S. Inagaki and T. Tatsumi, *Chem. Commun*., 2009, 2583.

257 A. Corma, M. J. Diaz-Cabanas, J. L. Jorda, C. Martinez and M. Moliner, M. *Nature*, 2006, **443**, 842.

258 A. Corma, M. Moliner, J. M. Serra, P. Serna, M. J. Diaz-Cabanas and L. A. Baumes, *Chem. Mater*., 2006, **18**, 3287.

259 A. Corma, M. J. Diaz-Cabanas, C. Martinez and F. Rey, *Stud. Surf. Sci. Catal*. 2008, **174**, 1087.

260 P. S. Petkov, H. A. Aleksandrov, V. Valtchev and G. N. Vayssilov, *Chem. Mater*., 2012, **24**, 2509.

261 X. L. Liu, U. Ravon and A. Tuel, *Chem. Mater*., 2011, **23**, 5052.

262 E. Verheyen, L. Joos, K. Van Havenbergh, E. Breynaert, N. Kasian, E. Gobechiya, K. Houthoofd, C. Martineau, M. Hinterstein, F. Taulelle, V. Van Speybroeck, M. Waroquier, S. Bals, G. Van Tendeloo, C. E. A. Kirschhock and J. A. Martens, *Nat. Mater*., 2012, **11**, 1059.

263 T. Blasco, A. Corma, M. J. Diaz-Cabanas, F. Rey, J. Rius, G. Sastre, J. A. Vidal-Moya, *J. Am. Chem. Soc*., 2004, **126**, 13414.

264 M. A. Zwijnenburg, S. T. Bromley, J. C. Jansen and T. Maschmeyer, *Microporous Mesoporous Mater*., 2004, **73**, 171.

265 O. V. Shvets, M. V. Shamzhy, P. S. Yaremov, Z. Musilova, D. Prochazkova and J. Čejka, *Chem. Mater*., 2011, **23**, 2573.

266 M. V. Shamzhy, O. V. Shvets, M. V. Opanasenko, L. Kurfirtova, D. Kubicka and J. Čejka, *ChemCatChem*, 2013, **5**, 1891.

267 M .V. Shamzhy, O. V. Shvets, M. V. Opanasenko, P. S. Yaremov, L. G. Sarkisyan, P. Chlubna, A. Zukal, V. R. Marthala, M. Hartmann and J. Čejka, *J. Mater. Chem*., 2012, **22**, 15793.

Chapter 2

Synthesis and characteristics of novel layered silicates HUS-2 and HUS-3 derived from a SiO_2–choline hydroxide–NaOH–H_2O system

1. Introduction

Inorganic layered materials are attractive owing to their (1) large surface area derived from multi-stacking ultrathin layers (socalled ‘‘nanosheets’’), (2) chemical and thermal stabilities, and (3) material diversity. Among them, crystalline layered silicates are functionalized by various modification methods such as cation exchange, silylation, and pillaring.[1,2] Organic derivatives with silane coupling reagents exhibit unique molecular recognition abilities, possibly due to the controlled spatial distribution of one or multiple kinds of functional groups in the interlayer nanospace. Furthermore, microporous and mesoporous materials that retain their original layered structure by pillaring show promise for use as adsorbents and catalyst supports.

Layered silicates have also attracted interest from the standpoint of zeolite synthesis. The silanol groups on the interlayer surfaces of layered silicates are condensed between layers and the layered structures are transformed into zeolite-like 3-D structures, a process that is called topotactic conversion. If the crystal structures

of the nanosheets of layered silicates are determined, then I can speculate easily about the framework structures of zeolites that are obtained by topotactic conversion via interlayer dehydration–condensation. There exist several research papers concerning the synthesis of zeolites from layered silicates. CDO (the three characters indicate the framework type-code),[3] NSI,[4] CAS-NSI,[5] RWR,[6–8] RRO,[9] and SOD[10] type zeolites have been prepared using layered silicates PLS-1[3] (isomorphic materials: PLS-4,[11] RUB-36,[12,13] MCM-47,[14] MCM-65,[15] UZM-13,[16] UZM-17,[16] and UZM-19[16]), Nu-6(1),[4] EU-19,[5] RUB-18,[17,18] RUB-39,[19] and RUB-15[20] respectively. Recently, their potential in catalytic applications has been investigated. The layered silicate PLS-1, which possesses tetramethylammonium hydroxide (TMAOH) between its interlayers, was found to exhibit catalytic activity when used in a Knoevenagel condensation reaction as a base catalyst. This reaction is a fundamental mechanism for bringing about C–C bond formation.[21] From such viewpoints, therefore, the synthesis of novel layered silicates with unique crystal structures is still a challenging area of research.

Very recently, Ikeda and Sano et al. succeeded in synthesizing a new layered silicate, HUS-1 (Hiroshima University Silicate-1), with the chemical composition $Si_{10}O_{24}H_8 \cdot 2(CH_3)_4N$.[22] HUS-1 consists of a halved sodalite cage framework structure and a tetramethylammonium (TMA) cation in the hemispherical sodalite cage acts as a structure-directing agent (SDA). It was hydrothermally synthesized by a complicated procedure, namely the interzeolite conversion method, in which locally ordered aluminosilicate species generated by decomposition/dissolution of the starting zeolite were used as nanosized parts for zeolite synthesis.[23] HUS-1 was synthesized through the decomposition of dealuminated FAU- and *BEA-type

zeolites by TMAOH and benzyltrimethyammonium hydroxide, respectively, followed by hydrothermal mixing of the two gels that were obtained.

In the present study, I succeeded in synthesizing novel layered silicates HUS-2 and HUS-3 by only using amorphous silica and choline hydroxide instead of TMAOH, and their crystal structures were investigated. I also studied the potentials of the layered silicates for use as base catalysts and zeoliteprecursors.

2. Experimental

2.1. Synthesis of layered silicates

Layered silicates were synthesized by the hydrothermal treatment of starting gels containing fumed silica (Cab-O-Sil M5, CABOT Co.), choline hydroxide (48–50 wt%, Aldrich), sodium hydroxide (>99%, High Purity Chemical Inc., Japan), and distilled water. The starting gel, which had the chemical composition SiO_2:0.2–0.6 choline hydroxide:0.2–0.4 NaOH:5.5–15.5H_2O, was transferred into a Teflon-lined stainless steel vessel and heated under static conditions at temperatures between 125 and 170 °C for 3–7 d. The solid product that was obtained was separated by centrifugation and washed with distilled water. It was then dried at 70 °C overnight. Lithium hydroxide (>99%, Wako Pure Chemical Ind. Ltd., Japan), potassium hydroxide (>99%, Wako Pure Chemical Ind. Ltd., Japan), rubidium hydroxide (>99%, Aldrich), and cesium hydroxide (>99%, High Purity Chemical Inc., Japan) were also employed instead of sodium hydroxide. A detailed description of the synthesis conditions is given in Table 2-1.

2.2. Characterization

Most of the characterizations were carried out for the assynthesized layered silicates. Powder X-ray diffraction (XRD) patterns of the solid products were collected using a powder X-ray diffractometer (Rigaku, MiniFlex) with graphite-monochromatized Cu Kα radiation at 30 kV and 15 mA. The crystal morphologies of the solid products were observed using a scanning electron microscope (SEM, Hitachi S-4800). ^{29}Si MAS NMR spectra were recorded at 119.17 MHz on a Varian 600PS solid NMR spectrometer using a 5 mm diameter zirconia rotor, which was spun at 10 kHz. The spectra were acquired using 6.7 ms pulses and a 200 s recycle delay over 1000 scans. 3-(Trimethylsilyl) propionic-2,2,3,3-d_4 acid sodium salt was used as a chemical shift reference. ^{1}H MAS NMR spectra were measured with a spinning frequency of 20 kHz and a single pulse sequence operated at 599.85 MHz. ^{1}H–^{13}C CP MAS NMR spectra were also measured at a spinning frequency of 20 kHz, a 90° pulse length of 2.2 ms, and a cycle delay of 100 s. The ^{1}H and ^{13}C chemical shifts were referenced to adamantane and hexamethylbenzene respectively. Nitrogen adsorption isotherms at −196 °C were obtained using a conventional volumetric apparatus (Bel Japan, BELSORP-mini). Prior to the adsorption measurements, the samples (ca. 0.1 g) were evacuated at 400 °C for 10 h. Thermal analyses were carried out using a thermogravimetry/differential thermal analysis (TG/DTA) apparatus (SSC/5200 Seiko Instruments). A sample (ca. 7 mg) was heated from room temperature to 800 °C at 10 °C min^{-1} in air flowing at 50 ml min^{-1}.

2.3. Structural analysis of HUS-2

For accurate structural analyses, powder XRD data were collected at room temperature on an ADVANCE D8-Vαrio1 (Bruker AXS, Japan) powder diffractometer with modified Debye–Scherrer geometry and Cu $K\alpha_1$ radiation that was emitted from a Ge(111) primary monochromator. The diffractometer was equipped with a linear position-sensitive detector VÅNTEC-1 (2θ 8°) and operated at 40 kV and 50 mA. The samples were sealed in borosilicate capillary tubes with an inner diameter of 0.5 mm. The μr (μ: linear absorption coefficient, r: sample radius) values of these sample tubes, which were determined by transmittance measurements, were 0.22. Therefore, there was no need to correct for X-ray absorption.

The crystal structure of HUS-2 was determined by *ab initio* structural analysis. The indexing of reflections with the program N-TREOR, which is built into the program EXPO2009, successfully gave lattice parameters and indices for the reflections.[24] The space group was determined from the reflection conditions that were derived from these indices. The observed integrated intensities, $|F_{obs}|^2$, were extracted by the Le Bail method using EXPO2009.[25] Then, a structural model for HUS-2 was constructed by the direct method using EXPO2009. The molecular geometry of HUS-2 was analyzed by the paralleltempering method, which is a kind of direct-space method, using the program FOX.

The lattice and structural parameters of HUS-2 were refined by the Rietveld method using the program RIETAN-FP on the basis of the above-mentioned structural model.[26] A split pseudo-Voigt profile function and a background function comprising 11^{th} order Legendre polynomials were used in the refinement. Partial profile relaxation with a modified split pseudo-Voigt function was applied to some reflections with highly asymmetric profiles in the low 2θ region.[27] During the early

stage of refinement, I imposed restraints upon all of the Si–O bond lengths, *i.e.,* l(Si–O) . 1.60 ± 0.02 Å, and all the O–Si–O bond angles, *i.e.,* ϕ(O–Si–O) . 109.47 ± 2.0°. Furthermore, restraints were imposed upon all of the bond lengths and bond angles, which were based on the molecular geometry of choline hydroxide, during the final stage of the structural refinement. The degrees of the restraints were gradually decreased as the structural refinement progressed.

The electron density distribution (EDD) in the unit cell of HUS-2 was calculated from the observed structural factors, Fobs, by the maximum entropy method (MEM) using the program Dysnomia.[28] After the first MEM analysis, the EDD was redetermined by MEM-based pattern fitting (MPF).[28] Table 2-2 summarizes the experimental conditions for the powder XRD measurements and part of the results of the Rietveld refinement for HUS-2. The final structural model and EDD were visualized using the program VESTA.[29]

2.4. Catalytic testing

The Knoevenagel condensation reaction as a test reaction for a base catalyst was carried out as follows. A mixture of benzaldehyde (1.0 mmol), ethyl cyanoacetate (1.2 mmol), and naphthalene (0.10 mmol, as an internal standard) in methanol (0.5 ml) was added to a flask containing solid HUS-2 (or HUS-3; 25 mg). The reaction was carried out at 25–70 °C under stirring. After filtering the solid, the filtrate was analyzed by using a gas chromatograph equipped with a FID-type detector on a Zebron ZB-1 column to determine the conversion of benzaldehyde and theproduct yield.

3. Results and discussion

3.1. Synthesis of HUS-2, HUS-3, and HUS-4

Table 2-1 Synthesis conditions for the novel layered silicates

Sample no.	Synthesis conditions						Product	
	Choline/ SiO_2	H_2O/ SiO_2	Additive	Additive/ SiO_2	Temperature (ºC)	Time (days)	Phase	Yield (%)
1	0.4	5.5	NaOH	0.2	150	3	No product	-
2	0.4	5.5	NaOH	0.2	150	5	HUS-2	48
3	0.4	5.5	NaOH	0.2	150	7	HUS-2	76
4	0.4	10.5	NaOH	0.2	150	7	HUS-2	77
5	0.4	15.5	NaOH	0.2	150	7	HUS-3	68
6	0.2	5.5	NaOH	0.4	150	7	HUS-3	84
7	0.6	5.5	NaOH	0.2	150	7	HUS-4	96
8	0.4	5.5	NaOH	0.4	150	7	HUS-2	32
9	0.4	5.5	NaOH	0.2	125	7	No product	-
10	0.4	5.5	NaOH	0.2	170	7	Kenyaite	89
11	0.4	5.5	LiOH	0.2	150	7	HUS-2	Trace
12	0.4	5.5	KOH	0.2	150	7	HUS-4	69
13	0.4	5.5	RbOH	0.2	150	7	HUS-4	100
14	0.4	5.5	CsOH	0.2	150	7	HUS-4	68

New layered silicates with a halved sodalite cage-like structure such as β-HLS and HUS-1 have become the focus of interest because of the belief that they can be used as precursors of new types of microporous materials with silicate frameworks. Such silicates have been hydrothermally synthesized using TMA cations as an SDA at relatively low H_2O/SiO_2 ratios.[30] These results motivated me to synthesize layered silicates using organic SDAs other than TMA cations at low H_2O/SiO_2 ratios.

Among several organics, I selected choline hydroxide, which was effective for interzeolite conversion of FAU-type zeolite.[23] Typical hydrothermal synthesis conditions are listed in Table 2-1.

At first, preliminary experiments were carried out under the synthesis conditions that were similar to those used for the synthesis of HUS-1. The reaction was conducted at 150 °C using the starting gel with a H_2O/SiO_2 ratio of 5.5 and a $NaOH/SiO_2$ ratio of 0.2, and choline hydroxide was employed instead of TMAOH as an SDA. When the crystallization time was 3 d, no product was obtained (Sample 1). However, when the crystallization time was prolonged to 5 d, as expected, *a new type of layered silicate* was obtained (Sample 2). The yield increased by increasing the crystallization time (Sample 3) and the product was named HUS-2 (Hiroshima University Silicate-2). When the H_2O/SiO_2 ratio in the starting gel was increased from 5.5 to 10.5, HUS-2 was also obtained in high yield (Sample 4). In the case of a H_2O/SiO_2 ratio of 15.5, however, another layered silicate, HUS-3, was obtained (Sample 5). The effects of the choline/SiO_2 ratio on the starting gel were also investigated. When the choline/SiO_2 ratio was changed from 0.4 to 0.2, HUS-3 was obtained in a yield of 84% (Sample 6). On the other hand, when the choline/SiO2 ratio was 0.6, another layered silicate, HUS-4, was obtained in a yield of 96% (Sample 7). In the case of the $NaOH/SiO_2$ ratio being 0.4, HUS-2 was also obtained, but the yield decreased (Sample 8). These results strongly indicate that the choline/SiO_2 ratio in the starting gel is a critical factor for the selective synthesis of layered silicates. It was also found that HUS-2 synthesis is sensitive to the crystallization temperature (Samples 9 and 10). Since it is well known that alkaline metal cations act as inorganic SDAs during zeolite synthesis, the effect of the type of

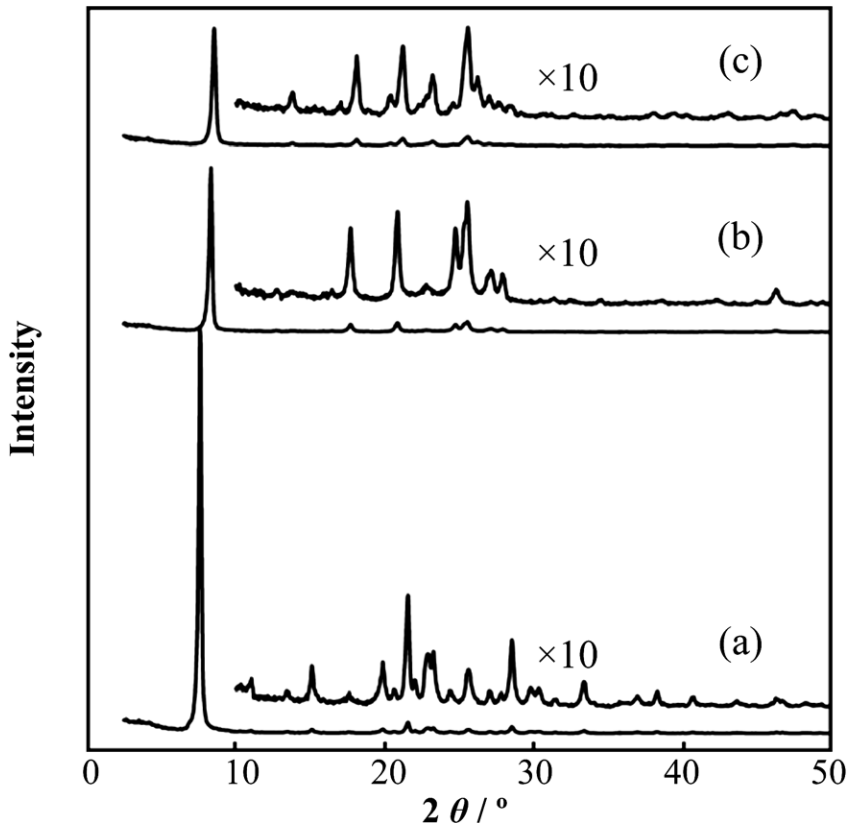

Fig. 2-1 XRD patterns of layered silicates synthesized with different choline/SiO_2 ratios. (a) HUS-2 (Sample 3), (b) HUS-3 (Sample 6), and (c) HUS-4 (Sample 7).

alkaline metal was investigated. LiOH, KOH, RbOH, and CsOH were therefore employed instead of NaOH. As can be seen for samples 11–14 in Table 2-1, NaOH was very effective for the synthesis of HUS-2, whereas KOH, RbOH, and CsOH were effective for the synthesis of HUS-4.

Fig. 2-1 shows the XRD patterns of the obtained layered silicates.HUS-2 was a new type of layered silicate. Its crystal structure is discussed in the second section. Although the crystal structure of HUS-3 was not determined, the transformation of HUS-3 into a CDO-type zeolite occurred by calcination (see the fourth section). The crystal structure of HUS-4 was similar to that of the layered silicate PLS-1, which is synthesized using TMAOH as an SDA.[31] As can be seen in Fig. 2-2, all of the

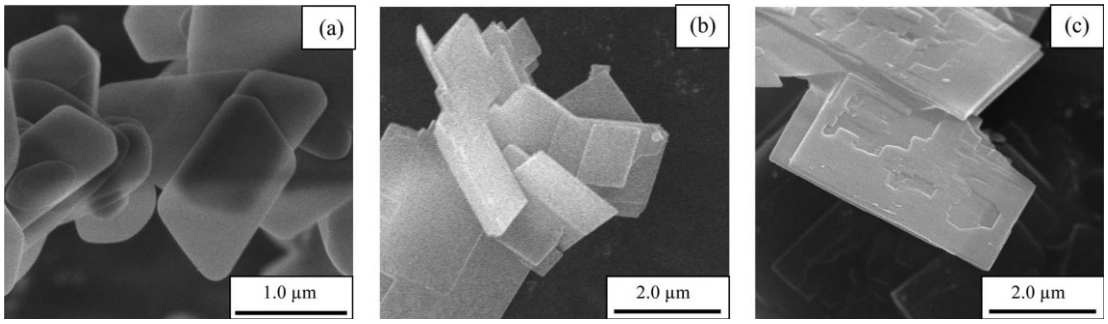

Fig. 2-2 SEM images of (a) HUS-2 (Sample 3), (b) HUS-3 (Sample 6), and (c) HUS-4 (Sample 7).

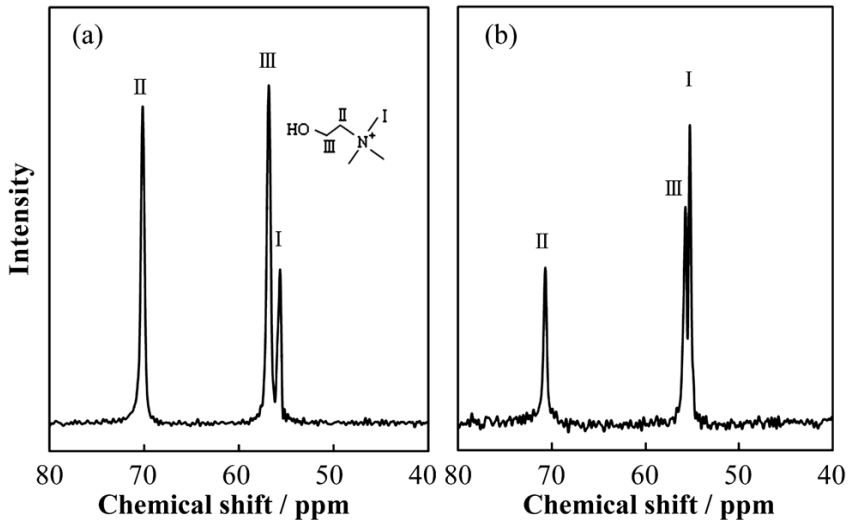

Fig. 2-3 ^{13}C CP MAS NMR spectra of (a) HUS-2 (Sample 3) and (b) HUS-3 (Sample 6).

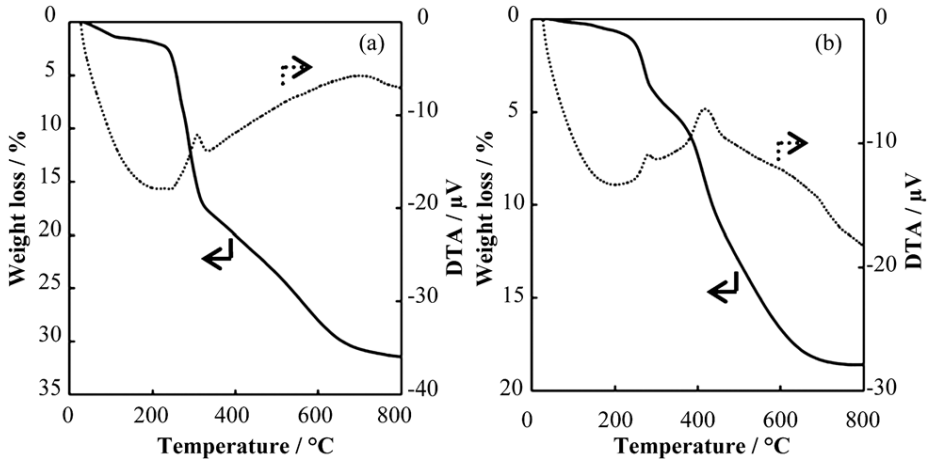

Fig. 2-4 TG/DTA curves of (a) HUS-2 (Sample 3) and (b) HUS-3 (Sample 6).

layered silicates had square plate-like particles. The particle sizes were 0.8 × 1.2 mm for HUS-2, 1.5 × 2.5 mm for HUS-3, and 2.0 × 4.5 mm for HUS-4. Fig. 2-3 depicts the ^{13}C CP/MAS NMR spectra of the obtained HUS-2 and HUS-3. Both spectra revealed the presence of three resonance peaks that were centered at ca. 55, 57, and 70 ppm, although the relative peak intensities were different between HUS-2 and HUS-3. The resonance peak at ca. 55 ppm indicated the presence of methyl groups attached to N, namely $–CH_3$ of $N–CH_3$, while the resonance peaks at ca. 70 and 57 ppm correspond to the methylene groups of $N–CH_2–$ and $–CH_2–OH$ respectively. Therefore, the choline cation was the only organic species present in HUS-2 and HUS-3. From ^{13}C CP/MAS NMR spectra of the obtained HUS-4, it was also found that the choline cation was also present in the interlayer nanospaces of HUS-4. The TG/DTA curves of HUS-2 and HUS-3 are presented in Fig. 2-4. For the DTA curve of HUS-2, the thermal profiles were categorized into three zones: (I) 25–250 °C, (II) 250– 350 °C, and (III) 350–700 °C. The first zone had an endothermic profile that corresponded to the desorption of water. The second zone had an exothermic profile that can probably be attributed to the decomposition/oxidation of either choline hydroxide that had occluded the pores or choline cations that were interacting with the silanol groups of crystal defects. The third zone had an exothermic profile and was assigned to the oxidation of carbonaceous materials that were generated by the decomposition of choline hydroxide or choline cations. Based on these thermal profiles, the weight loss that occurred between 250 and 700 °C, which corresponded to the total decomposition of the organic moieties, was about 28.0–31.5 wt%. The TG/DTA curves of HUS-3 also exhibited similar thermal behavior with a weight loss of ca. 17.0 wt%. Fig. 2-5

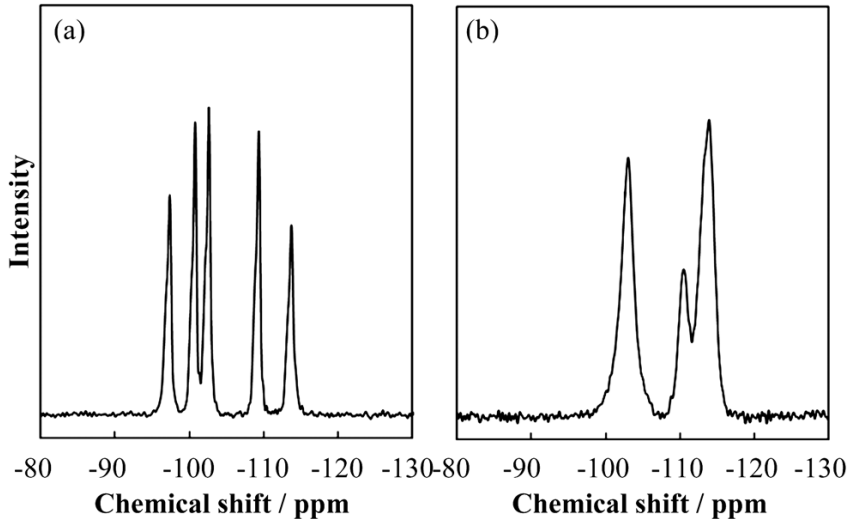

Fig. 2-5 ^{29}Si MAS NMR spectra of (a) HUS-2 (Sample 3) and (b) HUS-3 (Sample 6).

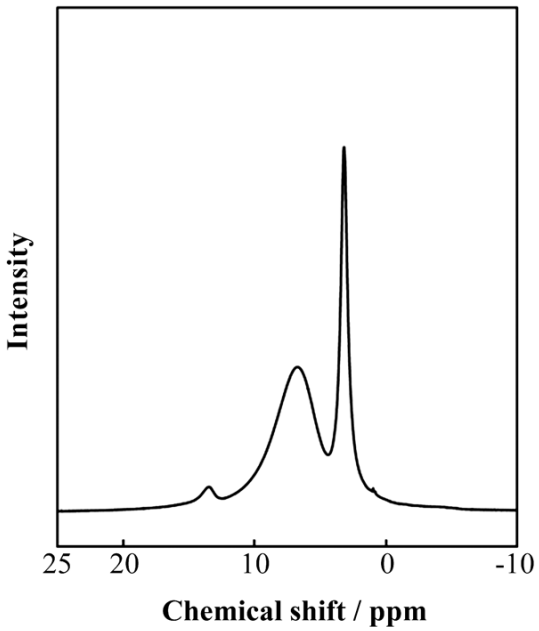

Fig. 2-6 ^{1}H MAS NMR spectrum of HUS-2 (Sample 3).

shows the ^{29}Si MAS NMR spectra of HUS-2 and HUS-3. In the spectrum of HUS-2, Q^3[(–SiO)$_3$Si–OH] and Q^4[(–SiO)$_4$Si] structures were clearly observed. Two resonance peaks at −97 and −101 ppm were assigned to the Q^3 structure, whereas three resonance peaks at ca. −103, −109, and −114 ppm were assigned to the Q^4 structure. The resonance peak at −103 ppm was seemingly attributed to the Q^3

structure. However, this peak was assigned to the Q^4 structure by virtue of the ^1H–^{29}Si CP MAS NMR measurements for various contact times. In the spectra, the intensities of the three resonance peaks at −103, −109, and −114 ppm were relatively elevated with increasing contact time as compared to those of the other two peaks. This finding indicated that the Si nuclei of the resonance peaks at −97 and −101 ppm were easily affected by the cross-polarization effect between $^1H$and ^{29}Si nuclei even if the contact time was short. Specifically, the Si nuclei of the latter two resonance peaks had hydroxyl groups (–OH). The peak intensity of the Q^4/Q^3 ratio 1.55 suggested the existence of a large number of interlayer silanol groups. In the spectrum of HUS-3, however, only three broad peaks were observed at ca. −103, −110, and −114 ppm, and were probably due to Q^3 (−103 ppm) and Q^4 (−110 and −114 ppm) structures respectively. The broad peaks seemed to be because of the poor crystallinity of HUS-3.

Fig. 2-6 shows the ^1H MAS NMR spectrum of HUS-2, where one sharp peak and two broad resonance peaks were observed. The sharp peak at 3.4 ppm was assigned to a methyl group, while the two broad peaks at 6.7 and 13.5 ppm were due to SiO–H/ $^-$OSi hydrogen bonds. These NMR results suggested the presence of a characteristic hydrogen bonding between the adjacent silicate sheets in the layered silicate or between adjacent silanol groups on the surface of the silicate layer.

3.2. Crystal structure of HUS-2

The crystallographic information that I obtained for HUS-2 is summarized in Table 2-2. Indexing the reflections gave a monoclinic unit cell of a = 0.734 nm, b = 2.358 nm, c = 0.958 nm, and b = 116.0° with acceptable figures of merit of $F20$ = 53

Table 2-2. Conditions for the powder XRD experiment and crystallographic information obtained therein for HUS-2.

Sample	HUS-2	
Estimated chemical formula	$Si_{20}O_{40}(OH)_4 \cdot 4(C_5H_{14}NO) \cdot 1.03H_2O$	
Space group	$P2_1/c$ (No. 14, set.1)	
a / nm	0.734341(12)	
b / nm	2.35821(3)	
c / nm	0.958426(14)	
β / °	116.0000(12)	
Unit-cell volume / nm^3	1.49176(4)	
Z	4	
Wavelength / nm	0.1540593 (λ = Cu Kα_1)	
2θrange / °	5.0–101.0	
Step size (2θ) / °	0.017368	
Profile range in FWHM	20	
FWHM / °	0.099 (at 2θ = 20.6°)	
Number of observations		5514
Number of contributing reflections		1540
Number of refined structural parameters	125	
Number of background coefficients		11
Number of constraints		107
R-factors obtained by Rietveld analysis		
R_{wp}	0.038	
R_F	0.012	
R_{Bragg}	0.008	
R_e	0.028	
χ^2	1.92	

and $M20 = 22$. The reflection conditions derived from the indexed reflections were $h + l = 2n$ for $h0l$, and $k = 2n$ for $0k0$, which led to the possible space group $P2_1/c$ (no. 14, setting 1). The $|F_{obs}|^2$ values of 1566 reflections in the region $d > 0.1$ nm were extracted by the Le Bail method. At first, I attempted to solve the layered framework structure of HUS-2 by the direct method and consequently detected five Si sites and eleven O sites. The presence of five independent T-sites was consistent with the observation of five resonance peaks in the ^{29}Si MAS NMR spectrum (Fig. 2-5(a)). As can be seen in Fig. 2-7(a)–(c), a framework topology composed of four-, five- and six-membered rings was clarified at this stage. Furthermore, the framework structure included the *bre* (10T)-type composite building unit (Fig. 2-7(d)).[32] There

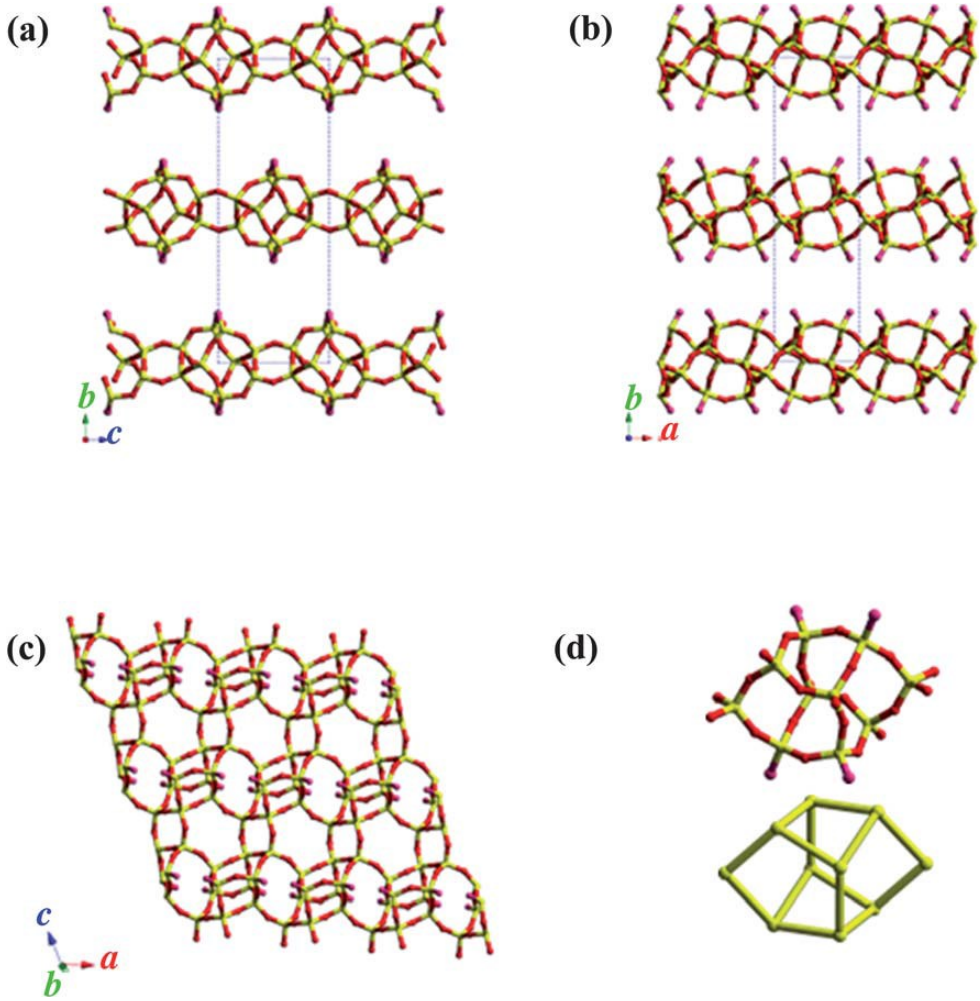

Fig. 2-7 Framework structures of layered silicate HUS-2 viewed along the (a) [100], (b) [001], and (c) [010] directions. The silicate layer consisted of 4-, 5-, and 6-membered rings and (d) bre-type composite building units.

were small hollow regions on both sides of the silicate layer. The maximum interlayer distance was estimated to be approximately 0.58 nm. The topology viewed along [100] direction (Fig. 2-7(a)) was similar to that of the HEU-type framework viewed along [001] direction.[32] At this stage, a few atoms that were attributed to choline cations were also found in the interlayers. Double silicate layers were included in the unit cell.

The distribution of choline cations in the interlayers was investigated by the

parallel-tempering method using the program FOX.[33] In this analysis, the molecular structure of the choline cation including the H atom was introduced into a structural model as a single atomic group with bond lengths and angles restrained within very narrow regions. In addition, the positions of all of the framework atoms were fixed at positions determined by the direct method. From this analysis, choline cations were located along the hollow region of the framework surface and adjacent cations were distributed along the *a*-axis. These findings, coupled with the results of the TG/DTA and ^{13}C CP/MAS NMR measurements, showed the presence of choline cations in the interlayers.

The EDD obtained by a preliminary MEM analysis strongly suggested the presence of hydrogen bonds, O–H···O, between terminal oxygen sites O1–O8, which lay parallel to the a-axis. A proton site at (0.065, 0.172, −0.005) for site H1 was then added to the structural model because these positions corresponded to the weighted centers of the hydrogen bonds in the EDD images. Additionally, small localized electron densities were observed close to site O1 at (0.60, 0.684, 0.53), probably suggesting the presence of an adsorbed water molecule at site WO1. The amount of adsorbed H2O derived from WO1 was calculated to be one molecule per unit cell.

In the final Rietveld refinement, five Si sites, twelve O sites, one N site, four C sites, oneWOsite, and fifteen H sites were included in the asymmetric unit. The scattering amplitude of H was added to site WO to maintain the charge balance. All of the isotropic atomic displacement parameters, B, for the Si sites were constrained to be equal: *B*(Si1) = *B*(Si*n*: *n* . 2–5). Simple approximations of *B*(O1) = *B*(O*n*: *n* = 2–11) and *B*(C*n*: *n* = 1–4) = *B*(N6) = *B*(O7b) = *B*(H*n*: *n* = 9–21) were also imposed on the *B* parameters of the O sites and the C, N, and H sites respectively. The *B*

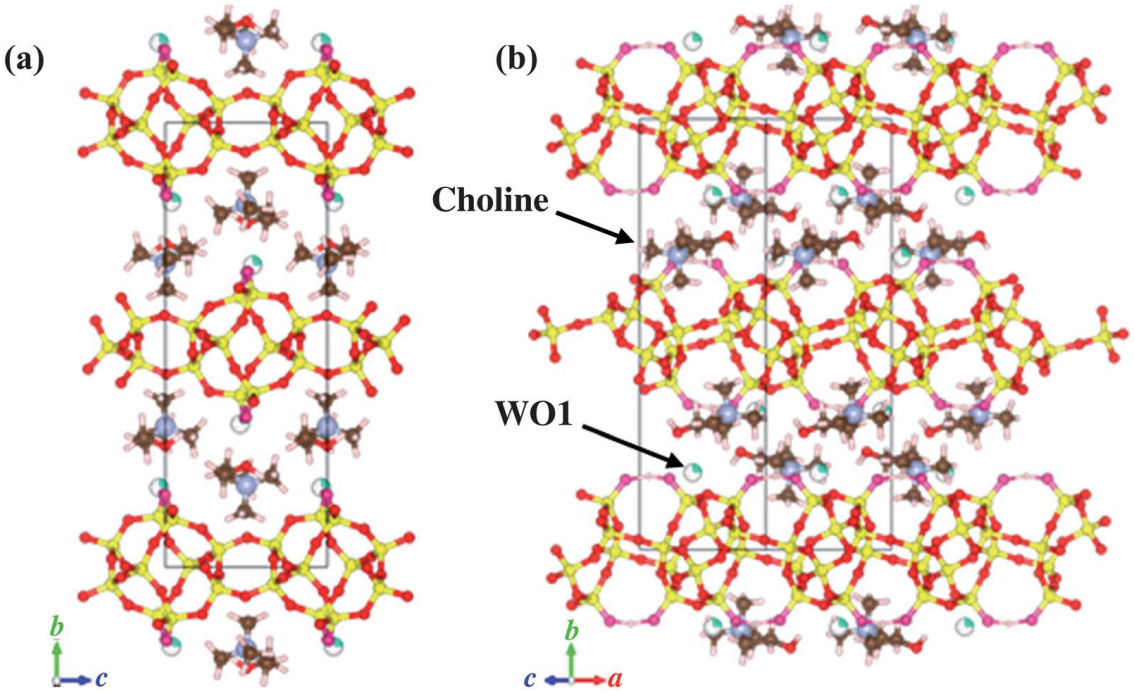

Fig. 2-8 Crystal structure model of HUS-2 determined by Rietveld analysis along the (a) [100] and (b) [101] directions.

values of the WO1 and H1 sites were fixed at 5.0 Å^2 for convenience. Finally, the *R* factors were decreased to sufficiently low levels, *i.e.*, R_{wp} = 3.8% (*S* = 1.4), R_F = 1.2%, and R_B = 0.8%.

The chemical formula of HUS-2 was estimated to be $Si_{20}O_{40}(OH)_4 \cdot 4(C_5H_{14}NO) \cdot 1.03H_2O$ according to the results of the structural refinement. If it is supposed that HUS-2 changed completely to amorphous silica (*i.e.* $Si_{20}O_{40}(OH)_4 \cdot 4(C_5H_{14}NO) \cdot 1.03H_2O \rightarrow Si_{20}O_{40}$), the total weight loss was calculated as being 29.6 wt%, which was almost in agreement with the observed weight loss of 28.0–31.5 wt% determined by the TG/DTA analysis. Although a small quantity of silanols might have remained due to incomplete condensation, the TG results were strong evidence in support of the chemical formula. Thus, the results of the chemical analysis were in accordance with the chemical formula estimated by structural

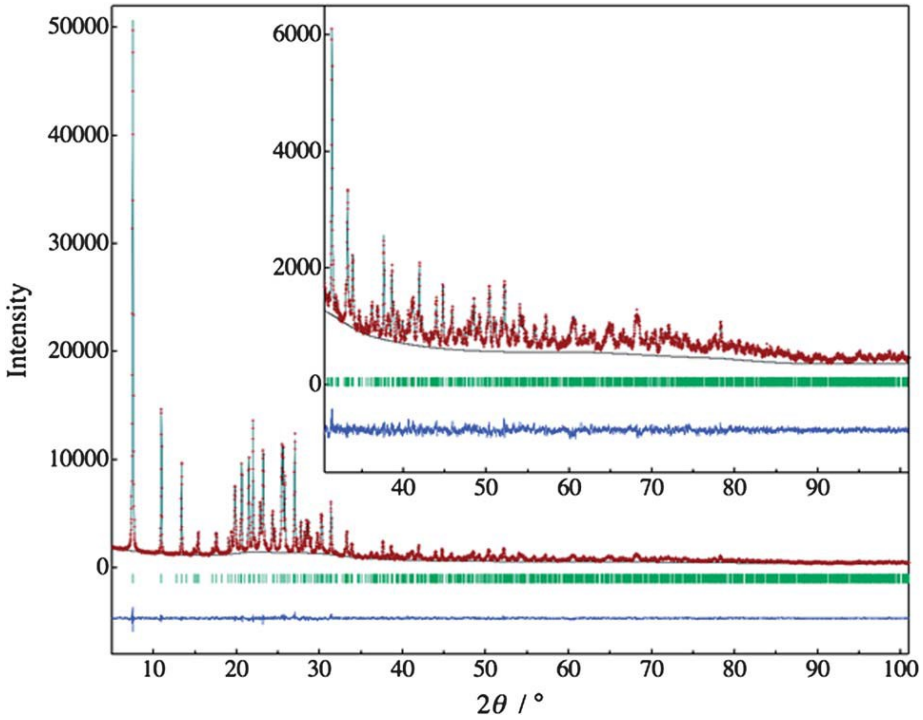

Fig. 2-9 Observed pattern (red crosses), calculated pattern (light blue solid line), and difference pattern (blue) obtained by Rietveld refinement for HUS-2. The tick marks (green) denote the peak positions of possible Bragg reflections. The inset shows magnified patterns from 30° to 101°.

analysis.

Fig. 2-8 shows the structural model of HUS-2 that we finally obtained. The narrowest width between the adjacent layers was estimated to be *ca*. 0.36 nm. Choline cations were accommodated into the interlayer space and the interatomic distance of H14–O7b between the nearest molecules along the a-axis was ca. 0.28 nm. The nearest atomic distance between neighboring silanol groups, *l*(O–O), was *l*(O1–O8) = 2.55(2) Å, which was in good agreement with the value of 2.53 Å calculated from the ^{1}H MAS NMR spectrum.[34] Sites Si1, Si4, and Si5 corresponded to the Q^4 structure, whereas sites Si2 and Si3 corresponded to the Q^3 structure, *i.e*., terminal silanol. The calculated Q^4/Q^3 ratio on the basis of the framework geometry was 1.5, which was consistent with the value (*ca*. 1.55) estimated from the ^{29}Si MAS

Table 2-3. Structural parameters *g*, *x*, *y*, *z,* and *B* of HUS-2 obtained by Rietveld refinement. Estimated standard deviations are given as uncertainties in the last reported decimal place.

Site	Wycoff	*g*	*x*	*y*	*z*	B_{iso}(Å^2)
Si1	4e	1.0	0.0906(7)	0.0395(3)	0.3320(6)	0.76(3)
Si2	4e	1.0	0.7908(8)	0.1082(3)	0.0449(5)	=*B*(Si1)
Si3	4e	1.0	0.3361(8)	0.1147(3)	–0.0383(6)	=*B*(Si1)
Si4	4e	1.0	0.2330(7)	0.0481(2)	0.6773(5)	=*B*(Si1)
Si5	4e	1.0	0.3427(7)	0.0048(2)	0.1478(5)	=*B*(Si1)
O1	4e	1.0	0.228(2)	0.1663(5)	–0.0094(11)	0.61(6)
O2	4e	1.0	0.7598(14)	0.0534(5)	–0.0689(10)	=*B*(O1)
O3	4e	1.0	0.0239(14)	0.0181(5)	0.6680(9)	=*B*(O1)
O4	4e	1.0	0.2620(13)	0.0230(5)	0.2732(9)	=*B*(O1)
O5	4e	1.0	–0.0570(14)	0.0857(4)	0.2271(11)	=*B*(O1)
O6	4e	1.0	0.268(2)	0.1051(5)	0.7725(11)	=*B*(O1)
O7	4e	1.0	0.2892(14)	0.0554(5)	0.0246(10)	=*B*(O1)
O8	4e	1.0	0.8856(14)	0.1623(5)	–0.0011(13)	=*B*(O1)
O9	4e	1.0	0.2010(14)	0.0664(4)	0.5043(12)	=*B*(O1)
O10	4e	1.0	0.4155(13)	0.0015(5)	0.7550(9)	=*B*(O1)
O11	4e	1.0	0.585(2)	0.1280(5)	0.0453(11)	=*B*(O1)
C1	4e	1.0	0.737(3)	0.2042(12)	0.657(3)	=*B*(O1b)
C2	4e	1.0	0.664(3)	0.1255(12)	0.486(2)	=*B*(O1b)
C3	4e	1.0	0.877(4)	0.1939(10)	0.474(3)	=*B*(O1b)
C4	4e	1.0	0.535(4)	0.2168(10)	0.374(3)	=*B*(O1b)
C5	4e	1.0	0.329(3)	0.2087(10)	0.367(3)	=*B*(O1b)
N6	4e	1.0	0.698(3)	0.1845(8)	0.498(2)	=*B*(O1b)
Ob	4e	1.0	0.305(2)	0.2270(7)	0.504(2)	3.6(2)
H8	4e	1.0	0.81(3)	0.244(9)	0.69(2)	=*B*(O1b)
H9	4e	1.0	0.60(2)	0.209(10)	0.67(2)	=*B*(O1b)
H10	4e	1.0	0.82(3)	0.171(9)	0.73(2)	=*B*(O1b)
H11	4e	1.0	0.73(2)	0.105(7)	0.42(2)	=*B*(O1b)
H12	4e	1.0	0.74(3)	0.109(9)	0.60(2)	=*B*(O1b)
H13	4e	1.0	0.50(3)	0.120(7)	0.44(2)	=*B*(O1b)
H14	4e	1.0	0.92(2)	0.240(7)	0.50(2)	=*B*(O1b)
H15	4e	1.0	0.00(2)	0.164(7)	0.55(2)	=*B*(O1b)
H16	4e	1.0	0.84(2)	0.190(9)	0.35(2)	=*B*(O1b)
H17	4e	1.0	0.58(2)	0.261(7)	0.39(2)	=*B*(O1b)
H18	4e	1.0	0.54(3)	0.206(8)	0.27(2)	=*B*(O1b)
H19	4e	1.0	0.22(2)	0.233(8)	0.26(2)	=*B*(O1b)
H20	4e	1.0	0.30(3)	0.162(8)	0.36(2)	=*B*(O1b)
H21	4e	1.0	0.31(2)	0.200(8)	0.59(2)	=*B*(O1b)
WO1	4e	0.259(12)	0.603(6)	0.677(2)	0.532(5)	5.0**
H1*	4e	1.0	0.065	0.172	–0.005	5.0**

Note: (*) The atomic coordinate parameters of site H1 were fixed. (**) The U_{iso} parameters of sites WO1 and H1 were fixed.

NMR spectrum. Fig. 2-9 shows the observed, calculated, and difference patterns, indicating that the structural model that we obtained explained the powder XRD data well. The average bond length *l*(Si–O) and bond angle ϕ(O–Si–O), which were close

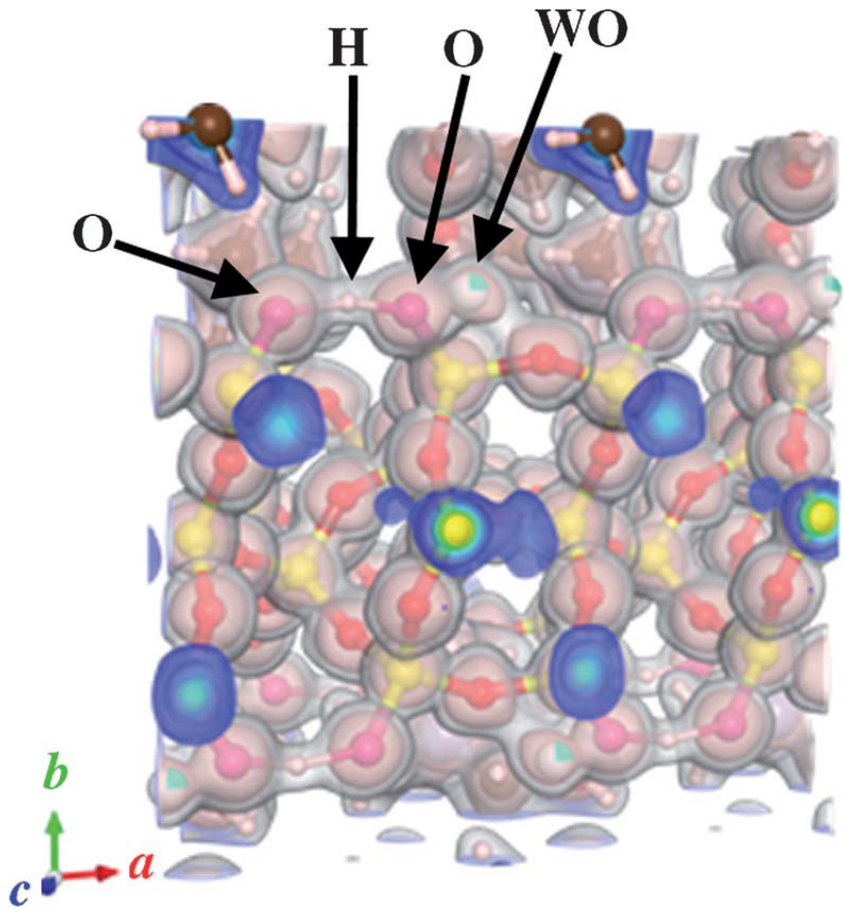

Fig. 2-10 An EDD image of HUS-2 obtained by MPF analysis: electron densities (−0.4 < x < 1.4, −0.245 < y < 0.3, −0.4 < z < 1.18) viewed along the c axis. Wqui-surface levels were set at 0.4 and 1.0 e □A□3. The spatial resolution was 74 × 236 × 96 pixels per unit cell.

to the expected values,[35] fell within 1.54–1.69 Å and 105.94–114.5° respectively. The refined structural parameters for site occupancy, atomic coordinate and isotropic atomic displacement are summarized in Table 2-3.

Fig. 2-10 shows EDD images of HUS-2 obtained by MPF refinement with equi-surface levels of 0.4 and 1.0 eÅ^{-3}. Covalent bonds of Si–O in the framework and N–C and C–C in the choline cation are clearly visible. Electron densities attributed to hydrogen bonds are clearly seen between sites O1 and O8. The electron densities of site WO1 are elongated toward sites O1, O11, and Si3, suggesting a disorderly distribution of adsorbed H_2O. This led to the idea that site WO1 may have

been attributed to not only a water molecule but also a proton. These findings coincided with the results of the ^{1}H MAS NMR measurements. Because the EDD determined by MPF showed a highly ordered arrangement of choline cations in the interlayers, the choline species were believed to be cations. Furthermore, the molecular motion of the choline cation was estimated to be considerably restricted. The MPF analysis lowered the weighted R_F(MEM) from 1.45% to 1.01% and the R_F(MEM) from 1.60% to 1.17% after two cycles.

3.3. Knoevenagel condensation reaction over HUS-2 and HUS-3

Table 2-4. Knoevenagel condensation reaction over HUS-2 and HUS-3[a]

Entry no.	Catalyst	Reactiojn conditions		Yield[b] (%)
		Temperature (°C)	Time (h)	
1	HUS-2	25	3.5	61
2	HUS-2	40	3.5	71
3	HUS-2	70	3.5	96, 92[c], 91[d]
4	HUS-2	70	0.5	38
5	HUS-2	70	1.5	89
6	HUS-3	70	3.5	95

[a] The reactions were carried out by using benzaldehyde (1.0 mmol), ethyl cyanoacetate (1.2 mmol), and naphthalene (0.10 mmol) as an internal standard and layered silicate (HUS-2 and HUS-3) (25 mg), in methanol (0.5 ml).

[b] Determined by gas chromatography. [c] 2nd use. [d] 3rd use.

In order to clarify the potential for using the layered silicates that I obtained as base catalysts, the Knoevenagel condensation reaction of benzaldehyde with ethyl cyanoacetate was investigated as a model reaction. From preliminary experiments, separate 25 mg quantities of layered silicates were used in conjunction with 1.0 mmol benzaldehyde. Typical results of the Knoevenagel condensation reaction over HUS-2 (Sample 3) and HUS-3 (Sample 6) are listed in Table 2-4. The reaction over HUS-2 occurred quantitatively even at room temperature (25 °C) to yield the product (ethyl-2-cyano-3-phenylacrylate) with a selectivity of 98%. The conversion of

benzaldehyde increased with increasing reaction temperature. For the reaction conditions of 70 °C for 3.5 h, the product yield was approximately 100%. There was no difference in the product yield between HUS-2 and HUS-3. The catalytic activities of HUS-2 and HUS-3 were similar to that of the layered silicate PLS-1 reported by Komura *et al*.[21]

The reusability of these layered silicates was also examined. As shown in Table 2-4 (entry no. 3), the product yields over HUS-2 after run 2 and run 3 were 92% and 91%, respectively, which were almost the same as for the first run of 96%. It was confirmed from XRD measurements that the framework structure of HUS-2 was completely retained even after run 3. TG/DTA analysis also showed no significant difference in weight loss corresponding to the decomposition of choline cations, namely no extraction of choline cations in the interlayers. These results strongly indicate that layered silicates of HUS-2 and HUS-3 actually performed as solid base catalysts in spite of their lower basicity and could be recycled without any significant loss in their catalytic abilities.

3.4. Transformation of HUS-3 into CDO-type zeolite by calcination

The possibility of transforming the obtained layered silicates into zeolites was examined next. When the as-synthesized HUS-3 heated at 450 °C for 20 h, a CDO-type zeolite was obtained, as shown in Fig. 2-11. Since the crystal structure of HUS-3 has not been determined, I could not explain exactly the transformation process that occurred. It is likely that the CDO-type zeolite was formed by a dehydration–condensation reaction that took place between the silanol groups on the interlayers. This was confirmed by the ^{29}Si MAS NMR spectrum of the obtained

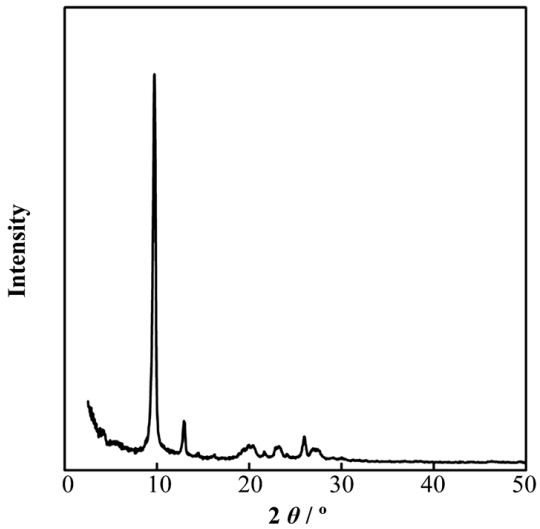

Fig. 2-11 The XRD pattern of HUS-3 calcined at 450 °C for 20 h.

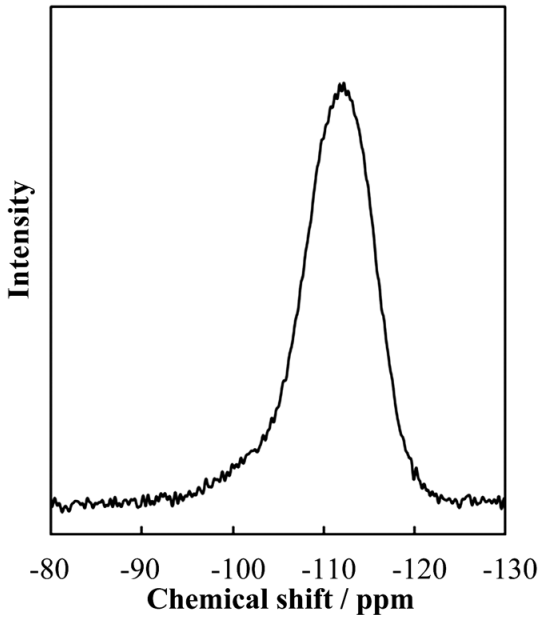

Fig. 2-12 The ^{29}Si MAS NMR spectrum of HUS-3 calcined at 450 °C for 20 h.

CDO-type zeolite. Fig. 2-12 shows only a broad peak at around −112 ppm that was mostly due to the Q^4 structure and possibly contained a small amount of Q^3. Although N_2 adsorption hardly occurred on the as-synthesized HUS-3, the BET surface area of the CDO-type zeolite calculated from the N_2 adsorption isotherm was 240 m^2 g^{-1}. From these findings, I guess that the crystal structure of HUS-3 was

similar to the disordered structure of PLS-1 with stacking faults in each layer. On the other hand, HUS-2 became amorphous when it was calcined. This was due to an inappropriate layer stacking sequence, as shown in Fig. 2-8.

4. Conclusions

I succeeded in synthesizing three kinds of layered silicates, HUS-2, HUS-3, and HUS-4, from a SiO_2–choline hydroxide–NaOH–H_2O system. HUS-2 had a layered structure, which was composed of four-, five-, and six-membered rings. Its framework topology is partially similar to that of a HEU-type zeolite including *bre* (10T)-type composite building units. Choline cations that were used as an SDA were present between the interlayers. Double silicate layers were present in each unit cell. The effective interlayer distance was estimated to be *ca*. 0.36 nm. The crystal structure of HUS-3 could not be determined. However, it was found that HUS-3 was converted into a CDO type zeolite by calcination at 450 °C for 20 h, indicating that the structure of HUS-3 was partially similar to that of a precursor of the CDO-type zeolite. The crystal structure of HUS-4 with choline cations in its interlayers was similar to that of PLS-1, which was synthesized using TMA cations. In addition, it was demonstrated that the layered silicates HUS-2 and HUS-3 could be employed as base catalysts for a Knoevenagel condensation reaction. These findings strongly suggest the high potential of HUS-2 and HUS-3 for applications as functional materials.

References

1 (a) M. Ogawa and K. Kuroda, *Bull. Chem. Soc. Jpn*., 1997, **70**, 2593; (b) T. Okada, Y. Ide and M. Ogawa, *Chem.–Asian J*., 2012, **7**, 1980.

2 N. Takahashi and K. Kuroda, *J. Mater. Chem*., 2011, **21**, 14336.

3 T. Ikeda, Y. Akiyama, Y. Oumi, A. Kawai and F. Mizukami, *Angew. Chem., Int. Ed*., 2004, **43**, 4892.

4 S. Zanardi, A. Alberti, G. Cruciani, A. Corma, V. Fornes and M. Brunelli, *Angew. Chem., Int. Ed*., 2004, **43**, 4933.

5 B. Marler, M. A. Camblor and H. Gies, *Microporous Mesoporous Mater*., 2006, **90**, 87.

6 B. Marler, N. Stroter and H. Gies, *Microporous Mesoporous Mater*., 2005, **83**, 201.

7 Y. Oumi, T. Takeoka, T. Ikeda, T. Yokoyama and T. Sano, *New J. Chem*., 2007, **31**, 593.

8 T. Ikeda, Y. Oumi, T. Takeoka, T. Yokoyama, T. Sano and T. Hanaoka, *Microporous Mesoporous Mater*., 2008, **110**, 488.

9 Y. Wang, B. Marler, H. Gies and U. Muller, *Chem. Mater*., 2005, **17**, 43.

10 T. Moteki, W. Chaikiiisilp, A. Shimojima and T. Okubo, *J. Am. Chem. Soc*., 2008, **130**, 15780.

11 T. Ikeda, S. Kayamori and F. Mizukami, *J. Mater. Chem*., 2009, **19**, 5518.

12 J. Song and H. Gies, *Stud. Surf. Sci. Catal*., 2004, **154A**, 295.

13 B. Marler, Y. Wang, H. Song and H. Gies, *Abstracts of Papers, 15th International Zeolite Conference, 2007*, Beijing, China, August 12-17, 2007, p. 599.

14 A. Burton, R. J. Accardi, R. F. Lobo, M. Falcioni and M. W. Deem, *Chem. Mater*., 2000, **12**, 2936.

15 D. L. Dorset and G. J. Kennedy, *J. Phys. Chem. B*, 2004, **108**, 15216.

16 L. M. Knight, M. A. Miller, S. C. Koster, M. G. Gatter, A. I. Benin, R. R. Willis, G. J. Lewis and R. W. Broach, *Stud. Surf. Sci. Catal*., 2007, **170A**, 338.

17 A. J. Blake, K. R. Franklin and B. M. Lowe, J. Chem. Soc., *Dalton Trans*., 1988, 2513.

18 S. Vortmann, J. Rius, S. Siegmann and H. Gies, *J. Phys. Chem. B*, 1997, **101**, 1292.

19 Y. X. Wang, H. Gies and J. H. Lin, *Chem. Mater*., 2007, **19**, 4181.

20 U. Oberhagemann, P. Bayat, B. Marler, H. Gies and J. Rius, *Angew. Chem., Int. Ed. Engl*., 1996, **35**, 2869.

21 K. Komura, T. Kawakami and Y. Sugi, *Catal. Commun*., 2007, **8**, 644.

22 (a) T. Ikeda, Y. Oumi, K. Honda, T. Sano, K. Momma and F. Izumi, *Inorg. Chem*., 2011, **50**, 2294; (b) Y. Ide, M. Torii, N. Tsunoji, M. Sadakane and T. Sano, *Chem. Commun*., 2012, **48**, 7073.

23 (a) H. Jon, K. Nakahata, B. Lu, Y. Oumi and T. Sano, *Microporous Mesoporous Mater*., 2006, **96**, 72; (b) H. Jon, S. Takahasni, H. Sasaki, Y. Oumi and T. Sano, *Microporous Mesoporous Mater*., 2008, **113**, 56; (c) M. Itakura, T. Inoue, A. Takahashi, T. Fujitani, Y. Oumi and T. Sano, *Chem. Lett*., 2008, **39**, 908; (d) H. Sasaki, T. Jon, M. Itakura, T. Inoue, T. Ikeda, Y. Oumi and T. Sano, *J. Porous Mater*., 2009, **16**, 465; (e) T. Inoue, M. Itakura, H. Jon, A. Takahashi, T. Fujitani, Y. Oumi and T. Sano, *Microporous Mesoporous Mater*., 2009, **122**, 149; (f) M. Itakura, Y. Oumi, M. Sadakane and T. Sano, *Mater. Res. Bull*., 2010, **45**, 646; (g) S. Shimata, M. Itakura, Y. Ide, M. Sadakane and T. Sano, *Microporous Mesoporous Mater*., 2011, **138**, 32; (h) K. Honda, A. Yashiki, M. Itakura, Y. Ide, M. Sadakane and T. Sano, *Microporous Mesoporous Mater*., 2011, **142**, 161.

24 A. Altomare, M. Camalli, C. Cuocci, C. Giacovazzo, A. Moliterni and R. J. Rizzi, *Appl. Crystallogr*., 2009, **42**, 1197.

25 A. Le Bail, H. Duroy and J. L. Fourquet, *Mater. Res. Bull*., 1988, **23**, 447.

26 F. Izumi and K. Momma, *Solid State Phenom*., 2007, **130**, 15.

27 T. Ohta, F. Izumi, K. Oikawa and T. Kamiyama, *Phys. B*, 1997, **234**, 1093.

28 F. Izumi and K. Momma, *Materials Science and Engineering*, 2011, **18**, 022001, Proceeding of ICC3: Symposium 1: Advanced Structural Analysis and Characterization of Ceramics Materials.

29 K. Momma and F. Izumi, *J. Appl. Crystallogr*., 2011, **44**, 1272.

30 (a) T. Ikeda, Y. Akiyama, F. Izumi, Y. Kiyozumi, F. Mizukami and T. Kodaira, *Chem. Mater*., 2001, **13**, 1286; (b) Y. Akiyama, T. Ikeda, A. Kawai, Y. Kiyozumi and F. Mizukami, *Mater. Chem. Phys*., 2004, **86**, 112.

31 A. Kawai, T. Ikeda, Y. Kiyozumi, H. Chiku and F. Mizukami, Mater. *Chem. Phys*., 2006, **99**, 470.

32 *Atlas of Zeolite Framework Types*, ed. Ch. Baerlocher, W. M. Meier and D. H. Olson, Elsevier, 6th edn, 2007, p. 374.

33 V. Favre-Nicolin and R. J. Cerny, *Appl. Crystallogr*., 2002, **35**, 734.

34 X. Xue and M. Kanzaki, *J. Phys. Chem. B*, 2007, **111**, 13156.

35 *International Tables for Crystallography*, ed. T Hahn, Springer, Dordrecht, The Netherlands, 2005, 5th edn, vol. A, p. 35.

Chapter 3

Synthesis and characteristics of novel layered silicate HUS-7 using benzyltrimethylammonium hydroxide and its unique and selective phenol adsorption behavior

2. Introduction

Frameworks of crystalline-layered silicates (CLSs) are composed exclusively of silicon oxide tetrahedra (SiO_4). As the interlayer surfaces are covered with silanol (SiOH) and silanolate (SiO^-) groups charge-balanced by alkali metal or organic cations, the layered silicates are easily functionalized by various modifications such as cation exchange, silylation, and pillaring. Therefore, CLSs have attracted interest in many applications such as catalysis and adsorption.[1,2] Another important application of layered silicates is their use as precursors for zeolite synthesis by the topotactic conversion method.[3,4] The conversion of a layered silicate into a zeolite proceeds through the topotactic dehydration–condensation of periodic and reactive silanol groups on both sides of the interlayer. If the crystal structures of the layered silicate nanosheets are determined, the framework structures of the zeolites obtained can be easily determined. This method has been already demonstrated previously. CDO (the three letters indicate the framework-type code),[3] NSI,[5] CAS–NSI,[6] RWR,[7–9] RRO,[10] and SOD[11]-type zeolites were prepared using layered silicates

PLS-1,[3] (isomorphic materials: PLS-4,[12] RUB-36,[13,14] MCM-47,[15] MCM-65,[16] UZM-13,[17] UZM-17,[17] and UZM-19[17]), Nu-6(1),[5] EU-19,[6] RUB-18,[18,19] RUB-39,20 and RUB- 15,[21] respectively. These layered materials incorporate organic cations, especially quaternary alkylammonium cations, in their interlayers, which are used as structural directing agents (SDAs) for the synthesis of each material. The quaternary alkylammonium cations are regularly located at crystallographically defined positions in these as-synthesized CLSs. In the case of the insertion of quaternary alkylammonium cations into the interlayer of CLSs by ion exchange,[22–25] it is not necessarily easy to immobilize the ion species at exactly defined locations, which limits the applicability of ion-exchanged CLSs. Based on these observations, to investigate the physicochemical properties of as-synthesized CLSs having regularly distributed interlayer cations would be quite interesting. Therefore, the synthesis of novel layered silicates with unique framework structures or regularity of interlayer molecules is a challenging area of research.

Recently, Sano et. al and I reported the successful syntheses and structural analyses of new layered silicates, the Hiroshima University Silicates HUS-1 and HUS-2, which were synthesized using tetramethylammonium (TMA) and choline hydroxides, respectively.[26,27] I also investigated their adsorption and ionexchange properties.[28–30] HUS-1 modified with dimethyldichlorosilane effectively and selectively adsorbed TMA^+ from water even in the presence of aqueous phenol.[28a] Also, HUS-2 selectively and effectively adsorbed propionic acid from water containing three acid components (formic, acetic, and propionic acids) (Chapter 4).[29] Very recently, during the further analytical study of HUS-1, I found that the crystal structure of HUS-5 with an ABAB stacking order was converted to HUS-1 with an

AAAA stacking order during washing treatment. These layered silicates exhibited different ion-exchange behaviors. The interlayer distance of HUS-5 could be expanded by ion exchange with bulky organic cations, while no expansion of the interlayer distance was observed for HUS-1. I also found that HUS-5 that had been treated *via* ion exchange with the hexadecyltrimethylammonium cation was converted to a novel nanoporous silica (HUS-6), with a Brunauer–Emmett–Teller (BET) surface area of 983 m^2 g^{-1} and an average pore diameter of 1.6 nm, by acetic acid treatment and subsequent calcination (Chapter 5).[30]

In this work, I succeeded in synthesizing the novel layered silicate HUS-7 using both benzyltrimethylammonium (BTMA) hydroxide and biphenyl, and I investigated its crystal structure. The structural refinement of HUS-7 by the Rietveld method showed that the BTMA cations used as SDAs existed as dimers in the interlayer with unique regularity. Although it is well recognized that the physicochemical properties of layered silicates are influenced by the stacking state and the interlayer distance of the silicate layers,[9,11,29] there are few reports concerning the adsorption properties of layered silicates having unique spaces formed by interlayer molecules. Thus, I also investigated the adsorption ability of HUS-7 using benzene and phenol molecules.

2. Experimental

2.1. Sunyhesis of layered silicate

The starting mixture was prepared using fumed silica (Cab-Osil ® M5, Cabot Corp.), benzyltrimethylammonium hydroxide (BTMAOH, Tokyo Chemical Ind. Co. Ltd., (TCI) Japan), sodium hydroxide (>99%, Kojundo Chemical Laboratory, Japan),

biphenyl (TCI), and distilled water. The resultant hydrogel with a chemical composition of SiO_2 : 0.2–0.4 BTMAOH : 0.2 NaOH : 0–0.2 biphenyl : 5.5–10.5 H_2O was transferred into a 30 mL Teflon®-lined stainless steel vessel and heated under static conditions at 125 °C for 7–14 days. The obtained solid product, the layered silicate, was separated by centrifugation and repeatedly washed with distilled water. Detailed synthesis conditions for HUS-7 are given in Table 3-1.

2.2. Characterization

Powder X-ray diffraction (XRD) patterns of the solid products were collected using a powder X-ray diffractometer (Rigaku MiniFlex) with graphite-monochromatized Cu Kα radiation at 30 kV and 15 mA. The crystal morphology was observed using a Hitachi S-4800 scanning electron microscope (SEM) coupled with an energy-dispersive X-ray (EDX) analyzer. ^{29}Si magic-angle spinning (MAS) NMR spectra were recorded at 119.17 MHz on a Varian 600PS solid NMR spectrometer using a 3.2 mm diameter zirconia rotor. The rotor was spun at 20 kHz. The spectra were acquired using 6.7 ms pulses, a 50 s recycle delay, and 1000 scans. 3-(Trimethylsilyl)propionic-2,2,3,3-d_4 acid sodium salt was used as a chemical shift reference. ^{1}H MAS NMR spectra were measured with a spinning frequency of 20 kHz and a single pulse sequence operated at 599.85 MHz. Furthermore, ^{1}H–^{13}C cross-polarized (CP)-MAS NMR spectra were also measured with a spinning frequency of 20 kHz, a 90° pulse length of 2.2 ms, and a cycle delay time of 50 s. The ^{1}H and ^{13}C chemical shifts were referenced to adamantine and hexamethylbenzene, respectively. Thermal analyses were carried out using a thermogravimetric/differential thermal analysis (TG/DTA) apparatus (SSC/5200,

Seiko Instruments). A sample (*ca*. 3 mg) was heated in a flow of air (50 mL min^{-1}) at a heating rate of 10 °C min^{-1} from room temperature to 800 °C. Elemental analysis was carried out using a PerkinElmer 2400 II CHN analyzer at the Natural Science Center for Basic Research and Development (N-BARD), Hiroshima University. UV-vis diffuse reflectance spectra of the obtained samples were recorded on a UV-vis spectrometer (JASCO V-570, Jasco, Japan) with $BaSO_4$ as a reference.

2.3. Structural analysis of HUS-7

For accurate structural analyses, PXRD data were collected at room temperature on a D8 ADVANCE with Vario1 (Bruker-AXS, Japan) powder diffractometer with a modified Debye–Scherrer geometry, Cu $K\alpha_1$ radiation, and a linear position-sensitive detector (VÅNTEC-1, Bruker). The sample was sealed in a borosilicate capillary tube with an inner diameter of 0.7 mm. The empirical μr (μ: linear absorption coefficient, r: sample radius) value was 0.353, which was applied for X-ray absorption corrections.

The crystal structure of HUS-7 was determined by *ab initio* analysis. Indexing of reflections with the program N-TREOR built in the integrated package EXPO2013[31] successfully gave lattice parameters and indices of the reflections. The spac group was determined from reflection conditions derived from these indices. Observed integrated intensities, $|F_{obs}|^2$, were extracted by the Le Bail method[32] using EXPO2013. Then, an initial structural model for HUS-7 was elucidated by a combination of the direct method with EXPO2013 and the direct space method with the program FOX.[33] The detailed analytical procedure has been described elsewhere.[26,27]

The obtained initial structural model of HUS-7 was refined by the Rietveld method using the program RIETAN-FP.[34] In the refinement, to enable the solution to converge easily, I imposed restraints upon all the Si–O bond lengths (*i.e., l*(Si–O) = 1.60 ± 0.02 Å) and all the O–Si–O bond angles (*i.e., l*(O–Si–O) = 109.47 ± 5.0°) on geometrical parameters. Likewise, softrestraints were imposed upon all bond lengths and bond angles which were based on the molecular geometry of BTMA.

To clarify the packing density of BTMA and the effective size of the nano-space in the interlayer, the electron density distribution (EDD) in the unit cell of HUS-7 was calculated from the observed structure factors, F_{obs}, by the maximum entropy method (MEM) using the program Dysnomia.[35] Furthermore, the calculated EDD was refined by MEM-based pattern fitting (MPF).[34] The MPF analysis is very effective in visualizing chemical bonds and disordered arrangements of chemical species. Table 3-2 summarizes the experimental conditions for the PXRD measurements and partial results for the Rietveld refinement of HUS-7. The structural model and EDD were visualized using the program VESTA.[36]

2.4. Adsorption tests

The adsorption of benzene and phenol from single- and binarycomponent acetonitrile solutions was studied at room temperature in batch mode. The benzene/phenol molar ratio in the binary-component acetonitrile solution was 1.0. An adsorbent (20 mg) was introduced into acetonitrile (20 mL) containing benzene and phenol at different concentrations in a glass vessel, and shaken at room temperature for 24 h. After a predefined contact time, the adsorbent was removed from the mixture by filtration. Then, the residual amounts of benzene and phenol in

the supernatant were analyzed by high-performance liquid chromatography with UV detection on an Ascentis Express C18 column. As a reference, I also investigated the adsorption behavior of RUB-51, which had similarly been synthesized using BTMAOH as an SDA.

3. Results and discussion

3.1. Synthesis of HUS-7

As described above, I successfully obtained the new layered silicates HUS-2, which was synthesized at relatively lower H_2O/SiO_2 ratios using choline hydroxides as SDAs. This motivated me to synthesize layered silicates using organic SDAs other than choline cations at lower H_2O/SiO_2 ratios. It is already reported that the organic cation was also effective for hydrothermal conversion of FAU-type zeolites to LEV-type zeolites.[37,38] Therefore, I selected the benzyltrimethylammonium (BTMA) cation as an SDA, which was effective for FAU–CHA interzeolite conversion.[39] In the hydrothermal syntheses of zeolites and mesoporous materials, it is also recognized that several organic molecules such as hydrocarbons and alcohols can be added into the starting gel to control the size and morphology of the products.[40,41] Therefore, I investigated the effect of the addition of hydrocarbons such as hexane, toluene, and biphenyl on the synthesis of the layered silicates. Typical hydrothermal synthesis conditions are listed in Table 3-1. To prevent decomposition of the organic molecules during the hydrothermal synthesis,

Table 3-1 Hydrothermal synthesis conditions for novel layered silicate HUS-7[a]

Sample no.	Synthesis conditions						Product	
	SDA	SDA/SiO_2	Additive	Additive/SiO_2	H_2O/SiO_2 / ºC	Time / days	Phase	Yield (%)
1	BTMA	0.2	-	-	5.5	7	Amorphous	39
2	BTMA	0.2	Biphenyl	0.05	5.5	7	HUS-7	80
3	BTMA	0.2	Biphenyl	0.1	5.5	7	HUS-7	88
4	BTMA	0.2	Biphenyl	0.1	10.5	7	No product	-
5	BTMA	0.2	Biphenyl	0.1	5.5	14	HUS-7	64
6	BTMA	0.4	Biphenyl	0.1	5.5	7	RUB-51	100
7	BTMA	0.2	Tolene	0.1	5.5	7	HUS-7	85
8	BTMA	0.2	Hexane	0.1	5.5	7	HUS-7	74

[a] Synthesis conditions: $NaOH/SiO_2$ = 0.2, temperature = 125 °C.

experiments were carried out at relatively lower temperatures compared with HUS-1 (140 °C) and HUS-2 (150 °C).

At first, the reaction was conducted at 125 °C for 7 days using a starting gel with a H_2O/SiO_2 ratio of 5.5, a $NaOH/SiO_2$ ratio of 0.2, and a $BTMAOH/SiO_2$ ratio of 0.2. Only amorphous phase was obtained (Sample 1). When biphenyl was added in the starting gel (biphenyl/SiO_2 ratio = 0.05), however, a new type of layered silicate was obtained in high yield (80%, Sample 2). The yield increased with an increase in the biphenyl/SiO_2 ratio (Sample 3), and the product was named HUS-7 (Hiroshima University Silicate-7). When the H_2O/SiO_2 ratio in the starting gel was increased from 5.5 to 10.5, no product was obtained (Sample 4). Instead, the starting gel was completely dissolved without subsequent crystallization. Prolonged reaction time did not improve the product yield (Sample 5). By changing the $BTMAOH/SiO_2$ ratio from 0.2 to 0.4, RUB-51 was obtained in 100% yield (Sample 6). It is known that the BTMA cation is effective as an SDA for the synthesis of RUB-51.[42] These results strongly indicated that both the $BTMAOH/SiO_2$ and biphenyl/SiO_2 ratios in the

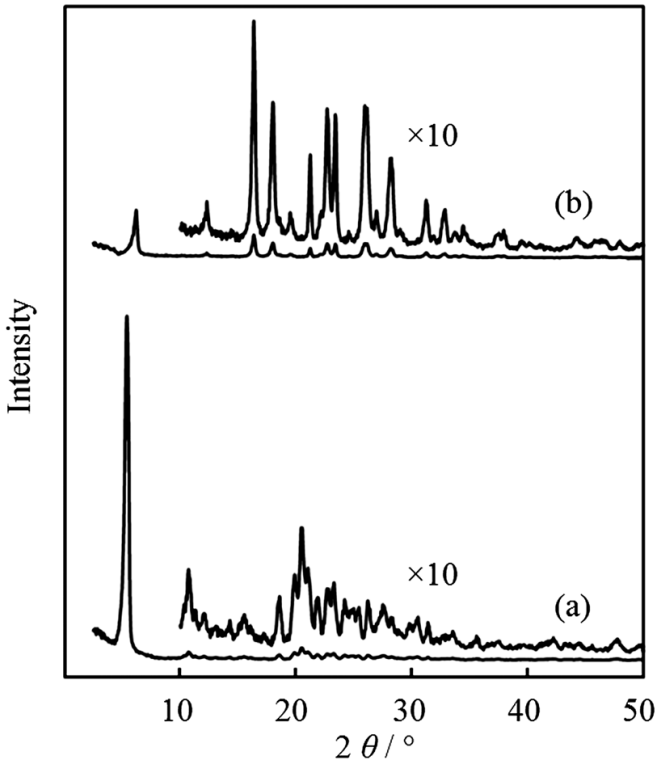

Fig. 3-1 XRD patterns of as-synthesized (a) HUS-7 (Sample 3) and (b) RUB-51 (Sample 6).

starting gel were critical factors for the selective synthesis of HUS-7. Toluene and hexane could also be employed instead of biphenyl, although the yields of HUS-7 were slightly lower (Samples 7 and 8). From these results, I concluded that a combination of BTMAOH with biphenyl allows me to effectively synthesize the novel layered silicate HUS-7 in high yield.

Fig. 3-1 shows the XRD pattern of as-synthesized HUS-7 (Sample 3). For a reference, the XRD pattern of RUB-51 (Sample 6) is also shown, because RUB-51 is synthesized using the same SDA (BTMA). The diffraction pattern of RUB-51 was consistent with that previously described in the literature.[42] On the other hand, the obtained HUS-7 was found to be a new type of layered silicate. Its crystal structure is discussed in the following section. As can be seen in Fig. 3-2, HUS-7 was formed as square plate-like particles, *ca*. 2.0 mm × 3.0 mm. Fig. 3-3(A) depicts the ^{13}C

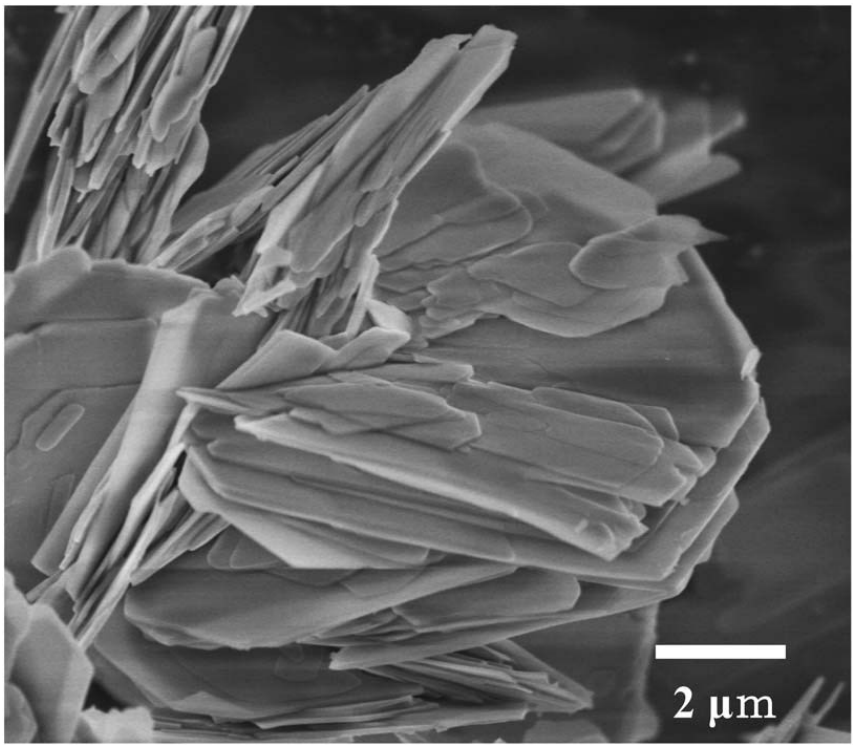

Fig. 3-2 SEM image of as-synthesized HUS-7 (Sample 3).

CP-MAS NMR spectrum of the as-synthesized HUS-7, which revealed the presence of several resonance peaks assigned to the BTMA cation. The peak at *ca*. 54.0 ppm was assigned to the three methyl groups attached to N, and the peak at *ca*. 71.3 ppm corresponded to the benzylic methylene group ($N–CH_2–$). The resonance peaks between 120 and 150 ppm were attributed to the phenyl groups. Surprisingly, no peaks assignable to the biphenyl molecules were observed. These results indicated that the BTMA cation with the C/N atomic ratio of 10 was the only organic species present in HUS-7. The presence of the BTMA cation was also confirmed by CHN analysis, producing a C/N atomic ratio of 9.7. The total amount of BTMA cation was approximately 29.4 wt%. The TG/DTA curves of HUS-7 are presented in Fig. 3-4. The thermal profiles were categorized into three zones: (I) 25–100 °C, (II) 100–350 °C, and (III) 350–700 °C. The first zone had an endothermic profile, which

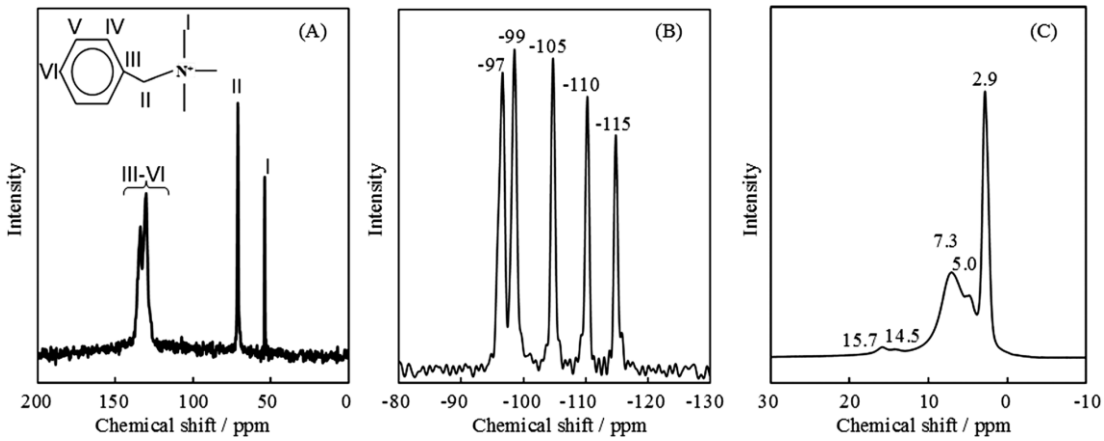

Fig. 3-3 (A) ^{13}C CP-, (B) ^{29}Si and (C) ^{1}H MAS NMR spectra of as-synthesized HUS-7 (Sample 3).

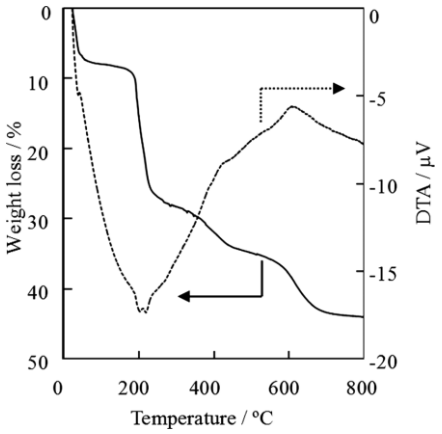

Fig. 3-4 TG/DTA curves of as-synthesized HUS-7 (Sample 3).

corresponded to the desorption of water adsorbed on the outer surfaces of the solid by weak interactions. The second zone also displayed an endothermic profile, which can probably be attributed to the desorption of water and/or the BTMA cations that interact with $SiOH/SiO^-$ groups in the interlayer. The third zone had an exothermic profile, which was assigned to the decomposition/oxidation of the BTMA cation and the oxidation of the carbonaceous materials that were generated by this decomposition. Based on these thermal profiles, the weight loss occurred between 100 and 700 °C and corresponded to the total amount of the organic moieties and water, which was about 35.8 wt%. Fig. 3-3(B) shows the ^{29}Si MAS NMR spectrum

of HUS-7. Q^3[(–SiO)$_3$Si–OH] and Q^4[(–SiO)$_4$Si] structures were clearly observed. The two resonance peaks at −97 and −99 ppm were assigned to the Q^3 structure, whereas the three resonance peaks at ca. −105, −110, and −115 ppm were assigned to the Q^4 structure. The resonance peak at −105 ppm was seemingly attributed to the Q^3 structure. However, this peak was assigned to the Q^4 structure by virtue of the ^{1}H–^{29}Si CP-MAS NMR measurements for different contact times. In the spectra, the intensities of the three resonance peaks at −105, −110, and −115 ppm were relatively elevated with increasing contact time as compared to those of the other two peaks. This finding indicates that the Si nuclei that resonated at −97 and −99 ppm were easily affected by the cross-polarization effect between ^{1}H and ^{29}Si nuclei, even if the contact time was short. Specifically, the Si nuclei of the latter two resonance peaks bear hydroxyl groups (–OH). The ratio of the Q^4/Q^3 peak intensities (1.43) suggested the existence of a large number of interlayer silanol groups. Fig. 3-3(C) shows the ^{1}H MAS NMR spectrum of HUS-7, in which one sharp and four broad resonance peaks were observed. The sharp peak at 2.9 ppm was assigned to the protons of the methyl groups of the BTMA cations. Two broad peaks at 5.0 and 7.3 ppm may be assigned to the protons of either the phenyl groups of the BTMA cations or the adsorbed hydrogen-bonded water molecules (SiOH/H_2O or H_2O/H_2O), respectively. The broad peaks at 14.5 and 15.7 ppm were attributed to silanol groups with strong hydrogen bonding (SiOH/SiO^-). These NMR results suggested the presence of a characteristic hydrogen bond between silanol groups on both sides of the interlayer or between adjacent intralayer silanol groups.

3.2. Crystal structure of HUS-7

Table 3-2. Conditions for the PXRD experiment and crystallographic information obtained therein for HUS-2.

Compound name	HUS-7
Estimated chemical formula	$Si_{40}O_{72}(OH)_{16}\cdot(C_{10}H_{16}N)_8\cdot(H_2O)_{23.7}$
*F*w	4176.244
Space group	*C2*/*c* (No. 15, setting no. 1)
a / nm	1.71112(3)
b / nm	0.73945(2)
c / nm	33.0249(2)
β / °	94.401(12)
Unit-cell volume / nm^3	4116.3(4)
Wavelength / nm	0.1540593 (λ = Cu Kα_1)
2*θ*range / °	3.0–100.1
Step size (2*θ*) / °	0.017368
Counting time per step/s	8111
Rietveld analysis	
Profile range in the unit of FWHM	12
Number of intensity data	5536
Number of contributing reflections	2199
Number of refined structural parameters	148
Number of background parameters	12
Number of nonlinear restraints	132
R_{wp} (Rietveld)	0.033
R_F (Rietveld)	0.012
R_B (Rietveld)	0.010
R_e (Rietveld)	0.017
wR_F (MPF)	0.016
wR_F (MPF)	0.015

The indexing of the reflections gave a monoclinic unit cell of a = 1.711 nm, b = 0.739 nm, c = 0.3303 nm, and β = 95.9° Reflection conditions derived from the indexed reflections were $h + k = 2n$ for hkl and $hk0$, h, l = 2n for $h0l$, k = 2n for $0kl$ and $0k0$, h = 2n for $h00$, and l = 2n for 00l, which gives the possible space group: *C*2*c* (no. 15, setting 1). $|F_{obs}|_2$ values of 1472 reflctions in the region d > 0.114 nm were extracted by the Le Bail method. The direct method analysis detected five Si and eleven O sites in a unit cell. The presence of five independent Si sites including three Q^4 and two Q^3 sites was consistent with the observation of five resonance peaks in the ^{29}Si MAS NMR spectrum (Fig. 3-3(B)). The layered framework composed of four-, five-, and sixmembered rings was clarified by the observed Si–O

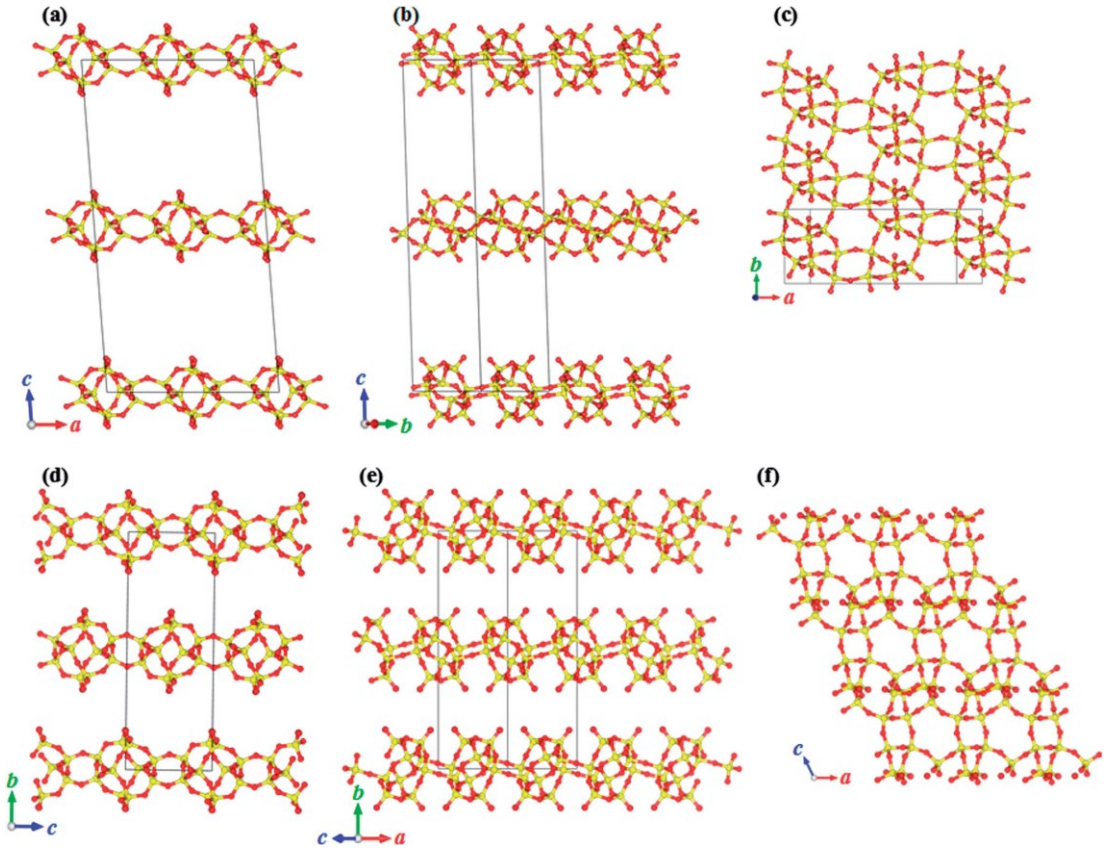

Fig. 3-5 Layered framework structure of HUS-7 determined by the direct method analysis along the (a) [010], (b) [□110], and (c) [001] directions and HUS-2 as described in ref. 26 along the (d) [100], (e) [101], and (f) [010] directions. The stacking period and interlayer distance of both layered silicates greatly vary.

connectivity. As shown in Fig. 3-5, the layered framework topology was identical to that of HUS-2, that is, the framework included the *bre* (10T)-type composite building unit (CBU).[43] However, the stacking sequence of the silicate layers in HUS-7 was different from that of HUS-2, namely, adjacent alternate layers of HUS-7 were shifted by 1/2 period along the *a*-axis in comparison with that of HUS-2 viewed from the [100] direction. The maximum interlayer distance was estimated to be *ca*. 1.73 nm, which was three times longer than HUS-2 (*ca*. 0.58 nm). The presence of a few atoms attributable to a BTMA cation or an adsorbed H_2O molecule was suggested in the interlayer. From the direct space method analysis, a double

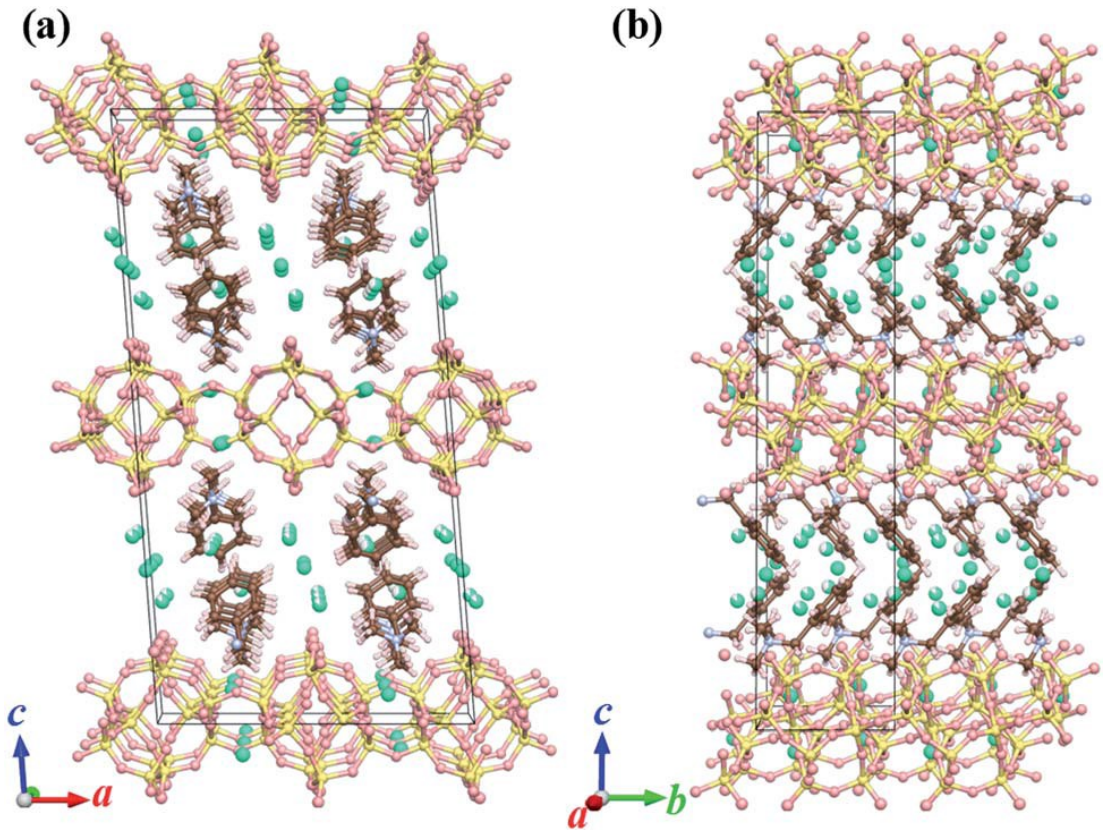

Fig. 3-6 Crystal structure model of HUS-7 determined by Rietveld analysis along the (a) [010] and (b) [100] directions.

BTMA layer, consisting of two different molecular orientations, was formed in the interlayer along the *c*-axis. Adjacent BTMA cations were perpendicular to the alternation along the *b*-axis viewed from the [100] direction. The $-(CH_2)N(CH_3)_3$ group of the BTMA cation faced the surface of the silicate layer. The major axis of the phenylene group in the BTMA molecule inclined to the *b*-axis direction, *ca*. 48.4° against the *a*–*b* plane. A one-dimensional nano-space between adjacent BTMA bridges was formed with an effective pore diameter of 0.35 nm × 0.79 nm (as can be seen in Fig. 3-6(a)). These findings, coupled with the results of the TG/DTA and ^{13}C MAS NMR measurements, showed the presence of BTMA cations in the interlayers. The preliminary MEM analysis could not reveal the presence of hydrogen bonds

between terminal oxygen sites (O9–O11), as was shown in HUS-2, whereas the presence of O–H···O bonds was detected in the ^{1}H MAS NMR spectra. The nearest atomic distance between neighboring silanol groups, l(O–O), was l(O9–O11) = 2.43(4) Å, which was in good agreement with the values of 2.46–2.50 Å according to a previous report,[44] estimated from the ^{1}H MAS NMR spectrum. Therefore, a minor hydrogen bond will be formed between O9 and O11 sites. Additionally, four localized electron densities were observed, which could be attributed to adsorbed H_2O molecules or OH^- anions (these sites are abbreviated as WO). Sites WO1 and WO2 were located in the one-dimensional nano-space. Site WO3 was located near the middle of the adjacent BTMA cation. Site WO4 was distributed near the center of the six-membered Si ring surrounded by four neighboring *bre*-type CBUs.

In the Rietveld analysis, the positions of the four H_2O sites were refined. Among them, site WO3 was found near one methyl group of the BTMA cation, suggesting that site WO3 would be the OH^- anion of the BTMA cation. Because the amount of site WO3 calculated from its occupancy did not coincide with that of BTMA, this site was assumed to be H_2O for convenience. Finally, the atomic coordinates of five Si sites, eleven O sites, ten C sites, one N site, sixteen H sites, and four WO sites were refined. The scattering amplitude of H was added to sites O9 and O11 in terminal silanol groups to maintain the charge balance. Fig. 3-6 shows the structural model of HUS-7 obtained by Rietveld analysis, viewed along the (a) [100] and (b) [010] directions.

The chemical formula of HUS-7 was estimated to be $Si_{40}O_{72}(OH)_{16}\cdot(C_{10}H_{16}N)_8\cdot(H_2O)_{23.7}$ according to the results of the structural refinement. The resulting organic content, which was calculated to be 28.8 wt%, was

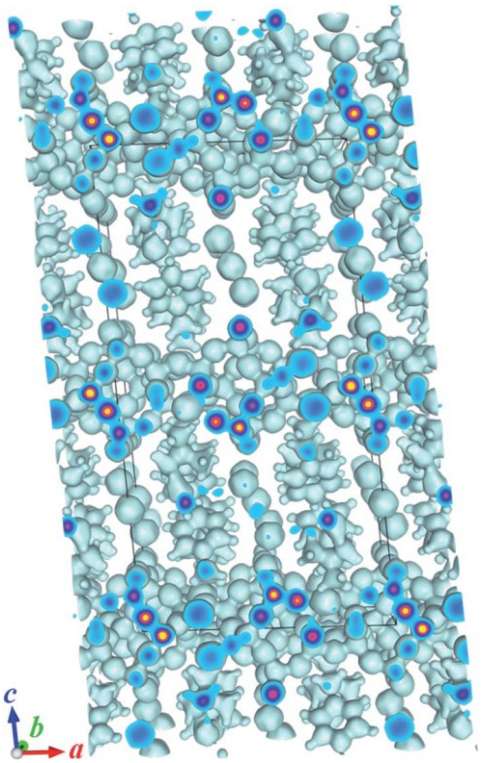

Fig. 3-7 An EDD image of HUS-7 obtained by MPF analysis: electron densities ($0.4 < x < 1.4$; $0.245 < y < 0.3$; $0.4 < z < 1.18$) viewed along the c-axis. Equi-surface level was set at 0.65e $Å^{-3}$. The spatial resolution was 170 × 74 × 330 pixels per unit cell.

in very good agreement with that determined by CHN analysis (ca. 29.4 wt%). The total amount of H_2O (including OH^-) was estimated to be 10.2 wt%. If it is supposed that HUS-7 changes to amorphous silica completely (*i.e.*, $Si_{40}O_{72}(OH)_{16}\cdot(C_{10}H_{16}N)_8\cdot(H_2O)_{23.7} \rightarrow Si_{40}O_{80}$), the total weight loss would be calculated to be 42.5 wt%, which is almost in agreement with the observed weight loss of 43.9 wt%by the TG profile. Although a small number of silanols might remain due to incomplete condensation, the TG result strongly supports the chemical formula estimated by the structural analysis. Thus, it was found that the results of the chemical analysis were in accordance with the chemical formula estimated by the structural analysis.

The average bond lengths *l*(Si–O) and bond angles φ(O–Si–O), which were close

to expected values, fell within the ranges 1.55–1.69 Å and 102.0–117.9°, respectively. Fig. 3-7 shows an EDD image of HUS-7. Because the EDD determined by MPF showed an ordered arrangement of BTMA in the interlayer, the BTMA molecules were believed to be cations. Furthermore, the molecular motion of BTMA was estimated to be considerably restricted. Final R-factors after the MPF analysis were sufficiently low: wR_F = 1.6% and R_F = 1.5%.

3.3. Adsorption tests

As described above, the interlayer of HUS-7 possesses unique spaces, which were composed of alternately and regularly located BTMA dimers and the silanol groups on the silicate layers. It has already been reported that layered silicates modified with two kinds of organic functional units showed selective and effective adsorption abilities as a result of the cooperative interaction between the substrate molecules and the two spatially arranged functional units.[45] In light of this, I investigated the adsorption of benzene and phenol, which are known water contaminants as well as important industrial commodity chemicals, on HUS-7 from single- and binary-component acetonitrile solutions. Fig. 3-8(A) shows the adsorption isotherms of benzene and phenol on HUS-7 from single-component acetonitrile solutions. HUS-7 hardly adsorbed benzene at any equilibrium concentrations. On the other hand, the adsorption isotherm of phenol on HUS-7 exhibited the H-type, according to the Giles classification,[46] suggesting strong interactions between HUS-7 and phenol molecules. The adsorption capacity of phenol on HUS-7 was estimated to be 0.60mmol g^{-1}. Fig. 3-8(B) depicts the adsorption isotherms of benzene and phenol on HUS-7 from a binary-component acetonitrile solution (benzene/phenol molar

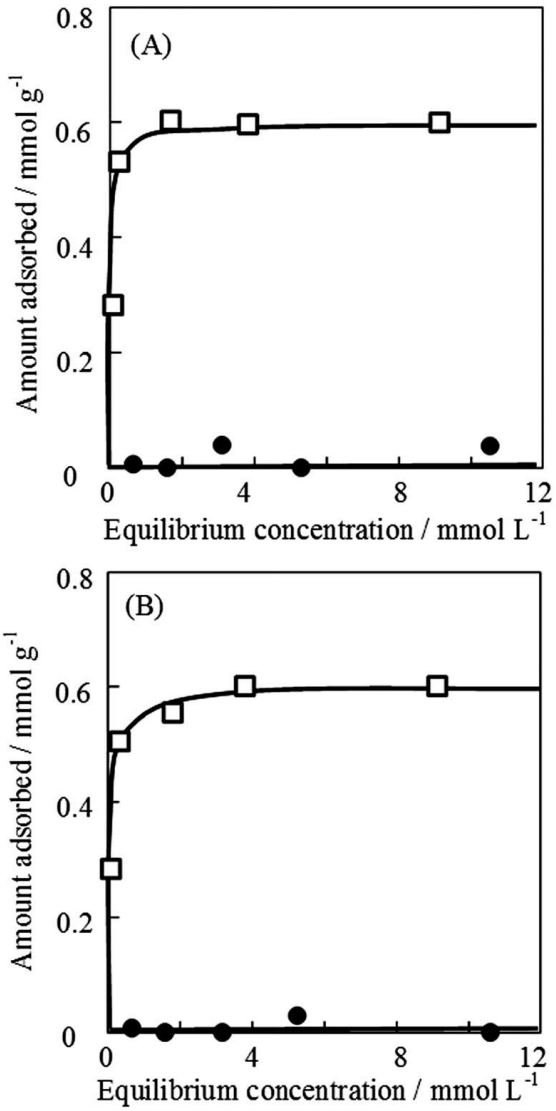

Fig. 3-8 Adsorption isotherms of (●) benzene and (□) phenol on HUS-7 from (A) single- and (B) binary-component acetonitrile solutions at room temperature.

ratio of 1). There were no differences in the adsorbed amounts of benzene and phenol between the single- and binary-component adsorption isotherms at any equilibrium concentrations. This clearly indicates that the presence of benzene did not disturb phenol adsorption on HUS-7.

To obtain information concerning organic molecules present in the interlayer space of HUS-7 after the adsorption experiment, ^{13}C CP-MAS NMR and UV-vis measurements were carried out. In the ^{13}C CP-MAS NMR spectrum of HUS-7

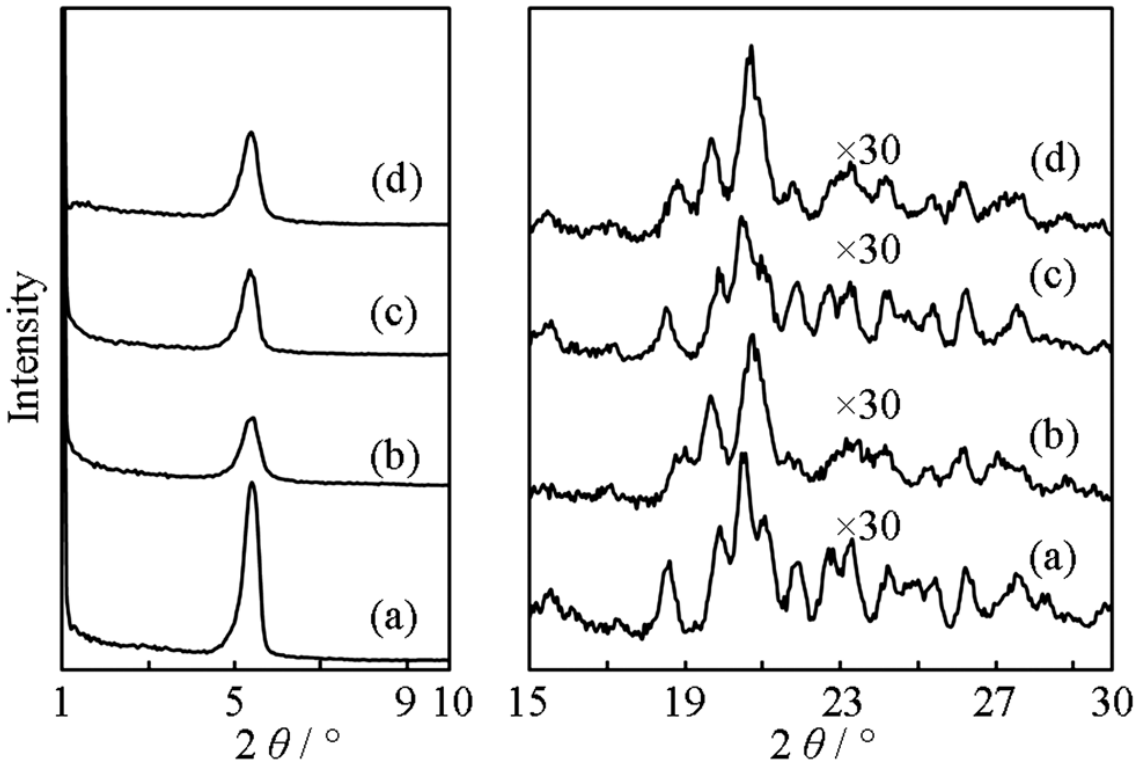

Fig. 3-9 XRD patterns of (a) as-synthesized HUS-7 and HUS-7s containing phenol (b) before and after washing with (c) water and (d) acetone.

treated with acetonitrile containing phenol, resonance peaks attributed to phenol at around 116 ppm were observed together with the peaks of BTMA cations, whereas no peaks assignable to benzene or acetonitrile were observed. The presence of phenol molecules as well as BTMA cations was also confirmed by UV-vis analysis. The UV-vis spectrum of the parent HUS-7 showed two absorption bands around 262 and 212 nm, which were indicative of the presence of BTMA cations. On the other hand, HUS-7 after phenol adsorption from acetonitrile solution gave a strong absorption band around 284 nm together with these two peaks (the band at 262 was a shoulder peak). The band at 284 nm might be due to phenol molecules in the interlayer of HUS-7 with the BTMA cations. Namely, the adsorption of phenol was expected to occur through the exchange of water molecules in the interlayer.

To clarify the reversibility of the adsorption/desorption of phenol molecules, the HUS-7 containing phenol was washed with water, and then, phenol adsorption was carried out again. For comparison, washing with acetone was also performed Fig. 9 shows XRD patterns of the as-synthesized HUS-7 and the HUS-7s containing phenol before and after washing with water and acetone, respectively. The XRD patterns of the HUS-7 containing phenol showed a different peak pattern at 2θ = 15–30° compared with the as-synthesized HUS-7, while the basal spacing (2θ = 5.4°) was not changed. This strongly indicated that the interlayer distance did not change and the regularity of the conformation of interlayer cations was only changed by insertion of phenol into the interlayer. After the HUS-7 containing phenol was washed with water, the XRD pattern was consistent with that of the as-synthesized HUS-7, suggesting the removal of phenol molecules from the interlayer. However, the acetone wash did not affect the XRD pattern, indicating no removal of phenol molecules. To confirm the removal of phenol molecules from the interlayer by washing with water, the ^{13}C CP-MAS NMR spectrum of HUS-7 after washing with water was measured. The resonance peaks around 116 ppm attributed to phenol completely disappeared, whereas the peaks due to the BTMA cation were clearly observed.

Next, I checked the possibility of reuse. The adsorption of phenol was again carried out using the HUS-7 washed with water. The amount of re-adsorbed phenol (0.61 mmol g^{-1}) was consistent with that (0.60 mmol g^{-1}) of the as-synthesized HUS-7. This strongly indicated that the selective adsorption of phenol on HUS-7 proceeds by replacing the interlayer water molecules with phenol. It is also suggested that the crystal structure of HUS-7 containing BTMA cation dimers in the

interlayer can flexibly change during the phenol adsorption/desorption process. Taking into account the fact that the adsorption of phenol did not occur on RUB-51, which also has BTMA cations in the interlayer space, the unique crystal structure of HUS-7 composed of the dimers of BTMA cations and surface silanol groups plays an important role in the selective adsorption of phenol. The unique adsorption ability of HUS-7 might be applied to the partial oxidation reaction of benzene to phenol. If HUS-7 promptly and selectively captures the product phenol from the reaction system, overoxidation reactions such as the oxidation of phenol into hydroxyphenols and CO_2 can be prevented.[47] I am now investigating this possibility.

4. Conclusions

I succeeded in synthesizing a new type of layered silicate, HUS-7, from a SiO_2–BTMAOH–NaOH–biphenyl–H2O system. HUS-7 had a layered structure, which was composed of four-, five-, and six-membered rings. Its framework topology was partially similar to that of a HEU-type zeolite, including the *bre* (10T)-type composite building unit. BTMA cations used as SDAs were incorporated as dimers with unique regularity in the interlayers. Double silicate layers were present in each unit cell. The effective interlayer distance was estimated to be ca. 1.73 nm. I also investigated the adsorption of benzene and phenol on HUS-7 from single- and binary-component acetonitrile solutions; HUS-7 selectively and effectively adsorbed phenol from the acetonitrile solutions. It was also found that HUS-7 repeatedly adsorbed phenol after washing with water. The XRD, ^{13}C CP-MAS NMR, and UV-vis results of HUS-7 before and after the adsorption

experiments revealed that the adsorption of phenol occurred through the exchange of water molecules in the interlayer.

References

1 N. Takahashi and K. Kuroda, *J. Mater. Chem*., 2011, **21**, 14336.

2 (a) M. Ogawa and K. Kuroda, *Bull. Chem. Soc. Jpn*., 1997, **70**, 2593; (b) T. Okada, Y. Ide and M. Ogawa, *Chem.–Asian J*., 2012, **7**, 1980.

3 T. Ikeda, Y. Akiyama, Y. Oumi, A. Kawai and F. Mizukami, *Angew. Chem., Int. Ed*., 2004, **43**, 4892.

4 B. Marler and H. Gies, *Eur. J. Mineral*., 2012, **24**, 405.

5 S. Zanardi, A. Alberti, G. Cruciani, A. Corma, V. Fornes and M. Brunelli, *Angew. Chem., Int. Ed*., 2004, **43**, 4933.

6 B. Marler, M. A. Camblor and H. Gies, *Microporous Mesoporous Mater*., 2006, **90**, 87.

7 B. Marler, N. Stroter and H. Gies, *Microporous Mesoporous Mater*., 2005, **83**, 201.

8 Y. Oumi, T. Takeoka, T. Ikeda, T. Yokoyama and T. Sano, *New J. Chem*., 2007, **31**, 593.

9 T. Ikeda, Y. Oumi, T. Takeoka, T. Yokoyama, T. Sano and T. Hanaoka, *Microporous Mesoporous Mater*., 2008, **110**, 488.

10 Y. Wang, B. Marler, H. Gies and U. Muller, *Chem. Mater*., 2005, **17**, 43.

11 T. Moteki, W. Chaikiiisilp, A. Shimojima and T. Okubo, *J. Am. Chem. Soc*., 2008, **130**, 15780.

12 T. Ikeda, S. Kayamori and F. Mizukami, *J. Mater. Chem*., 2009, **19**, 5518.

13 J. Song and H. Gies, *Stud. Surf. Sci. Catal*., 2004, **154A**, 295.

14 B. Marler, Y. Wang, H. Song and H. Gies, in *Abstracts of Papers, 15th International Zeolite Conference*, Beijing, China, August 12–17, 2007, p. 599.

15 A. Burton, R. J. Accardi, R. F. Lobo, M. Falcioni and M. W. Deem, *Chem. Mater*., 2000, **12**, 2936.

16 D. L. Dorset and G. J. Kennedy, *J. Phys. Chem. B*, 2004, **108**, 15216.

17 L. M. Knight, M. A. Miller, S. C. Koster, M. G. Gatter, A. I. Benin, R. R. Willis, G. J. Lewis and R. W. Broach, *Stud. Surf. Sci. Catal*., 2007, **170A**, 338.

18 A. J. Blake, K. R. Franklin and B. M. Lowe, *J. Chem. Soc., Dalton Trans*., 1988, 2513.

19 S. Vortmann, J. Rius, S. Siegmann and H. Gies, *J. Phys. Chem. B*, 1997, **101**, 1292.

20 Y. X. Wang, H. Gies and J. H. Lin, *Chem. Mater*., 2007, **19**, 4181.

21 U. Oberhagemann, P. Bayat, B. Marler, H. Gies and J. Rius, *Angew. Chem., Int. Ed. Engl*., 1996, **35**, 2869.

22 T. Yanagisawa, T. Shimizu, K. Kuroda and C. Kato, *Bull. Chem. Soc. Jpn*., 1990, **63**, 988.

23 S. Inagaki, Y. Fukushima and K. Kuroda, *J. Chem. Soc., Chem. Commun*., 1993, 680.

24 S. Inagaki, A. Koiwai, N. Suzuki, Y. Fukushima and K. Kuroda, *Bull. Chem. Soc. Jpn*., 1996, **69**, 1449.

25 T. Kimura, T. Kamata, M. Fuziwara, Y. Takano, M. Kaneda, Y. Sakamoto, O. Terasaki, Y. Sugahara and K. Kuroda, *Angew. Chem., Int. Ed*., 2000, **39**, 3855.

26 T. Ikeda, Y. Oumi, K. Honda, T. Sano, K. Momma and F. Izumi, *Inorg. Chem*., 2011, **50**, 2294.

27 N. Tsunoji, T. Ikeda, Y. Ide, M. Sadakane and T. Sano, *J. Mater. Chem*., 2012, **22**, 13682.

28 (a) Y. Ide, M. Torii, N. Tsunoji, M. Sadakane and T. Sano, *Chem. Commun*., 2012, **48**, 7073; (b) K. Honda, Y. Ide, N. Tsunoji, M. Torii, M. Sadakane and T. Sano, *Bull. Chem. Soc. Jap*., 2014, **1**, 160.

29 N. Tsunoji, Y. Ide, M. Torii, M. Sadakane and T. Sano, *Chem. Lett*., 2013, **42**, 244.

30 N. Tsunoji, M. Fukuda, K. Yoshida, Y. Sasaki, T. Ikeda, Y. Ide, M. Sadakane and T. Sano, *J. Mater. Chem. A*, 2013, **1**, 9680.

31 A. Altomare, N. Corriero, C. Cuocci, A. Moliterni and R. J. Rizzi, *J. Appl. Crystallogr*., 2013, **46**, 779.

32 A. Le Bail, H. Duroy and J. L. Fourquet, *Mater. Res. Bull*., 1988, **23**, 447.

33 V. Favre-Nicolin and R. J. Cerny, *J. Appl. Crystallogr*., 2002, **35**, 734.

34 F. Izumi and K. Momma, *Solid State Phenom*., 2007, **130**, 15.

35 K. Momma, T. Ikeda, A. A. Belik and F. Izumi, *Powder Diffr*., 2007, **28**, 184.

36 K. Momma and F. J. Izumi, *J. Appl. Crystallogr*., 2011, **44**, 1272.

37 H. Jon, S. Takahashi, H. Sasaki, Y. Oumi and T. Sano, *Microporous Mesoporous Mater*., 2008, **113**, 56.

38 A. Yashiki, K. Honda, A. Fujimoto, S. Shibata, Y. Ide, M. Sadakane and T. Sano, *J. Cryst. Growth*, 2008, **113**, 56.

39 M. Itakura, T. Inoue, A. Takahashi, T. Fujitani, Y. Oumi and T. Sano, *Chem. Lett*., 2008, **37**, 908.

40 S. Arazaki, T. Kusuno, T. Sano, Y. Kawakami and H. Shoji, *Nippon Kagaku Kaishi*, 1995, **8**, 606.

41 M. J. Kim and R. Ryoo, *Chem. Mater*., 1999, **11**, 487.

42 Z. Li, B. Marler and H. Gies, *Chem. Mater*., 2008, **20**, 1896.

43 *Atlas of Zeolite Framework Types*, ed. W. M. Meier and D. H. Olson, Elsevier, Amsterdam, 6th edn, 2007, ch. Baerlocher, p. 374.

44 X. Xue and M. Kanzaki, *J. Phys. Chem. B*, 2007, **111**, 13156.

45 Y. Ide, S. Iwasaki and M. Ogawa, *Langmuir*, 2011, **27**, 2522.
46 C. H. Giles, T. H. MacEwan, S. N. Nakhwa and D. Smith, *J. Chem. Soc*., 1960, 3973.
47 Y. Ide, M. Torii and T. Sano, *J. Am. Chem. Soc*., 2013, **135**, 11784.

Chapter 4

Molecular recognitive adsorption of aqueous propionic acid on Hiroshima University Silicate-2 (HUS-2)

3. Introduction

The concentration of ions and molecular species from water on solid surfaces is a topic covering a wide variety of scientific and practical applications for such purposes as the removal of toxic compounds and the collection of noble elements. Adsorption-based processes are among the most promising strategies; therefore, designing adsorbents has been actively conducted. Layered materials have a strong historical background in adsorbents because of i) the large surface area derived from well-defined nanostructures composed of nanosheets, ii) chemical and thermal stabilities, and iii) surface tunable properties.[1] The modification of layered materials via ion exchange,[2] grafting,[3] and pillaring[4] is useful in designing molecular recognition abilities. However, these methods often require step-by-step operations, which take a lot of time and labor. On the other hand, there are several literature reports on the successful concentration of a particular species on pristine layered materials;[5] for example, the selective and effective adsorption of Zn^{2+} from seawater on a layered alkali silicate (magadiite, $Na_2Si_{14}O_{29}$) via cation exchange with the interlayer Na^+ has been reported.[5d]

Recently, I reported the synthesis of a novel layered silicate, Hiroshima

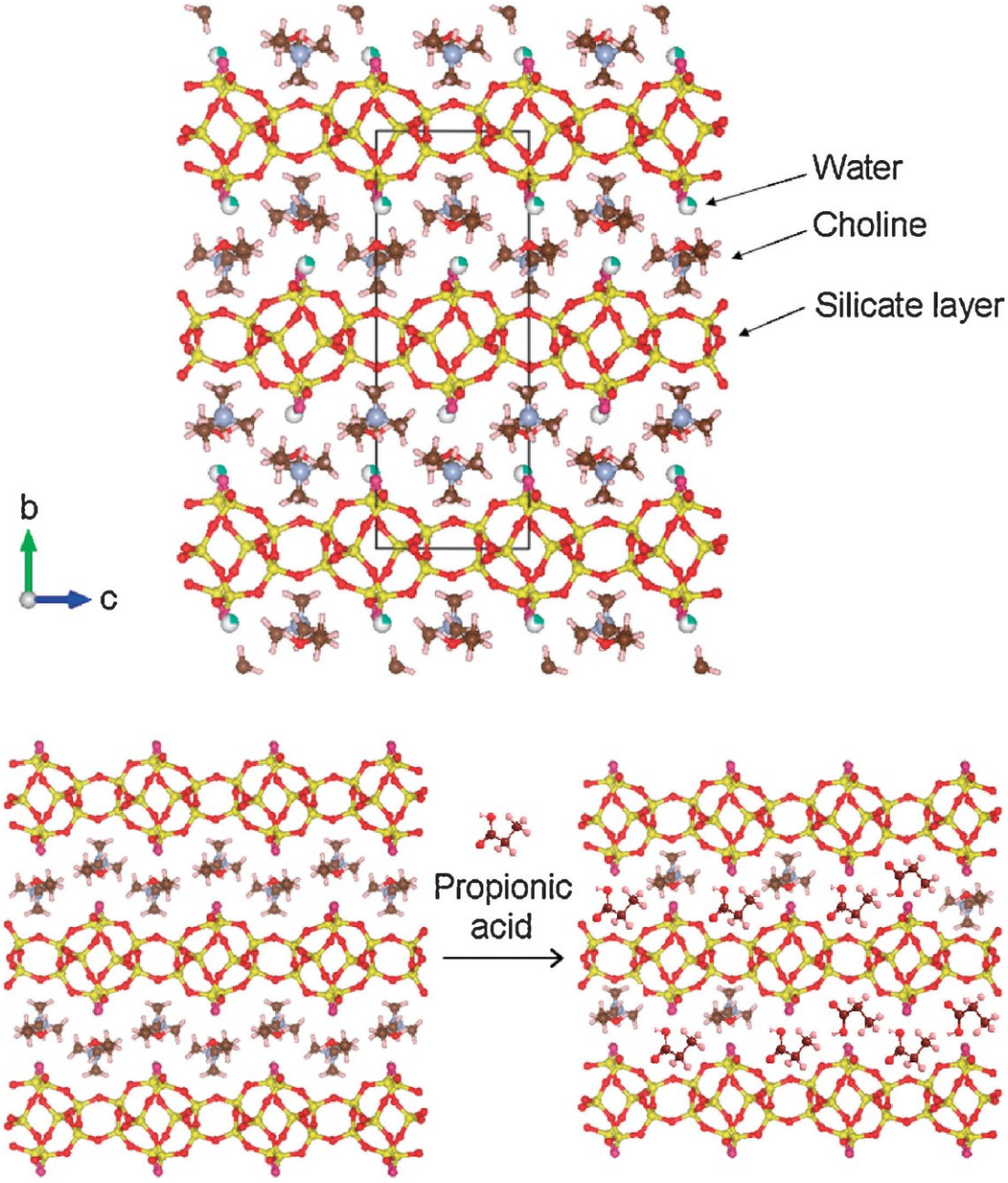

Fig. 4-1 (top) Structure of HUS-2 and (bottom) schematic drawing of the intercalation of propionic acid into HUS-2.

University Silicate-2 (HUS-2, $Si_{20}O_{40}(OH)_4 \cdot 4[C_5H_{14}NO]\cdot nH_2O$), composed of silicate layers and chargecompensating interlayer choline cations (Figure 4-1, top).[6] In this work, I report the molecular recognitive adsorption of propionic acid (which is a known water contaminant[7] but an important commodity chemical in industry[8])

on HUS-2 from water. I examined the adsorption of three carboxylic acids, formic, acetic, and propionic acids, on HUS-2 from water, since these molecules coexisted in wastewater and possibly competed because of their structural similarities.

2. Experimental

2.1. Synthesis of layered silicates HUS-2

Layered silicate HUS-2 was synthesized by the hydrothermal treatment of starting gels containing fumed silica (Cab-O-Sil M5, CABOT Co.), choline hydroxide (48–50 wt%, Aldrich), sodium hydroxide (>99%, High Purity Chemical Inc., Japan), and distilled water. The starting gel, which had the chemical composition SiO_2:0.4 choline hydroxide:0.2 NaOH:5.5 H_2O, was transferred into a Teflon-lined stainless steel vessel and heated under static conditions at temperatures at 150 °C for 7 d. The solid product that was obtained was separated by centrifugation and washed with distilled water. It was then dried at 70 °C overnight.

2.2. Adsorption test

Adsorption test was conducted by mixing 100 mg of HUS-2 (or magadiite) and an aqueous solution (20 mL) of formic, acetic, or propionic acid or their aqueous mixture at room temperature for 3 d (the concentration of carboxylic acids: RCOOH/$Si_{20}O_{40}(OH)_4$ molar ratio = 0.320). HUS-2 treatment with carboxylic acids was conducted using an aqueous solution of carboxylic acids with RCOOH/$Si_{20}O_{40}(OH)_4$ molar ratio of 20. The pH values of the starting solution were

3.6–2.7, 4.0–3.2, or 4.1–3.2 for aqueous solutions of formic, acetic, or propionic acid, respectively, and 3.5–2.8 for their aqueous mixtures.

2.3. Characterization

Powder X-ray diffraction (XRD) patterns of the solid products were collected using a powder X-ray diffractometer (Rigaku, MiniFlex) with graphite-monochromatized Cu Kα radiation at 30 kV and 15 mA. ^{1}H MAS NMR spectra were measured with a spinning frequency of 20 kHz and a single pulse sequence operated at 599.85 MHz. ^{1}H–^{13}C CP MAS NMR spectra were also measured at a spinning frequency of 20 kHz, a 90° pulse length of 2.2 ms, and a cycle delay of 100 s. The ^{1}H and ^{13}C chemical shifts were referenced to adamantane and hexamethylbenzene respectively. Elemental analysis was carried out using a PerkinElmer 2400 II CHN Analyzer at the Natural Science Center for Basic Research and Development (N-BARD), Hiroshima University.

3. Results and discussion

Figure 4-2a shows the adsorption isotherms of formic, acetic, and propionic acids on HUS-2 from water. The adsorption isotherm of propionic acid exhibited the C type, according to the Giles classification[9] and showed relatively strong interactions between HUS-2 and propionic acid. On the other hand, formic or acetic acid was hardly adsorbed on HUS-2 at lower concentration levels. Depicted in Figure 4-2b are the adsorption isotherms of the three carboxylic acids on HUS-2 from an aqueous mixture. It should be noted here that the presence of formic and acetic acids does not

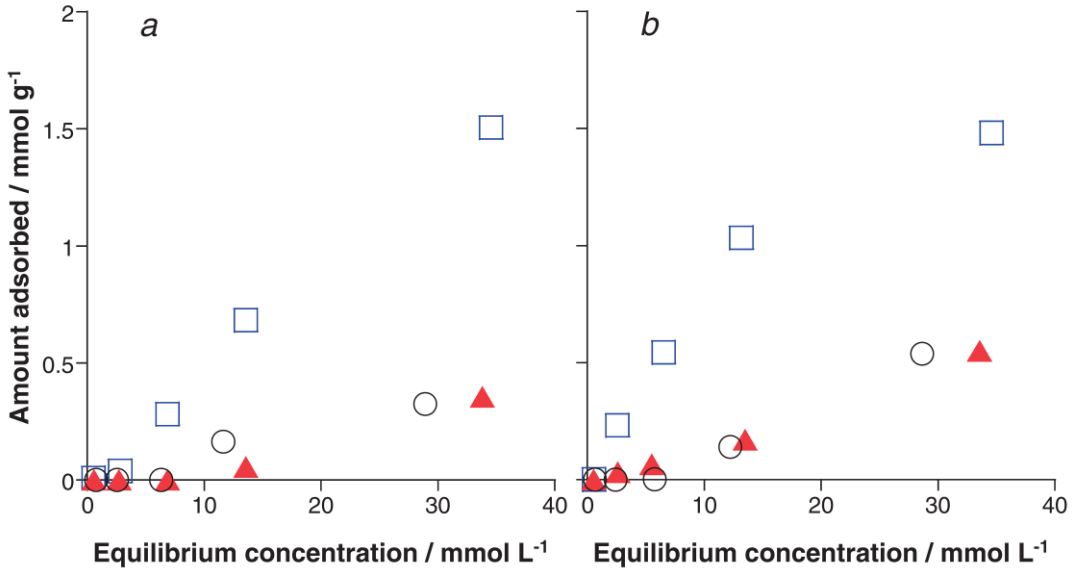

Fig. 4-2 Adsorption isotherms of (○) formic acid, (▲) acetic acid , and (□) propiocnic acid on HUS-2 from (a) water and (b) their aqueous mixture.

disturb propionic acid adsorption on HUS-2, which is confirmed by the L-type adsorption[9] of propionic acid from the aqueous mixture with formic and acetic acids. The change of propionic acid adsorption from the C type to the L type indicates that interactions between propionic acid and HUS-2 become stronger when formic and acetic acids are present,[9] although it is difficult to explain the phenomenon (the difference between the solubility of propionic acid in pure water and in the aqueous mixture with formic and acetic acids may be involved). The adsorption capacity of propionic acid on HUS-2 was estimated to be >1.5mmol g^{-1}, which was comparable to that (ca. 2 mmol g^{-1}) on organic resins.[10] Selective and effective adsorption of aqueous propionic acid on HUS-2 was, therefore, shown.

The state and the location of propionic acid adsorbed on HUS-2 were investigated. Shown in Figure 4-3 are the ^{13}C CP/MAS NMR spectra of HUS-2 and HUS-2 treated with an aqueous solution of the three carboxylic acids. In the spectrum of the

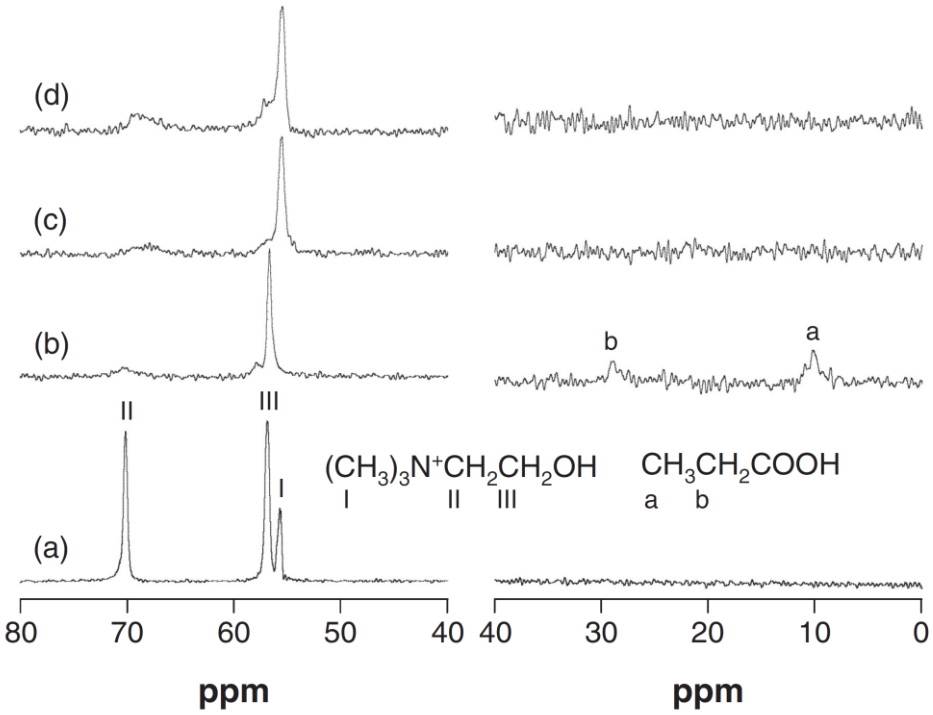

Fig. 4-3 ^{13}C CP/MAS NMR spectra of (a) HUS-2 and HUS-2 treated with an aqueous solution of (b) propionic acid, (c) acetic acid, and (d) formic acid.

propionic acid-treated HUS-2, signals from propionic acid were observed, and the positions of these signals were slightly shifted from those observed in the liquid state (data not shown), implying intercalation of propionic acid into HUS-2. Signals for the interlayer choline cations, which appear in the spectrum of pristine HUS-2, were also observed, indicating that part of the interlayer choline remained. From the N content (2.1 wt%) of the elemental analysis of the propionic acid-adsorbed HUS-2 with the largest amount (ca. 1.5mmol g^{-1}) of adsorbed propionic acid in Figure 4-2a, the composition of the product was determined to be $Si_{20}O_{40}(OH)_4 \cdot 1.4[H+] \cdot 2.6[C_5H_{14}NO] \cdot 2.6\text{-}[C_3H_6O_2]$ (H^+ exists as SiOH). Therefore, when mixed with aqueous propionic acid, HUS-2 probably desorbed the interlayer choline upon proton exchange (conversion of the surface SiO^- group to an SiOH

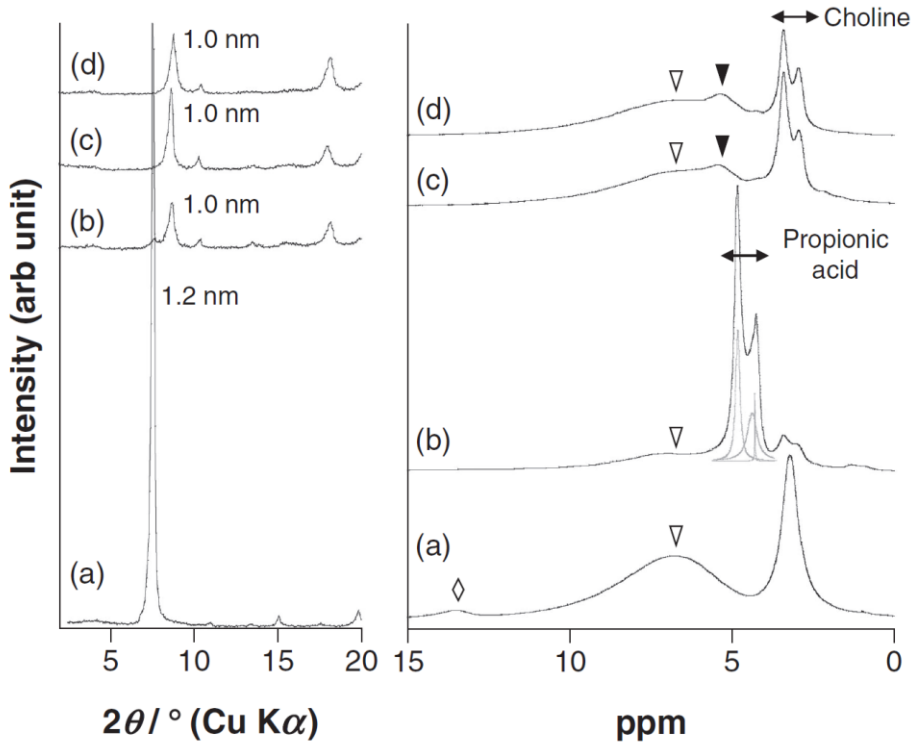

Fig. 4-4 (left) XRD patterns and (right) ^{1}H MAS NMR spectra of (a) HUS-2 and HUS-2 treated with an aqueous solution of (b) propionic acid, (c) acetic acid, and (d) formic acid.

group, which will be confirmed below) and then adsorbed propionic acid by size-matching with the interlayer pores and hydrogen-bonding interactions with the surface SiOH (Figure 4-1, bottom).[11] On the other hand, in the case of treatment with formic or acetic acid, signals associated with the carboxylic acids were not clearly detected in the ^{13}C CP MAS NMR spectra (Figures 4-3c and d). Taking into account the elemental analyses (data not shown) of formic and acetic acid-treated HUS-2, the treatment of HUS-2 with aqueous formic or acetic acid hardly causes intercalation of the carboxylic acid but causes replacement of the interlayer cholines with protons (the change in the signals of choline after treatment with formic or acetic acid is presumably caused by the change in the arrangement of cholines upon proton exchange and hydration of the interlayer spaces).

The mechanism of the successful molecular recognition of aqueous propionic acid by HUS-2 was discussed on the basis of comparison of the structure before and after adsorption. Figure 4-4 (left) shows the XRD patterns of HUS-2 before and after treatment with an aqueous solution of formic, acetic, and propionic acids. The basal spacings of all the products were identical (1.0 nm), although only propionic acid was effectively intercalated into HUS-2. In the XRD pattern at the higher 2θ region of the propionic acid-treated HUS-2, the peaks attributed to the (121), (131), and (180) lattice planes of HUS-2 were observed (data not shown), confirming that the structural regularity of HUS-2 is retained after the intercalation of propionic acid. Figure 4-4 (right) compares the 1HMASNMR spectrum of HUS-2 to those of HUS-2 treated with the three carboxylic acids. HUS-2 exhibited two broad peaks at 13.5 and 6.7 ppm from hydrogen bonds between SiO^- and SiOH and those between SiOH and SiOH (or H_2O), respectively.[6] The former signal was hardly detected after the carboxylic acids treatment, since the SiO^- group was converted to an SiOH group by proton exchange. In the spectrum of formic or acetic acidtreated HUS-2, a new signal appeared at 5.4 ppm. Peaks resulting from hydrogen bonding of silanol groups are known to shift downfield with a decrease in the adjacent O–O distance,[12] and then the new signal is assigned to a hydrogen bond between SiOH with an O–O atomic distance shorter than that observed at 6.7 ppm.[13h] The new signal was not detected in the spectrum of HUS-2 treated with propionic acid, which was confirmed after deconvolution of the peaks from propionic acid at around 5 ppm (Figure 4-4, left, b).

Moreover, in the XRD patterns of HUS-2 and the carboxylic acids-treated HUS-2 after calcination at 450 °C (Figure 4-5), crystallized products were formed when

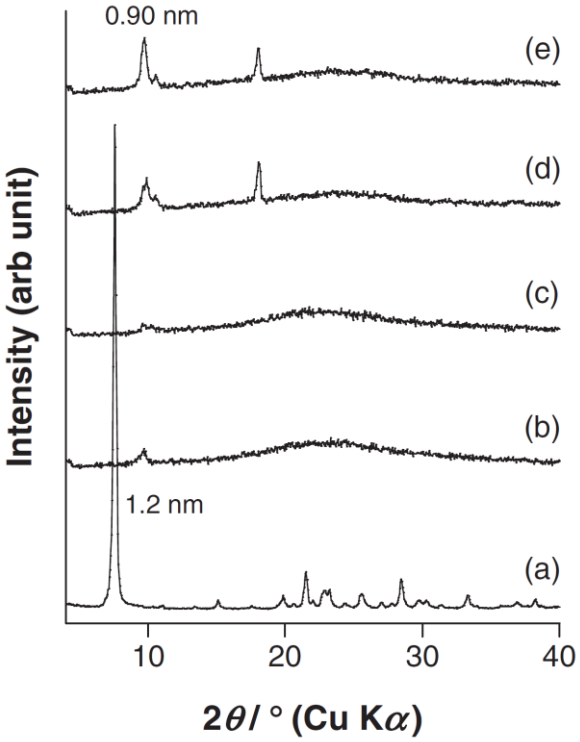

Fig. 4-5 XRD patterns of (a) HUS-2 and calcined products at 450 ℃ of (b) HUS-2 and HUS-2 treated with an aqueous solution of (c) propionic acid, (d) acetic acid, and (e) formic acid.

formic and acetic acids were used; on the other hand, pristine HUS-2 and the propionic acid-treated HUS-2 gave considerably lower-crystalline products after calcination. All the results suggest that the intercalation of propionic acid, which can fit over the interlayer pores of HUS-2, inhibits the translation of the neighboring silicate layers along the *ac* plane (Figure 4-1, bottom); in contrast, formic or acetic acid treatment of HUS-2 causes the shift of the neighboring silicate layers to give crystallized products after dehydration and condensation of silanol groups on the neighboring silicate layers. In some studies on zeolite synthesis through topotactic condensation of layered silicates,[13] it is considered that the intercalation of organic species such as acetic acid into layered silicates is an essential step to shift the neighboring layers along a direction parallel to the silicate layers and to position

silanol groups so that they can react to bridge the neighboring layers. For example, Okubo and co-workers have reported that acetic or propionic acid-treated RUB-15 gives well-crystallized sodalite after calcination and speculated that the intercalation of a carboxylic acid that can fit over the sodalite half-cups of RUB-15 moves the single silicate layers along a direction parallel to the layers.[13i] For HUS-2, although acetic acid (or formic acid) cannot adsorb on the interlayer spaces, the treatment leads to the lateral shift; the occluded propionic acid inhibits the lateral shift. The differences among the pK_a values of formic, acetic, and propionic acids (3.8, 4.8, and 4.9, respectively) were not a key factor for selective propionic acid adsorption on HUS-2, since the pH of the starting solution used for the present adsorption tests was considerably lower than the pKa of the carboxylic acids.

Magadiite, which is a naturally occurring Na-type layered silicate and has interlayer silanol groups, adsorbed formic and acetic acids, as well as propionic acid, from the aqueous mixture. This result shows the merit of HUS-2 in concentrating propionic acid from water. In the XRD patterns of magadiite treated with aqueous solutions of formic, acetic, and propionic acids, the basal spacing of the products increased depending on the size of the carboxylic acids, and all the products maintained hkl diffraction peaks characteristic of pristine magadiite at 2θ = 20–30°, implying that all the carboxylic acids intercalated without the lateral shift of the neighboring silicate layers. I assume that magadiite, the structure of which is not known, has an interlayer structure that can occlude the three carboxylic acids.

4. Conclusions

I reported the effective and selective adsorption of propionic acid on HUS-2 (Hiroshima University Silicate-2) from an aqueous mixture with formic and acetic acids. This phenomenon was explained by suggesting that propionic acid could fit over the interlayer structure. The present result motivates me to look at the structures of existing layered materials or synthesize new layered materials with different structures and thus open a door to finding the molecular recognition abilities of pristine layered materials simply and rationally.

References

1 T. Okada, Y. Ide, M. Ogawa, *Chem. –Asian J*. 2012, **7**, 1980.

2 (a) M. A. M. Lawrence, R. K. Kukkadapu, S. A. Boyd, *Appl. Clay Sci*. 1998, **13**, 13; (b) Q. Wei, T. Nakato, *Microporous Mesoporous Mater*. 2006, **96**, 84; (c) Y. Ide, Y. Nakasato, M. Ogawa, *J. Am. Chem. Soc.* 2010, **132**, 3601; (d) T. Okada, T. Matsutomo, M. Ogawa, *J. Phys. Chem. C* 2010, **114**, 539.

3 (a) J. W. Johnson, A. J. Jacobson, W. M. Butler, S. E. Rosenthal, J. F. Brody, J. T. Lewandowski, *J. Am. Chem. Soc*. 1989, **111**, 381; (b) G. Cao, T. E. Mallouk, *Inorg. Chem.* 1991, **30**, 1434; (c) M. Ogawa, S. Okutomo, K. Kuroda, *J. Am. Chem. Soc*. 1998, **120**, 7361; (d) D. Mochizuki, S. Kowata, K. Kuroda, *Chem. Mater*. 2006, **18**, 5223; (e) Y. Ide, M. Ogawa, *Angew. Chem., Int. Ed*. 2007, **46**, 8449; (f) Y. Ide, S. Iwasaki, M. Ogawa, *Langmuir* 2011, **27**, 2522; (g) Y. Ide, N. Kagawa, M. Itakura, I. Imae, M. Sadakane, T. Sano, *ACS Appl. Mater. Interfaces* 2012, **4**, 2186.

4 (a) T.W.Kim, S.-J. Hwang, S. H. Jhung, J.-S. Chang, H. Park, W. Choi, J. H. Choy, *Adv. Mater*. 2008, **20**, 539; (b) Y. Ide, M. Matsuoka, M. Ogawa, *J. Am. Chem. Soc*. 2010, **132**, 16762.

5 (a) Y. Komatsu, Y. Fujiki, *Chem. Lett*. 1980, 1525; (b) S. Komarneni, R. Roy, *Science* 1988, **239**, 1286; (c) R. Chitrakar, S. Tezuka, J. Hosokawa, Y. Makita, A. Sonoda, K. Ooi, T. Hirotsu, *J. Colloid Interface Sci*. 2010, **349**, 314; (d) Y. Ide, N. Ochi, M. Ogawa, *Angew. Chem., Int. Ed*. 2011, **50**, 654.

6 N. Tsunoji, T. Ikeda, Y. Ide, M. Sadakane, T. Sano, *J. Mater. Chem*. 2012, **22**, 13682.

7 S.H.Al-Lahham, M. P. Peppelenbosch, H. Roelofsen, R. J. Vonk, K. Venema, Biochim. Biophys. *Acta, Mol. Cell Biol. Lipids* 2010, **1801**, 1175.

8 M.V.Kirillova, M. L. Kuznetsov, J. A. L. da Silva, M. F. C. G. da Silva, J. J. R. F. da Silva, A. J. L. Pombeiro, *Chem. Eur. J*. 2008, **14**, 1828.

9 C. H. Giles, T. H. MacEwan, S. N. Nakhwa, D. Smith, *J. Chem. Soc.* 1960, **111**, 3973.

10 H. Uslu, İ. İnci, Ş. S. Bayazit, G. Demir, *Ind. Eng. Chem. Res*. 2009, **48**, 7767.

11 (a) M. Tagaya, M. Ogawa, *Chem. Lett*. 2006, **35**, 108; (b) Y. Ide, M. Torii, N. Tsunoji, M. Sadakane, T. Sano, *Chem. Commun*. 2012, **48**, 7073.

12 (a) X. Xue, M. Kanzaki, *J. Phys. Chem. B* 2007, **111**, 13156; (b) T. Ikeda, Y. Oumi, K. Honda, T. Sano, K. Momma, F. Izumi, *Inorg. Chem*. 2011, **50**, 2294.

13 (a) R. Millini, G. Perego, W. O. Parker, Jr., G. Bellussi, L. Carluccio, *Microporous Mater*. 1995, **4**, 221. (b) L. Schreyeck, P. Caullet, J. C. Mougenel, J. L. Guth, B. Marler, *Microporous Mater*. 1996, **6**, 259; (c) T. Ikeda, Y. Akiyama, Y. Oumi, A.

Kawai, F. Mizukami, *Angew. Chem., Int. Ed*. 2004, **43**, 4892; (d) S. Zanardi, A. Alberti, G. Cruciani, A. Corma, V. Fornés, M. Brunelli, *Angew. Chem., Int. Ed*. 2004, **43**, 4933; (e) B. Marler, N. Ströter, H. Gies, *Microporous Mesoporous Mater*. 2005, **83**, 201; (f) Y. X. Wang, H. Gies, B. Marler, U. Müller, *Chem. Mater*. 2005, **17**, 43; (g) T. Moteki, W. Chaikittisilp, A. Shimojima, T. Okubo, *J. Am. Chem. Soc*. 2008, **130**, 15780; (h) T. Ikeda, Y. Oumi, T. Takeoka, T. Yokoyama, T. Sano, T. Hanaoka, *Microporous Mesoporous Mater*. 2008, **110**, 488; (i) T. Moteki, W. Chaikittisilp, Y. Sakamoto, A. Shimojima, T. Okubo, *Chem. Mater*. 2011, **23**, 3564.

Chapter 5

Characterization of layered silicate HUS-5 and formation of novel nanoporous silica through transformation of HUS-5 ion-exchanged with alkylammonium cations

4. Introduction

Frameworks of crystalline layered silicates (CLSs) are composed exclusively of SiO4 tetrahedra. Because reactive SiOH/SiO^- groups are located on the interlayer surface, the layered silicate is easily functionalized by various modification methods such as cation exchange, silylation, and pillaring. CLSs are used in many applications such as catalysts and adsorbents.[1,2] They can also be deployed in the synthesis of porous materials such as zeolite and mesoporous silica.[3–5] In the case of zeolite synthesis, transformation of a layered silicate into zeolite is called topotactic conversion. Here, the silanol groups on the interlayer surfaces of the layered silicates are condensed between the layers, and the layered structures are transformed into zeolite-like 3D structures. If the crystal structures of the layered silicate nanosheets are determined, the framework structures of zeolites obtained by topotactic conversion using the interlayer dehydration–condensation process can be easily determined. Several studies have been conducted on the synthesis of zeolites fromlayered silicates. CDO (the three letters indicate the framework type-code),[3]

NSI,[6] CAS–NSI,[7] RWR,[8–10] RRO,[11] and SOD[12]-type zeolites were prepared using layered silicates PLS-1,3 (isomorphic materials: PLS-4,[13] RUB-36,[14,15] MCM-47,[16] MCM-65,[17] UZM-13,[18] UZM-17,[18] and UZM-19[18]), Nu-6(1),[6] EU-19,[7] RUB-18,[19,20] RUB-39,[21] and RUB-15,[22] respectively. In some cases, organic cations are intercalated into the interlayer to control the layer-stacking sequence.

Formation of ordered mesoporous silica derived from layered silicates, especially kanemite, was extensively investigated by the Kuroda group.[23–26] They concluded that the formation of mesophase silicates from layered silicates with a single silicate sheet depends on a combination of factors, including the reactivity of the layered silicates, presence of layered intermediates, variations in the silicate sheet, and assembly of surfactant molecules in the interlayer.[23–27] FSM-16-type mesoporous silica is formed via layered intermediates composed of fragmented silicate sheets and alkyltrimethylammonium (C_nTMA) cations. KSW-2 mesoporous silica can be prepared by bending the individual silicate sheets using intralayer and interlayer condensation. These findings indicate that the layered silicates have high potential for use in the synthesis of ordered mesoporous silica. However, only a few studies have been conducted on transformation of layered silicates, other than kanemite, into mesoporous materials.[27] Therefore, the synthesis of novel layered silicates with unique crystal structures and their conversion to porous materials remain challenging subjects of research.

Recently, Sano et. al reported the successful synthesis and structural analysis of a new layered silicate, HUS-1 ($Si_{10}O_{24}H_8 \cdot 2(CH_3)_4N$).[28] HUS-1 consists of a half sodalite cage framework structure and a tetramethylammonium cation (TMA^+) in the hemispherical sodalite cage, which acts as a structure-directing agent (SDA).

Although the interlayer distance of HUS-1 was estimated to be approximately 0.15 nm, which was unusually short compared to those of other layered silicates. I found that the HUS-1 modified with dimethyldichlorosilane effectively and selectively adsorbed TMA^+ from water, even in the presence of aqueous phenol.[29] Although HUS-1 was obtained by the hydrothermal treatment and then thorough washing, recently, during a further analytical study on HUS-1, I discovered that the crystal structure of the assynthesized HUS-1 changed with the number of washings performed. The crystal structure of as-synthesized HUS-1 with 1–3 washings, named as HUS-5, was structurally similar to β-HLS,[30] whose interlayer distance was much greater than that of HUS-1 obtained by thorough washing. It is well recognized that the physicochemical properties of layered silicates are influenced by the stacking state as well as the interlayer distance of silicate layers.[10,12,31] This fact motivated mes to investigate the difference between the respective ion-exchange behaviors of HUS-1 and HUS-5, for which they were ion-exchanged with bulky organic cations, namely dodecyltrimethylammonium ($C_{12}TMA$), hexadecyltrimethylammonium ($C_{16}TMA$), and benzyltrimethylammonium (BTMA). I also studied the potential of ion-exchanged layered silicates for use as base catalysts and their suitability for transformation into porous materials by post-treatment.

2. Experimental

2.1. Sunyhesis of HUS-5

The starting synthesis mixture was prepared using fumed silica (Cab-O-Sil M5, CABOT Co., USA), tetramethylammonium hydroxide (TMAOH, 48–50 wt%,

Aldrich), sodium hydroxide (>99%, High Purity Chemical Inc., Japan), and distilled water. The resulting hydrogel, with a chemical composition of SiO2 : 0.6 TMAOH : 0.2 NaOH : 5.5H_2O, was transferred to a Teflon-lined stainless steel vessel and heated under static conditions at 140 °C for 3 days. The solid product obtained (layered silicate) was separated by centrifugation and repeatedly washed with about 50 mL of distilled water. HUS-5 was obtained after 1–3 washings, whereas HUS-1 was obtained by thorough washing until the supernatant became neutral.

2.2. Ion-exchange of HUS-1 and HUS-5

Various ion-exchange processes of HUS-1 and HUS-5 were carried out using dodecyltrimethylammonium chloride (C_{12}TMACl, Tokyo Chemical Ind. Co. Ltd., Japan), hexadecyltrimethylammonium chloride (C_{16}TMACl, Tokyo Chemical Ind. Co. Ltd., Japan), and benzyltrimethylammonium chloride (BTMACl, Tokyo Chemical Ind. Co. Ltd., Japan) as alkylammonium surfactants. The layered silicate (0.1 g) was dispersed in an aqueous solution (20 mL) of alkylammonium chloride (1.1 mmol). The mixture was stirred at room temperature for 0.5 h and then centrifuged to remove the supernatant. This procedure was repeated three times.

2.3. Catalytic test

The Knoevenagel condensation reaction, which is used as a test reaction for a base catalyst, was carried out as follows. A mixture of benzaldehyde (4.0 mmol), ethyl cyanoacetate (3.5 mmol), and naphthalene (0.35 mmol, as an internal standard) in ethanol (3 mL) was added to a flask containing the layered silicate (HUS-1 or HUS-5

ion-exchanged with organic surfactants) as a catalyst (25 mg). The reaction was carried out at room temperature under stirring. After filtration of the solid, the filtrate was analyzed using a GC equipped with an FID-type detector on a Zebron ZB-1 column to determine the conversion of ethyl cyanoacetate and product yield.

2.4. Transformation of ion-exchanged HUS-5 into porous silica

Transformation of HUS-5, ion-exchanged with various alkylammonium cations, into a porous material was carried out by acid treatment, followed by calcination. The alkylammonium ion-exchanged HUS-5 (200 mg) was dispersed in distilled water (20 mL), and then 1.0 M acetic acid aqueous solution was added dropwise to the mixture to adjust the pH value between 2.5 and 5.5. The resulting mixture was then stirred at room temperature for 1 day. Next, the obtained solid product was separated by filtration, dried at 70 °C, and then calcined at 550 °C for 6 h to completely remove organic fractions.

2.5. Characterization

Powder X-ray diffraction (XRD) patterns of the solid products were collected using a powder X-ray diffractometer (Rigaku, Mini Flex) with graphite-monochromatized Cu Kα radiation at 30 kV and 15 mA. Crystal morphology and elemental composition were determined using a Hitachi S-4800 scanning electron microscope (SEM) coupled to an energy-dispersive X-ray (EDX) analyzer. ^{29}Si MAS NMR spectra were recorded at 119.17 MHz on a Varian 600PS solid NMR spectrometer using a 6 mm diameter zirconia rotor. The rotor was spun at 7 kHz. The spectra were acquired using 6.7 ms pulses, a 100 s recycle delay, and

1000 scans. 3-(Trimethylsilyl)propionic-2,2,3,3-d_4 acid sodium salt was used as a chemical shift reference. ^{1}H MAS NMR spectra were measured using a spinning frequency of 20 kHz and a single pulse sequence operated at 599.85 MHz using a 3.2mmdiameter zirconia rotor. Furthermore, ^{1}H-^{13}CCP MAS NMR spectra were also measured with a spinning frequency of 20 kHz, a 90° pulse length of 2.2 ms, and a cycle delay time of 100 s using a 3.2 mm diameter zirconia rotor. The ^{1}H and ^{13}C chemical shifts were referenced to adamantine and hexamethylbenzene, respectively. Nitrogen adsorption–desorption isotherms were obtained at −196 °C using a conventional volumetric apparatus (Bel Japan, BELSORP-mini). Prior to the adsorption measurements, the samples (ca. 0.1 g) were evacuated at 200 °C for 3 h. Thermal analyses were carried out using a TG/DTA apparatus (SSC/5200, Seiko Instruments). A sample (*ca*. 3 mg) was heated in a flow of air (50 mL min^{-1}) at a heating rate of 10 °C min^{-1} from room temperature to 800 °C. Elemental analysis was carried out using a Perkin-Elmer 2400II CHN analyzer at the Natural Science Center for Basic Research and Development (N-BARD), Hiroshima University. Transmission electron microscopy (TEM) images of nanoporous silica were taken using a Hitachi H9500 microscope at an acceleration voltage of 300 kV. IR spectra were recorded using an FT-IR spectrometer (NICOLET 6700) with a resolution of 4 cm□1 at room temperature. The sample was first pressed into a self-supporting thin wafer (*ca*. 10 mg cm^{-2}), and then placed into a quartz IR cell equipped with CaF_2 windows.

3. Results and discussion

3.1. Synthesis and characteristics of HUS-5

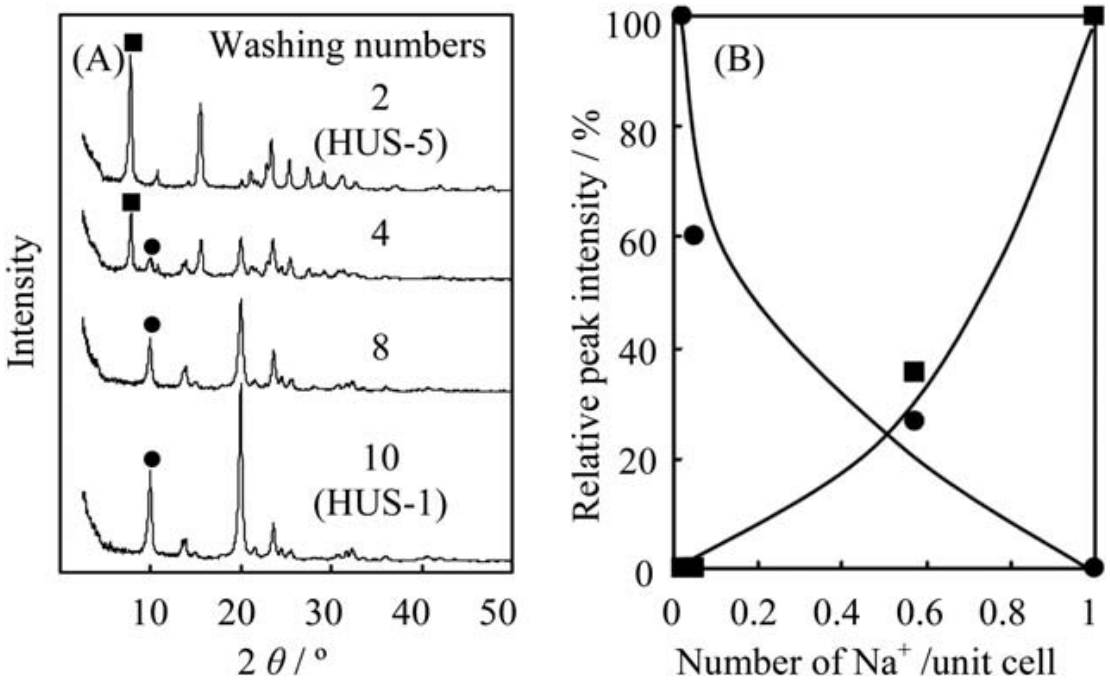

Fig. 5-1 (A) XRD patterns of as-synthesized HUS-1 obtained with different washing numbers and (B) relationship between relative peak intensities of (■) 2θ =7.8° (HUS-5) and (●) 2θ =9.9° (HUS-1) and the number of Na^+ in the unit cell.

Fig. 5-1(A) shows the XRD patterns of the as-synthesized layered silicates. When the number of washings was < 2, the peaks assigned to HUS-1 were not observed, indicating the formation of another type of layered silicate with a different crystal structure, which was named HUS-5. After 3 washings, diffraction peaks that correspond to HUS-1 phase became observable and the peak intensities increased with washing. The product obtained after 10 washings had the well-defined HUS-1 structure. [28] The basal spacing of HUS-5 (d = 1.13 nm, 2θ =7.8°) was greater than that of HUS-1 (d = 0.89 nm, 2θ = 9.9°). Fig. 5-1(B) shows the relationship between the peak intensities at 7.8° and 9.9° and the number of Na^+ cations per unit cell. The amounts of Na^+ cations in the products were determined by SEM/EDX. The peak intensity at 7.8° decreased with a decrease in the number of Na^+ cations,

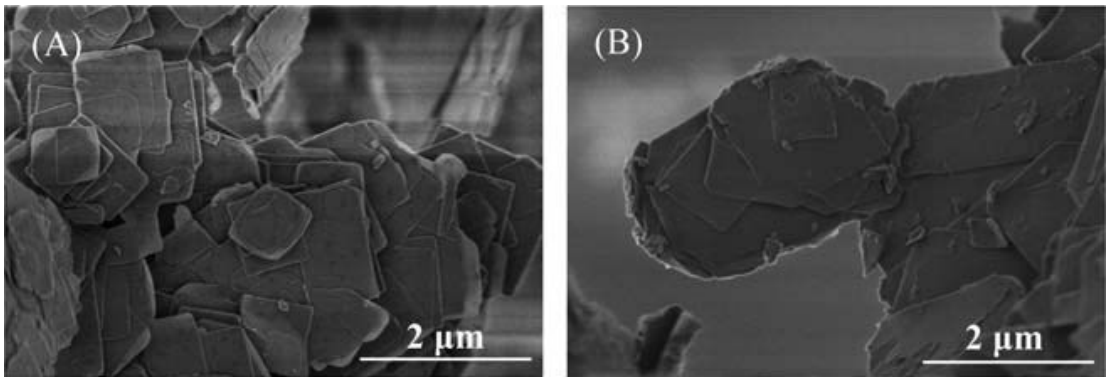

Fig. 5-2 SEM images (A) HUS-5 and (B) HUS-1.

whereas the peak intensity at 9.9° increased with a decrease in the number of Na+ cations. This observation strongly indicates that Na^+ cations were substituted with protons and de-intercalated from the interlayer during washing. Fig. 4-2 shows the SEM images of HUS-5 and HUS-1. There are no differences in the morphology (square, plate-like) and particle sizes (0.8 × 1.2 mm) between HUS-1 and HUS-5, indicating that the crystal structure was retained after washing.

In the ^{13}C CP MAS NMR spectra of both HUS-5 and HUS-1, a sharp resonance peak centered at *ca*. 58 ppm was observed. The peak can be assigned to methyl groups attached to N, namely the CH_3 moiety of N–CH_3. Therefore, TMA^+ was the only organic species present in HUS-1 and HUS-5. To quantify the amount of TMA^+ present, TG/DTA measurements were performed. As presented in Fig. 5-3, the thermal profiles can be categorized into three temperature zones: (I) 25–250 °C, (II) 250–350 °C, and (III) 350–700 °C. The first zone has an endothermic profile due to desorption of water. Approximately 11% weight loss is observed for HUS-5, whereas there is negligible mass loss observed for HUS-1. Thus, apparently, the interlayer of HUS-5 is more hydrophilic, compared with that of HUS-1. The second zone has an exothermic profile that can probably be attributed to the

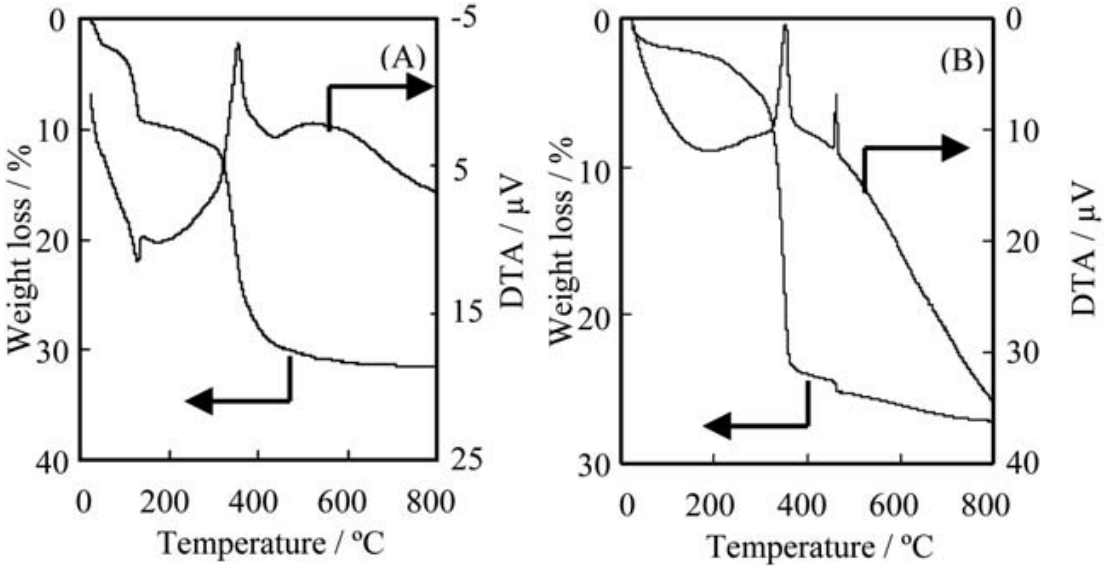

Fig. 5-3 TG-DTA curves of (A) HUS-5 and (B) HUS-1.

decomposition/oxidation of TMA^+ that interacts with $SiOH/SiO^-$ groups. The third zone, with an exothermic profile, could be assigned to further oxidation of carbonaceous materials generated by the decomposition of TMA^+. Although I could not assign the sharp exothermic peak at 450 °C at the present time, the mass losses between 250 and 700 °C for HUS-1 and HUS-5 were approximately 21 and 23 wt%, respectively, indicating no significant release of TMA+ from the interlayers during washing. Fig. 5-4(A) shows the ^{29}Si MAS NMR spectra of HUS-5 and HUS-1. In the spectrum of HUS-1, four resonance peaks are clearly observed, of which three at −102, −105, and −107 ppm may be assigned to the $Q^3[(–SiO)_3Si–OH]$ structure, whereas the fourth at ca. −114 ppm may be assigned to the $Q^4[(–SiO)_4Si]$ structure.[28] In contrast, in the case of HUS-5, only two peaks are observed at ca. −104 and −114 ppm, which are because of Q^3 and Q^4 structures, respectively. The Q^3/Q^4 ratio (83/17) of HUS-5 was consistent with that of HUS-1 (81/19), indicating that the silicate sheet structure was retained during the washing treatment. Therefore, the change in the spectrum could probably be attributed to the presence of Na^+ cations

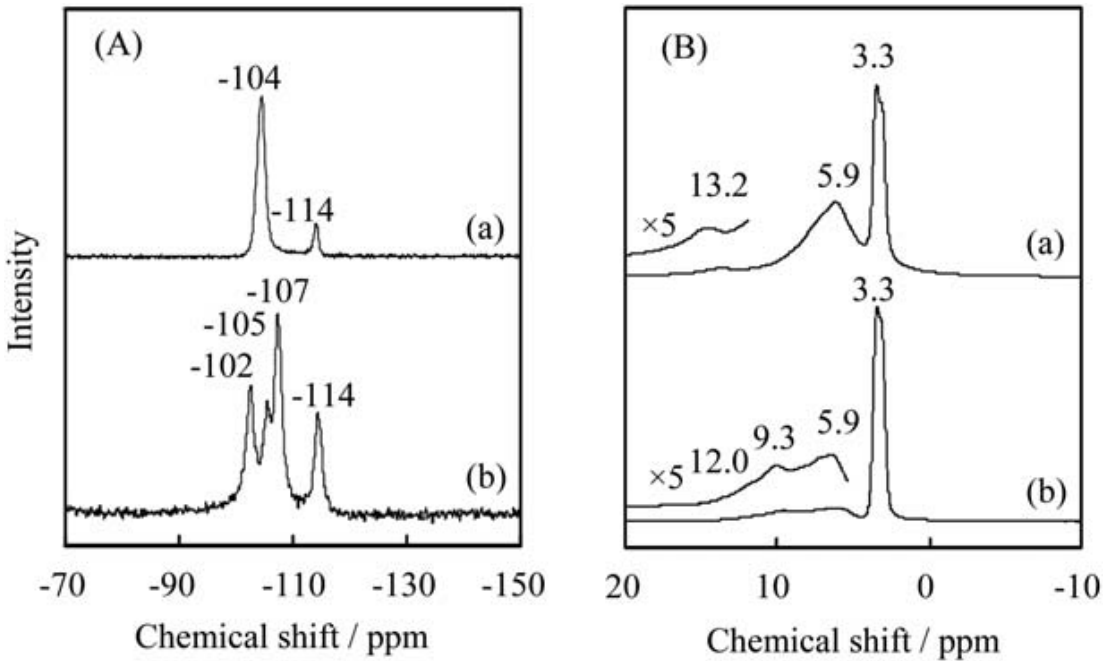

Fig. 5-4 (A) ^{29}Si and (B) ^{1}H MAS NMR spectra of (a) HUS-5 and (b) HUS-1.

and hydrated water in the interlayers of HUS-5. To investigate the configuration of silanol groups, ^{1}H MAS NMR measurements were performed. Fig. 5-4(B) shows the ^{1}H MAS NMR spectra of HUS-1 and HUS-5. The sharp and broad peaks at 3.3 and 5.9 ppm may be assigned to the protons of the methyl groups of TMA^{+} cations and to adsorbed hydrogen-bonded water molecules ($SiOH^{\cdots}H_2O$ or $H_2O^{\cdots}H_2O$), respectively. The broad peaks at 9.3, 12.0, and 13.2 ppm are attributed to silanol groups with strong hydrogen bonding ($SiOH^{\cdots}OSi$). These NMR results suggest that strong hydrogen bonding exists between the silanol groups on both sides of the interlayer, as well as between the vicinal silanols in the intralayer of both HUS-5 and HUS-1.

Taking into account the data obtained by CHN elemental analysis and EDX, together with the above results, the chemical composition of HUS-5 was estimated to be $Si_{10}O_{24}H5 \cdot 1.9[(CH_3)_4N] \cdot 1.0Na \cdot 4.5H_2O$. Furthermore, from the structural analysis obtained by powder XRD, it can be seen that the structure-type of HUS-5 is similar

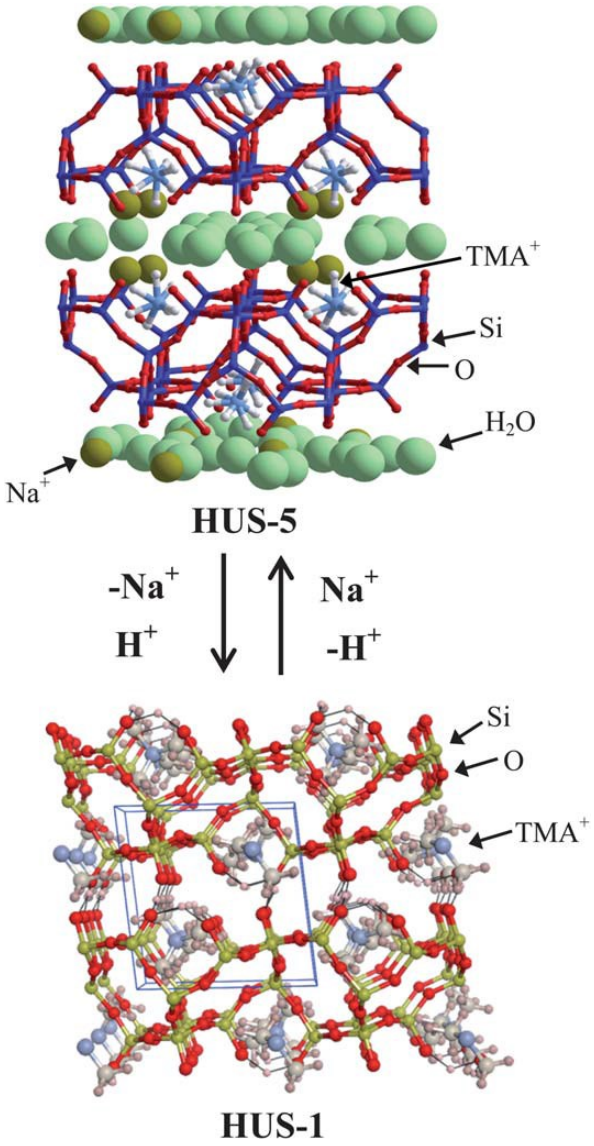

Fig. 5-5 Crystal structure models of HUS-5 and HUS-1.

to that of β-HLS; in particular, HUS-5 had Na^+, TMA^+, and hydrated water in the interlayer.[30] The stacking sequence of the neighboring layers in HUS-1 is entirely different from that in HUS-5. However, their framework topologies are similar to each other. This shows that HUS-5, with ABAB stacking order, converts to HUS-1, with AAAA stacking order, because of washing. To obtain further information concerning the structural transformation process, the following ion-exchange experiments were conducted. When HUS-1 was ion-exchanged using 0.5 M NaCl

aqueous solution, there was no change in the XRD patterns of HUS-1 before and after ion-exchange. In contrast, HUS-1 was completely transformed into HUS-5 when the ion-exchange was carried out under an alkaline condition using 0.5 M NaOH aqueous solution. These results strongly suggest that the transformation of HUS-1 into HUS-5 occurs by ion-exchange of protons from silanol groups in the interlayers of HUS-1 with Na^+ cations, which is activated at basic pH. Lastly, the transformation between HUS-5 and HUS-1 is a reversible process. Fig. 5-5 shows crystal structure models of HUS-5 and HUS-1.

3.2. Ion-exchange behavior of HUS-1 and HUS-5

As described above, the interlayer distance of HUS-5 was greater than that of HUS-1 because of the presence of both Na^+ cations and hydrated water in the interlayers. This suggests the possibility of further expansion of the interlayers by ion-exchange of TMA^+ and Na^+ cations in the interlayer with bulky organic cations. Therefore, HUS-5 was ion-exchanged in three separate samples with $C_{12}TMA^+$, $C_{16}TMA^+$ and $BTMA^+$, all of which are quaternary ammonium cations. For comparison, HUS-1 was also ion-exchanged with these cations. Fig. 5-6(A) shows the XRD patterns of HUS-5 ion-exchanged with $C_{12}TMA^+$ ($C_{12}TMA$–HUS-5), $C_{16}TMA^+$ ($C_{16}TMA$–HUS-5), and $BTMA^+$ (BTMA–HUS-5). The interlayer distance of HUS-5 increased to 1.65, 2.35, and 0.85 nm for $C_{12}TMA$–HUS-5, $C_{16}TMA$–HUS-5, and BTMA–HUS-5, respectively. In contrast, (Fig. 5-6(B)), there were no differences in the XRD patterns of HUS-1 recorded before and after ionexchange, suggesting that the alkylammonium cations were not intercalated in the interlayer of HUS-1. Fig. 5-7 shows the ^{13}C CP/MAS NMR spectra of

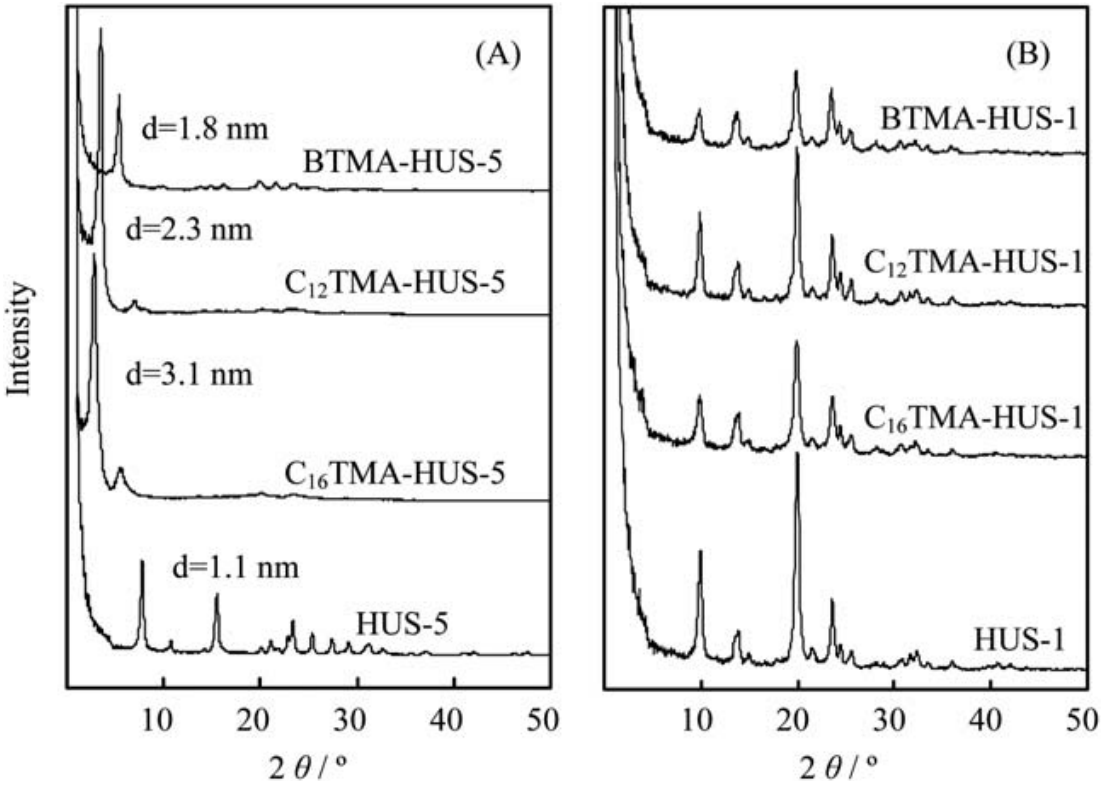

Fig. 5-6 XRD patterns of (A) HUS-5 and (B) HUS-1 ion-exchanged with various quaternary alkylammonium cations.

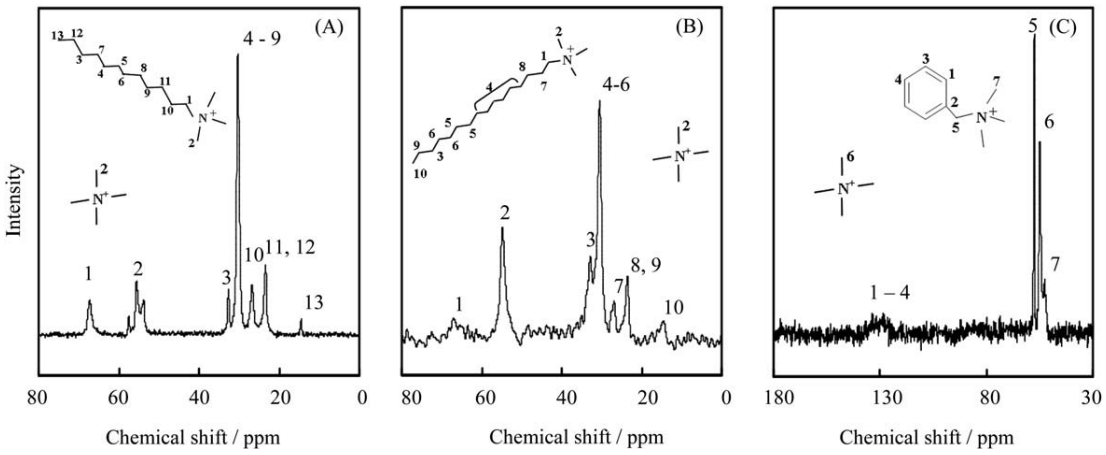

Fig. 5-7 ^{13}C CP/MAS NMR spectra of (A) C_{12}TMA–HUS-5, (B) C_{16}TMA–HUS-5, and (C) BTMA–HUS-5.

C_{12}TMA–HUS-5, C_{16}TMA–HUS-5, and BTMA–HUS-5. In addition to the TMA^+ cation, the presence of C_nTMA cations was confirmed in these spectra. Based on the results of TG/DTA and elemental analysis, the chemical compositions of

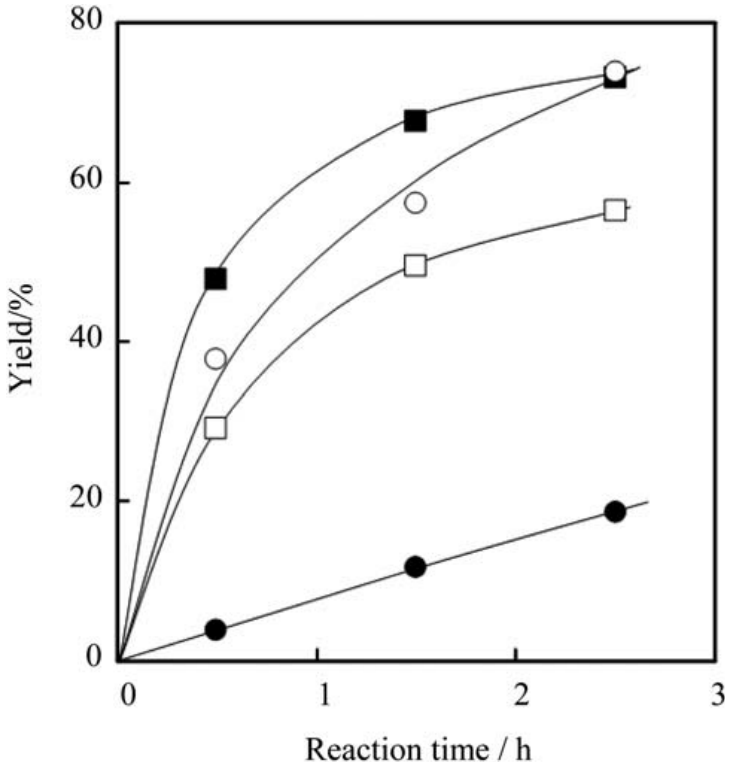

Fig. 5-8 Knoevenagel reaction over (●) HUS-1, (○) BTMA–HUS-5, (■) C_{12}TMA–HUS-5, and (□) C16TMA–HUS-5.

C_{12}TMA–HUS-5, C_{16}TMA–HUS-5, and BTMA–HUS-5 were estimated to be $Si_{10}O_{24}H_6 \cdot 0.5[TMA] \cdot 1.5[C_{12}TMA]$, $Si_{10}O_{24}H_{5.7} \cdot 0.4[TMA] \cdot 1.9[C_{16}TMA]$, and $Si_{10}O_{24}H_6 \cdot 0.7[TMA] \cdot 1.3[BTMA]$, respectively. Moreover, it was found that the expansion of the interlayer spacing of HUS-5 was due to the ionexchange of Na^+ cations, and some TMA^+ cations in the interlayer, with these bulky ammonium cations. Furthermore, as Na^+ cations were not detected in the ion-exchanged HUS-5, it is thought that several SiO^- groups were protonated and converted to SiOH.

Recently, the layered silicate PLS-1, which possesses TMAOH in the interlayers, was found to exhibit catalytic activity when used in a Knoevenagel condensation reaction as a base catalyst. The latter reaction is a fundamental means of encouraging C–C bond formation.[33] However, there are few reports concerning the catalytic

activity of layered silicates, other than PLS-1, or the literature on the effect of the interlayer expansion of layered silicates on the catalytic performance in the Knoevenagel condensation. Therefore, in order to clarify the respective potentials of C_{12}TMA–HUS-5, C_{16}TMA–HUS-5, and BTMA–HUS-5 for use as base catalysts, the Knoevenagel condensation reaction of benzaldehyde with ethyl cyanoacetate was investigated. For comparison, the catalytic performance of HUS-1 was also evaluated. The reaction occurred quantitatively, even at room temperature (25 °C), to yield the product (ethyl-2-cyano-3-phenylacrylate) with a selectivity of >95%. Fig. 5-8 shows the results of the Knoevenagel condensation reaction over these catalysts. The respective catalytic activities of C_{12}TMA–HUS-5, C_{16}TMA–HUS-5, and BTMA–HUS-5 are considerably higher than that of HUS-1. These high catalytic performances were probably due to large interlayer spacings that facilitated easier diffusion of reagents and products. The difference in the respective catalytic activities of C_{12}TMA–HUS-5, C_{16}TMA–HUS-5, and BTMA–HUS-5 seems to be because of the difference in diffusion limitation between reagents and products. Furthermore, the catalytic performance was much higher as compared with other types of layered silicates such as HUS-2, HUS-3 and PLS-1.[32,33]

3.3. Conversion of HUS-5, ion-exchanged with alkylammonium cations, into porous silica

Alkylammonium-layered silicate complexes have been used as precursors of mesoporous silica.[23–26] Kimura et al. reported the formation of KSW-2 with square and lozenge one-dimensional (1D) by mild acid treatment of a layered alkylammonium–kanemite complex.[26] In previous work, Sano et. al also succeeded

Table 5-1 Characteristics of the HUS-5 ion-exchanged with various alkylammonium cations after acid treatment followed by calcination at 550 ºC for 6 h

Sample no.	Acid treatment condition				BET surface rea[a] / m^2g^{-1}	Pore diamter[b] / nm
	Alkylammonium cation	pH value	Temperature / ºC	Time / h		
1	C_{16}TMA				200	
2	C_{16}TMA	5.5	150	24	440	
3	C_{16}TMA	4.5	150	24	780	1.28
4	C_{16}TMA	2.5	150	24	983	1.62
5	C_{16}TMA	2.5	150	24	165	
6	BTMA	2.5	150	24	209	

[a] Determined by the BET method. [b] Determined by the BJH plot.

in the preparation of a microporous material, which had an average pore diameter of 0.55 nm, from intermediates.[34] The latter were obtained by the intercalation of acetic acid molecules and TMA^+ cations into the interlayer of layered silicate magadiite and converted to the microporous material through the dehydration–condensation of silanol groups on both sides of the interlayer. It became clear that the control of both the stacking sequence and the configuration of the silanol groups, on both sides of the interlayer, are important factors for the zeolitization of layered silicates. Although the layered framework structure of HUS-1 is more complicated than those of kanemite and magadiite, these facts motivated us to use alkylammonium–HUS-5 complexes as precursors for porous materials. The HUS-5, which contained TMA^+ cations in the interlayer, was thermally treated at 550 °C. However, only broad and hollow peaks, corresponding to amorphous materials, were observed in the XRD pattern, indicating the degradation of the layered structure of HUS-5; probably, the state of the silicate layers, such as the stacking sequence, was not suitable for formation of the porous material. Therefore, I attempted to convert HUS-5,

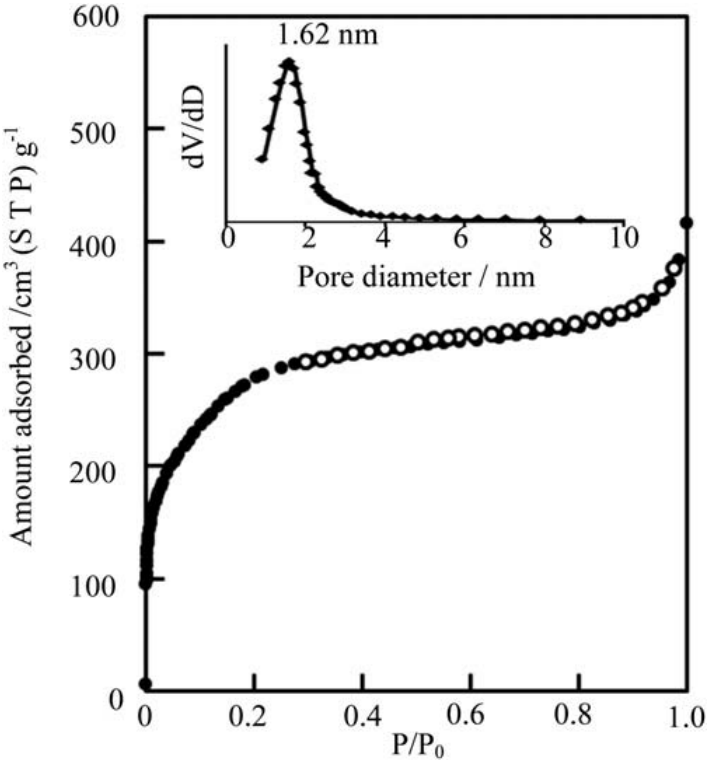

Fig. 5-9 N_2 adsorption (●)–desorption (○) isotherms and pore size distribution of HUS-6 (sample no. 4).

ionexchanged with alkylammonium cations, to a porous material by a multi-stage process that involved acid treatment and subsequent calcination.

Typical treatment conditions and characteristics of the products obtained are listed in Table 5-1. When C_{16}TMA–HUS-5 was calcined at 550 °C for 6 h (sample no. 1), the product had a BET surface area of 200 $m^2\ g^{-1}$. However, when C_{16}TMA–HUS-5 was treated in acetic acid aqueous solutions with various pH values, considerable increases in BET surface areas were observed, especially at a pH value of 2.5 (sample no. 4), which was named HUS-6. The N_2 adsorption–desorption isotherms of HUS-6 are shown in Fig. 5-9. The pore size distribution, calculated from the adsorption branch, is also shown. The BET surface area, pore volume, and average pore diameter of the HUS-6 were calculated to be 983 $m^2\ g^{-1}$, 0.45 $cm^3\ g^{-1}$, and 1.62

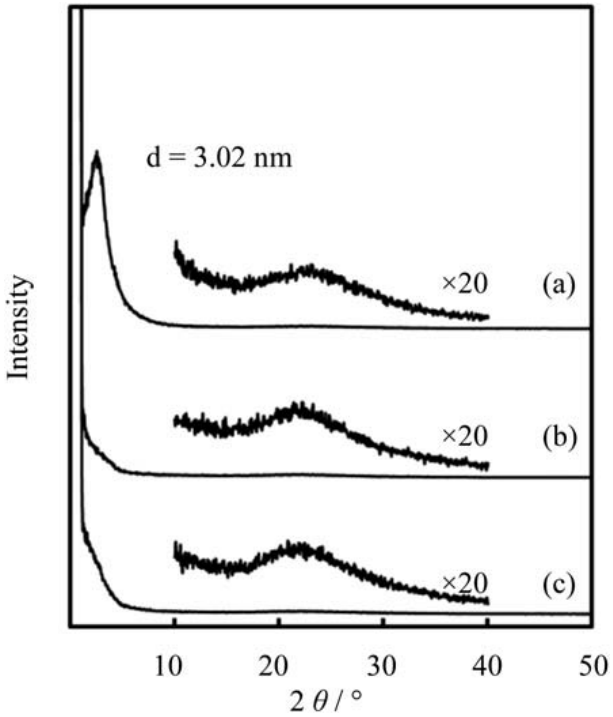

Fig. 5-10 XRD patterns of (a) HUS-6 (sample no. 4), (b) sample no. 5, and (c) sample no. 6.

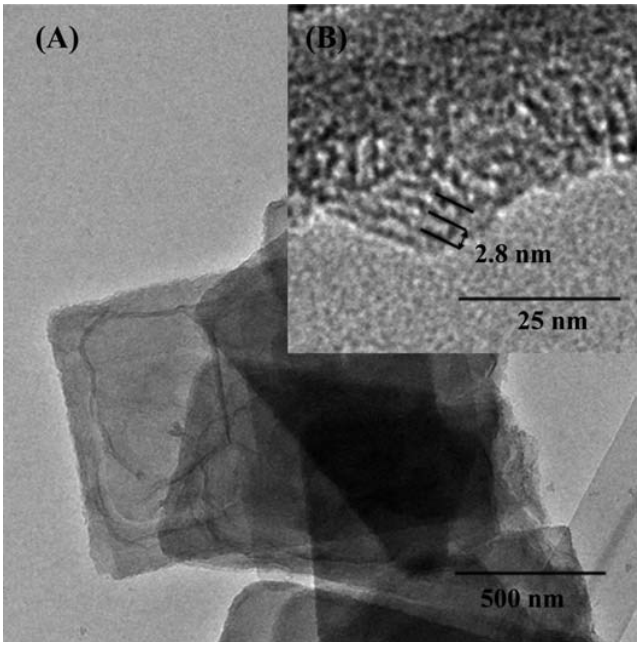

Fig. 5-11 TEM image of HUS-6 (sample no. 4).

nm, respectively. The N_2 adsorption isotherm exhibited a steep increase in the N_2 adsorption amount at low relative pressure; this suggests the existence of nanopores. Fig. 5-10(a) shows the XRD pattern of the HUS-6 (sample no. 4). Although no peaks

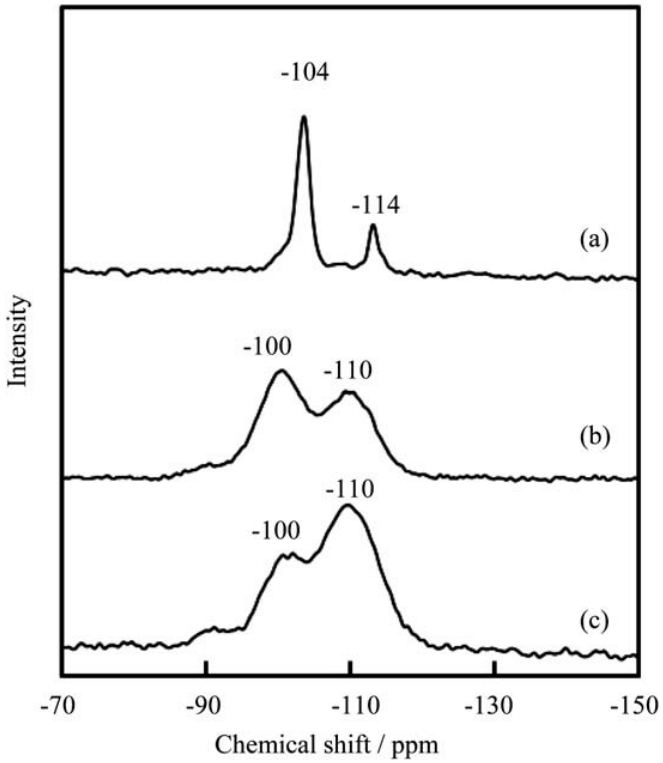

Fig. 5-12 ^{29}Si MAS NMR spectra of (a) C16TMA–HUS-5, (b) C16TMA–HUS-5 after only acetic acid treatment (no calcination), and (c) C16TMA–HUS-5 after acetic acid treatment and subsequent calcination (HUS-6).

are observed in the range 2θ = 10–50°, a broad peak is seen at ca. 2.9°, corresponding to a basal spacing of 3.02 nm, indicating regulation of pore formation in the HUS-6. Fig. 5-11 shows the TEM images of the HUS-6. The slightly disordered nanopores with a pore size range of 1.0–2.0 nm are clearly observed. The periodic distance of adjacent pores (*ca*. 2.8 nm) was in agreement with the basal d-spacing of HUS-6 (3.02 nm). It was also found that no morphology change occurred after the acid and calcination treatments, which indicated that there was no dissolution of silicate layers during the post-treatment involved acid treatment and subsequent calcination. Although the posttreatment of C_{12}TMA–HUS-5 and BTMA–HUS-5 was also carried out, no significant formation of ordered nanopores was observed in XRD patterns (Fig. 5-10(b) and (c)).

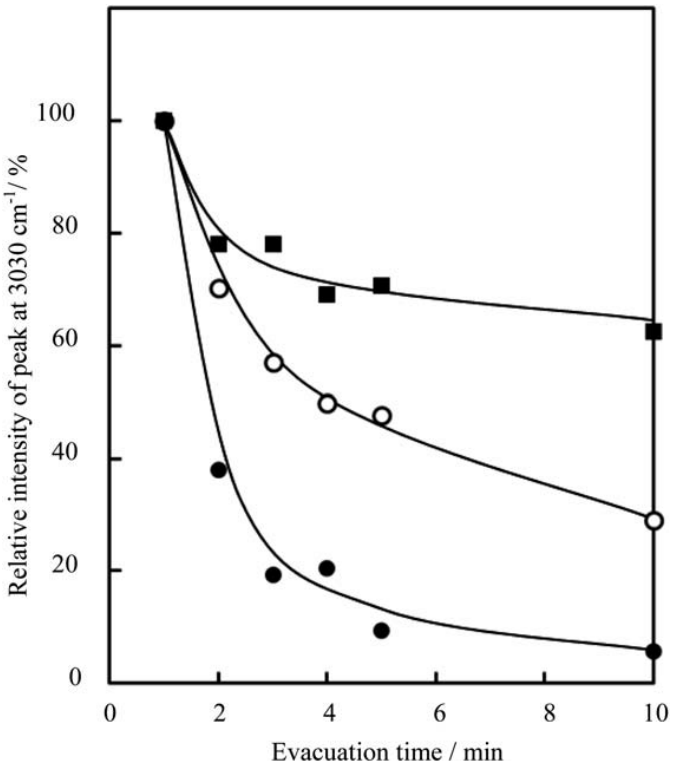

Fig. 5-13 Relationship between relative intensity of the peak at 3030 cm^{-1} and evacuation time on (○) HUS-6, (●) MCM-41, and (□) silicalite-1.

To obtain further information concerning the formation process of HUS-6, ^{29}Si MAS NMR spectra were obtained (Fig. 5-12). The latter shows the following spectra: C_{16}TMA–HUS-5, C_{16}TMA–HUS-5 after acetic acid treatment only, and C_{16}TMA– HUS-5 after both acid treatment and subsequent calcination (HUS-6). In the spectrum of C_{16}TMA–HUS-5, only two peaks are observed at ca. −104 and −114 ppm, which are assigned to Q^3 and Q^4 structures, respectively. As the spectrum was consistent with that of the as-synthesized HUS-5, it was found that the framework structure of HUS-5 was retained during the ionexchange. In contrast, the profile of C16TMA–HUS-5 after acid treatment was different to that of C_{16}TMA–HUS-5. The latter showed broad Q^3 and Q^4 peaks at −100 and −110 ppm, espectively. The Q^3/Q^4 ratio of C_{16}TMA–HUS-5 after acid treatment was 59/41.

Furthermore, this value for HUS-6 changed to 38/62. This strongly indicates that the dehydration–condensation of silanol groups in the interlayer or intralayer occurred by acid treatment and subsequent calcination.[26] Moreover, since the Q^2 peak was not observed, the cleavage of Si–O–Si bonds in the framework was negligible, so that, essentially, the framework structure of the silicate sheets was retained after the acid treatment and calcination.[35] However, there is room for examination of the exact formation mechanism of the nanopores in HUS-6 at the present time, and I am conducting further investigation on the transformation.

As stated above, the pore size of the HUS-6 obtained was smaller than that of MCM-41 (*ca*. 2.9 nm), which was synthesized using hexadecyltrimethylammonium bromide. To my knowledge, there are few reports concerning the preparation of ordered nanoporous silica with a pore size of 1–2 nm,[36] which indicates that the HUS-6 with its unique pore structure can be used as a shape-selective catalyst and adsorbent. In order to determine any influence of pore size on the adsorption–desorption behavior of porous silica, I investigated the desorption behavior of toluene on HUS-6. MCM-41 (*ca*. 2.9 nm) as mesoporous silica and silicalite-1 (*ca*. 0.6 nm) as MFI type pure silica zeolite were used as references. These samples were evacuated at 400 °C for 3 h, and then adsorption of toluene was carried out at 25 °C for 1 h. Afterwards, samples were evacuated at room temperature for various times, and then the samples' FT-IR spectra were measured to evaluate the amount of the remaining toluene. Fig. 5-13 shows the relationship between the intensity of the peak at ca. 3030 cm^{-1} that is assigned to the C–H stretching vibration of the toluene molecule and the evacuation time for HUS-6, MCM-41, and silicalite-1. For MCM-41, the peak intensity decreases rapidly with evacuation time, suggesting that

toluene molecules had been weakly adsorbed in the mesopores of MCM-41. On the other hand, for silicalite-1, approximately 63% of toluene molecules were still present even after 10 min evacuation. In the case of HUS-6, approximately 29% of toluene molecules remained in the nanopores after 10 min evacuation. These results strongly indicate that nanopores of HUS-6 present a unique adsorption space when compared with both micropores (*ca*. 0.6 nm) of silicalite-1 and mesopores (*ca*. 2.9 nm) of MCM-41.

4. Conclusions

I prepared the HUS-1 precursor, HUS-5, whose crystal structure was similar to that of *β*-HLS layered silicate. The interlayer distance of HUS-5 was 0.4 nm, and TMA^+, Na^+ , and hydrated water were present in the interlayer. HUS-5 with ABAB stacking order was converted to HUS-1 with AAAA stacking order during washing treatment. An increase in the interlayer distance of HUS-5 was observed when the latter was ion-exchanged with bulky organic cations such as dodecyltrimethylammonium, hexadecyltrimethylammonium, and benzyltrimethylammonium. In addition, HUS-5, ion-exchanged with any of the several organic cations tested, could be employed as a base catalyst. Also, the alkylammonium ion-exchanged HUS-5 variants exhibited high catalytic activities in Knoevenagel condensation reactions. Separately, I also succeeded in the conversion of HUS-5, ionexchanged with hexadecyltrimethylammonium cations, to novel nanoporous silica (HUS-6) by an acetic acid treatment and subsequent calcination. The BET surface area, pore volume, and average pore diameter of HUS-6 were 983

$m^2\ g^{-1}$, 0.45 $cm^3\ g^{-1}$, and 1.62 nm, respectively. In order to determine any influence of pore size on the adsorption properties of porous silica with different pores sizes, desorption experiments were performed for HUS-6, MCM-41, and silicalite-1. The adsorption–desorption behavior of toluene on HUS-6 showed that there was an intermediate state between MCM-41 and silicalite-1. Therefore, it was found that nanopores (mean size *ca*. 1.6 nm) of HUS-6 present a unique adsorption space as compared to micropores (mean size *ca*. 0.6 nm) of silicalite and mesopores (mean size *ca*. 2.9 nm) of MCM-41.

References

1 N. Takahashi and K. Kuroda, *J. Mater. Chem*., 2011, **21**, 14336.

2 (a) M. Ogawa and K. Kuroda, *Bull. Chem. Soc. Jpn*., 1997, **70**, 2593; (b) T. Okada, Y. Ide and M. Ogawa, *Chem.–Asian J*., 2012, **7**, 1980.

3 T. Ikeda, Y. Akiyama, Y. Oumi, A. Kawai and F. Mizukami, *Angew. Chem., Int. Ed*., 2004, **43**, 4892.

4 B. Marler and H. Gies, *Eur. J. Mineral*., 2012, **24**, 405.

5 T. Kimura and K. Kuroda, *Adv. Funct. Mater*., 2009, **19**, 511.

6 S. Zanardi, A. Alberti, G. Cruciani, A. Corma, V. Fornes and M. Brunelli, *Angew. Chem., Int. Ed*., 2004, **43**, 4933.

7 B. Marler, M. A. Camblor and H. Gies, *Microporous Mesoporous Mater*., 2006, **90**, 87.

8 B. Marler, N. Stroter and H. Gies, *Microporous Mesoporous Mater*., 2005, **83**, 201.

9 Y. Oumi, T. Takeoka, T. Ikeda, T. Yokoyama and T. Sano, *New J. Chem*., 2007, **31**, 593.

10 T. Ikeda, Y. Oumi, T. Takeoka, T. Yokoyama, T. Sano and T. Hanaoka, *Microporous Mesoporous Mater*., 2008, **110**, 488.

11 Y. Wang, B. Marler, H. Gies and U. Muller, *Chem. Mater*., 2005, **17**, 43.

12 T. Moteki, W. Chaikiiisilp, A. Shimojima and T. Okubo, *J. Am. Chem. Soc*., 2008, **130**, 15780.

13 T. Ikeda, S. Kayamori and F. Mizukami, *J. Mater. Chem*., 2009, **19**, 5518.

14 J. Song and H. Gies, *Stud. Surf. Sci. Catal*., 2004, **154A**, 295.

15 B. Marler, Y. Wang, H. Song and H. Gies, *Abstracts of Papers, 15th International Zeolite Conference*, 2007, Beijing, China, August 12–17, 2007, p. 599.

16 A. Burton, R. J. Accardi, R. F. Lobo, M. Falcioni and M. W. Deem, *Chem. Mater*., 2000, **12**, 2936.

17 D. L. Dorset and G. J. Kennedy, *J. Phys. Chem. B*, 2004, **108**, 15216.

18 L. M. Knight, M. A. Miller, S. C. Koster, M. G. Gatter, A. I. Benin, R. R. Willis, G. J. Lewis and R. W. Broach, *Stud. Surf. Sci. Catal*., 2007, **170A**, 338.

19 A. J. Blake, K. R. Franklin and B. M. Lowe, *J. Chem. Soc., Dalton Trans*., 1988, 2513.

20 S. Vortmann, J. Rius, S. Siegmann and H. Gies, *J. Phys. Chem. B*, 1997, **101**, 1292.

21 Y. X. Wang, H. Gies and J. H. Lin, *Chem. Mater*., 2007, **19**, 4181.

22 U. Oberhagemann, P. Bayat, B. Marler, H. Gies and J. Rius, *Angew. Chem., Int. Ed*., 1996, **35**, 2869.

23 T. Yanagisawa, T. Shimizu, K. Kuroda and C. Kato, *Bull. Chem. Soc. Jpn*., 1990, **63**, 988.

24 S. Inagaki, Y. Fukushima and K. Kuroda, *J. Chem. Soc., Chem. Commun*., 1993, 680.

25 S. Inagaki, A. Koiwai, N. Suzuki, Y. Fukushima and K. Kuroda, *Bull. Chem. Soc. Jpn*., 1996, **69**, 1449.

26 T. Kimura, T. Kamata, M. Fuziwara, Y. Takano, M. Kaneda, Y. Sakamoto, O. Terasaki, Y. Sugahara and K. Kuroda, *Angew. Chem., Int. Ed*., 2000, **39**, 3855.

27 R. Garc´ıa, I. D´ıaz, C. M´arquez-´Alvarez and J. P´erez-Pariente, *Chem. Mater*., 2006, **18**, 2283.

28 T. Ikeda, Y. Oumi, K. Honda, T. Sano, K. Momma and F. Izumi, *Inorg. Chem*., 2011, **50**, 2294.

29 Y. Ide, M. Torii, N. Tsunoji, M. Sadakane and T. Sano, *Chem. Commun*., 2012, **48**, 7073.

30 T. Ikeda, Y. Akiyama, F. Izumi, Y. Kiyozumi, F. Mizukami and T. Kodaira, *Chem. Mater*., 2001, **13**, 1286.

31 N. Tsunoji, Y. Ide, M. Torii, M. Sadakane and T. Sano, *Chem. Lett*., 2013, **42**, 244.

32 N. Tsunoji, T. Ikeda, Y. Ide, M. Sadakane and T. Sano, *J. Mater. Chem*., 2012, **22**, 13682.

33 K. Komura, T. Kawakami and Y. Sugi, *Catal. Commun*., 2007, **8**, 644.

34 Y. Oumi, K. Takagi, T. Ikeda, H. Sasaki, T. Yokoyama and T. Sano, *J. Porous Mater*., 2009, **16**, 641.

35 L. Liebau, *Structural Chemistry of Silicates*, Springer, Heidelberg, 1985.

36 M. J. Kim and R. Ryoo, *Chem. Mater*., 1999, **11**, 487.

Chapter 6

Design of layered silicate by grafting with metal acetylacetonate for high activity and chemoselectivity in photooxidation of cyclohexane

5. Introduction

Metallosilicate catalysts such as zeolites and mesoporous silicas with tetrahedrally coordinated transition metals species, especially Ti and V, covalently linked into silicate frameworks, have been utilized as oxidation catalysts for various reactions because of the specific property of the active sites.[1–3] They give specific and highly selective catalytic activities for epoxidation of alkenes and for oxidation of alkanes and alcohols by using oxidant or photoirradiation. The catalytic performances are quite different from those of bulk TiO_2 and V_2O_3, which consists of octahedrally coordinated species. Accordingly, the synthesis of more effective and active metallosilicate catalysts has been extensively investigated.[4–10] The amount of transition metal incorporated into the silicate framework, which directly affects the catalytic performances, can be controlled to some extent by changing the composition of starting materials.[4,6] When the amount of incorporated transition metal is greatly increased to improve their catalytic performances by conventional methods, however, generation of unconvenient species such as metal and metal

oxide are often observed because of the limitation of the amount of incorporated transition metals, which causes decrease in the activity and selectivity. To overcome such limitation of catalyst preparation, therefore, development of a novel route for design of catalysts with high activity and chemoselectivity by increasing density of active sites effectively is required.

Inorganic layered materials are attractive because of their large surface area derived from multistacking ultrathin layers having chemical and thermal stability and material diversity.[11] The grafting (covalent attachment) of functional units onto interlayer surfaces of layered materials is one of the most promising methods for design of the composite materials with hetero elements because of the regularity and numerousness of the connectable points between incorporated functional units and interlayer surfaces. Especially, the surface density of silanol groups of interlayer silicates, which can be regarded as connectable points, is higher than that of other materials such as zeolites and mesoporous silicas. The grafting was first reported by Rojo and Ruiz-Hitzky, who demonstrated the silylation of interlayer silanol group of a layered silicate with a silane coupling reagent.[12] Recently, in addition to silane coupling reagents,[13−20] alcohols,[21−23] phosphonic acids[24,25] and other hydroxyl-bearing organic molecules[26] have been successfully grafted onto the interlayer surfaces of various layered materials. Such grafting reactions allow control of the density and the interunit distance of the immobilized functional units in two-dimensional nanospaces at the angstrom level, which is important for the design of advanced materials such as single-site heterogeneous catalysts and photofunctional materials. Because the guest is irreversibly immobilized onto the interlayer surfaces, the resulting hybrid materials are sufficiently suitable for use in

challenging practical applications. However, there are still few reports concerning the grafting of metal or metal oxide on the surfaces of layered materials,[27] which has the possibility to freely design advanced and innovative catalysts.

In this study, I report the grafting of titanium(IV) acetylacetonate as a representative metal acetylacetonate onto the interlayer surface of a layered silicate. I also show that the modified layered silicates with a controlled amount (density) of the grafted Ti are excellent photocatalysts for fine chemical synthesis under solar light irradiation when the acetylacetonate ligand is removed by calcination. Because a wide variety of metal acetylacetonates and various layered silicates with different framework topology are available, the present method may enable the design of diverse single-site heterogeneous catalysis.

2. Experimental

2.1. Preparation of Ti-Incorporated HUS-2

Layered silicate HUS-2[28] were synthesized by the hydrothermal treatment of starting gel, which had the chemical composition SiO_2:0.4 choline hydroxide:0.2 NaOH:5.5H_2O, at temperature 150 °C for 2 d. Hexhadecyltrimethylammonium (C_{16}TMA)-exchanged HUS-2 (C_{16}TMA-HUS) was prepared by the reaction of HUS-2 with an aqueous solution of hexadecyltrimethylammonium chloride. Ti-incorporated HUS-2 (*x* denotes grafted Ti residues per $Si_{20}O_{40}(OH)_4$ unit) was synthesized by the reaction of C_{16}TMA-HUS with $Ti(acac)_4$ followed by the removal of C_{16}TMA with washing. $Ti(acac)_4$ in isopropyl alcohol (ca. 63%, Wako) was used as received. C_{16}TMA-HUS (1.0 g) was mixed with the $Ti(acac)_4$ solution (5.38 mL

of $Ti(acac)_4$) in ethanol/hexane (3:17 vol/vol; 100 mL) at room temperature for 3 d. After the evaporation of the solvent, the solid was washed twice with 0.1 M HCl/ethanol (1:1 vol/vol; 20 mL,), affording $Ti_{2.3}$-HUS. $Ti_{1.5}$-HUS and $Ti_{1.2}$-HUS were synthesized by a similar method except that C_{16}TMA-HUS was mixed with $Ti(acac)_4$ at 60 °C for $Ti_{1.5}$-HUS and room temperature in the presence of 2,2′ -bipyridyl for $Ti_{1.2}$-HUS and the solids were separated by centrifugation, not by evaporation. For grafting of funcational units onto silica surfaces, heterocyclic compounds such as pyridine and 2,2'-bipyridyl are often used to change the reactivity between interlayer silanol groups and gest species grafted. Therefore, I used the bipyridyl to control the amount of Ti incorporated.

2.2. Catalyst Tests

Photocatalytic oxidation reactions were carried out by photoirradiation with solar simulator (San-Ei Electric Co., Ltd.) in a closed stainless steel container equipped with a 75 mL of Pyrex glass vessel containing a mixture of catalyst (30 mg) and O_2-saturated solution of cyclohexane (2 mL) in acetonitrile (18 mL). The container was placed ca. 30 cm away from the light source to irradiate the mixture by 1 solar (1000 Wm^{2-}) power light at 42 °C for 24 h with shaking. CO_2 and organic compounds were quantitatively analyzed by GC-FID and GC-TCD, respectively. Only cyclohexane, cyclohexanone, and cyclohexanol were detected in GC-FID.

3. Results and discussion

Metal acetylacetonates can be grafted onto oxide surfaces via ligand exchange

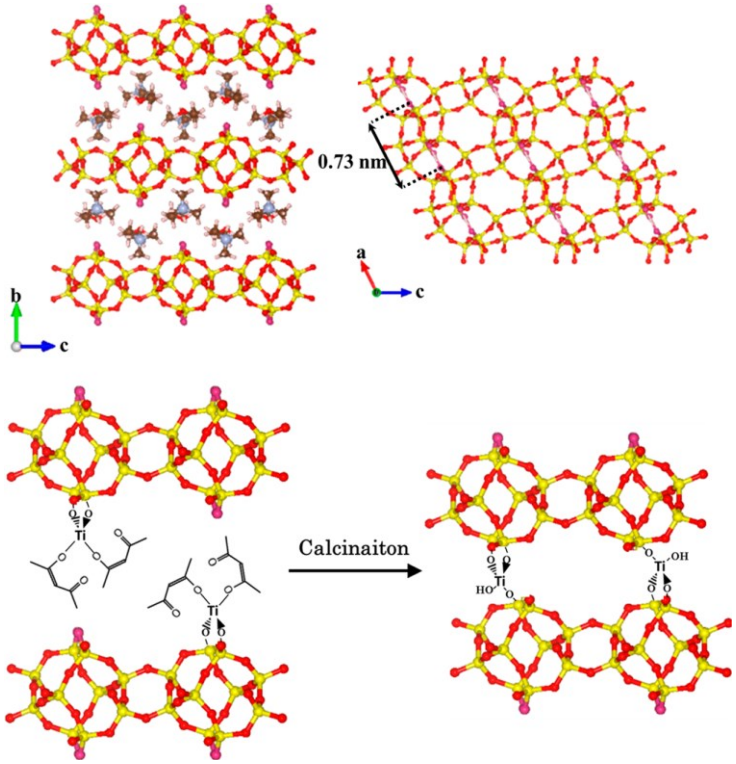

Fig. 6-1 (top) Framework structure of HUS-2 and (bottom) scheme for grafting of Ti(acac)4 onto interlayer surface of HUS-2.

with the surface hydroxy groups.[29,30] In this study, titanium(IV) acetylacetonate ($Ti(acac)_4$) was chosen as a typical metal acetylacetonate representative because Ti-containing porous silicas such as zeolite and mesoporous silica have been widely investigated as photocatalysts.[7–10] HUS-2 (Hiroshima University Silicate-2, $Si_{20}O_{40}(OH)_4 \cdot 4[C_5H_{14}NO]$), having interlayer choline cations and silanol groups (Figure 6-1),[28] was used as the layered silicate. Grafting of bulky organic molecules onto the interlayer surfaces of layered materials is usually accomplished by using the corresponding long-chain alkylammonium-exchanged forms as intermediates. Accordingly, the interlayer choline cations were first exchanged with hexadecyltrimethylammonium cations ($C_{16}TMA$) to afford $C_{16}TMA$-exchanged HUS-2 ($C_{16}TMA$-HUS), which then reacted with $Ti(acac)_4$, affording Ti_x-HUS.

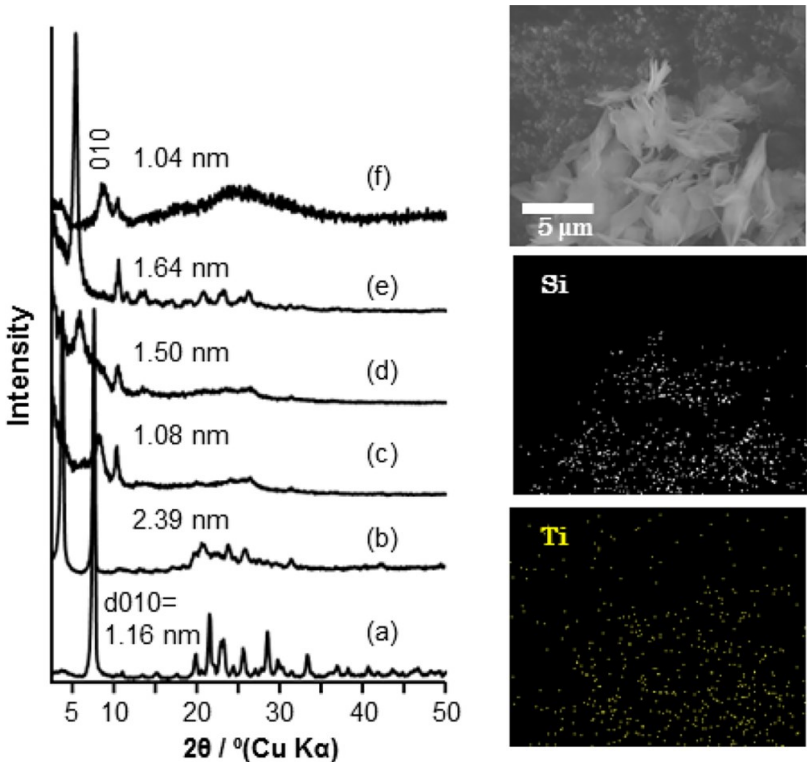

Fig. 6-2 (left) Powder X-ray diffraction patterns of (a) HUS-2, (b) C_{16}TMA-HUS, (c) $Ti_{1.2}$-HUS, (d) $Ti_{1.5}$-HUS, (e) $Ti_{2.3}$-HUS, and (f) calcined $Ti_{2.3}$-HUS. Insets show variation of basal spacing of Tix-HUS as a function of amount of grafted $Ti(acac)_4$. (right) FE-SEM image of $Ti_{2.3}$- HUS and corresponding elemental mapping (bottom).

Figure 6-2 (left) compares the X-ray diffraction (XRD) patterns of Ti_x-HUS to those of HUS-2 and C_{16}TMA-HUS. In the XRD patterns of Ti_x-HUS, the peaks attributed to basal spacing diffraction and in-plane diffraction were observed around 5 and 10 degrees, respectively. The basal spacings of Ti_x-HUS differ from that of HUS-2 in a manner that dependent on the amount of the grafted $Ti(acac)_4$. The ^{29}Si MAS NMR spectra of Ti_x-HUS are also shown in Figure 6-3(left). The two resonance peaks between −90 and −100 ppm were assigned to the Q^3 structure, whereas the three resonance peaks between −105 and −120 ppm were assigned to the Q^4 structure, based on the ^{1}H−^{29}Si CP-MAS NMR measurements. The integral ratio of Q^3/Q^4 signals, which reflects the amount of interlayer silanol groups, is substantially smaller for Ti_x-HUS relative to C_{16}TMA-HUS and decreases with

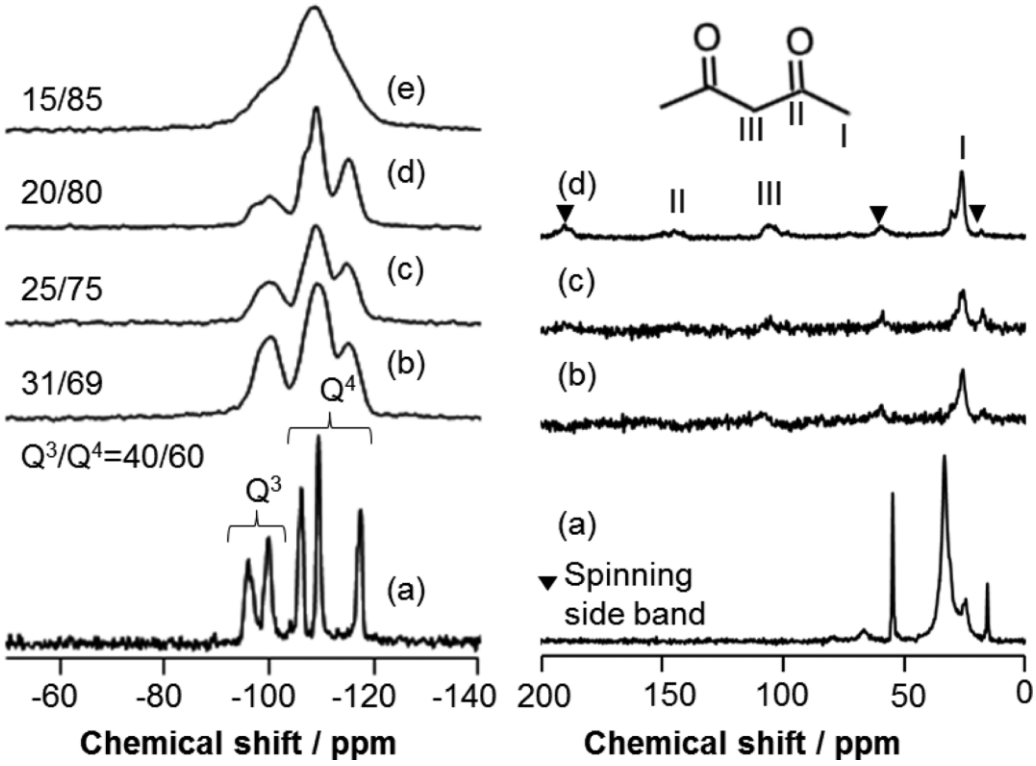

Fig. 6-3 (left) ^{29}Si MAS NMR spectra of (a) C^{16}TMA-HUS, (b) $Ti_{1.2}$-HUS, (c) $Ti_{1.5}$-HUS, (d) $Ti_{2.3}$-HUS, and (e) calcined $Ti_{2.3}$-HUS. (right) ^{13}C CP-MAS NMR spectra of (a) C_{16}TMA-HUS, (b) $Ti_{1.2}$-HUS, (c) $Ti_{1.5}$-HUS, and (d) $Ti_{2.3}$-HUS.

increasing the amount of $Ti(acac)_4$ grafted. Furthermore, in the ^{13}C CP-MAS NMR spectra of Ti_x-HUS, signals from $Ti(acac)_4$ are observed whereas those from C_{16}TMA are not (Figure 6-3(right)). The above results indicate that $Ti(acac)_4$ was immobilized onto the silicate sheet vi covalent Si−O−Ti bonds and C_{16}TMA barely remained in Ti_x- HUS. The compositions of the grafted $Ti(acac)_4$ for $Ti_{1.2}$-HUS, $Ti_{1.5}$-HUS, and $Ti_{2.3}$-HUS were calculated as $Ti(C_5H_7O_2)_{1.4}$, $Ti(C_5H_7O_2)_{1.8}$, and $Ti(C_5H_7O_2)_{1.8}$, respectively, based on the amounts of Ti and acetylacetonate ligand (Table 6-1). Therefore, approximately half of the acetylacetonate ligands of $Ti(acac)_4$ in Ti_x-HUS remain. Judging from (1) the basal spacing (1.08−1.64 nm), (2) the long distance (0.73 nm) between the adjacent SiOH/SiO$^-$ pairs on the silicate sheet, indicating no possibility for formation of Ti−O−Ti covalent bond between the

grafted Ti species, and (3) the convenient distance (0.25 nm) between two reactive functional groups (SiO^-/SiOH) for dipodal grafting of $Ti(acac)_4$, $Ti(acac)_4$ are grafted in a dipodal fashion with Ti−O−Si bridges, not but pillars the adjacent sheets, to leave two acetylacetonate ligands in Ti_x-HUS (Figure 6-1). As shown in Figure 6-2, the XRD patterns of Ti_x-HUS are indicative of a single phase (if the grafted $Ti(acac)_4$ are segregated, the basal spacing (010) peaks should split) and the basal spacings of Ti_x-HUS increase with increasing the amount of grafted $Ti(acac)_4$. Also, in the elemental mapping of Ti_x-HUS (Figure 6-2(right)), Ti was evenly distributed in the product. Similar results have been shown for the organic derivatives of layered materials with silane coupling reagents, in which the spatial distribution of the grafted silyl groups appears to be controlled.[14]

The remaining acetylacetonate ligand in Ti_x-HUS was removed by calcination at 400 °C for 6 h as evidenced by the ^{13}C CP-MAS NMR spectra, thermogravimetry-differential thermal analyses and CHN elemental analyses of Ti_x-HUS after calcination. Spectra a and b in Figure 6-4 show the UV−vis spectra of $Ti_{2.3}$-HUS before and after calcination, respectively. Upon calcination, the 320−450 nm absorption band from the π−π* transition in the acetylacetonate ligand[29] disappears and an absorption band appears at 220 nm. This band is often observed in Ti-incorporated zeolites such as TS-1 (Figure 6-4e) and is indicative of the presence of isolated tetrahedral Ti species. The absorbance at 220 nm increases with increasing the amount of grafted $Ti(acac)_4$. These results strongly suggest that the grafted $Ti(acac)_4$ is homogeneously distributed on the silicate sheet. Also, the basal spacing drastically decreases (Figure 6-2f) and the integral ratio of Q^3/Q^4 signals for

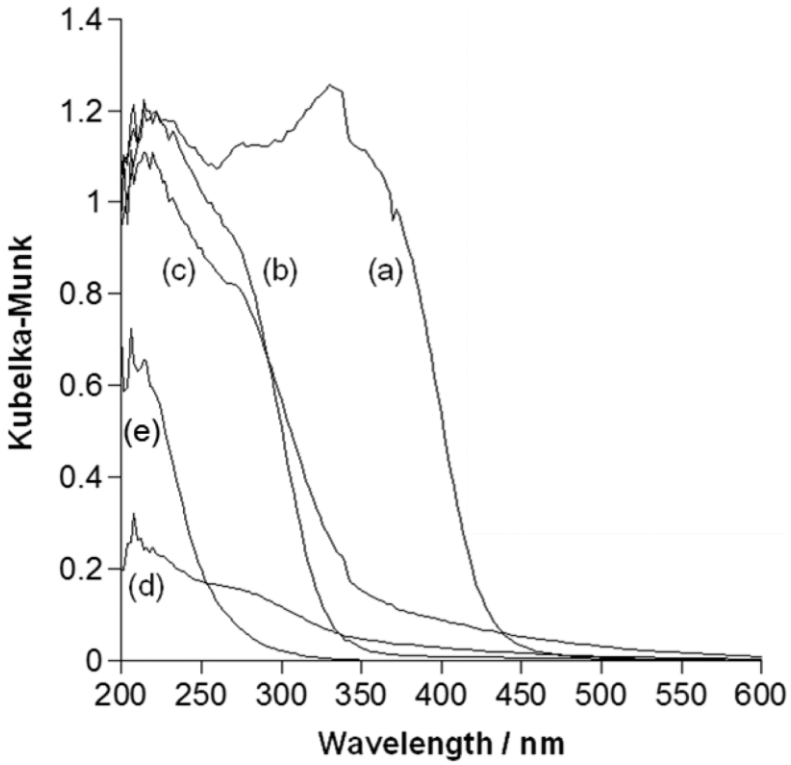

Fig. 4 UV−vis spectra of (a) $Ti_{2.3}$-HUS, (b) calcined $Ti_{2.3}$-HUS, (c) calcined $Ti_{1.5}$-HUS, (d) calcined $Ti_{1.2}$-HUS, and (e) TS-1.

$Ti_{2.3}$-HUS slightly decreases upon calcination. From the FT-IR measurment of $Ti_{2.3}$-HUS cal, a peak assigned to Si−O−Ti bond was observed at ca. 960 cm^{-1}, indicating effective grafting of Ti species onto interlayer surfaces of HUS-2. Furthermore, the N_2 adsorption isotherms of $Ti_{2.3}$-HUS before and after calcination showed that the amount of micropore-adsorbed N_2 increased upon calcination. All Ti_x-HUS cal showed basal spacings of ~1.0 nm, which were larger than that of HUS-2 calcined and dependent on the amount of the grafted Ti, indicating that upon the removal of the remaining acetylacetonate ligands, a part of the grafted $Ti(acac)_4$ links to the surface silanol group forming pillars that connect the adjacent silicate sheets (Figure 6-1). Because square-planar configuration for Ti is unlikely, one of the two remaining acetylacetonate ligands is likely to be converted to a hydroxy

group (Figure 6-1). The shoulders observed in the 250−450 nm range in the UV−vis spectra of calcined Ti_x-HUS (Figure 6-4) likely indicate the presence of such Ti−OH species.[6] However, I could not rule out the possible presence of octahedral Ti species in the calcined Ti_x-HUS. Although TEM observation was carried out, I could not find out any Ti oxide particles. The oxidation state of Ti species incorporated in Ti_x-HUS was measured by XPS. The peak of $Ti2p_{3/2}$ attributed to Ti^{4+} (isolated tetrahedral Ti species) in the silicate framework was clearly observed at 460 eV of binding energy. However, the peak at 457.9 eV attributed to TiO_2 was hardly observed, indicating no formation of Ti oxide particles.

Zeolites and mesoporous silicas with isolated tetrahedral Ti are important single-site photocatalysis due to electron transfer from O^{2-} to Ti^{4+} ions upon excitation by UV irradiation, resulting in the formation of pairs of trapped hole (O^-) and electron (Ti^{3+}) centers.[10] I carried out the partial oxidation of cyclohexane to cyclohexanol (CHol) and cyclohexanone (CHone), one of the most important synthetic reactions in chemical industry, using Ti_x-HUS (before and after calcination) as photocatalysts under simulated solar light irradiation. TS-1, typical Ti-containing zeolite, and P25, a mixture of anatase and rutile type TiO_2, were used as references under the same irradiation conditions (Table 6-1). Although TiO_2 (P25) exhibited lower chemoselectivity because of the generation of a large amount of CO_2, TS-1 showed close to 100% chemoselectivity for partial oxidation. The completely oxidized product CO_2 barely formed. Ti_x-HUS also showed ~100% chemoselectivity. The yields of CHone and CHol were 3.4 and 4.1 μmol for $Ti_{1.2}$-HUS, 3.0 and 4.0 μmol for $Ti_{1.5}$-HUS, and 4.9 and 7.5 μmol for $Ti_{2.3}$-HUS. These values were higher than those for TS-1 (2.4 μmol of CHone and 3.7 μmol of

Table 6-1 Compositions and Photocatalytic Performance of Ti_x-HUS before and after Calcination in the Selective Cyclohexane Oxidation under Simulated Solar Light

Sample no.	acac/Ti[d]	Ti(wt %)	Yield (μmol)[e]			Product
			CHone	CHol	CO_2	[CHone+CHnol] selectivity (%)[f]
$Ti_{1.2}$-HUS	1.4	4.0	3.4	4.1	n.d.	>99
$Ti_{1.2}$-HUS cal[a]		6.0	4.4	6.1	n.d.	>99
$Ti_{1.5}$-HUS	1.8	4.9	3.0	4.0	n.d.	>99
$Ti_{1.5}$-HUS cal		5.6	6.1	6.7	n.d.	>99
$Ti_{2.3}$-HUS	1.8	6.5	4.9	7.5	n.d.	>99
$Ti_{2.3}$-HUS cal[a]		8.3	12.7	12.6	n.d.	>99
TS-1[b]		2.2	2.4	3.7	n.d.	>99
TiO_2(P25)[c]			39.7	13.6	126.0	72

[a]Calcined at 400 °C under air flow. [b]A reference catalyst, ARCTS1CL, Catalysis Society of Japan (Si/Ti molar ratio of 35). [c]Irradiation time, 6 h. [d]Molar ratio calculated from the amounts of Ti and acetylacetonate determined by the inductively coupled plasma atomic emission spectroscopy of the dissolved products and thermogravimetric-differential thermal analysis under air flow of the products, respectively. The mass loss from 250 to 500 °C was assumed because of the oxidative decomposition of acetylacetonate. [e]CHone and CHol are cyclohexannoe and cyclohexanol, respectively. [f][formed CHone] + [formed CHol]}/{[formed CHone] + [formed CHol] + 1/6[formed CO2]} × 100.

CHol). When the reaction was carried out over the $Ti_{2.3}$-HUS under no irradiation condition, CHol, CHone and CO_2 were not formed. The considerable increase in the yields of CHone and Chol was observed when the calcined Ti_x-HUS was used. The yields of CHone and CHol were 4.4 and 6.1 μmol for $Ti_{1.2}$-HUS cal, 6.1 and 6.7 μmol for $Ti_{1.5}$-HUS, and 12.7and 12.6 μmol for $Ti_{2.3}$-HUS, respectively. Accordingly, both the interlayer pores created by removing of acetylacetonate ligands and pillaring of HUS-2 with $Ti(acac)_4$ and the isolated and tetrahedrally coordinated Ti grafted onto the silicate sheets played important roles in photocatalysis. Moreover, it was also found that the yields of CHone and CHol increased with the amount of

incorporated Ti. These results strongly suggest that the larger amount of incorporated Ti yielded more effectively CHone and CHol because the isolated and tetrahedrally coordinated Ti species was homogeneously distributed in the silicate surfaces and acted as a single active site. This conceptually new methodology can be used for the accurate construction of similar composite materials. Co-grafting of other metal acetylacetonates is now under investigation for further optimization of the photocatalytic performance.

4. Conclusions

I successfully grafted titanium(IV) acetylacetonate onto the interlayer surface of the layered silicate HUS-2. The Ti-incorporated (pillared) layered silicate showed a high photocatalytic activity and excellent chemoselectivity in the partial cyclohexane oxidation to cyclohexanone and cyclohexanol under simulated solar light irradiation.

References

1 G. Centi and F. Trifiro, *New Developments in Selective Oxidation*; Elsevier: Amsterdam, 1990.

2 I. W. C. E. Arends, R. A. Sheldon, M. Wallau and U. Schuchardt, *Angew. Chem., Int. Ed*. 1997, **36**, 1144.

3 B. Notari, *Stud. Surf. Sci. Catal*. 1991, **60**, 343.

4 T. Blasco, M. A. Camblor, A. Corma, P. Esteve, J. M. Guil, A. Martinez, J. A. Perdigón-Melón and S. Valencia, *J. Phys. Chem. B* 1998, **102**, 75.

5 Q.-H. Xia, X. Chen and T. Tatsumi, *J. Mol. Catal. A:Chem*. 2001, **176**, 179.

6 W. Fan, R. G. Duan, T. Yokoi, P. Wu, Y. Kubota and T. Tatsumi, *J. Am. Chem. Soc*. 2008, **130**, 10150.

7 A. Corma and H. Garcia, *Chem. Commun*. 2004, 1443.

8 Y. Shiraishi, N. Saito and T. Hirai, *J. Am. Chem. Soc*. 2005, **127**, 8304.

9 S. Rodrigues, K. T. Ranjit, S. Uma, I. N. Martyanov and K. Klabunde, *J. Adv. Mater*. 2005, **17**, 2463.

10 K. Mori, H. Yamashita and M. Anpo, *RSC Adv*. 2012, **2**, 3165.

11 T. Okada, Y. Ide and M. Ogawa, *Chem. Asian J*. 2012, **7**, 1980.

12 E. Ruiz-Hitzky and J. M. Rojo, *Nature* 1980, **287**, 28.

13 N. Takahashi and K. Kuroda, *J. Mater. Chem*. 2011, **21**, 14336.

14 M. Ogawa, S. Okutomo and K. Kuroda, *J. Am. Chem. Soc*. 1998, **120**, 7361.

15 Y. Ide and M. Ogawa, *Chem. Commun*. 2003, **11**, 1262.

16 Y. Ide and M. Ogawa, *Angew. Chem., Int. Ed*. 2007, **46**, 8449.

17 Y. Ide, M. Torii,; N. Tsunoji, M. Sadakane and T. Sano, *Chem. Commun*. 2012, **48**, 7073.

18 F. E. Osterloh, *J. Am. Chem. Soc*. 2002, **124**, 6248.

19 V. S. O. Ruiz, G. C. Petrucelli and C. Airoldi, *J. Mater. Chem.* 2006, **16**, 2338.

20 Y. Matsuo, T. Tabata, T. Fukunaga, T. Fukutsuka and Y. Sugie, *Carbon* 2005, **43**, 2875.

21 J. J. Tunney and C. Detellier, *Chem. Mater*. 1993, **5**, 747.

22 Y. Mitamura, Y. Komori, S. Hayashi, Y. Sugahara and K. Kuroda, *Chem. Mater*. 2001, **13**, 3747.

23 S. Takahashi, T. Nakato, S. Hayashi, Y. Sugahara and K. Kuroda, *Inorg. Chem*. 1995, **34**, 5065.

24 J. L. Guimarães, P. Peralta-Zamora, F. Wypych, *J. Colloid Interface Sci*. 1998, **206**, 281.

25 A. Shimada, Y. Yoneyama, S. Tahara, P. H. Mutin and Y. Sugahara, *Chem. Mater*. 2009, **21**, 4155.

26 C. Wang, K. Tang, D. Wang, Z. Liu, L. Wang, Y. Zhu and Y. Qian, *J. Mater. Chem*. 2012, **22**, 11086.

27 T. D. Baerdemaeker, B. Yilmaz, M. Feyen, U. Müller and D. D. Vos, *Proceedings of the 17th International Zeolite Conference*; Moscow, Russia, July 7−12, 2013 ; International Zeolite Association, 2013; Vol. B, pp 37−38.

28 N. Tsunoji, T. Ikeda, Y. Ide, M. Sadakane and T. Sano, *J. Mater. Chem*. 2012, **22**, 13682.

29 H. Tada, Q. Jin, H. Nishijima, H. Yamamoto, M. Fujishima, S. Okuoka, T. Hattori, Y. Sumida and H. Kobayashi, *Angew. Chem., Int. Ed*. 2011, **50**, 3501.

30 H. Hattori, Y. Ide, S. Ogo, K. Inumaru, M. Sadakane and T. Sano, *ACS Catal*. 2012, **2**, 1910.

Chapter 7

Design of novel microporous material HUS-10 by interlayer silylation of layered silicate HUS-2 with trichloromethylsilane and its molecular sieving ability and potential for separation of CO_2

6. Introduction

Zeolites having solid acidity, high internal surface area, molecular sieving and ion-exchange ability are a class of microporous crystalline aluminosilicate. Because of their attractive properties, they has been utilized as catalysts, adsorbents and ion-exchangers even in environmentally friendly and economically beneficial applications such as hydrocarbon conversions in petroleum and separation processes in chemical industries.[1-3] The attractive properties of zeolites are derived from their various structural features. Especially, the pore structure, pore size and connectivity, bring the important properties for controlling their functionalities such as diffusion of molecules, catalytic abilities and separation selectivity. Therefore, a lot of efforts have been made in synthesis of various novel zeolites having new framework types using complex structure-directing agents, isomorphous substitution of Si with other appropriate atoms and controlling other synthesis condition.[4-7] To date, because the development of zeolite synthesis has been achieved by continuing preparation and the research of fundamental properties of zeolite, design of their structural features and

desired physicochemical properties on an atomic scale are still most critical issue for innovative zeolite synthesis.

To achieve more free and rational construction of microporous materials, another synthesis approach using two-dimensional silicate precursors as a "structural building unit" has attracted considerable attention.[8-13] The layered precursors, layered zeolitic materials and layered silicates, have reactive neighboring silanol (SiOH and SiO^-) groups regularly located in the interlayer surface. Because the layered precursors are easily functionalized by various modifications such as cation exchange, silylation, and pillaring, they have attracted interest in many applications such as catalysis and adsorption.[9,14,15] Furthermore, the layered precursors can be transformed into 3D-porous structures by post treatment of the interlayer silanol groups including dehydration and condensation (topotactic conversion)[16-34] and silylation reaction.[35-50] The advantage of these procedures is that if the crystal structures of the layered precursors are determined, the framework structures of porous materials obtained thorough the modification processes we can be easily determined. Conventional such transformation processes are shown in Fig. 7-1A. The conversion of a layered precursor into a zeolite proceeds through the topotactic dehydration–condensation of periodic and reactive silanol groups on both sides of the interlayer (Fig. 7-1A top). In contrast, the interlayer silylation process gives more designable construction of interlayer structure. New Si-O-Si linkages are incorporated into the SiOH and SiO^- groups in the interlayer and the up-and-down silicate layers are connected by the incorporated tetrahedral units, affording construction of larger pore (Fig. 7-1A bottom). Layered silicates and layered zeolitic materials including PLS-1,[35,39,41] PLS-3,[39] PLS-4,[39] RUB-36,[43-45,48,50] RUB-39,[40,42,43] RUB-51,[49] Nu-6(1),[47] MWW(P),[36,41,46] MCM-47[46] and PREFER,[36,38,39] have been silylated with chlorosilane or alkoxysilane. Inagaki et al. prepared the organic-inorganic hybrid zeolite IEZ (Interlayer Expanded Zeolite)-1 by interlayer silylation of the layered silicate PLS-1 and also investigated the adsorption ability for

benzene.[35] Ruan et al. elucidated the interlayer 12- membered pore structure in the IEZ-1 by the HR-TEM observations.[38] The crystal structure of interlayer expanded porous materials were determined by Ikeda et al.[39] and Gies et al.[40] using XRD. Several groups concluded that more accessible channels in the interlayer expanded zeolites gave a higher catalytic activity than unexpanded materials.[37,41-43,45,46] Furthermore, several literatures report the successful the silylation of another type of layered precursors and the formation of artful 3-D structures. Roth et al. report the synthesis of two type of zeolites, IPC-2 and IPC-4 having different pore diameter, by the interlayer condensation and silylation reaction of IPC-1P, layered material with UTL like layers removed framework germanium.[25] Silylation of layered silicate RUB-51 with halved sodalite cages and the potential of the silylated derivative as a separation medium were reported by Asakura et al.[43] From such perspectives, the development of the silylation technique for creation of new pore structure using novel layered precursor is important for more free design of advanced and innovative porous materials. Although, when the interlayer silylation processes is categorized, they are similar strategy, which is the immobilization of one SiO_4 tetrahedral unit between the interlayer. Because the 3-D porous structures obtained through the transformation cannot exhibit totally different structure from layered precursors due to the structural similarity, a small number of the construction method disturb the diversification and further development of zeolite synthesis. To overcome such limitation and to change the zeolite synthesis more directly and freely, therefore, a novel synthesis route using new layered precursor for design of interlayer micropore is required.

Recently, Sano and I et. al reported the successful synthesis and structural analysis of new layered silicates, Hiroshima University Silicates (HUSs), which were synthesized using alkylammonium cations with various structures.[51-58] I also investigated their adsorption, ion-exchange properties, and potential as the precursors for the catalysts and porous materials. Among of those, layered silicate

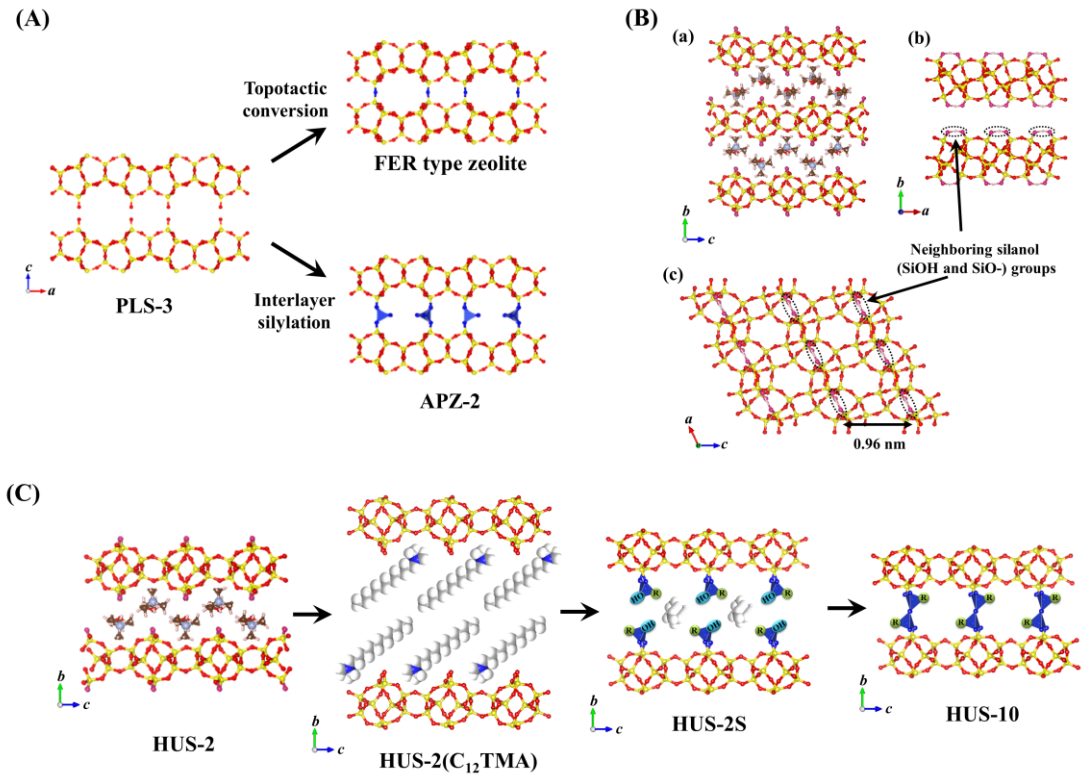

Fig. 7-1 (A) Formation of interlayer micropore in the layered silicate PLS-3, (B) (a) crystal structure and framework structure of HUS-2 along the (b) *c* and (c) *b* axis, and (C) formation scheme of ordered micropore in the interlayer of HUS-2.

HUS-2 has a unique framework structure, which is partially similar to that of a HEU-type zeolite including *bre* (10T)-type composite building units, and interlayer choline cations (Scheme 1B). The interlayer SiOH and SiO^- groups linearly located along the *a* axis with hydrogen bond interacted each other against the surface of the silicate layer. In this study, I report the novel method for the design of ordered microporous material HUS-10 by the two step method including the interlayer silylation and subsequent calcination of layered silicate HUS-2. The preparation strategy for the design of interlayer micropore in the interlayer of HUS-2 is depicted in Fig. 7-1C. First, choline cation in the interlayer of HUS-2 is ion-exchanged with bulky molecule, dodecyltrimethylammonium, affording ion-exchanged

HUS-2(HUS-2(C_{12}TMA)). Subsequently, HUS-2(C_{12}TMA) is silylated using trichloromethylsilane. The introduced tetrahedral unit with hydroxyl groups from trichloromethylsilane is immobilized on the interlayer surface in a dipodal fashion. Finally, by calcination, the dehydration-condensation of remaining hydroxyl groups of the immobilized tetrahedral units on both sides of the interlayer take place and up-and-down silicate layers are connected via Si-O-Si covalent bond, yielding the HUS-10 having 3D-porous structure. From structural determination using MAS NMR measurement, it was concluded that the HUS-10 has porous structure consist of 2-dimansional 8- and 12- membered rings with methyl and hydroxyl groups on the pore surface. I also studied the molecular sieve ability of HUS-10 by the molecular prove method using various gas molecules having different molecular sizes. Furthermore, in order to clarify the potential application for CO_2 adsorption separation, the adsorption behevior of CO_2, CH_4 and N_2 at room temperature were investigated.

2. Experimental

2.1. Preparation of crystalline porous silicas

Synthesis of layered silicate HUS-2. HUS-2 ($Si_{20}O_{40}(OH)_4 \cdot 4[C_5H_{14}NO]$)[25] was synthesized by hydrothermal treatment of starting gels containing fumed silica (Cab-O-Sil® M5, Cabot Co.), choline hydroxide (48–50 wt%, Aldrich), sodium hydroxide (>99%, High Purity Chemicals Inc., Japan), and distilled water. The starting gel, with the chemical composition SiO_2:0.4 choline hydroxide:0.1 NaOH:5.5 H_2O, was

transferred into a Teflon-lined stainless steel vessel and heated under static conditions at 150 °C for 2 d. The solid product obtained was separated by centrifugation, washed with distilled water, and dried at 70 °C overnight.

Ion-exchange of HUS-2 with dodecyltrimethylammonium cation (HUS-2(C_{12}TMA)). HUS-2 ion-exchanged with dodecyltrimethylammonium cation (HUS-2(C_{12}TMA)) was prepared as follow. HUS-2 (10 g) was dispersed in an aqueous solution (500 ml) of dodecyltrimethylammonium chloride (C_{12}TMACl, Tokyo Chemical Ind. Co. Ltd., Japan, 0.33 mol). The mixture was stirred at 60 °C for 24 h and then centrifuged to remove the supernatant. This procedure was repeated three times. The obtained solid separated by centrifugation was washed with water/ethanol (50/50 vol%) solution and then dried at 70 °C overnight.

Interlayer silylation and calcination of HUS-2 (HUS-2S, HUS-10(200-550), PHUS-10(400)). HUS-2(C_{12}TMA) (2.0 g), dried in vacuum at 70 °C for 3 h, was dispersed in dehydrated toluene (50 ml). An excess amount (1.5 g, 5 equiv of 4 SiO^-/SiOH groups) of trichloromethylsilane (Tokyo Chemical Ind. Co. Ltd.) and 2,2'-Bipyridyl (3.3 g, Tokyo Chemical Ind. Co. Ltd.) were added to the mixture and stirred at 100 °C for 3 d under N_2 atmosphere. The resultant solid product was centrifuged and washed with toluene and then dried at 70 °C overnight. To transform the HUS-2S into a 3D-porous material through the interlayer dehydration-condensation reaction, the HUS-2S was calcined at 200, 400, 500, 550 and 600 °C for 6 h, named HUS-10(200), HUS-10(400), HUS-10(500), HUS-10(550) and HUS-10(600), respectively. For a reference, the as-synthesized HUS-2 was also silylated and then calcined at 400 °C for 6 h, named PHUS-2S and PHUS-10(400), respectively.

2.2 Characterization

Powder X-ray diffraction (XRD) patterns of the solid products were collected using a powder X-ray diffractometer (Rigaku MiniFlex) with graphite-monochromatized Cu Kα radiation at 30 kV and 15 mA. The crystal morphology was observed using a Hitachi S-4800 scanning electron microscope (SEM) coupled with an energy-dispersive X-ray (EDX) analyzer. ^{29}Si magic-angle spinning (MAS) NMR spectra were recorded at 119.17 MHz on a Varian 600PS solid NMR spectrometer using a 6 mm diameter zirconia rotor. The rotor was spun at 7 kHz. The spectra were acquired using 6.7 μs pulses, a 100 s recycle delay, and 1000 scans. 3-(Trimethylsilyl)propionic-2,2,3,3-d_4 acid sodium salt was used as a chemical shift reference. ^{1}H-^{13}C cross-polarized (CP)-MAS NMR spectra were measured with a spinning frequency of 7 kHz, a 90° pulse length of 2.2 μs, and a cycle delay time of 100 s. The ^{13}C chemical shifts were referenced to hexamethylbenzene. Thermal analyses were carried out using a thermogravimetric/differential thermal analysis (TG/DTA) apparatus (SSC/5200, Seiko Instruments). A sample (ca. 3 mg) was heated in a flow of air (50 mL min^{-1}) at a heating rate of 10 °C min^{-1} from room temperature to 800 °C. Nitrogen and argon adsorption isotherms were obtained at −196 and −189 °C, respectively, using a conventional volumetric apparatus (BELSORP-max, Bel Japan). Prior to performing the adsorption measurements, the calcined samples (ca. 50 mg) were heated at 200 °C for 3 h under evacuation. Adsorption measurements of H_2O, CO_2, CH_4, C_2H_6, n-butane and isobutene were also conducted. Elemental analysis was carried out using a PerkinElmer 2400 II CHN analyzer at the Natural Science Center for Basic Research and Development (N-BARD), Hiroshima University. Transmission electron microscopy (TEM) images of nanoporous silica were taken using a Hitachi H9500 microscope at an acceleration

voltage of 300 kV.

3. Results and discussion

3.1. Ion-exchange and interlayer silylation of HUS-2

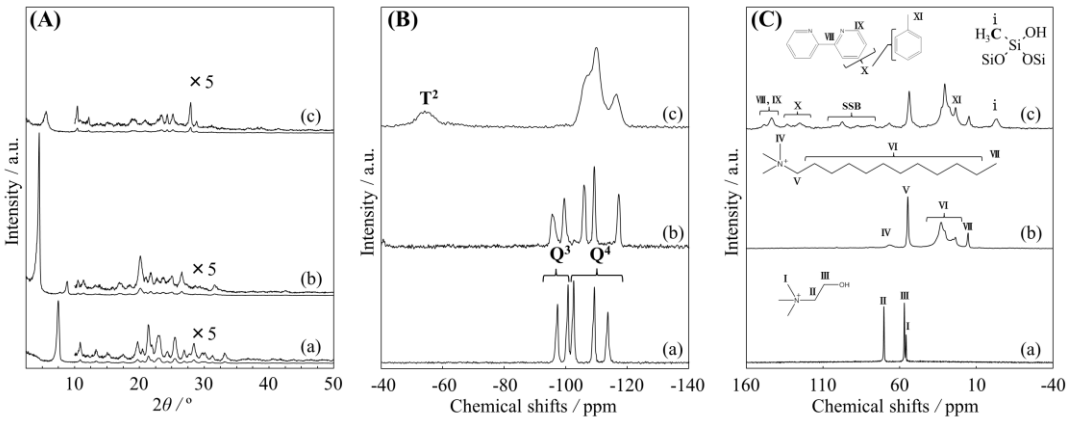

Fig. 7-2 (A) XRD patterns, (B) ^{29}Si MAS NMR spectra and ^{13}C CP MAS NMR spectra of (a) HUS-2, (b) HUS-2(C12TMA) and (c) HUS-2S.

Fig. 7-2A shows the XRD patterns of HUS-2, HUS-2(C_{12}TMA), and HUS-2S. The peaks attributed to basal spacing diffractions were observed in the low 2 theta region between 2.5° and 10°. The XRD pattern of HUS-2 showed a peak at 7.5° with a d-spacing of 1.2 nm. The basal spacing of HUS-2(C_{12}TMA) was 1.96 nm, whereas that of HUS-2S was 1.62 nm. Fig. 7-2B depicts the ^{29}Si MAS NMR spectra of HUS-2, HUS-2(C_{12}TMA), and HUS-2S. In the ^{29}Si MAS NMR spectra of HUS-2 and HUS-2(C_{12}TMA), the two resonance peaks between −90 and −105 ppm are assigned to a Q^3 structure, whereas the three resonance peaks between −105 and −120 ppm are assigned to a Q^4 structure. The Q^3/Q^4 peak intensity ratios are listed in Table 7-1. There are no changes in the peak intensity ratios of Q^3/Q^4 between HUS-2 and HUS-2(C_{12}TMA), indicating no collapse of the framework structure of HUS-2 during

Table 7-1 Characteristics determined by N_2 adsorption isotherms and ^{29}Si MAS NMR spectra

	BET surface area[a] / m^2g^{-1}	Micropore volume[b] / cm^3g^{-1}	Average pore diameter[c] / nm	Relative intensity ratio in ^{29}Si MAS NMR spectra				
				T^2	T^3	Q^3	Q^4	$(T^2+T^3+Q^3):Q^4$
HUS-2	-	-	-	0	0	40	60	40:60
HUS-2(C_{12}TMA)	-	-	-	0	0	40	60	40:60
HUS-2S	-	-	-	16	0	0	84	16:84
HUS-10(200)	-	-	-	16	0	0	84	16:84
HUS-10(400)	385	0.15	0.50	0	14	3	83	17:83
HUS-10(500)	378	0.14	0.50	0	10	7	83	17:83
HUS-10(550)	362	0.13	0.50	0	5	13	82	18:82
HUS-10(600)	105	0.03	-	0	0	21	79	21:79

[a] Determined by the BET method..

[b] Determined using the t-plot.

[c] Determined using the Ar adsorption isotherms and SF method.

the ion-exchange process. In the spectrum of HUS-2S, a new signal at −54 ppm was observed. From ^1H-^{29}Si CP MAS NMR measurements, it was found that the peak intensity at −54 ppm was relatively enhanced with increasing a contact time as compared to the other peaks between −100 and −120 ppm, indicating that peak at −54 ppm is attributable to T^2 ($(CH_3)\underline{Si}(OSi)_2(OH)$) structure. It was also found that there was no Q^3 peak in the ^{29}Si MAS NMR spectrum of HUS-2S. This strongly indicates the formation of Si-O-Si covalent bond between introduced tetrahedral unit (trichloromethylsilane) and interlayer silanol group of HUS-2. Taking into account that (1) the degree of silylation calculated from the Q^3/Q^4 ratio was ca. 100% and (2) the peak intensity ratio of T^2/Q^4 in the HUS-2S (16/84) was consistent with the value expected from silyalated HUS-2 in which two Q^3 silicon species on the interlayer surface reacted with one introduced tetrahedral unit, the introduced tetrahedral unit was uniformly immobilized on the interlayer surface with dipodal fashion remaining a hydroxyl group. The ^{13}C CP MAS NMR spectra of HUS-2, HUS-2(C_{12}TMA) and HUS-2S are

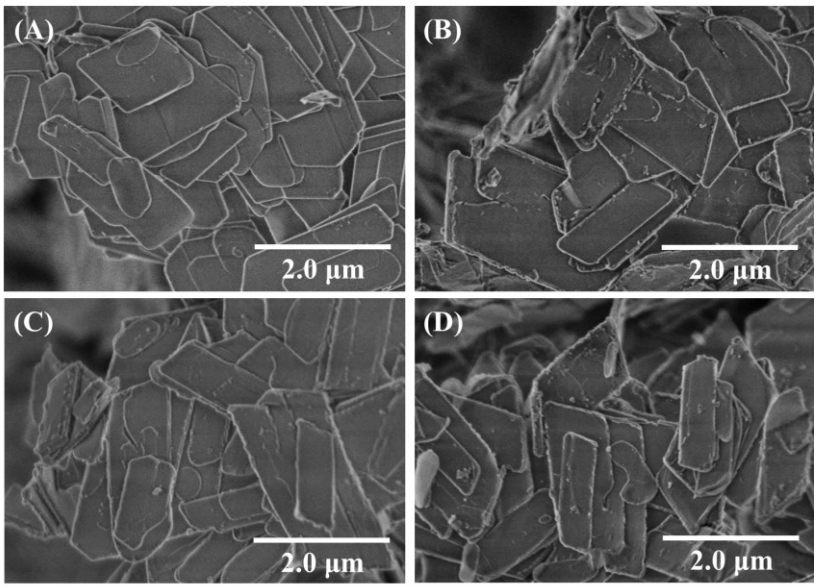

Fig. 7-3 (A) SEM images of (A) HUS-2, (B) HUS-2(C12TMA), (C) HUS-2S and (D) HUS-10(400).

shown in Fig. 7-2C. In the ^{13}C CP MAS NMR spectrum of HUS-2, three resonance peaks that were centered at ca. 55, 57, and 70 ppm were observed, indicating the presence of choline cation in the interlayer. The HUS-2(C_{12}TMA) showed several peaks between 10-80 ppm, which are attributable to dodecyltrimethyammonium cation. From the CHN elemental analysis results that the C/N ratio of HUS-2 and HUS-2(C_{12}TMA) were 5.0 and 14.8, respectively, it was confirmed that choline cation in the interlayer of HUS-2 was completely ion-exchanged with dodecyltrimethyammonium cation. In the spectrum of HUS-2S, the resonance peak assigned to the methyl groups on the T^2 silicon was observed at ca. −2.9 ppm. It was also found from the observation of several resonance peaks between 110-160 ppm that toluene and 2,2'-bipyridyl molecules were presented in the HUS-2S. SEM images of HUS-2, HUS-2(C_{12}TMA) and HUS-2S are shown in Fig. 7-3. There are no differences in the morphology (square, plate-like) and particle sizes (1.0 × 3.0 μm) among the samples.

3.2. Interlayer dehydration and condensation of HUS-2S

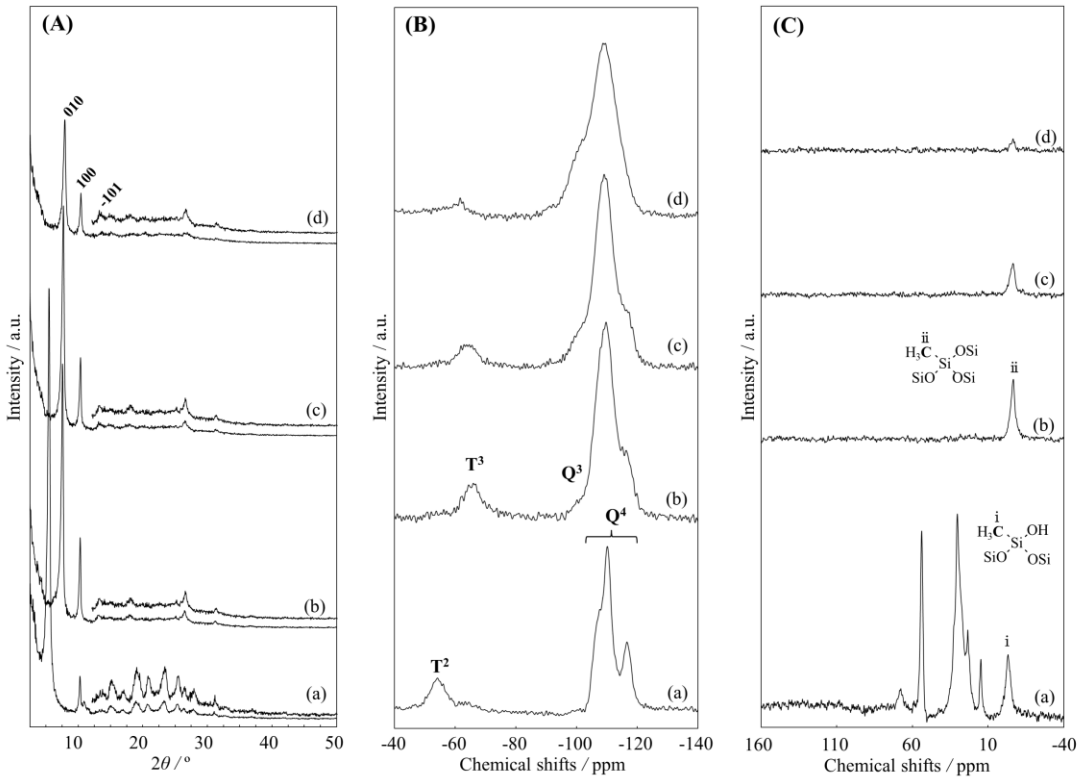

Fig. 7-4 (A)XRD patterns, (B) ^{29}Si MAS NMR and (C) ^{13}C CP MAS NMR spectra of (a) HUS-10(200), (b) HUS-10(400), (c) HUS-10(500) and (d) HUS-10(550).

To form the interlayer pore by the dehydration-condensation reaction of the remaining hydroxyl groups of the introduced tetrahedral unit on both sides of interlayer, HUS-2S was calcined at various temperatures of 200, 400, 500 550 and 600 °C for 6 h, affording HUS-10(200), HUS-10(400), HUS-10(500), HUS-10(550) and HUS-10(600), respectively. The HUS-2S calcined at 400 °C (HUS-10(400)) showed square a plate-like morphology, which reflected the morphology of as-synthesized HUS-2 (Fig. 7-3D). Fig. 7-4A shows the XRD pattern of HUS-10(200), HUS-10(400), HUS-10(500) and HUS-10(550). As shown in Fig. 7-4A, the XRD patterns of all HUS-10s are indicative

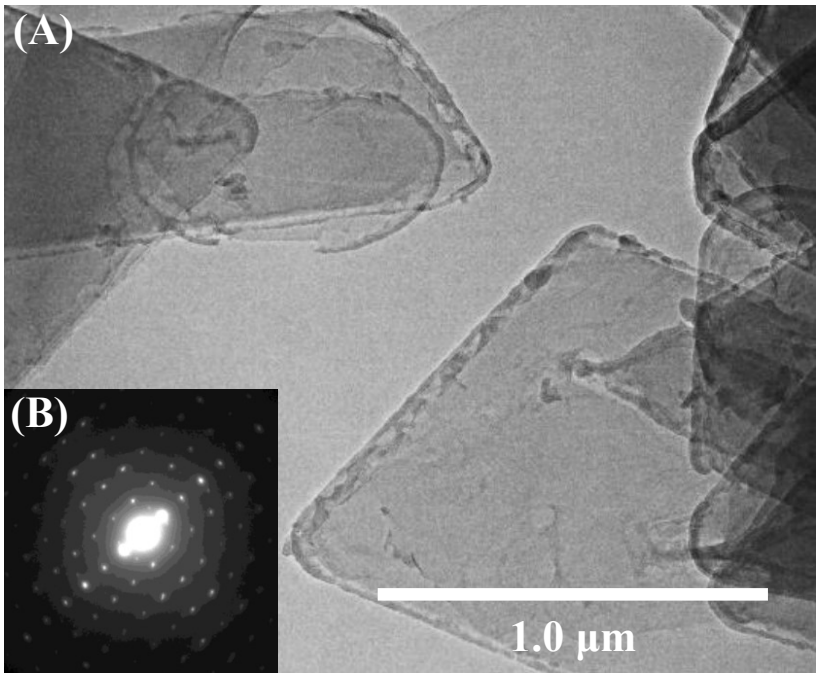

Fig. 7-5 (A) TEM image and (B) electron diffraction pattern of HUS-10(400).

of a single phase. If the interlayer structure is disordered, the basal spacing of (010) peaks should split or become broad. Although there were no changes in the basal spacing before and after calcination at 200 °C, whereas in the case of HUS-10(400), the diffraction peak at 2 theta of ca. 7.6 ° with basal spacing of ca. 1.17 nm was observed, which is shorter than that of HUS-10(200), indicating the decrease in the interlayer distance. Even if the calcination temperature was elevated to 500 and 550 °C, the basal spacing values of calcined products were hardly changed. In the high 2 theta region, HUS-10s maintained *h0l* in-plane diffraction peaks characteristic of as-synthesized HUS-2 at 2 theta of ca. 10.2 and 13.4°, indicating that the framework structure of original silicate layer was retained through the post treatment including silylation and subsequent calcination. However, when the HUS-2S was calcined at 600 °C, the further decrease in the interlayer distance was observed, indicating the possibility of the change

of the interlayer structure. The TEM image and electron diffraction pattern of HUS-10(400) is shown in the Fig. 7-5. The plate-like particle with the size of 1.0 × 3.0 μm was clearly observed. As shown in the Fig. 7-5B, the net pattern was observed for the HUS-10(400). This demonstrates that this plate like particle was well crystallized. The *d*-spacings of several electron diffractions were in good agreement with that of XRD.

To obtain further information concerning the interlayer structure, ^{29}Si MAS NMR measurements of calcined HUS-2Ss were carried out. Fig. 7-4B shows the ^{29}Si MAS NMR spectra of HUS-10(200), HUS-10(400), HUS-10(500) and HUS-10(550). ^{13}C CP MAS NMR spectra of calcined products were also shown in the Fig. 7-4C. There was no change in the ^{29}Si MAS NMR spectra before and after calcination at 200 °C for 6 h, indicating that the interlayer structure was maintained. In addition to the ^{13}C CP MAS NMR spectrum of HUS-10(200), several resonance peaks due to C_{12}TMA molecule was observed between 10 - 80 ppm. As shown in the Figure 7-4C, the remaining C_{12}TMA molecule was completely removed by calcination at ≥400 °C and only one resonance peak was observed at −6.5 ppm. Taking into the fact that the resonance peak can be assigned to methyl group of $(\underline{C}H_3)Si(OSi)_3$, it is indicates that the formation of interlayer new Si-O-Si covalent bond. The difference in the chemical shift after calcination at ≥400 °C, −2.9 to −6.5 ppm, seem to be the changing of chemical state of methyl group on the T structure silicon. In the ^{29}Si MAS NMR spectra HUS-2(400), HUS-2(500) and HUS-2(550), new resonance peaks assigned to T^3 ($(CH_3)\underline{Si}(OSi)_3$) and Q^3 ($\underline{Si}(OSi)_3(OH)$) structures were clearly observed at −65 and −100 ppm, respectively. The presence of T^3 structure strongly indicates the dehydration and condensation reaction between the remaining silanol groups of tetrahedral units immobilized on the

up-and-down silicate layers surfaces. The peak intensity of Q^4 in the ^{29}Si MAS NMR spectra of HUS-10s were hardly changed during calcination at temperatures between 400 - 550 °C, which indicates that the cleavage of Si–O–Si bonds in the framework was negligible. This result strongly indicates that the new resonance Q^3 peak appeared at −100 ppm is attributed to the introduced tetrahedral unit on the silicate layers. The peak intensity of Q^3 gradually increased with increasing the calcination temperature, whereas that of T^3 decreased monotonously. In addition, during the calcination, the decrease in the peak intensity at −6.5 ppm in the ^{13}C CP MAS NMR spectra and the decrease in the organic entities contents in the HUS-10s measured by CHN elemental analysis were observed. These results strongly indicate that the remaining methyl group of the tetrahedral unit immobilized on the interlayer was gradually substituted to hydroxyl group by calcination without collapse of the silicate framework. In contrast, the ^{29}Si MAS NMR spectrum of HUS-10(600) revealed the partial collapse of the silicate framework because of the high peak intensity of Q^3 compared to HUS-10(400), HUS-10(500) and HUS-10(550). It was also found that there are no methyl groups in the HUS-10(600) as evidenced by ^{13}C CP MAS NMR spectrum and CHN elemental analysis.

3.3. Porosity and adsorption property of HUS-10s

Next, I investigated the porosity of HUS-10s. The N_2 adsorption-desorption isotherms of HUS-10(200), HUS-10(400), HUS-10(500) and HUS-10(550) are shown in the Fig. 7-6A. The textural properties of the products calculated from N_2 and Ar adsorption isotherms are also listed in Table 7-1. For the HUS-2S calcined at 200 °C, the micropore volume (0.01 cm^3g^{-1}) and BET surface area (10 m^2g^{-1}) were very low due

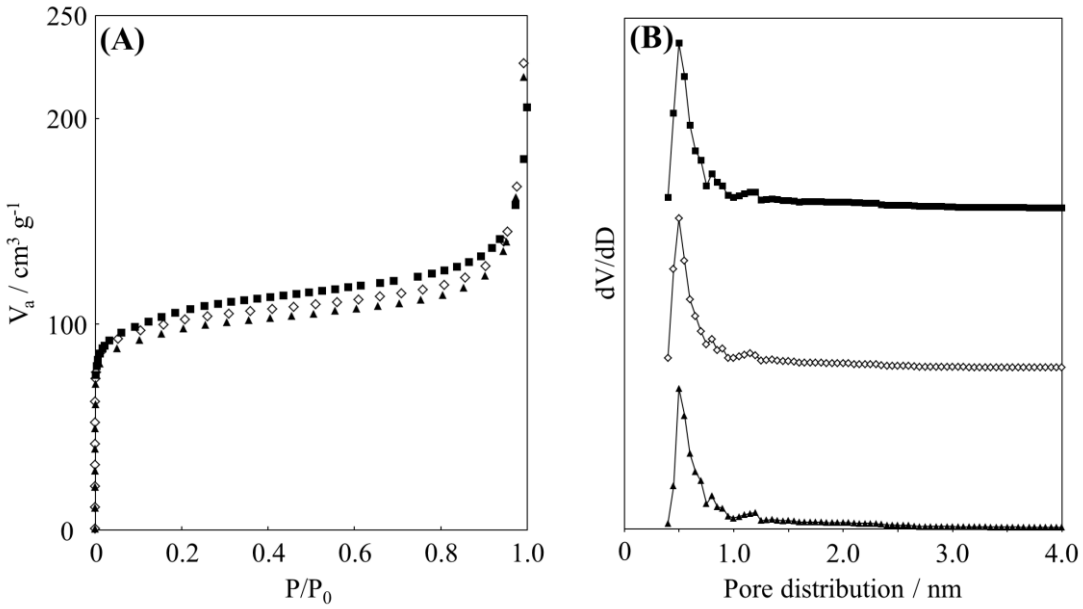

Fig. 7-6 (A) N_2 adsorption isotherms and (B) pore size distributions of (■) HUS-10(400), (◊) HUS-10(500) and (▲) HUS-10(550). The pore size distribution was measured by Ar adsorption.

to the presence of C_{12}TMA molecule occluded in interlayer space. In contrast, the N_2 adsorption isotherms of the HUS-10(400), HUS-10(500) and HUS-10(550) exhibited a steep increase in the adsorption amount at low relative pressure; this suggests the existence of micropores. The BET surface area and micropore volume of HUS-10(400) was calculated to be 385 m^2 g^{-1} and 0.16 cm^3 g^{-1}. HUS-10(600) showed lower BET surface area (105 m^2 g^{-1}) and micropore volume (0.03 cm^3 g^{-1}), which are indicative of the collapse of interlayer pore structure by calcination at higher temperatures. The pore size distributions, calculated from the adsorption branch of Ar adsorption using the SF method, are shown in the Fig. 7-6B. As shown in the Fig. 7-6B, a very narrow pore size distribution with average pore diameter of 0.50 nm was clearly observed in the HUS-10(400), HUS-10(500) and HUS-10(550). As there are no differences in the textual properties of HUS-10(400), HUS-10(500) and HUS-10(550), it is suggested that the amounts of methyl and hydroxyl group in the interlayer pore was successfully

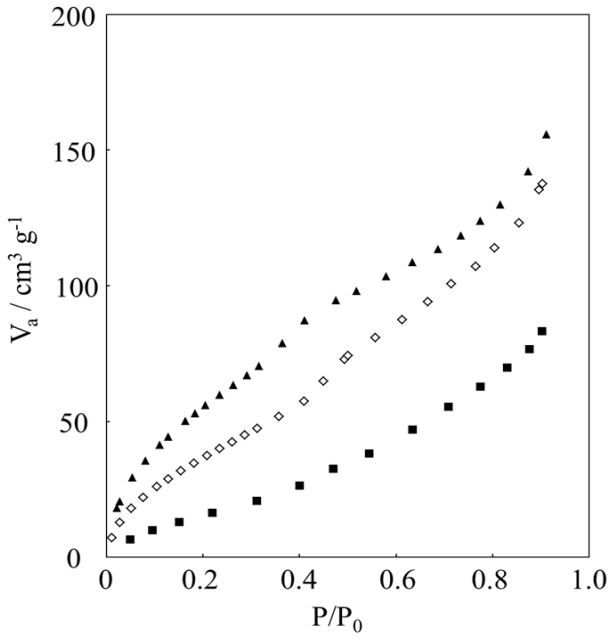

Fig. 7-7 (A) H_2O adsorption isotherms of (■) HUS-10(400), (◊) HUS-10(500) and (▲) HUS-10(550).

controlled by varying the calcination temperature without changing the pore structure. Such organic functionalized microporous material would allow a wide range of applications because of the unique surface property, which can control adsorption behavior of various guest molecules into the micropores. Next, I studied the adsorption behavior of H_2O molecules on the obtained porous materials having different amounts of hydroxyl and methyl groups. Fig. 7-7 shows the adsorption isotherms of H_2O on the HUS-10(400), HUS-10(500) and HUS-10(550) at 25 °C. The amount of adsorbed H_2O increased with increasing the calciation temperature. Thus, apparently, the interlayer micropores generated in HUS-10(550) are more hydrophilic than that of HUS-10(400) due to the presence of larger amounts of hydorxy groups of HUS-10(550). Accordingly, it is found that hydrophilicity of the interlayer space of HUS-10s can be controlled by only calcination process.

Crystalline microporous materials including zeolite and MOF show various useful

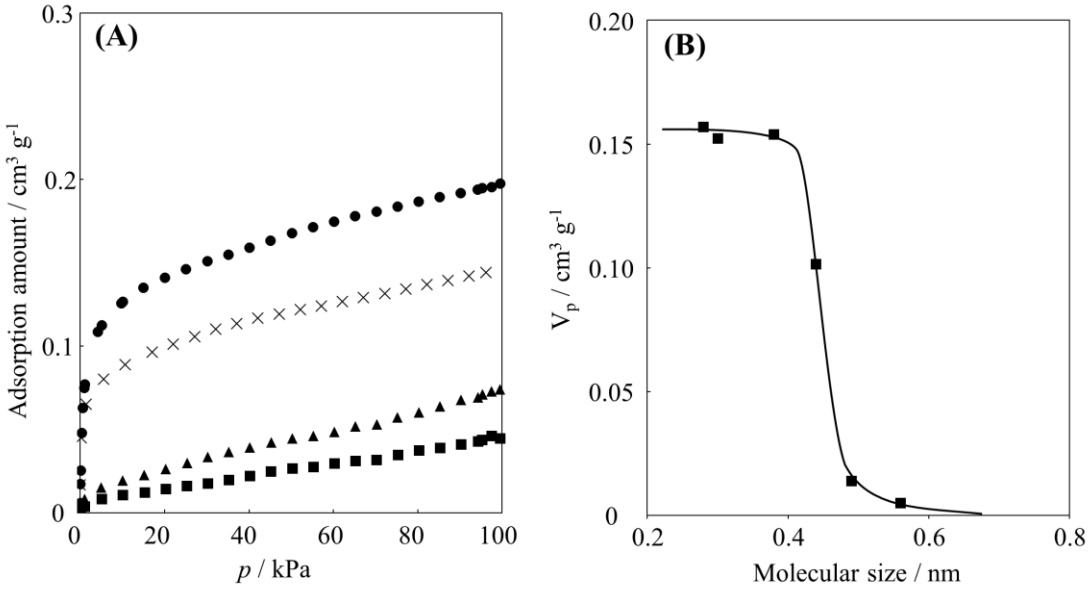

Fig. 7-8 (A) Adsorption isotherms of CO_2, C_2H_6, n-butane and isobutene on HUS-10(400). (B) Relationship between micropore volumes using probe molecules, such as CO_2, N_2, Ar, C_2H_6, n-butane and isobutene, and adsorbed molecular size. The micropore volumes were calculated from their adsorption isotherms.

properties. Especially, the molecular sieving ability, which recognizes the difference in the molecular sizes, is very important for the development of catalysts and adsorbents in industry. Although interlayer silylation of layered precursor gives an accurate construction of interlayer structure, there are few reports concerning the accurate pore size and adsorption behavior of interlayer space. Therefore, to clarify the actual molecular sieving ability of obtained porous materials, the molecular probe method using the various probe molecules with different molecular sizes was applied. Fig. 7-8A shows the adsorption isotherms of CO_2, C_2H_6, n-butane, isobutene of HUS-10(400). Adsorption measurements were performed under the conditions of near the boiling point of these molecules. Fig. 7-8B shows the relationship between the micropore volume of HUS-10(400) calculated form gas adsorption isotherms of CO_2, N_2, Ar, C_2H_6, n-butane and isobutene using the DR method, and the molecular sizes of probe molecules. The

HUS-10(400) hardly adsorbed isobutene and n-butane, whose molecular sizes were 0.58 nm and 0.49 nm, respectively. The micropore volumes estimated using isobutene and n-butane were 0.005 $cm^3\ g^{-1}$ and 0.014 $cm^3\ g^{-1}$, respectively. On the other hand, the micropore volume calculated using C_2H_6 was 0.10 $cm^3\ g^{-1}$. In addition, further increase of micropore volume was observed on the Ar. Although several molecules smaller than Ar exhibit different molecular sizes, the molecular sizes of CO_2 (0.28 nm), N_2, Ar and C_2H_6 (0.42 nm) were 0.28, 0.30, 0.38 and 0.44 nm, respectively, no changes in adsorbed amount between was observed among these molecules. The maximum pore volume (0.15 cm^3g^{-1}) determined by the molecular probe method was consistent with that (0.16 cm^3g^{-1}) of calculated from N_2 adsorption isotherm using by the t method. Furthermore, the average pore diameter (0.45 nm) estimated by the molecular probe method as shown in Fig. 7-8B was well consistent with that (0.50 nm) from Ar adsorption isotherm. These results strongly indicate that HUS-10(400) has ordered micropore like a zeolite and can adsorb smaller molecule than ethane, indicating the high molecular sieving ability. I also confirmed that both HUS-10(500) and HUS-10(550) showed the similar molecular sieving ability. Accordingly, the atomic scale separation ability comparable with that of zeolite was achieved by the accurate design of the interlayer structure of HUS-2. To the best of my knowledge, this is the first report that the microporous material synthesized from silicate layered precursors exhibited the separation ability in the angstrom level.

As described in the above section, the HUS-10 exhibits a unique pore structure, which consists of 8 and 12 membered rings with methyl and hydroxy groups regularly located on the open framework. In the light of this, I investigated an effect of the unique pore structure of HUS-10 on the adsorption behavior of CO_2, CH_4, and N_2, which are known as important test molecules helping for understanding the separation ability of

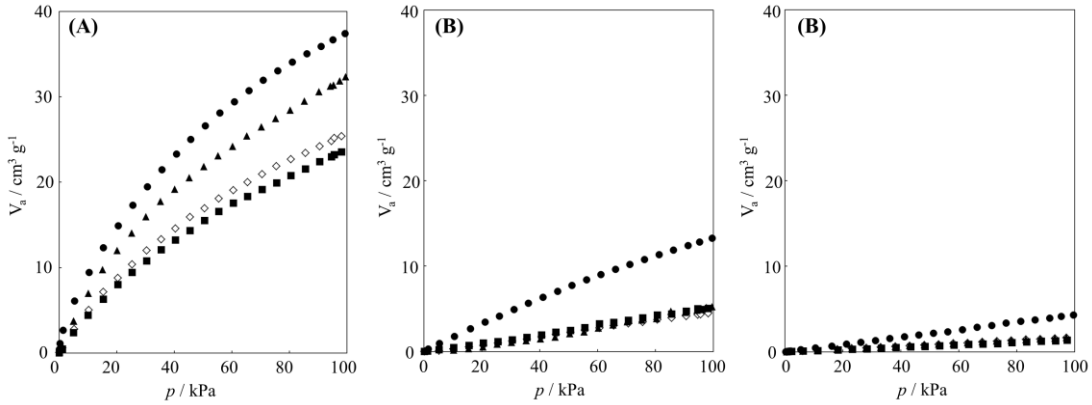

Fig. 7-9 (A) CO_2, (B) CH_4 and (C) N_2 adsorption isotherms of (■) HUS-2S(400), (◊) HUS-2S(500), (▲) HUS-2S(550) and (●) silicalite-1 at 25 °C.

porous materials for various gas mixtures containing CO_2, such as natural gases and exhaust gases. For a reference, the adsorption experiments on silicalite-1, all-silica MFI type zeolite, whose texture properties are approximately equal to HUS-10 were also performed. Fig. 7-9 shows the adsorption isotherm of CO_2, CH_4 and N_2 at 25 °C. The large amounts of CO_2 adsorbed on the HUS-10s were observed. The adsorption amount of CO_2 increased with increasing calcination temperature, indicating an increase of hydrophilicity on HUS-10s. The adsorbed amount of CO_2 on HUS-10(550) at 100 kPa is 32 cm^3g^{-1}, which was comparable to that on silicalite-1. Although CH_4 and N_2 were adsorbed on silicalite-1 to same extent (13 cm^3g^{-1} (CH_4) and 4.3 cm^3g^{-1} (N_2) 100kPa), HUS-2Ss hardly adsorbed CH_4 and N_2 (5.2 cm^3g^{-1} (CH_4) and 1.9 cm^3g^{-1} (N_2) at 100kPa on HUS-10(550), respectively). It is well known that the CO_2 can be effectively separated from gas mixtures of CO_2 and CH_4 (or N_2), if the CO_2/CH_4 and CO_2/N_2 adsorption ratio is higher. The CO_2/CH_4 and CO_2/N_2 ratios of HUS-2S(550) were considerably higher than those of silicalite-1. The CO_2/CH_4 adsorption ratio of HUS-2S(550) were 9.9 at 10 kPa and 5.8 at 100 kPa, while those of silicalite-1 were 5.2 at 10 kPa and 2.8 at 100 kPa, respectively. Furthermore, the high CO_2/N_2 adsorption

ratio was also observed on HUS-2S(550) (CO_2/CH_4 = 36.6 at 10 kPa, 17.9 at 100 kPa). These values on HUS-2S(550) are comparable with those on several MOFs and zeolites having excellent CO_2 separation ability. MOF with flexible organic framework unit with high mobility often shows selective and effective CO_2 adsorption ability.[59-61] Therefore, taking into account that there are almost no difference in the pore characteristics between HUS-10s and silicalite-1, the excellent adsorption property of HUS-2S(400) may be due to obstruction of CH_4 and N_2 derived from the unique pore structure with methyl and hydroxy groups with high mobility which are regularly located on the pore surfaces. In general, zeolite is composed exclusively of silicon or aluminium atoms with Q^4 strucuture and the design synthesis of zeolites with desirable structure and composition is very difficult, whereas the interlayer silylation process, which is observed for IEZ like materials, often enables to design specific structure unlike conventional zeolites having a large amount of T^2 or Q^2 structure.[35,39] The present result motivated me to look at novel process of interlayer silylation, resulting in finding the more artful function of microporous materials.

4. Conclusion

A novel microporous material HUS-10 was synthesized from layered silicate HUS-2 through silylation with trichloromethylsilane and subsequent calcination. From DFT calculation, HUS-10 had 2-dimansional 8- and 12- membered pore structure with methyl and hydroxyl groups, which were attributed to immobilized trichloromethylsilane located on the pore surfaces. Furthermore, HUS-10 showed excellent CO_2 adsorption ability compared to silicalite-1. Silicalite-1 adsorbed CO_2, CH_4 and N_2 to some extent, while the large amount of CO_2 adsorbed was adsorbed

on HUS-10, which was 5 times and 10 times larger than the amounts of CH_4 and N_2 adsorbed, suggesting the excellent potential for the separation of CO_2 from various gas mixtures. I am speculating that this adsorption behavior is achieved by accurate design of microporous structure with unique adsorption space in the interlayer of HUS-2. The present result will be the help for the diversification and rationalization of design of functional microporous materials by using various silane coupling agents and layered precursors.

References

1 A. Corma, *Chem. Rev*., 1995, **95**, 559.

2 M. E. Davis, *Nature*, 2002, **417**, 813.

3 S. I. Zones, *Microporous Mesoporous Mater*., 2011, **144**, 1.

4 R. M. Barrer, *Zeolites*, 1981, **1**, 130.

5 M. E. Davis and R. F, Lobo, *Chem. Mater*., 1992, **4**, 756.

6 C. S. Cundy and P. A. Cox, *Chem. Rev*., 2003, **103**, 663.

7 J. X. Jiang, J. H. Yu and A. Corma, *Angew. Chem., Int. Ed*., 2010, **49**, 3120.

8 W. J. Roth and J. Čejka, *Catal. Sci. Technol*., 2011, **1**, 43.

9 N. Takahashi and K. Kuroda, *J. Mater. Chem*., 2011, **21**, 14336.

10 B. Marler and H. Gies, *Eur. J. Mineral*., 2012, **24**, 405.

11 F. S. O. Ramos, M. K. de Pietre and H. O. Pastore, *RSC Adv*., 2013, **3**, 2084.

12 W. J. Roth, P. Nachtigall, R. E. Morris and J. Čejka, *J. Chem. Rev*., 2014, **114**, 4807.

13 U. Díaz and A. Corma, *Dalton Trans*., 2014, **43**, 10292.

14 M. Ogawa and K. Kuroda, Bull. *Chem. Soc. Jpn*., 1997, **70**, 2593

15 T. Okada, Y. Ide and M. Ogawa, *Chem.–Asian J*.,2012, **7**, 1980.

16 M. E. Leonowicz, J. A. Lawton, S. L. Lawton and M. K. Rubin, *Science*, 1994, **264**, 1910.

17 L. Schreyeck, P. Caullet, J. C. Mougenel, J. L. Guth and B. Marler, *Microporous Mater.*, 1996, **6**, 259.

18 T. Ikeda, Y. Akiyama, Y. Oumi, A. Kawai and F. Mizukami, *Angew. Chem. Int. Ed*., 2004, **43**, 4892.

19 S. Zanardi, A. Alberti, G. Cruciani, A. Corma, V. Fornes, M. Brunelli, *Angew. Chem. Int. Ed*., 2004, **43**, 4933.

20 B. Marler, N. Stroter, H. Gies, *Microporous Mesoporous Mater*., 2005, **83**, 201.

21 Y. X. Wang, H. Gies, B. Marler and U. Muller, *Chem. Mater*., 2005, **17**, 43.

22 B. Marler, M. A. Camblor and H. Gies, *Microporous Mesoporous Mater*., 2006, **90**, 87.

23 Y. X. Wang, H. Gies, and J. H. Lin, *Chem. Mater*., 2007, **19**, 4181.

24 Y. Oumi, T. Takeoka, T. Ikeda, T. Yokoyama and T. Sano, *New J. Chem*., 2007, **31**, 593.

25 T. Ikeda, Y. Oumi, T. Takeoka, T. Yokoyama, T. Sano and T. Hanaoka, *Microporous Mesoporous Mater*., 2008, **110**, 488.

26 T. Moteki, W. Chaikittisilp, A. Shimojima and T. Okubo, T. *J. Am. Chem. Soc*., 2008, **130**, 15780.

27 Y. Oumi, K. Takagi, T. Ikeda, H. Sasaki, T. Yokoyama and T. Sano, *J. Porous Mater*., 2009, **16**, 641.

28 W. J. Roth and D. L. Dorset, *Struct. Chem*., 2010, **21**, 385.

29 T. Moteki, W. Chaikittisilp, Y. Sakamoto, A. Shimojima and T. Okubo, *Chem. Mater.*, 2011, **23**, 3564.

30 Z. Zhao, W. Zhang, P. Ren, X. Han, U. Müller, B. Yilmaz, M. Feyen, H. Gies, F. S. Xiao, D. D. Vos, T. Tatsumi and X. Bao, *Chem. Mater*., 2013, **25**, 840.

31 W. J. Roth, P. Nachtigall, R. E. Morris, P. S. Wheatley, V. R. Seymour, S. E. Ashbrook, C. Pavla, L. Grajciar, M. Položij, A. Zukal, O. Shvets, J. Čejka, *Nat. Chem*., 2013, **5**, 628.

32 A. Rojas and M. A. Camblor, *Chem. Mater*., 2014, **26**, 1161.

33 Y. Asakura, R. Takayama, T. Shibue and K. Kuroda, *Chem.-Eur. J*., 2014, **20**, 1893.

34 B. Marler, Y. Wang, J. Song and H. Gies, *Dalton Trans*., 2014, **43**, 10396.

35 S. Inagaki, T. Yokoi, Y. Kubota and T. Tatsumi, *Chem. Commun*., 2007, 5188.

36 P. Wu, J. Ruan, L. Wang, L. Wu, Y. Wang, Y. Liu, W. Fan, M. He, O. Terasaki, T. Tatsumi, *J. Am. Chem. Soc*., 2008, **130**, 8178.

37 S. Inagaki and Tatsumi, *Chem. Commun*., 2009, 2583.

38 J. F. Ruan, P. Wu, B. Slater, Z. L. Zhao, L. L. Wu, O. Terasaki, *Chem. Mater*., 2009, **21**, 2904.

39 T. Ikeda, S. Kayamori, Y. Oumi and F. Mizukami, *J. Phys. Chem. C*, 2010, **114**, 3466.

40 H. Gies, U. Muller, B. Yilmaz, T. Tatsumi, B. Xie, F. S. Xiao, X. H. Bao, W. P. Zhang and D. De Vos, *Chem. Mater*. 2011, **23**, 2545.

41 S. Inagaki, H. Imai, S. Tsujiuchi, H. Yakushiji, T. Yokoi and T. Tatsumi, *Microporous Mesoporous Mater*. 2011, **142**, 354.

42 B. Tijsebaert, M. Henry, H. Gies, F-S. Xiao, W. Zhang, X. Bao, H. Imai, T. Tatsumi, U. Müller, B. Yilmaz, P. Jacobs and D. D. Vos, *J. Catal*., 2011, **282**, 47.

43 F.-S. Xiao, B. Xie, H. Zhang, L. Wang, X. Meng, W. Zhang, X. Bao, B. Yilmaz, U. Müller, H. Gies, H. Imai, T. Tatsumi and D. De Vos, *ChemCatChem*, 2011, **3**, 1442.

44 H. Gies, U. Muller, B. Yilmaz, M. Feyen, T. Tatsumi, H. Imai, H. Y. Zhang, B. Xie, F. S. Xiao, X. H. Bao, W. P. Zhang, T. De Baerdemaeker and D. De Vos, *Chem. Mater*., 2012, **24**, 1536.

45 B. Yilmaz, U. Muller, F. Feyen, H. Zhang, F.-S. Xiao, T. De Baerdemaeker, B. Tijsebaert, P. Jacobs, D. De Vos, W. Zhang, X. Bao, H. Imai, T. Tatsumi and H. Gies, *Chem. Commun*., 2012, **48**, 11549.

46 H. Xu, B. Yang, J.-G. Jiang, L. Jia, M. He and P. Wu, *Microporous Mesoporous Mater*., 2013, **169**, 88.

47 J. G. Jiang, L. L. Jia, B. T. Yang, H. Xu and P. Wu, *Chem. Mater*., 2013, **25**, 4710.

48 H. Li, D. Zhou, D. Tian, C. Shi, U. Müller, M. Feyen, B. Yilmaz, H. Gies, F.-S. Xiao, D. De Vos, T. Yokoi, T. Tatsumi, X. Bao and W. Zhang, *ChemPhysChem*, 2014, **15**, 1700.

49 Y. Asakura, Y. Sakamoto and K. Kuroda, *Chem. Mater.*, 2014, **26**, 3796.

50 T. De Baerdemaeker, W. Vandebroeck, H. Gies, B. Yilmaz, U. Müller, M. Feyen and D. Vos, *Catalsis Today*, 2014, **235**, 169.

51 T. Ikeda, Y. Oumi, K. Honda, T. Sano, K. Momma and F. Izumi, *Inorg. Chem*., 2011, **50**, 2294.

52 N. Tsunoji, T. Ikeda, Y. Ide, M. Sadakane and T. Sano, *J. Mater. Chem*., 2012, **22**, 13682.

53 Y. Ide, M. Torii, N. Tsunoji, M. Sadakane and T. Sano, *Chem. Commun*., 2012, **48**, 7073.

54 K. Honda, Y. Ide, N. Tsunoji, M. Torii, M. Sadakane and T. Sano, *Bull. Chem. Soc. Jpn*., 2014, **1**, 160.

55 N. Tsunoji, Y. Ide, M. Torii, M. Sadakane and T. Sano, *Chem. Lett*., 2013, **42**, 244.

56 N. Tsunoji, M. Fukuda, K. Yoshida, Y. Sasaki, T. Ikeda, Y. Ide, M. Sadakane and T. Sano, *J. Mater. Chem. A*, 2013, **1**, 9680.

57 N. Tsunoji, T. Ikeda, Y. Ide, M. Sadakane and T. Sano, *J. Mater. Chem. A*, 2014, **2**, 3372.

58 N. Tsunoji, Y. Ide, Y. Yagenji, M. Sadakane and T. Sano, *ACS Appl. Mater. Interfaces*, 2014, **6**, 4616.

59 L. Hamon, P. L. Llewellyn, T. Devic, A. Ghoufi, G. Clet, V. Guillerm, G. D. Pirngruber, G. Maurin, C. Serre, G. Driver, W. Beek, E. Jolimaître, A. Vimont, M. Daturi and G. Férey, *J. Am. Chem. Soc*., 2009, **131**, 17490.

60 B. Zheng, J. Bai, J. Duan, L. Wojtas and M. J. Zaworotko, *J. Am. Chem. Soc*., 2011, **133**, 748.

61 S. Henke, A. Schneemann, A. Wütscher and R. A. Fischer, *J. Am. Chem. Soc*., 2012, **134**, 9464.

Chapter 8

Summary

Chapter 1, to make the purpose of my thesis clear, the historical and experimental overview of layered silicate was described. In addition, the possibility of innovative material design by effective utilizing of several layered silicate was also shown. From these back grounds, novel layered silicate, having new crystal structure and framework topology, based functionalized material much interested me.

Therefore, in chapter 2 and chapter 3, I attempted to synthesis novel layered silicates. To achieve synthesis of novel layered silicates, I focused on the hydrothermal synthetic system with relative low H_2O/SiO_2 ratio in the starting synthetic gel. Then, a wide variety of synthesis conditions using various alkylammoniums with different structures as structure directing agents (SDAs) were investigated. As a result, several layered silicates with novel and unique structures were successfully synthesized, which were named Hiroshima University Silicates (HUSs).

Three kinds of layered silicates HUS-2, HUS-3 and HUS-4 were synthesized on SiO_2–choline hydroxide–NaOH–H_2O system. Structural analyses by powder X-ray diffractometry and solid-state magic-angle-spinning (MAS) NMR spectroscopy revealed that HUS-2 had a novel silicate framework topology which was composed of four-, five-, and six-membered rings. Its silicate framework topology had similar structure of bre (10T)-type composite building included in HEU-type zeolite. Although

HUS-4 exhibited similar structure of layered silicate PLS-1 synthesized using tetramethylammonium cation as an SDA and the crystal structure of HUS-3 was not able to be determined, they could be transformed into CDO type zeolite by calcination via dehydration and condensation reaction of interlayer silanol groups (topotactic conversion process). I also clarified the potential application of these layered silicates for a Knoevenagel condensation reaction as base catalysts.

In chapter 3, I investigated the influence of benzyltrimethylammonium cation on the synthesis of novel layered silicate in relative low H_2O/SiO_2 system. When benzyltrimethylammonium was employed as a SDA, novel layered silicate HUS-7 was successfully synthesized, which indicates that the synthesis strategy using various SDAs with different structures is very effective for synthesis of layered silicate. Although the silicate framework structure of HUS-7 is similar to HUS-2, benzyltrimethylammonium cations and water molecules were regularly located in the generated interlayer space with unique arrangement. This crystallographically defined interlayer space exhibited selective and effective adsorption of phenol from acetonitrile solution containing benzene and phenol through the exchange of water molecules in the interlayers with phenol. These results strongly indicate that not only novel layered silicate framework but also novel regularity of interlayer molecules are an important factor for materials design and the research focused on this point is also attracted in the synthesis of novel layered silicate.

In chapter 4, I investigated the ability of molecular recognition of HUS-2 through adsorption experiments of formic, acetic, and propionic acids with different molecular structure. The HUS-2 selectively and effectively adsorbed propionic acid from water containing formic, acetic, and propionic acids. As confirmed by ^{1}H MAS NMR and

XRD measurements of formic acetic and propionic acid treated HUS-2, it was thought that this selective adsorption was derived from the intercalation of propionic acid, which can fit over the interlayer pores of HUS-2. In contrast, magadiite, which is a naturally occurring Na-type layered silicate, adsorbed formic and acetic acids, as well as propionic acid, from the aqueous mixture, indicating the unique framework topology of HUS-2 played important role for selective adsorption. The present results motivate me to look at novel layered silicate framework topology with different structures to find the more artful molecular recognition abilities.

In chapter 5, the ion-exchange ability and the potential as a precursor of porous material of HUSs were investigated in detail. I found layered silicate HUS-5, whose crystal structure was similar to that of β-HLS, with tetramethylammonium and sodium cations in the interlayer was converted to HUS-1 with only tetramethylammoniun through washing with water. In addition, bulky organic cations were not incorporated into the interlayer of HUS-1, whereas the interlayer distance of HUS-5 was easily expanded by ion-exchang with such organic cations. This result strongly indicates the possibility of ion-exchanged HUS-5 intermediate as a precursor for preparation of porous material with high surface derived from its interlayer huge space. To design novel porous material by effective utilizing of their internal surface are and novel framework topology, several post treatments including ion-exchange, acid treatment and calcination were performed for the layered silicate HUS-5. Then, novel nano porous silica HUS-6, with high BET surface area of ca. 1000 m^2g^{-1} and average pore diameter of 1.6 nm, was obtained. Furthermore, the specific pore structure of HUS-6 gave an intermediate state between micropores (ca. 0.6 nm) of silicalite-1 and mesopores (ca. 2.9 nm) of MCM-41. Because there are few reports concerning the preparation of

ordered nanoporous silica with a pore size of 1–2 nm, the HUS-6 with its unique pore structure can be used as a shape-selective catalyst and adsorbent for specific area. Furthermore, as the pore characteristics of HUS-6 is markedly different these of mesoporous silicas such as FSM-16 and KSW-2 synthesized using other layered silicate kanemite, my discovery suggests the possibility of design of novel porous silicas using novel layered silicates as precursors.

In chapter 6, highly active and chemoselective titanosilicate catalysts were obtained by material design via grafting with metal acetylacetonate onto the surface of layered silicate HUS-2. XRD, SEM/EDX, ^{13}C CP and ^{29}Si MAS NMR and UV−vis measurements of Ti-incorporated HUS-2 confirmed that the isolated tetrahedral Ti species were homogeneously immobilized onto silicate sheets via Si−O−Ti covalent bond. Ti-incorporated HUS-2 showed ca. 100% selectivity for partial cyclohexane oxidation and considerably higher yields (cyclohexanol and cyclohexanone) than TS-1, a typical Ti-containing zeolite due to the large amounts of isolated and tetrahedrally coordinated Ti grafted onto the silicate sheets. Although, by many research groups, material design by effective utilizing of the grafting reaction of layered silicate using various reactants, this is the first report concerning the grafting of metal complex onto the layered silicate. As a wide variety of metal acetylacetonates with different compositions and various layered silicates with different framework topology are available, the present result may make the accurate and innovative design of composite materials based on metals or metal oxides.

In chapter 7, a new type of microporous material HUS-10 was successfully synthesized by silylation with trichloromethylsilane of layered silicate Hiroshima University Silicate (HUS)-2 and subsequent calcination. Through the silylation process,

tetrahedral $Si(CH_3)Cl_3$ unit reacted with two silanol groups on the both sides of the interlayer. By the subsequent calcination, the remaining hydroxyl groups of the tetrahedral $Si(OH)(OSi\text{-})_3$ unit on the up-and-down silicate layers were condensed, affording ordered microporous material, named HUS-10, was obtained. The BET surface area, micropore volume and average pore diameter of HUS-10 were ca. 400 m^2g^{-1}, 0.15 cm^3g^{-1} and 0.50 nm, respectively. Structural determination using MAS NMR measurements and DFT calculation results revealed that HUS-10 has a porous structure consist of 2-dimensional 8- and 12- membered rings with methyl and hydroxy groups regularity located. Control of hydrophilic or hydrophobic adsorption behavior was achieved by changing the amounts of methyl and hydroxyl groups through the calcination process. Molecular prove method using various probe molecules having different molecular sizes proved the actual molecular sieve ability like zeolite, which can adsorb smaller molecules than ethane. It was also found that the HUS-10 adsorbed a large amount of CO_2 at room temperature. Furthermore, although silicalite-1, all-silica MFI type zeolite having the approximately same porosity of HUS-10, adsorbed CH_4 and N_2 to some extent, whereas CH_4 and N_2 were hardly adsorbed on HUS-10, revealing that the unique pore structure of HUS-10 gave the potential for adsorption removal of contaminated CO_2 from various gas mixtures.

In this thesis, I successfully synthesized several novel layered silicates HUSs and showed these potential for catalysts, adsorbents and the precursor of porous material. As a consequence, the potential application of these HUSs was confirmed. Also, there are wonderful applicability and possibility of HUSs. In chapter 1, I described that structure features and applicability and possibility of layered silicate are directly affected from

the original crystal structure of layered silicates. In fact, in this thesis, HUSs actually exhibited numerous potential for material design through effective utilizing of their specific structural features such as their (1) interlayer large surface area, (2) ordered interlayer space, and (3) unique silicate framework. These facts strongly indicate that more numerous and innovative material design will become possible by increasing the diversity of novel layered silicate, which can be regarded as a new class of foundation for interesting structure design.

List of publications

1. Yoshiyasu Furumoto, Yasumitsu Harada, **Nao Tsunoji**, Atsushi Takahashi, Tadahiro Fujitani, Yusuke Ide, Masahiro Sadakane, and Tsuneji Sano, "Effect of acidity of ZSM-5 zeolite on conversion of ethanol to propylene", *Appl. Catal. A*, **399** 262-267, **2011**.
2. Yoshiyasu Furumoto, **Nao Tsunoji**, Yusuke Ide, Masahiro Sadakane, and Tsuneji Sano, "Conversion of ethanol to propylene over HZSM-5(Ga) co-modified with lanthanum and phosphorous", *Appl. Catal. A*, **417–418** 137-144, **2012**.
3. **Nao Tsunoji**, Takuji Ikeda, Yusuke Ide, Masahiro Sadakane, and Tsuneji Sano, "Synthesis and characteristics of novel layered silicates HUS-2 and HUS-3 derived from a SiO_2-choline hydroxide-NaOH-H_2O system", *J. Mater. Chem.*, **22** 13682-13690, **2012**.
4. Yusuke Ide, Masato Torii, **Nao Tsunoji**, Masahiro Sadakane, and Tsuneji Sano, "Molecular recognitive adsorption of aqueous tetramethylammonium on the organic derivative of Hiroshima University Silicate-1 with a silane coupling reagent" *Chem. Commun*., **48** 7073-7075, **2012**.
5. **Nao Tsunoji**, Yoshiyasu Furumoto, Yusuke Ide, Masahiro Sadakane, and Tsuneji Sano, "Conversion of ethanol into propylene over TON type zeolite", *J. Jpn. Petrol. Inst.,* **56** 22-30, **2013**.
6. **Nao Tsunoji**, Yusuke Ide, Masato Torii, Masahiro Sadakane, and Tsuneji Sano, "Molecular Recognitive Adsorption of Aqueous Propionic Acid on Hiroshima University Silicate-2 (HUS-2)", *Chem. Lett*., **42** 244-246, **2013**.
7. **Nao Tsunoji**, Miki Fukuda, Kaname Yoshida, Yukichi Sasaki, Takuji Ikeda, Yusuke Ide, Masahiro Sadakane and Tsuneji Sano, "Characterization of layered silicate HUS-5 and formation of novel nanoporous silica through transformation of HUS-5 ion-exchanged with alkylammonium cations", *J. Mater Chem A*, **1** 9680–9688, **2013**.
8. Toshihiro Maruo, Naoki Yamanaka, **Nao Tsunoji**, Masahiro Sadakane and Tsuneji Sano, "Facile Synthesis of AEI Zeolite by Hydrothermal Conversion of FAU Zeolite in the Presence of Tetraethylphosphonium Cations", *Chem. Lett.*, **43** 302-304, **2014**.
9. Kotaro Honda, Yusuke Ide, **Nao Tsunoji,** Masato torii, Masahiro Sadakane and Tsuneji Sano, "An Efficient Way to Synthesize Hiroshima University Silicate-1 (HUS-1) and the Selective Adsorption Property of Ni^{2+} from Seawater", *Bull. Chem.*

Soc. Jpn., **1** 160-166, **2014**.

10. **Nao Tsunoji**, Takuji Ikeda, Masahiro Sadakane and Tsuneji Sano "Synthesis and characteristics of novel layered silicate HUS-7 using benzyltrimethylammonium hydroxide and its unique and selective phenol adsorption behavior", *J. Mater. Chem. A*, **2** 3372-3380, **2014**.
11. **Nao Tsunoji**, Yusuke Ide, Yuya Yagenji, Masahiro Sadakane and Tsuneji Sano "Design of Layered Silicate by Grafting with Metal Acetylacetonate for High Activity and Chemoselectivity in Photooxidation of Cyclohexane", *ACS Appl. Mater. Interfaces* **6** 4616-4621, **2014**.
12. **Nao Tsunoji**, Takushi Sonoda, Yoshiyasu Furumoto, Masahiro Sadakane and Tsuneji Sano "Regeneration of Brønsted acid sites in phosphorus-modified HZSM-5(Ga) by modification with various metal cations", *Appl. Catal. A* **481** 161-168, **2014**.
13. **Nao Tsunoji**, Keita Takahashi, Masahiro Sadakane and Tsuneji Sano "Incorporation of heteropolyacids into layered silicate HUS-2 grafted with 3-aminopropyltriethoxysilane", *Bull. Chem. Soc. Jpn.* in press.
14. Takushi Sonoda, Toshihiro Maruo, Yoshitaka Yamasaki, **Nao Tsunoji**, Masahiro Sadakane and Tsuneji Sano, "Synthesis of high-silica AEI zeolites with enhanced thermal stability by hydrothermal conversion of FAU zeolites, and their activity in the selective catalytic reduction of NO_x with NH_3" *J. Mater. Chem. A*, in press.

Presentations in international conference

1. Miki Fukuda, **Nao Tsunoji**, Kaname Yoshida, Yukichi Sasaki, Takuji Ikeda, Yusuke Ide, Masahiro Sadakane and Tsuneji Sano, "Synthesis of nanoporous silica HPS-1 by transformation of layered silicate HUS-1" *6th International FEZA Conference*, P A3.14, University of Leipzig, Leipzig, Germany, (Sept., 2014). Poster
2. **Nao Tsunoji**, Takuji Ikeda, Masahiro Sadakane and Tsuneji Sano, "Synthesis and characteristics of novel layered silicate HUS-7 using BTMAOH and its unique and selective phenol adsorption behavior" *6th International FEZA Conference*, P A3.15, University of Leipzig, Leipzig, Germany, (Sept., 2014). Poster
3. **Nao Tsunoji**, Miki Fukuda, Kaname Yoshida, Yukichi Sasaki, Takuji Ikeda, Yusuke Ide, Masahiro Sadakane and Tsuneji Sano, "Synthesis of nanoporous silica HPS-1 by transformation of layered silicate HUS-1" *17th International Zeolite Conference*, P-1.1-54, Best Western Vega Hotel, Moscow, Russia, (July, 2013). Poster

4. **N. Tsunoji**, T. Ikeda, Y. Ide, M. Sadakane, T. Sano, "Synthesis of novel layered silicates HUS-2, HUS-3, and HUS-4 as precursors for zeolites and its post-synthesis alumination" *17th International Zeolite Conference*, RRR-1.1-08, Best Western Vega Hotel, Moscow, Russia, (July, 2013). Poster
5. **Nao Tsunoji**, Miki Fukuda, Kaname Yoshida, Yukichi Sasaki, Takuji Ikeda, Yusuke Ide, Masahiro Sadakane and Tsuneji Sano, "Transformation of layered silicate Hiroshima University Silicate-1 (HUS-1) to novel nanoporous silica HPS-1" *8th International Mesostructured Materials Symposium*, RRR-1-008, Awaji Island, Hyogo, Japan, (May, 21, 2013). Poster
6. **Nao Tsunoji**, Yoshiyasu Furumoto, Yusuke Ide, Masahiro Sadakane, Tsuneji Sano "Regeneration of Brønsted acid sites in phosphorus-modified HZSM-5(Ga) by modification with various metals" *7th international symposium on acid-base catalysis*, PA-19, TKP Garden city Shinagawa, Tokyo, Japan, (May, 13, 2013). Poster
7. Miki Fukuda, **Nao Tsunoji**, Yusuke Ide, Masahiro Sadakane, Tsuneji Sano "Modification of Layered Silicate HUS-1 Precursor with Organic Cations and its Base Catalytic Activity" *7th international symposium on acid-base catalysis*, PA-34, TKP Garden city Shinagawa, Tokyo, Japan, (May, 13, 2013). Poster
8. **Nao Tsunoji**, Masato Torii, Yusuke Ide, Masahiro Sadakane, Tsuneji Sano "Synthesis of novel layered silicate HUSs and their molecular recognitive adsorption properties" *International symposium on material chemistry of intercalation compounds*, No. 6, Waseda University, Tokyo, Japan, (May, 11, 2013). Short oral
9. Miki Fukuda, **Nao Tsunoji**, Kaname Yoshida, Yukichi Sasaki, Yusuke Ide, Masahiro Sadakane, Tsuneji Sano "Ion-exchange and transformation to novel nanoporous material of layered silicate HUS-1" *International symposium on material chemistry of intercalation compounds*, No. 7, Waseda University, Tokyo, Japan, (May, 11, 2013). Short oral
10. **N. Tsunoji**, Y. Ide, K. Honda, M. Torii, M. Miyamoto, M. Sadakane, T. Sano, "Synthesis of a New layered Silicate HUS-1 and the Selective Adsorption Property of Ni^{2+} from Seawater" *The 2nd Asian Clay Conference*, PP-5-18, ASTER PRAZA, Ewha Womans University, Seoul, Korea, (September, 2012). Poster
11. Yoshiyasu Furumoto, **Nao Tsunoji**, Yusuke Ide, Masahiro Sadakane, Tsuneji Sano "Effect of co-modification with lanthanum and phosphorous on conversion of ethanol to propylene over HZSM-5(Ga)" *International Symposium on Zeolites and Microporous Crystals 2012 (ZMPC2012)*, P-10, ASTER PRAZA, Hiroshima, Japan,

(August, 2012). Poster

12. **N. Tsunoji**, Y. Ide, K. Honda, M. Torii, M. Miyamoto, M. Sadakane, T. Sano, "Efficient Way to Synthesize Hiroshima University Silicate-1 (HUS-1) and the Selective Adsorption Property of Ni^{2+} from Seawater" *International Symposium on Zeolites and Microporous Crystals 2012 (ZMPC2012)*, P-035, ASTER PRAZA, Hiroshima, Japan, (August, 2012). Poster
13. M. Torii, Y. Ide, **N. Tsunoji**, M. Sadakane, T. Sano, "Adsorption of Aqueous Tetramethylammonium on the Organic Derivative of Hiroshima UniversitySilicate-1 (HUS-1) with Silane Coupling Reagents" *International Symposium on Zeolites and Microporous Crystals 2012 (ZMPC2012)*, P-080, ASTER PRAZA,Hiroshima, Japan, (August, 2012). Poster
14. **N. Tsunoji**, T. Ikeda, Y. Ide, M. Sadakane, T. Sano, "Synthesis and characteristics of novel layered silicate HUS-2" *International Symposium on Zeolites and Microporous Crystals 2012 (ZMPC2012),* RRR-038, ASTER PRAZA, Hiroshima, Japan, (August, 2012). Poster

Acknowledgements

I would like to express my gratitude to all people who have helped me with the preparation of this doctoral thesis. Especially, I am deeply indebted to my supervisor Prof. Dr. Tsuneji Sano for his advice, support, and invaluable suggestions concerning science. Without his patient guidance, it is almost impossible to finish my study. I also gratefully acknowledge Prof. Masahiro Sadakane and Dr. Yusuke Ide for teaching me laboratorial techniques and work as well as for valuable suggestions. I must also express special gratitude to Dr. Takuji Ikeda, Dr. Yoshimichi Kiyozumi, Dr. Tadahiro Fujitani (National Institute of Advanced Industrial Science and Technology) for providing input and some characterizations.

I am grateful to all of Sano Laboratory's members, Dr. S. Sumiya, Dr. M. Itakura, Dr. Y. Takamitsu, Dr. K. Honda, Dr. S. Ogo, Mr. S. Shibata, Mr. Y. Harada, J. Hujiwara, Ms. A. Yashiki, Mr. I. Goto, Mr. Y. Furumoto, Ms, S Moroi, Mr. N. Yamanaka, Mr. R. Ogino, Ms. N. Shimizu, Mr. K. Takahashi, Mr. M. Torii, Mr. H. Hattori, Mr. Y. Umehara, Ms. A. Suzuki, Mr. K. Nishiki, Ms. M. Fukuda, Mr. I. Igarashi, Mr. T. Kadota, Mr. Y. Koyama, Mr. A. Haioka, Mr. S. Maruo, Mr. Y. Yagenji, Mr. S. Yuki; and peers as well: Ms. A. Fujimoto, Ms. N Kagawa, Ms. Y. Kawamoto, Mr. H. Kitatomi, Mr. K. Sahiro, Mr. N. Nakamura for their help, cooperation and contributions to my study.

Hiroshima, March 2015

Nao Tsunoji